

https://dspace.org/

Biomass waste to energy: investigating syngas production from pyro-gasification of sawdust blends of invasive alien plants and tropical tree species

Michael, Okoro Nnanna-jnr

2020

https://hdl.handle.net/10539/31289

Downloaded from a DSpace repository. https://dspace.org/



Biomass waste to Energy: Investigating syngas production from pyro-gasification of sawdust blends of Invasive Alien Plants and Tropical tree species

Okoro Nnanna-jnr Michael

(1582331)

A thesis submitted to the Faculty of Engineering and the Built Environment, University of the Witwatersrand, Johannesburg, in fulfilment of the requirement for the degree of Doctor of Philosophy in Engineering

Supervisor: Prof. Kevin G. Harding

Co-Supervisor: Prof. Michael O. Daramola

September 2020

Declaration

I declare that this thesis is my own work. It is being submitted for the degree of Doctor of Philosophy in the University of Witwatersrand, Johannesburg. It has not been submitted before for any degree or examination in any other University.

Nnanna-jnr Michael Okoro



25th day of March, 2020

ABSTRACT

Conventional biomass gasification is associated with technical issues which limit its scale-up to full commercialization. These issues include but are not limited to high tar composition in the syngas produced, low syngas yield, and expensive and inefficient tar cleaning procedures. Biomass pyro-gasification can be defined as a hybrid or multi-stage integration of pyrolysis and gasification process, controlled independently to separate and restrict tar from being gasified alongside char. This is capable of producing high yields of syngas with less tar impurities suitable for downstream applications.

By employing pyro-gasification, this research aimed to investigate the properties of syngas contained in the product gas, produced from the thermochemical conversion of wood wastes. These enormous wood wastes samples were sourced from different Invasive Alien Plants (IAPs) and commercial sawmill tropical woods. Firstly, the individual samples were subjected to a series of characterisations to ascertain their fuel properties and suitability for pyro-gasification. These tests include their structural composition, proximate and elemental composition, char yield, char reactivity, higher heating value (HHV), bulk density, fuel ratio, and energy density. A fuel quality evaluation of the samples was conducted to rank the samples accordingly. This was used to gain better understanding of the behaviour of each sample when subjected to pyro-gasification. Furthermore, the samples were subjected to a thermogravimetric analysis to ascertain their rates of volatilization, char decomposition, and maximum decomposition temperatures. Based on their thermogravimetric analysis and differential thermogravimetry, a kinetic study was conducted to inform the viability of the samples and the selection of suitable operating parameters for optimum process efficiency.

Finally, in conducting the pyro-gasification experiment, the sawdust sizes of the wood waste samples were first pyro-gasified individually (i.e. 100 % wt. of the feedstock). Subsequently, the samples were blended with each other in three separate mix ratios – 30/70 (i.e. 30 % wt., and 70 % wt. of 20 g of the feedstock), 50/50 and 70/30. The product gas produced from each experimental run was

sampled at 900°C, 950°C, and 1000°C, and analysed using a TCD Gas Chromatograph (GC). The properties of the syngas (and those of its component gases CO and H_2) determined are the – percentage concentration in the product gas, syngas yield per gram of biomass feedstock, volumetric flow rate, rate of production of the gas and the physical properties of the flame generated when the syngas was ignited.

According to the data collated, syngas concentrations in the product gas were generally high across the board, averaging 96.4%. Meanwhile, trace concentrations of CH_4 and CO_2 were observed in the product gas. The ratio of H_2/CO in the syngas averaged 0.06 at 900°C and was observed to increase to averages of 0.16 and 0.46 with increase in temperature to 950°C and 1000°C respectively. The production rate of the syngas and those of its gaseous components – H_2 and CO, were also affected by the increase in temperature. The most significant increases in the gas production rate were observed with the H_2 as the temperature was increased from 900°C to 1000°C. In general, the IAPs showed the highest increases in H_2 production rate, attaining significant increases with the rise in temperature from 900°C to 1000°C. The 100% wt. of the Poplar feedstock, in particular, exhibited a significant increase in H_2 production rate from 130.12 mL/min/gram at 900°C to 3556.14 mL/min/gram at 1000°C. Meanwhile, the highest hydrogen production rate of 7937.07 mL/min/gram attained across the board was exhibited by the Eucalyptus-Jacaranda 30/70 blend. Most IAP blended samples exhibited higher syngas production rate than their associated individual samples at a lower temperature of 900°C. However, with an increase in temperature to 1000°C, the syngas production rate from most of these blended samples declined significantly.

The syngas yields (i.e. the volume of syngas produced from a gram of wood feedstock), from most samples were significantly high, particularly at 900°C. These yields were subsequently increased at 1000°C. The highest syngas yield of 744.42 mL/gram was obtainable from the Eucalyptus-Bugweed 30/70 blend, while the lowest yield of 518.05 mL/gram was obtainable from the Jacaranda-Poplar 30/70

amongst all IAP samples and their blends. Meanwhile, among the tropical samples and their blends, the highest syngas yield of 735.8 mL/gram of feedstock was obtainable from the Mahogany-Opepe 30/70 blend, while the lowest yield of 493.7 mL/gram of feedstock was obtainable from the African mahogany-Opepe 70/30 blend. These were generally higher than those obtained from the 100% wt. of the individual tropical wood samples.

This thesis has been carefully documented to (a) prove the viability of pyro-gasification as a tar removal process for syngas production at reduced gasification temperatures; (b) showcase the viability of wood wastes of invasive alien plants and commercial tropical trees which are yet to be explored for syngas production and; (c) showcase the possibility of optimizing syngas production by blending two wood species in different mix ratios. Some of the findings on results of the characterization of the samples, their thermogravimetric analyses, as well as data on their syngas production via pyro-gasification as described in chapters four, five and six respectively, have either been communicated as scientific articles in journals, presented in conferences or have been submitted and awaiting publication (see Appendix C for this list).

Acknowledgement

I am most grateful to God Almighty for life, good health and grace beyond words, and to the Holy Spirit for the continuous gift of knowledge, wisdom and guidance.

I am forever grateful to Prof. K.G Harding my supervisor and Prof. M.O Daramola, my co-supervisor, and research mentors for their patience, guidance, exceptional work ethic, humility and tireless efforts in imparting a great deal of knowledge to me, thereby moulding me into becoming a better researcher in the field of renewable energy. I am also forever indebted to Prof. E. Oguzie, my boss, research mentor and friend, who worked tirelessly to ensure I did not miss out on this opportunity. For being a father Sir, I am eternally grateful to you.

My special thanks also go to the immediate past and present Vice-chancellors of the Federal University of Technology, Owerri, the past and present Heads of Department of Environmental Management and the entire staff who worked diligently to ensure the success of my programme.

To the University of Witwatersrand Post-Graduate Merit Award (PGMA), The World Academy for Sciences (TWAS) and National Research Foundation (NRF), South Africa; none of these would have been possible without you. Thanks for supporting this project financially.

I would like to specially thank Mr. Motlatsi, who went the extra mile to ensure I completed my lab experiments on time even in critical moments. Also special thanks to Janet Smith, Rodney, Hopewell, Phathu for their unending love, support and hard work in supporting my research.

I also extend my appreciation to my colleagues; Olayile Ejekwu, Dr. Ayotunde Awosusi, Ashiegbu Darlington, Uzor Enwereuzor, Dr. Kevin Yoro, Dr. Maxwell Ozonoh, Dr. Thomas Aniokote, Dr. Wumi Sadare, Dr. Demilade Fayemiwo, Dr. Comas Uche, Dr. Moshood Onifade, Amira Mohammed, Ugochukwu Ikegwu and all other members of the SEERU group for their friendship, support and contribution to this project.

To my beloved Parents, Engr. & Barr. Nnanna Okoro and awesome siblings, Barr. Nneoma, Dr. Emeka, Dr. Chinyere and Engr. Obiageli for their prayers, sacrifices and unwavering support. My Uncles Prof. Toni Duruaku, Barr. Emeka Duruaku, and Barr. (Mrs) Chioma Toni-Duruaku, Thank you so much for your love and support.

Finally, Dr. “Ashiwaju Mazi Mike” Bodunrin, Yusuf Jimoh-Taiwo, Dr. Moshood Onifade and Ummukulthoum Bakare here is a big thank you for your guidance, continuous support and friendship in my times of need.

You are all numerous gems who I have been blessed with; Thanks for your support.

This thesis is dedicated to my Parents; Engr. & Barr. (Mrs) Nnanna Okoro

Table of Contents

ABSTRACT ..... ***iii***

Acknowledgement ..... ***vi***

Table of Contents ..... ***ix***

List of tables ..... ***xiii***

List of figures ..... ***xiv***

Chapter 1 ..... ***1***

Introduction ***1***

1.1 Background 1

1.1.1 Power situation in Sub-Sahara Africa an opportunity for bioenergy 2

1.1.2 Abundance of wood waste biomass in Sub Sahara Africa 6

1.2 Research questions, aim, and objectives 16

1.2.1 Research questions 16

1.2.2 Research aim 19

1.2.3 Research objectives 19

1.3 Report outline 19

1.4 Scope of work 21

Chapter 2 ..... ***24***

Literature Review ***24***

2.1 Introduction 24

2.2 Lignocellulosic Biomass (LCB) 24

2.2.1 Structural composition of LCB 25

2.2.2 Thermal behaviors of structural components of LCBs 28

2.2.3 Contribution of biomass structural components on biofuel type and yield 31

2.3 Biomass Thermochemical Conversion 36
2.3.1 Pyrolysis 38
2.3.2 Gasification 45
2.4 Tar in biomass gasification 65
2.4.1 Tar cleaning techniques 66
2.5 Pyro-gasification 72
2.6 Concluding remark 80
Chapter 3 83
Materials and Methods 83
3.1 Introduction 83
3.2 Wood sampling 83
3.2.1 Identification and harvesting of wood species 83
3.2.2 Wood sample pre-treatment 84
3.3 Experimental 84
3.3.1 Structural Analysis 84
3.3.2 Proximate and Ultimate Analysis 85
3.3.3 Ultimate analysis 86
3.3.4 Fuel Ratio 86
3.3.5 Higher Heating Value 86
3.3.6 Bulk and Energy Density 87
3.3.7 Char yield and reactivity 88
3.3.8 Fuel evaluation exercise 88
3.4 Thermo-decomposition Analysis (TGA) and Kinetic Study 91
3.4.1 Thermo-decomposition Analysis (TGA) 91
3.4.2 Kinetic Analysis 91

3.5 Pyro-gasification experiment 94

3.5.1 Description of the Pyro-gasification reactor 94

3.5.2 Description of the Pyro-gasification Rig 96

3.5.3 Operation of the Rig 98

3.5.4 Description of the pyro-gasification process 99

3.5.5 Novelty of this pyro-gasification method and rig design 102

3.5.6 Determination of yield and production rate of syngas, H_2 and CO 104

Chapter 4..... 106

Fuel examination of Invasive Alien Plants and Tropical hardwoods as feedstock in pyro-gasification..... 106

4.1 Introduction 106

4.2 Results and Discussion 108

4.2.1 Structural analysis 108

4.2.2 Proximate analysis 112

4.2.3 Ultimate analysis 116

4.2.4 Higher heating value 119

4.2.5 Bulk density 120

4.2.6 Char yield and reactivity 121

4.2.7 Fuel Quality Evaluation 124

4.3 Concluding remark 133

Chapter 5..... 139

Thermogravimetric Analysis (TGA) and Kinetic Study of the wood samples ... 139

5.1 Introduction 139

5.1.1 Thermogravimetric Analysis (TGA) / Derivative Thermogravimetry (DTG) 139

5.1.2 Kinetic study 139

5.2 Results and Discussion 141

5.2.1 TGA and DTG of wood samples 141

5.2.2 Determination of Activation energies: 155

5.3 Concluding remark 165

Chapter 6 168

Pyro-gasification of wood samples 168

6.1 Introduction 168

6.2 Results and Discussion 169

6.2.1 Dry product gas volumetric flow rate: 169

6.2.2 H_2, CO and Syngas production rate 176

6.2.3 Syngas yield 183

6.2.4 Bio-oil extracted and Char residue after process 186

6.2.5 Observed flame properties 194

6.4 Concluding remark 198

Chapter 7 201

Conclusions and Recommendations 201

7.1 Conclusions 201

7.2 Recommendations 211

References 214

Appendix A: Determination of Activation energies 234

Appendix B: Pyro-gasification experimental data of wood samples 242

Appendix C: List of publications from this study 286

List of tables

Table 2.1: Structural compositions of softwoods and hardwoods……..27

Table 2.2: Higher heating values of branches and trunks of hardwood samples……27

Table 2.3: Three modes of pyrolysis and their products in comparison to gasification……..44

Table 2.4: Allowable amounts of tar and impurities in syngas for downstream applications as reported in literature……66

Table 3.1: A sample of fuel evaluation table……90

Table 4.1: Experimental data of the eight wood samples……110

Table 4.2: Comparison of ash composition of woods in this study with others in literature……115

Table 4.3: Comparison of nitrogen composition of wood samples in this study with others in literature……118

Table 4.4: Higher heating values of wood samples in this study with literature……120

Table 4.5: Char properties of wood samples……..122

Table 4.6: Fuel evaluation scores of wood samples……125

Table 4.7: Comparison of proximate properties of wood samples in this study with literature……129

Table 5.1: TGA data of the wood samples……152

Table 5.2: Activation energies of the wood samples……164

Table 6.1: Observed flame properties of gases generated from wood samples.197

List of figures

Figure 1.1: World regional data on electricity. Sourced from literature ……5

Figure 1.2: Change in Global Consumption of Sawn Wood Products since 1961….7

Figure 1.3: Global consumption of Forest Product in Africa (m3) since 1961…….7

Figure 1.4: Environmental and air pollution caused by indiscriminate dumping and open-air burning of sawdust……8

Figure 1.5: IAP wood waste left on-site during a “slash and dump” mechanical control……..10

Figure 1.6: Sustainable sources of wood waste for bioenergy……11

Figure 1.7: Work Breakdown Structure (WBS) of this research project……..21

Figure 2.1: Thermal decomposition behaviours of the biomass structural components……..28

Figure 2.2: (a) Thermogravimetric (TG) and (b) Derivative thermogravimetry (DTG) thermograms of standard samples of cellulose, hemicellulose, and lignin……29

Figure 2.3: TGA and DTG thermograms of cellulose, xylan (hemicellulose) and lignin……33

Figure 2.4: DSC thermograms of hemicellulose, cellulose and lignin thermal decomposition……34

Figure 2.5: Effect of heating rate on (a) char yield and (b) Tar (bio-oil) yield, of different wood sizes – sawdust (SD), 2, 5 and 9 mm cylindrical wood pellets……35

Figure 2.6: Lignocellulosic biomass and their thermochemical conversion processes for biofuel products……37

Figure 2.7: Effect of increase in heating rate from 1 K/s to 30 K/s to the char reactivity of the same sample in different sizes – Sawdust (SD), 2, 5 and 9 mm diameter cylindrical wood pellets……45

Figure 2.8: Stages, processes, and products of the biomass gasification……46

Figure 2.9: Pathways for char phase reactions and gas-phase reactions of biomass gasification……..49

Figure 2.10: Classification of gasifiers……55

Figure 2.11: (a) Influence of S/B ratio variation on gas composition; (b) Effect of temperature variation on product gas yield……60

Figure 2.12: (a) Composition of products at varying temperatures (at a steam flow rate of 9.0 g/min); (b) Effect of S/B on Hydrogen increment by ASPEN simulation……61

Figure 2.13: (a) Effect of wood size on tar yield; (b) Effect of wood size on char yield; (c) Temperature histories at three locations within the wood cylinder during the pyrolysis at a heating rate of 30 K/s……62

Figure 2.14: A schematic representation of the thermochemical conversion process of bulk wood……64

Figure 2.15: Typical composition of biomass tar……65

Figure 2.16: Classification of tar removal methods with a focus on pyro-gasification……66

Figure 2.17: Schematic diagram of a typical dual fluidized bed gasifier……71

Figure 2.18: The pyro-gasification pathway……73

Figure 2.19: The Viking pyro-gasification combined heat and power (CHP) demonstration and research plant……75

Figure 2.20: : Schematic diagrams of pyro-gasification reactor designs reported in literature by (a) Alipour *et al.*; (b) Chen *et al.*; (c) Ahrenfeldt *et al.*; (d) Pattanotai *et al.*……76

Figure 3.1: (a) The soxhlet extraction process, (b) the vacuum filtration of the NaOH and extractive-free sample mixture after boiling for 3.5 h, and (c) the oven-dried sample residue……85

Figure 3.2: Measurement of dimensions and mass for the bulk density of the Jacaranda wood sample……87

Figure 3.3: Classification of fuel evaluators……89

Figure 3.4: Blueprint of the pyro-gasification reactor……95

Figure 3.5: Reactor after fabrication……96

Figure 3.6: Schematic diagram of the pyro-gasification rig……96

Figure 3.7: The pyro-gasification rig……97

Figure 3.8: Blending pattern of (a) IAP samples and (b) Tropical hardwood samples, in blend ratios: 50/50, 70/30, 30/70……101

Figure 4.1: A comparison of the Structural compositions of the eight wood samples……108

Figure 4.2: Chart depicting a comparison of the Char yield and Char reactivity fuel evaluation ranks of the wood samples relative to each other……133

Figure 4.3: Chart depicting the Fuel ratio and Energy density fuel evaluation ranking of the wood samples relative to each other……134

Figure 4.4: Chart depicting the Nitrogen content and Ash content fuel evaluation ranking of the wood samples relative to each other……135

Figure 4.5: Chart depicting the Total fuel superiority ranking of the wood samples relative to each other……136

Figure 5.1: Typical non-monolithic decomposition patterns of biomass structural components……139

Figure 5.2: TGA and DTG thermograms of Bugweed……142

Figure 5.3: TGA and DTG thermograms of Eucalyptus……143

Figure 5.4: TGA and DTG thermograms of Jacaranda……144

Figure 5.5: TGA and DTG thermograms of Poplar……145

Figure 5.6: TGA and DTG thermograms of the African mesquite……146

Figure 5.7: TGA and DTG thermograms of the African mahogany……147

Figure 5.8: TGA and DTG thermograms of the African oilbean……148

Figure 5.9: TGA and DTG thermograms of Opepe……149

Figure 5.10: An overlay of the DTG thermograms of the IAP wood samples depicting their peak rates of volatilization and char decomposition……150

Figure 5.11: An overlay of the DTG thermograms of the Tropical hardwood samples depicting their peak rates of volatilization and char decomposition……151

Figure 5.12: Separate decomposition patterns of Bugweed structural components……156

Figure 5.13: Separate decomposition patterns of Eucalyptus structural components……157

Figure 5.14: Separate decomposition patterns of Jacaranda structural components……158

Figure 5.15: Separate decomposition patterns of Poplar structural components……159

Figure 5.16: Separate decomposition patterns of African mesquite structural component……160

Figure 5.17: Separate decomposition patterns of African mahogany structural components……161

Figure 5.18: Separate decomposition patterns of African oilbean structural components……162

Figure 5.19: Separate decomposition patterns of Opepe structural components……163

Figure 6.1: Average dry product gas volumetric flow rate of individual IAP wood samples……170

Figure 6.2: Average dry product gas volumetric flow rate of Eucalyptus-Bugweed blend……171

Figure 6.3: Average dry product gas volumetric flow rate of Bugweed-Jacaranda blend……171

Figure 6.4: Average dry product gas volumetric flow rate of Bugweed-Poplar blend……172

Figure 6.5: Average dry product gas volumetric flow rate of Jacaranda-Poplar blend……173

Figure 6.6: Average dry product gas volumetric flow rate of Eucalyptus-Poplar blend……173

Figure 6.7: Average dry product gas volumetric flow rate of the individual Tropical hardwood samples……174

Figure 6.8: Average dry product gas volumetric flow rate of African mesquite-African oilbean blend……175

Figure 6.9: Average dry product gas volumetric flow rate of African mahogany-African oilbean blend……175

Figure 6.10: Rate of production of syngas and its components from the individual IAP samples at 900, 950 and 1000°C……177

Figure 6.11: Rate of production of H_2 and CO from the individual IAP samples and their blends at 900°C……178

Figure 6.12: Rate of production of H_2 and CO from the individual IAP samples and their blends at 950°C……178

Figure 6.13: Rate of production of H_2 versus CO from the individual IAP samples and their blends at 1000°C……179

Figure 6.14: Rate of production of syngas and its components from the individual Tropical hardwood samples at 900, 950 and 1000°C……180

Figure 6.15: Rate of production of H_2 versus CO from the individual Tropical hardwood samples and their blends at 900°C……181

Figure 6.16: Rate of production of H_2 versus CO from the individual Tropical hardwood samples and their blends at 950°C……182

Figure 6.17: Rate of production of H_2 versus CO from the individual Tropical hardwood samples and their blends at 1000°C……182

Figure 6.18: Syngas yield of all individual wood samples……184

Figure 6.19: Syngas yield of individual IAP samples and their blends at 900, 950 and 1000°C……185

Figure 6.20: Syngas yield of individual Tropical hardwood samples and their blends at 900, 950 and 1000°C……186

Figure 6.21: Bio-oil deposition through condensation of heavy pyrolysis gases……187

Figure 6.22: Varying volumes of Bio-oil extracted from the individual Tropical hardwoods and their blends……188

Figure 6.23: Varying volumes of Bio-oil extracted from the individual IAP samples and their blends……..188

Figure 6.24: Volume of Bio-oil extracted from Jacaranda-Bugweed 50/50 blend..……..189

Figure 6.25: Mass of char residue recovered from the reactor after the pyro-gasification of hardwoods (a) Poplar; (b) Eucalyptus; (c) African mahogany; (d) African mesquite; (e) Opepe; (f) African oilbean…..190

Figure 6.26: Mass of char residue recovered from the reactor after the pyro-gasification of hardwoods (a) African Mahogany and (b) Opepe; in comparison to their blends¬ Opepe-African mahogany – (c) 50/50; (d) 30/70; (e) 70/30……..191

Figure 6.27: Char residue of (a) Poplar and (b) Eucalyptus chars as well as those of their blends Poplar-Eucalyptus (c) 50/50; (d) 30/70; and (e) 70/30 after pyro-gasification at 1000°C……..….192

Figure 6.28: Mass of char residue recovered for the individual IAPs and their blends……..193

Figure 6.29: Mass of char residue recovered for the individual Tropical hardwood samples and their blends……..194

Figure 6.30: (a), (b) and (c) three types of flames generated from the syngas produced in this study; (d) flame produced from syngas of Eucalyptus-Jacaranda 30/70 blend at an instantaneous gas flow rate of 1735 mL/min……195

Chapter 1

Introduction

1.1 Background

Deficiencies in energy supply in economies across Sub-Sahara Africa (SSA) create a bottleneck to development and cause severe economic, environmental and social hardship in the region despite its diverse energy resources. One such resource continually being generated in abundance in most parts of SSA is wood waste. Wood sawdust generation from lucrative sawmills operating across the region, and the mechanical control of environmentally malicious invasive alien plants (IAPs), are two scenarios that serve as major sustainable sources of wood waste in SSA.

Wood, a type of lignocellulosic biomass (LCB), has remained an age-long source of domestic and industrial fuel. The thermochemical conversion of LCBs to biofuel such as syngas is proving to be a cleaner, more sustainable alternative to fossil fuels for energy generation. Off-grid power generation fuelled with sustainably and locally supplied LCB waste resources eliminates the demerits of insecurities in energy resource supply associated with fossil fuels. It may serve as an economically benign solution to the irregular power supply particularly in remote communities if the biomass waste is generated locally and close to a gas power plant. Such a scenario also creates opportunities for socio-economic growth through job creation across the supply chain.

Syngas production from LCBs involves the direct gasification of the feedstock through a sequence of four primary stages (drying, pyrolysis, partial oxidation, and reduction) taking place at temperatures normally between 800°C and 1200°C. However, gasification of biomass at these temperatures is associated with high tar generation and low syngas yield in the product gas. High tar composition in the syngas is undesirable and has been reported to damage power plant components, poison expensive fuel cell catalysts, clog pipelines and fittings as well as diminish syngas fuel properties. Previous studies have focused on minimizing tar content in syngas through various techniques that are either largely energy-intensive or

wholly expensive. These tar cleaning methods can be broadly divided into pre-syngas production and post-syngas production tar cleaning. Tar cleaning by high-temperature tar cracking and or by use of catalysts has frequently been reported in literature.

This study explores the use of pyro-gasification as an alternative thermochemical conversion method to minimize tar as well as maximize syngas yield from wood wastes at temperatures between 900°C and 1000°C. Pyro-gasification is a hybrid process incorporating a pyrolysis and gasification phase. It involves the extraction and trapping of tar in the form of bio-oil generated in the pyrolysis phase, midway through the process. This, therefore, leaves behind a carbon-rich and tar-free char residue which can then progress to the advanced stages of the gasification process. One main advantage of the pyro-gasification reactor fabricated for this research is its capability of a dual production of bio-oil and syngas from one biomass thermochemical conversion process.

1.1.1 Power situation in Sub-Sahara Africa an opportunity for bioenergy

Energy can be referred to as the soul of any economy whether classified as developed or developing. Furthermore, a diverse utilization of a region's natural energy resources for power generation provides a recipe for rapid economic growth, security of energy supply, and improved standard of living. Though this notion supports the actualization of the Seventh Sustainable Development Goal (Affordable and Clean Energy) of the United Nations, but remains a mirage in most developing countries particularly in Sub-Sahara Africa (SSA). The growth of the economy in SSA is plagued by unending irregular power supply [1]. One important parameter used as a yardstick for development is access to uninterrupted power supply (e.g. electricity). A recent World Bank statistic for access to electricity by percentage of a region's population reveals that apart from South Africa and Gabon, every other country in the region ranked below 60% in 2017 which was amongst the lowest in the world (see Fig. 1.1). In total only just 44.6% of the total

population of Sub-Saharan Africa (majority of which are rural communities) have access to electricity [2].

Africa's fastest-growing economies (i.e. South Africa and Nigeria) [3], rely heavily on fossil fuels for power generation. South Africa has over time, relied majorly on coal power plants for electricity generation [4,5]. With these, it has attained a benchmark of 84.4% in access to electricity (by percentage of population), going by the 2017 statistics [2]. Despite this, many remote areas in the country still experience limited or zero access to power. Moreover, South Africa in 2014 generated 67.5% of CO_2 from its total fuel combusted for electricity and heat production [2]. Nigeria on its part has been unable to make such giant leaps in her power sector. In the same year reported, it barely attained a 59% benchmark in electricity accessibility (by percentage of population) which is low when compared with those of other developing countries and this has not been a major shift from its 1990 figure of 41.8% [2]. Its power generation is mainly from natural gas power plants and hydro-electric sources [6]. In 2014, Nigeria generated 39.1% of CO_2 emissions from its total fuel combusted for electricity and heat production[2]. The high CO_2 emissions generated in both countries due to their sole dependence on fossil fuels can be minimized by supporting the existing power infrastructure with renewable power generation. One of such renewable energy solutions is the use of wood wastes as feedstock for bioenergy generation. The supply of electricity which has been either inconsistent or non-existent particularly to remote and off-grid areas, may be attributed to bottlenecks in the power sector. Such bottlenecks include, inadequate generation capacity of the power plants, obsolete power infrastructure, and limitations in the initial design of the national power transmission network which supplies power mostly to major cities. Therefore, there is need to support the existing power infrastructure with remote, off-grid power plants fuelled with renewable resources such as wood waste, locally generated in abundance in these remote communities.

Given the inadequate power supply and poor access to electricity, opportunities, therefore, abound in the conversion of these abundant woody biomass wastes,

continuously being generated in the aforementioned scenarios for bioenergy production. Huge potentials could be actualized in solving the environmental issues arising from their accumulation, as well as in improving the power situation in SSA. These may be in the form of:

a. On-site synthesis gas (syngas) production from wood waste, for off-grid power generation in remote communities;

b. Socio-economic empowerment through human capital development and job creation across the supply chain of wood waste management; and

c. A decrease in droughts and other environmental catastrophes by maximizing the use of wood wastes generated in abundance from commercial sawmills rather than from wood directly sourced from the illegitimate felling of trees from natural forests. Such wood wastes may also be sourced from the authorized mechanical control of environmental threatening Invasive trees.

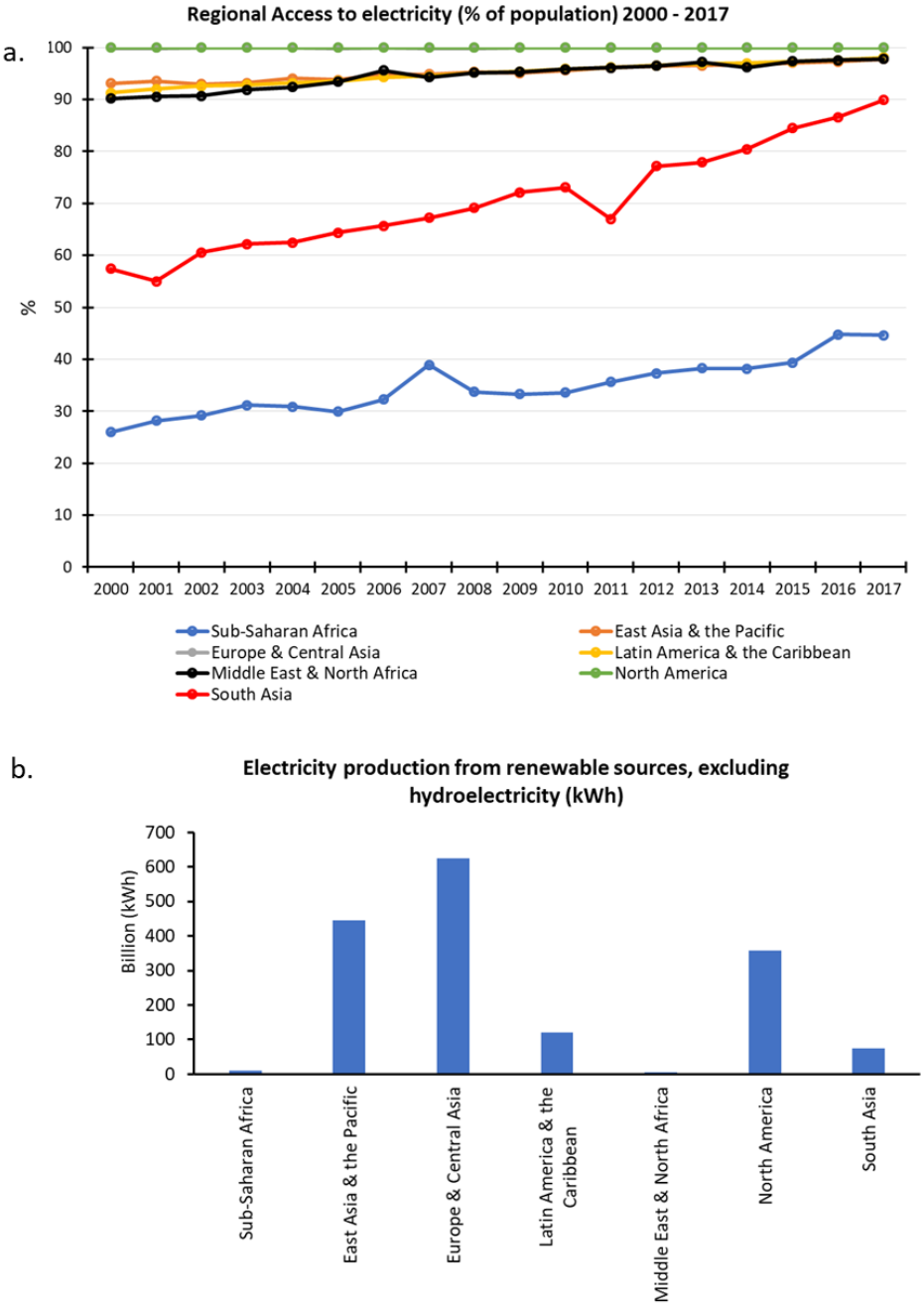


Figure 1.1: World regional data on electricity (Note: in Fig. 1.1 a, Europe & Central Asia share the same profile of 100% Access to electricity as North America and therefore is not visible on the graph). Sourced from literature [2].

This project is inspired by the urgent need to change the status quo and promote these opportunities by exploring the production of syngas from wood wastes for power production.

1.1.2 Abundance of wood waste biomass in Sub Sahara Africa

Biomass is defined as the residue of living and recently dead and decomposing organic material which can be used as fuel or production of value-added materials. Biomass can be classified into:

a. Fast-growing energy crops, grown for the sole purpose of being used as fuel, such as fast-growing trees, miscanthus or switchgrass;
b. Agricultural wastes and by-products, such as groundnut husks, corn cobs straw, sugarcane bagasse, rice hulls, palm kernel shells, etc.; and
c. Residues such as sawdust, wood chips and off-cuts from forestry, sawmilling, construction, pulp and paper and other wood related industries [7].

Globally, lignocellulosic biomass (LCB) such as wood undoubtedly remains one of the most essential and universally consumed materials for domestic and industrial activities both as fuel and timber, and its demand is unending. In Africa alone, the annual consumption of wood is estimated at 700 million m^3 [8]. Forests from which it is primarily sourced, are the most globally available and abundant sources of biomass. Hence, the preservation and sustainable exploitation of forest products is key to maintaining an equilibrium of the earth's carbon cycle.

Sub-Saharan Africa (SSA) alone boasts of about 16% of the global forest area [9]. It is home to the Congo Basin which is the second-largest forest estate after the Amazon in South America. The forest estates in SSA, spanning across different geographical and climatic zones, are blessed with an estimated 4500 – 6000 indigenous tree species [10], which sufficiently supports Africa's lucrative wood sawmilling and paper/pulp industries. Consequently, the regular activities of the sawmill industry continuously generate enormous amounts of wood waste as the consumption of sawn wood products increases (Figs. 1.2 & 1.3) [10–12].

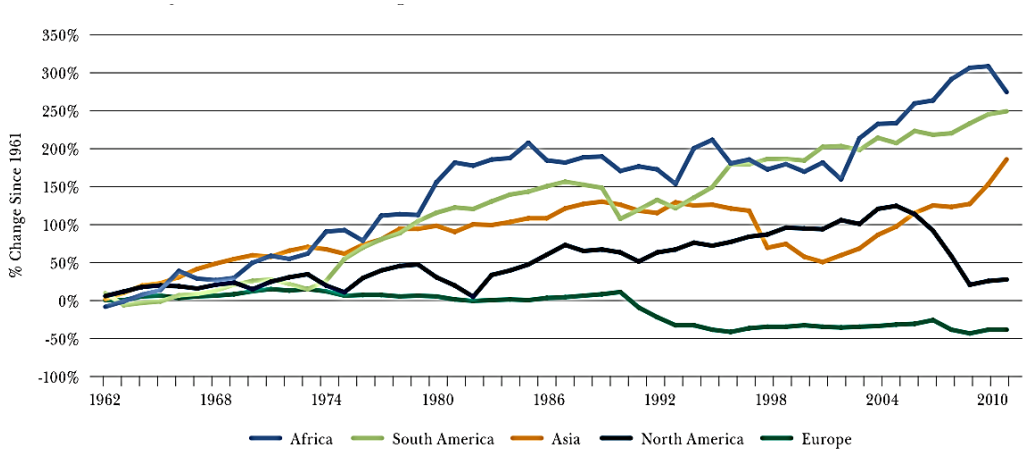


Figure 1.2: Change in global consumption of sawn wood products since 1961. Sourced from literature [10].

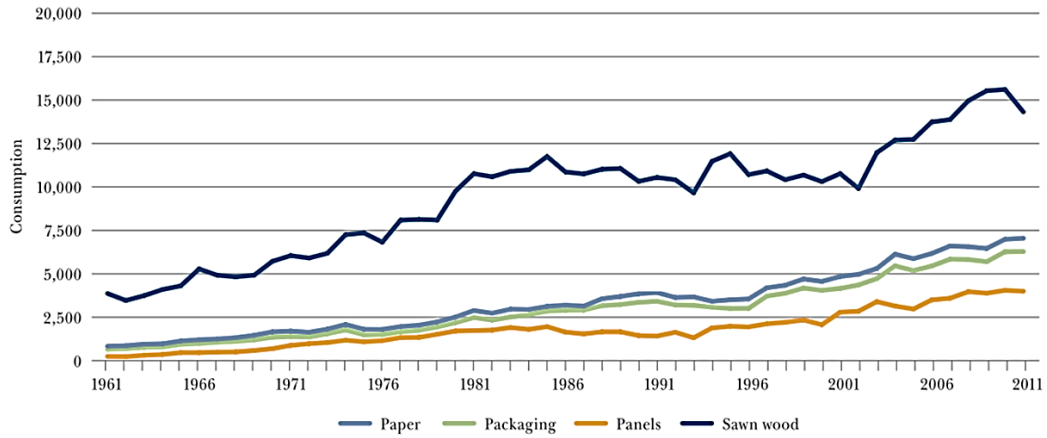


Figure 1.3: Global consumption of forest product in Africa (m^3) since 1961. Sourced from literature [10].

A trend however exists, whereby inadequate wood waste management and ineffective enforcement of environmental protection laws have posed a major setback particularly in less developed countries. Due to the huge financial implications of waste management, local small to medium-scale sawmill owners who make up the bulk of sawmill operators, indulge in either indiscriminate open-air burning or dumping of waste sawdust in unauthorized locations or by river banks [13]. This has led to respective environmental problems such as air pollution, biodegradation, and infiltration of unhealthy organic products into the soil or turbulence in nearby rivers thereby inhibiting sunlight beneficial to aquatic organisms [12,14]. A typical scenario in SSA is Nigeria's sawmill industry which

represents 93.2% of the total number of its wood-based industry and generates an estimated 1.8 million tons of sawdust annually [13]. This generated sawdust represents a fraction of 5.2 million tons of wood waste mostly incinerated or dumped in unauthorized locations (see Fig. 1.4) [12].

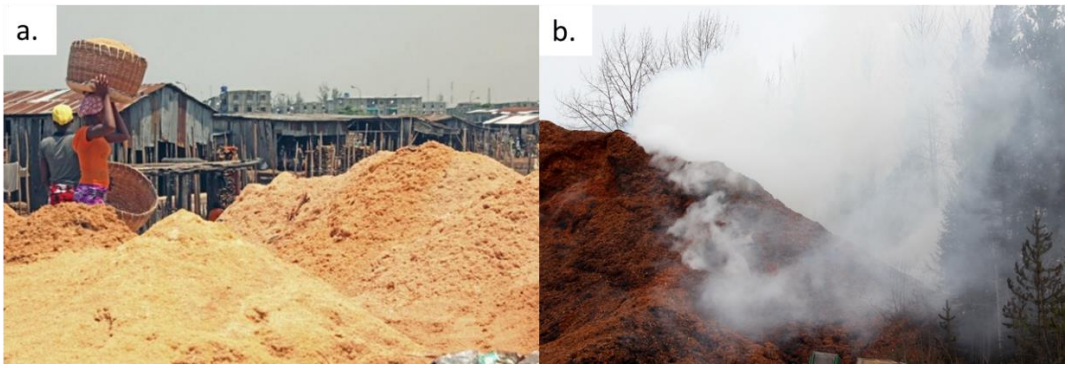


Figure 1.4: Environmental and air pollution caused by indiscriminate dumping and open-air burning of sawdust. Sourced from literature [15, 16].

Another major source of wood waste in SSA has been from the continuous control of environmentally disruptive Invasive Alien Plants (IAPs) in the southern region of SSA. South Africa in particular, is home to an estimated 750 tree and 8000 shrub IAP species introduced into the country since the mid-seventeenth century [17]. Renowned for their exceptional qualities and fast growth rate, these trees were previously cultivated for economic purposes such as for timber, fuelwood and charcoal production, aesthetics, wind barriers, soil stabilisation, and conservation. However, 161 of these and of which 68% are woody, have been classified as extremely invasive [17]. Ironically, the widespread incursion of over 10 million ha of natural forest estates by these IAPs, particularly in the wetter biomes of country, have continued to cause severe environmental and socio-economic problems that undermine the initial purpose of their introduction. Their unique rapid growth rate, ability to quickly invade natural habitats and disrupt the existing ecosystem has led to impacts such as:

a. Massive decrease in surface water flow and groundwater level estimated at 3 million m^3/yr, leading to intense droughts in affected regions;

b. Increasing forest wildfires leading to loss of lives and property, coupled with increased fire protection costs;

c. Increase in soil erosion as an aftermath of wildfires;

d. Alterations of soil nutrients caused by competing IAPs and indigenous plants;

e. Loss of natural habitat of native animals; and

f. Loss of productive agricultural lands and poisoning of grazing animals [17].

In a bid to control or eradicate these invasive species, the South African government had over the past 15 years, reportedly invested more than 3.2 billion rands (US$457 million) through its 'Working for Water' (WfW) programme, established primarily for this purpose [18]. Regulations were also set up to control the importation, sales, and planting of seeds of IAPs. However, these efforts to date, have remained insufficient in combating the spread of invasive species since their seeds are mostly dispersed by birds and wind [19]. This has prompted the Department of Environmental Affairs (DEA) under the policy framework of the National Environmental Management: Biodiversity Act (NEM: BA) No. 10 of 2004 [10], to adopt direct and intensive field control measures to curb the spread of these IAPs in the affected regions. The most common and effective of these control measures is the mechanical "slash and dump" which generates massive amounts of woody biomass wastes. Other common practices include the chemical method such as the use of herbicides and biological methods which employs a "pest-attack" technique to curb their growth [18,20]. In South Africa, it is estimated that over 165 million tonnes of woody biomass wastes from IAPs are obtainable within 44 million hectares of invaded land, which amounts to 36% of its total land area [21]. Unfortunately, due to their low economic value, the bulk of these wood wastes generated during felling operations are often left to rot on site and when exposed to drying under the thriving dry weather conditions, cause wildfire outbreaks [22].



Figure 1.5: IAP wood waste left on-site during a "slash and dump" mechanical control. Sourced from literature [23,24].

In recent years, there has been an increased global interest in harnessing these woody biomass wastes for energy production which has consequently increased the global trade of pellets [9]. South Africa is rated the highest consumer of wood bioenergy in Africa which makes it an ideal location for this research [25]. Moreover, like most other SSA countries it is yet to attain its full potentials in wood bioenergy production despite its success in wood pellets export mostly to Asia [9]. According to Bildirici & Ozaksoy [25], this potential is approximately above 1000 times its current level and would create opportunities in waste reduction, job creation, and meeting climate change policy obligations if fully exploited.

1.1.3 Sustainability of wood waste supply for bioenergy

Justifying the use of sawdust from sawmills and IAPs as the preferred feedstock to traditional bulk wood or wood pellets is vital to the economic significance of this research. The motivation behind harnessing sawdust as feedstock is its availability

as a waste product of sawmilling, which is a well-established and age-long industry that has created a niche for itself in supporting both developing and advanced economies.

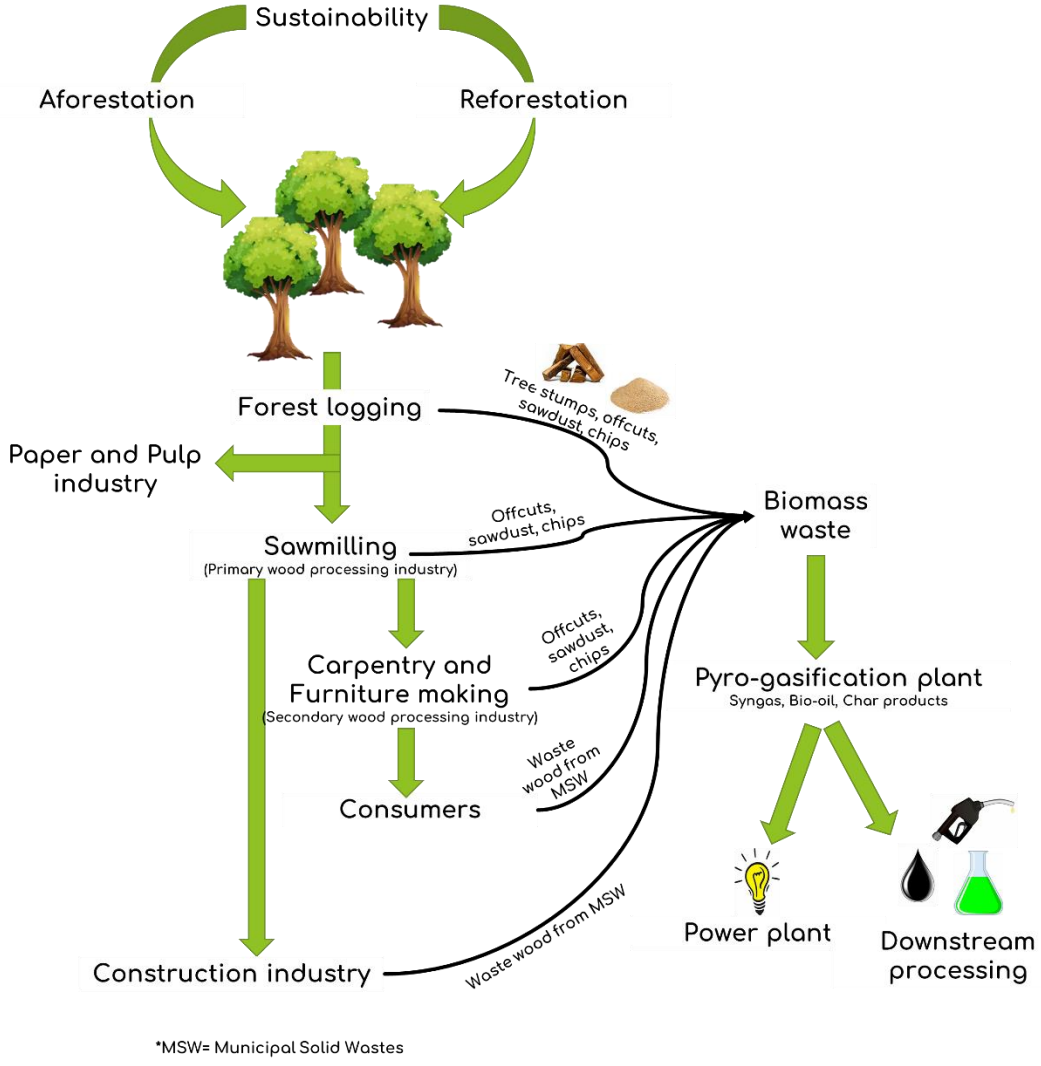


Figure 1.6: Sustainable sources of wood waste for bioenergy.

The wood industry products and by-products trade cuts across local and international markets and will continue to grow as global demand increases and regional shortages exist especially in the European Union (EU) and Asia (see Figs. 1.2 and 1.3) [7,26]. Most importantly, the raw material used – timber, if continually being sourced from well-managed forest plantations would ensure its sustainable and regular supply for sawmilling. These plantations in Africa cover a total area of 8,036,000 ha (4.3% of the total plantation area worldwide) of which 3,392,000 ha

were for industrial purposes as reported in 2000 by the Food and Agriculture Organisation (FAO) [27]. During this period the rate of tree planting was estimated at 194, 000 ha yr^{-1}. However, Africa's total plantation area and the rate of planting remain the lowest, globally. This justifies the need for a sustainable and efficient conversion of sawdust waste for energy generation to prevent the exploitation of the limited forest resources in the region.

Wood industry wastes have been categorized into avoidable and unavoidable [28]. The former constitutes those wood off-cuts generated during logging and milling due to poor working conditions of sawing equipment and/or inefficient cutting techniques by personnel which could be improved on to minimize waste. The latter, however, includes wastes like sawdust, chips, and shavings which are inevitable during milling and not subject to any improvements in milling efficiency and technique [28]. Interestingly, wood shavings are found to be more suitable for livestock bedding than sawdust due to ease of bacteria growth on the latter [29]. This discourages the use of sawdust for livestock farming and hence strengthens its availability as feedstock for bioenergy. Therefore, the supply of sawdust waste as feedstock in commercial quantities for power generation is sustainable.

In addition to sawdust from sawmills, sawdust from IAPs sourced in South Africa could also play a significant role in power generation. According to a "feasibility study of harvesting invasive alien plant species for energy" published in 2014 [30], there were commercially viable potentials in harnessing IAPs for off-grid power generation, particularly in remote areas. As described in one of the seven scenarios modelled, a partnership would be formed between energy companies and a National Resource Management (NRM) programme such as the WfW. The study and scenario modelling were conducted within a 50 km radius to a central power plant in the Nelson Mandela Metropolitan Municipality. The results revealed that if the WfW could bear the financial responsibility of harvesting and extraction of the IAPs (including a 60-day drying period of the biomass in-field); while the energy companies bore the cost of transportation and milling of the wood wastes to sawdust, the resultant unit cost of energy (including harvesting,

transportation, processing and externality costs) could be estimated between 24.8 to 28.7 ZAR/GJ. This would be much lower than that of coal power generation estimated at 49.0 ZAR/GJ (externality costs inclusive) [30]. Additionally, such a venture would lead to (a) a reduction in both the externalities caused by coal power generation and their impact include on the environment; (b) a reduction in invasions by IAPs and restoration of invaded ecosystems; (c) a contribution to the positives of clearing IAPs with cost reductions in fire control and loss of infrastructure as a result of wildfires; (d) job creation and economic empowerment [30].

1.1.4 Conventional thermochemical conversion of wood and their limitations

Inspired by an increased global call for cleaner, more sustainable energy supplies and improved efficiency in natural resource utilization and management, research particularly in the area of biomass waste beneficiation for energy production has been intensified. Gasification, pyrolysis, liquefaction, and combustion are four key thermochemical technologies traditionally employed for the conversion of low-grade carbonaceous materials such as wood wastes into useful energy. Gasification, pyrolysis, and liquefaction convert these carbonaceous materials into more useful, versatile fuels and chemical feedstock convenient for wide range applications. Meanwhile, combustion is mostly confined to the production of steam from the oxidation of such materials for heat and power generation. While combustion remains the most commercially deployed of the four technologies globally [31], most combustion plants operate at low efficiencies and are associated with many maintenance and technical issues which include slagging in the gasifier and high ash build-up [32, 33]. Moreover, the oxidation of the carbonaceous material to release its energy during combustion, produce very harmful and undesirable gaseous products with no useful energy value in such gases. This is contrary to the more environmentally benign pyrolysis, gasification and liquefaction processes which through a series of chemical reactions, transform the energy stored in biomass into clean liquid, solid and gaseous energy carriers suitable for downstream applications. These energy carriers can be utilized for heat and power

generation or further downstream conversion into transport fuels and chemicals [34,31].

Biomass pyrolysis can be defined as the low to medium temperature thermochemical breakdown of biomass structural components (cellulose, hemicellulose, and lignin) in an inert or low-oxygen atmosphere to form three major products – char (biochar), bio-oil (pyrolysis oil) and a mixture of combustible gases. Similar to pyrolysis is liquefaction, whereby biomass is treated in a solvent and pressurized to high values of up to 200 atm in the presence of a catalyst at low-temperature environments to also produce bio-oil [35,36]. Meanwhile, gasification enables the production of syngas from biomass at higher temperatures and in a sufficiently oxidized atmosphere.

However, inasmuch as biomass gasification is environmentally benign, the wide variations in biomass chemical and physical properties make their gasification process and end products unpredictable. Differences in wood species, soil type and climatic conditions of geographical locations where the wood is harvested, can result in differences in their chemical properties and also translate to variations in their fuel properties. This in-turn can yield unpredictable results that directly affect their use as feedstock for thermochemical conversion processes. Meanwhile, variations in the structural properties of different wood species can directly affect the reaction kinetics of the thermochemical process as well as the type and quality of the final biofuel product.

Moreover, undesirable compounds can be formed during biomass thermochemical conversion processes. NO_x and SO_x compounds can be formed from the oxidation of nitrogen and sulfur elements present in the wood feedstock. These gaseous compounds if released and absorbed into the atmospheric water-cycle can be hazardous to the surrounding air, soil, and water. Most significantly, however, is the generation of syngas with undesirable high amounts of tar which is common with wood gasification. As discussed in detail in Sect. 2.4 of this thesis, syngas with high tar composition is largely unsuitable for downstream application

such as in liquid biofuel production and use as gaseous fuel in power plants and fuel cells. Moreover, various tar cleaning methods have been investigated by researchers, some of which may have exhibited good tar cleaning capabilities but at the expense of high energy input.

During a biomass gasification process, the biomass pyrolysis phase is most critical because it forms the primary products (tar, char, and gas) which determine the quality of the final syngas product. The amount of tar and char formed in this early phase is largely dependent on the structural composition (cellulose, hemicellulose, and lignin) of the biomass feedstock. These components when decomposed are responsible for the release of tar-forming volatiles and char residue. Tar present in the reactor at the advanced stages of the gasification process form part of the final syngas product, if not 'cracked' at very high temperatures above 1200 °C. Therefore, high-temperature tar cracking during gasification or subjecting the syngas produced to a secondary tar-cleaning process after gasification is common practice. High-temperature tar cracking is however an energy-intensive and expensive process as it involves endothermic reactions that require an external heat supply of very high temperatures. Likewise, secondary tar cleaning is expensive as it requires the installation and maintenance of additional hot or cold syngas cleaning units as would be discussed in Sect. 2.4.1.

The two basic grey areas of biomass use for bioenergy are in: (a) The need to improve on the existing knowledge of biomass properties and composition as it pertains its use as feedstock for specific conversion processes; (b) The need to apply this knowledge for the development of advanced and more sustainable use of biomass as feedstock for bioenergy [37]. As part of this research, therefore, a modified gasification method called pyro-gasification was employed as an alternative to the traditional gasification process for the production of syngas from the biomass wood wastes. Pyro-gasification is a hybrid of pyrolysis and gasification with the capability of extracting the tar in form of bio-oil, from the reactor at the point of its volatilization during the biomass decomposition phase of the process, before the production of syngas in the char gasification phase. The aim is to

prevent the progression of tar alongside char into the gasification phase. To realize this, a bench-scale pyro-gasification reactor was fabricated and used for the thermochemical conversion of sawdust of the wood wastes to syngas.

To ascertain their suitability as feedstock for syngas production via pyro-gasification, eight wood waste samples sourced from the sawmill industry in Nigeria and from the IAP control programme in South Africa were characterised for their fuel properties. Each sample was pyro-gasified during this study and a measurement/calculation of the concentration, rate of production and yields of the syngas and its components (CO and H_2) in the product gas was conducted. Furthermore, samples with low syngas yields were blended with those of higher syngas yields in three sawdust mix ratios of 30/70; 50/50; and 70/30, to ascertain any changes in syngas production. The volume of bio-oil recovered from each run was also measured. Other observations made in the course of the pyro-gasification conversion process such as flame ignition, flame colour, and flame combustion propensity, have also been discussed in this report.

1.2 Research questions, aim, and objectives

Against the aforementioned background, this research aimed to explore the use of pyro-gasification for syngas production from wood wastes generated in two distinct SSA regions. These include those sourced from four tropical wood species commonly processed in commercial sawmills across West and Central Africa, as well as those sourced from four category 1 and 2 invasive alien trees being controlled in Southern Africa. The tropical commercial species harvested include the following – African mahogany, African mesquite, African oil bean, and Opepe. Meanwhile, the Southern African invasive alien tree species include the – Eucalyptus, Bugweed, Poplar, and Jacaranda.

1.2.1 Research questions

This research was intended to provide answers to the following questions:

a. *Due to variations in chemical and structural properties common with biomass materials which affect their fuel properties, how suitable are these wood*

species for pyro-gasification? It is common knowledge that LCBs are characterized by variations in their proximate and ultimate properties. These properties greatly affect the thermochemical reaction kinetics, yield, and quality of the final biofuel products.

However, there is limited data on their chemical and structural properties as well as their fuel properties as they affect feedstock suitability for pyro-gasification. Moreover, research reveals that in most cases, where some of these wood species have been characterized in literature, there are still wide variations in the properties of wood samples of the same species of tree, but grown in different regions due to contrasts in the climatic and geological/soil conditions of the regions [38,39]. Therefore, available published data on wood samples similar to those used for this project may not be completely relied upon in conducting this research.

Moreover, with the extraction of tar during the pyrolysis phase of the pyro-gasification process, char residue is left behind for reduction reactions to take place. It, therefore, becomes increasingly important to identify those wood samples which exhibit good char reactivity and yield to maximize syngas production at gasification temperatures. Therefore, samples exhibiting high char yield with low to medium char reactivity (or rates of decomposition) may be blended with those which do not exhibit such characteristics. However, these may not necessarily determine the final syngas yield and those of its components – hydrogen and carbon monoxide. This is due to the additional influence of other parameters such as temperature, steam to biomass (S/B) ratio and heating rate on the gasification phase reactions

b. *What are the thermo-decomposition and kinetic behaviors of the wood samples when subjected to thermal treatment at different temperatures?* The Thermogravimetric analysis (TGA) helps in ascertaining the ideal operating conditions for optimum biofuel production such as pyrolysis and gasification temperatures, and heating rate, as they affect the rate of thermal

decomposition of the wood material. Moreover, determining the thermal decomposition kinetic parameter such as the activation energy (E_a) of the wood to be used as feedstock for a thermochemical conversion process is vital to the design, operation, and economics of the entire process. Besides, a study of the peak rates of thermal decomposition and thermogram patterns of the various wood samples at different stages of the process gives an idea of the feedstock residence time and yield of the biofuel product to be expected at each stage. It also aids in predicting the temperatures at which the pyrolysis and gasification phases commence. Hence there is a need to conduct a Thermogravimetric Analysis (TGA) and understand the reaction kinetics of the individual wood samples before use for pyro-gasification.

c. *What differences in the production rate and yield of syngas (and those of its components H_2 and CO) can be observed from the pyro-gasification of the individual wood samples and that of their associated blends?* Providing solutions to questions 1 & 2 serves as a prerequisite to ascertaining the differences in the production rate and yield of syngas obtainable from each wood sample and their blends when pyro-gasified under the same conditions. Moreover, it is important to test the functionality of the pyro-gasification process and ascertain the volume of tar obtainable from each wood sample.

d. *What is the importance of the outcome of this research to stakeholders?* Several studies on the environmental impacts, control, and feasibility of utilizing these wastes as feedstock for bioenergy and other value-added products – particularly from a socio-economic stand-point have been reported [12,25,46,47,28,30,40–45]. However, experimental data on the fuel properties and syngas yields which highlight the suitability or limitations of these wood species for biofuel production need to be made available to industry stakeholders. Moreover, the viability of pyro-gasification as an alternative to other traditional tar removal processes is of utmost importance to this research. Knowledge of the actual experimental pyro-gasification of wood

wastes sourced from IAPs and commercial woods is needed to promote and fast-track their implementation for bioenergy production.

1.2.2 Research aim

This research was aimed at investigating the syngas production from the pyro-gasification of individual and blended sawdust samples sourced from invasive alien trees in South Africa and tropical trees in Nigeria using a fabricated bench-scale pyro-gasification rig.

1.2.3 Research objectives

Below were the investigated objectives that addressed the above-listed research questions:

a. To assess the proximate, ultimate and fuel properties of the wood samples for suitability as feedstock for thermochemical conversion.

b. To examine the thermogravimetric performance, derivative thermogravimetry (DTG) and derive the kinetic parameter of the individual wood samples.

c. To identify the gasification phase temperatures for optimum H_2, CO and Syngas yields as well as the volume of bio-oil extracted during pyro-gasification of sawdust of individual wood samples under selected gasifier parameters.

d. To examine variations in H_2, CO, and syngas rate of production and yield from pyro-gasification of individual samples and their associated blends in mix ratios of 30/70, 50/50 and 70/30.

1.3 Report outline

This report has been divided into seven chapters, namely:

a. *Chapter 1 (Introduction)*: In this chapter the project's background, statement of problem/research questions, research aim and objectives, and scope of work have been presented;

b. *Chapter 2 (Literature Review):* This chapter, reviews available literature discussing the beneficiation of lignocellulosic biomass via traditional pyrolysis and gasification processes. It also highlights existing tar removal methods in biomass gasification and introduces pyro-gasification and its working principles.

c. *Chapter 3 (Materials and Methods):* In this chapter, all materials and equipment used as well as methods adopted in the course of carrying out the activities of this research will be presented. Also, the fabrication of the pyro-gasification rig and its working principles will be discussed in detail.

d. *Chapter 4 (Fuel examination of Invasive Alien Plants and Tropical hardwoods as feedstock in pyro-gasification):* This chapter presents all the characterizations conducted on the wood samples. In addition, a fuel quality evaluation of the samples using data collated from their characterizations will be carried out to rank the suitability of each sample as feedstock for pyro-gasification based on six feedstock evaluators.

e. *Chapter 5 (Thermogravimetric Analysis and Kinetic study):* In this chapter, a thermogravimetric analysis and kinetic study of each sample when treated thermally in inert conditions will be conducted and the data collated will be presented and discussed.

f. *Chapter 6 (Pyro-gasification of wood samples):* The data such as the concentration, rate of production, and yield of the syngas produced from the individual samples as well as from their associated blends have been presented and discussed in this chapter. Also, observations made on their flame properties when the gases produced were ignited were also highlighted.

g. *Chapter 7 (Conclusion and Recommendation):* This chapter concludes the project and makes recommendations for further studies.

1.4 Scope of work

The core of this research is centred on two studies: (a) developing a lab-scale pyro-gasification concept with a tar removal capability in the conversion of wood sawdust to syngas and; (b) exploring the blending sawdust of different wood species for syngas production.

As depicted in Fig. 1.7, the Work Breakdown Structure (WBS) of the entire research project is subdivided into six main stages namely: Literature review, Sample sourcing, and preparation, Characterization, Thermogravimetric Analysis, Fabrication of the pyro-gasification rig and the Pyro-gasification of the wood samples. Also depicted in Fig. 1.7 are highlights of the activities conducted in each stage.

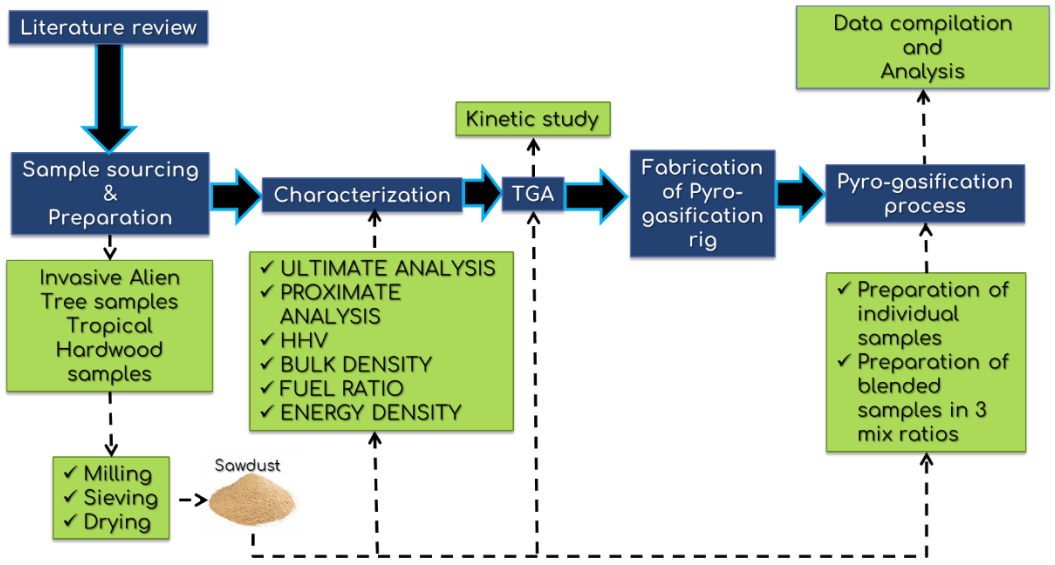


Figure 1.7: Work Breakdown Structure (WBS) of this research project.

The activities carried out throughout the period of this research as depicted on the WBS diagram are briefly described below:

a. Literature review

This first stage involved a study of existing literature discussing previous research on conventional pyrolysis and gasification of biomass as well as issues particularly relating to tar generation in conventional biomass gasification. This also included

a review of existing tar cleaning methods. Several studies on the blending of biomass feedstock for thermochemical conversion were also covered to identify any gaps in knowledge.

b. Sample sourcing and Preparation

After extensive research and consultations with experts in the forestry industry, both in Nigeria and South Africa, an identification and sourcing of the wood samples used for this research was conducted. The tropical wood samples were harvested from the Enugu State forest reserves in Nigeria and sawn into sizeable chunks for transportation to South Africa. Meanwhile, the Invasive Tree species were harvested locally from a densely invaded forest in Johannesburg, by the help of experts at Servest Pty. Limited. The samples were dried and milled to sawdust and sieved at the laboratories of the School of Chemical and Metallurgical Engineering, University of the Witwatersrand.

c. Characterization

A series of tests were conducted on the wood samples to ascertain their fuel properties and suitability as feedstock for pyro-gasification. The tests include – Ultimate analysis, Proximate analysis, determination of Higher Heating Value (HHV), Bulk density, Fuel ratio, and Energy density. Also, a pyro-gasification feedstock evaluation was conducted on each sample.

d. Thermogravimetric Analysis

To ascertain and compare their thermo-decomposition behaviours and thermal stability, a Thermogravimetric Analysis (TGA) and Derivative Thermogravimetry (DTG) of the individual wood samples was conducted. These were conducted in an inert atmosphere at a constant heating rate. Their thermograms were also analysed to gain important information about their rates of volatilization decomposition, char yields, char rates of decomposition and final decomposition temperatures in both inert and oxidizing atmospheres. Also, calculations to derive the activation energy of each sample was conducted at this stage.

e. Fabrication of the Pyro-gasification rig

This represented an important part of this research. A bench-scale Pyro-gasification concept was developed for the production of a tar-free syngas from wood. The rig was fabricated with the help of the workshop technicians. After a series of test runs were conducted, several modifications to the original concept were made to resolve the technical issues detected.

Chapter 2

Literature Review

2.1 Introduction

In this chapter, a comprehensive and critical review of the fuel properties of woods or lignocellulosic biomass (LCB) relating to their suitability for thermochemical conversion is presented. Furthermore, previous studies reported on the blending of biomass feedstock for thermochemical conversion processes were critically reviewed and contrast. To describe biomass pyro-gasification and its relevance, an overview of biomass pyrolysis and gasification was carried out. This also includes the issue of tar generation during biomass gasification and existing tar cleaning methods employed during syngas production. Other published literature highlighting pilot studies where pyro-gasification has been employed, were also reviewed and documented in this chapter.

2.2 Lignocellulosic Biomass (LCB)

Biomass can be defined as any organic material produced as waste by living organisms or sourced from a recently decaying organism, which is capable of being utilized as feedstock for bioenergy production [48]. Lignocellulosic biomass is a versatile carbonaceous type of biomass material which is primarily made up of three structural components namely – Hemicellulose, Cellulose, and Lignin. They provide bioenergy when used directly as fuel or as feedstock for both thermochemical and biochemical conversion processes. They provide an environmentally benign alternative to coal combustion and can also be blended with coal when carbonized or torrefied, to cut down on emissions. The properties of LCBs such as their structural, elemental and proximate compositions as well as their fuel properties such as heating value, energy density, and fuel ratios, are however widely variable due to the following reasons:

a. The biomass type, and in the case of plant biomass, the specie, and part of plant;

b. The factors affecting the growth of the plant biomass such as sunlight intensity, geographical factors, and climate of the location, the particular season of growth, proximity to the sea (i.e. salt water) or a polluted area, etc.

c. The plant's age before its harvesting and use as feedstock;

d. The type and concentration of soil improvement additive used, such as fertilizers;

e. Presence of major sources of pollution such as coal power plants, factories, and locations with high carbon footprints (e.g. densely populated cities);

f. Storage, handling and pre-processing conditions of the biomass, whereby they are likely to come in contact with impurities [49 (and references therein)].

The relative composition of its structural components determines the suitability of an LCB as feedstock for either thermochemical or biochemical conversion processes [50].

2.2.1 Structural composition of LCB

As previously highlighted, LCBs such as wood are generally comprised of hemicellulose and cellulose, which are collectively known as *holocellulose*, and are tightly bound together by another structural component called lignin. The proportions of each of these components relative to each other in the LCB is one important factor considered in the selection of suitable feedstock for conversion to biofuel [50].

Hemicellulose is an amorphous organic polymer consisting of water-soluble, branched six-carbon (mannose, galactose, glucose, and 4-O-methyl-d-glucuronic acid) and five-carbon (arabinose and xylose) monosaccharides [51]. These branches are easily detachable from the main stem of its chain and decomposed to volatiles when exposed to thermal treatment at low to medium temperatures. Their amorphous nature makes them readily extractable by hydrothermal treatment and hydrolysis, as they are also easily dissolved in hot water [52].

Unlike hemicellulose, cellulose is crystalline, comprising of long, straight-chain polymers with no branches, thus making them more resistant to thermal decomposition and less soluble in hot water than hemicellulose. It is the core structural component of an LCB material and makes up most of a tree's cell wall[53].

Meanwhile, lignin which serves as a binding material is a complex structural component exhibiting high molecular-weight and made up of polymers of phenolic monomers with no sugar present. It provides mechanical strength and contributes to wood hydrophobicity, resistance to pest and microbial attack as well as supports tree growth [54,55]. It is the most thermally resistant of the three structural components and exhibits plasticity when thermally treated at elevated temperature. This state is however reversed as it hardens when cooled. Due to its lower rate of oxidation, woods with high lignin composition generally exhibit higher calorific values [56,57].

LCBs also contain an important non-structural component know as *extractives*. These are vital components of trees, largely responsible for preventing them from attacks by insects and biotic organisms. It also contributes to the physical attributes of LCBs such as colour, scent, and hydrophobicity in addition to acting as energy storages [35,58]. Extractives are also known to have a positive influence on the HHV of wood [59,60], and in most trees are known to contain carbon-rich triterpenes which augment the total carbon composition [61].

Generally, a dry woody LCB comprises of approximately 40–60% cellulose, 20–40% hemicellulose, 10–25% lignin, extractives of about 1–10%, as well as negligible amounts of inorganic minerals [62–64]. As have been observed in literature, these compositions may vary significantly depending on the type of wood (hardwood or softwood), the specie of tree, the part of the tree, as well as variations in geographical conditions where the tree is grown [39,50,65].

Hardwoods and softwoods exhibit very distinct proportions of these three components which serve as a contributing factor to the variations in their biofuel products as shown in Table 2.1.

Table 2.1: *Structural compositions of softwoods and hardwoods* [53].

Component	Softwood (%)	Hardwood (%)
Cellulose	40-50	40-50
Hemicellulose	20-30	25-35
Lignin	25-35	15-25
Extractives	1-5	1-15

Different parts of the same tree are also reported to exhibit variations in the proportions of these structural components [66]. This may also explain the higher calorific values exhibited by trunks as cited in a recent study [39], evaluating the calorific values of trunks and branches of 11 tropical tree species (see Table 2.2).

Table 2.2: *Higher heating values of branches and trunks of hardwood samples* [39].

Botanic name of Tree	Gross Heating Value (MJ/kg)	
	Branch	Trunk
Lophira lanceolata	18.70	20.72
Pentaclethra macrophylla	18.80	20.10
Brachistigia eurycoma	18.92	20.92
Prosopis africana	18.94	22.41
Erythophleum suaveolens	18.95	20.83
Dialium guinensis	19.43	20.20
Albizie ferruginea	19.60	20.81
Morinda lucida	19.62	19.82
Tectonia grandis	20.30	19.75
Nauclea diderichii	21.20	21.44
Afzelia africana	21.40	20.80

2.2.2 Thermal behaviors of structural components of LCBs

Lignocellulosic biomass is described as exhibiting sequential thermal decomposition patterns, particularly at low heating rates. This involves the initial expulsion of moisture followed by an early decomposition of hemicellulose, a rapid breakdown of cellulose and a subtler lignin decomposition [67]. Such sequential decomposition patterns can be attributed to the differences in their thermal resistance and structures as earlier described.

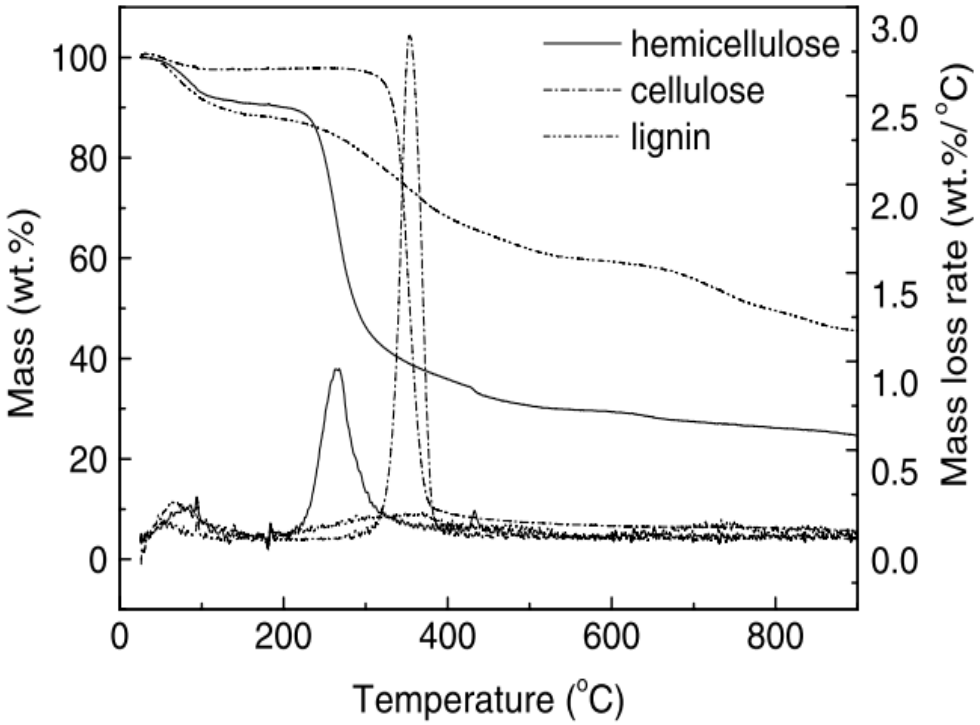


Figure 2.1: Thermal decomposition behaviors of the biomass structural components. Sourced from literature [65].

When subjected to thermal decomposition, the hemicellulose and cellulose thermograms were observed to attain peaks in mass loss rate in the active pyrolysis stage, while that of lignin with no significant peak in mass loss rate spreads across both the active and passive pyrolysis stages [68,69]. Instances of such behavior reported in literature are depicted in the pyrolysis plots of the three components as shown in Figures 2.1 and 2.2.

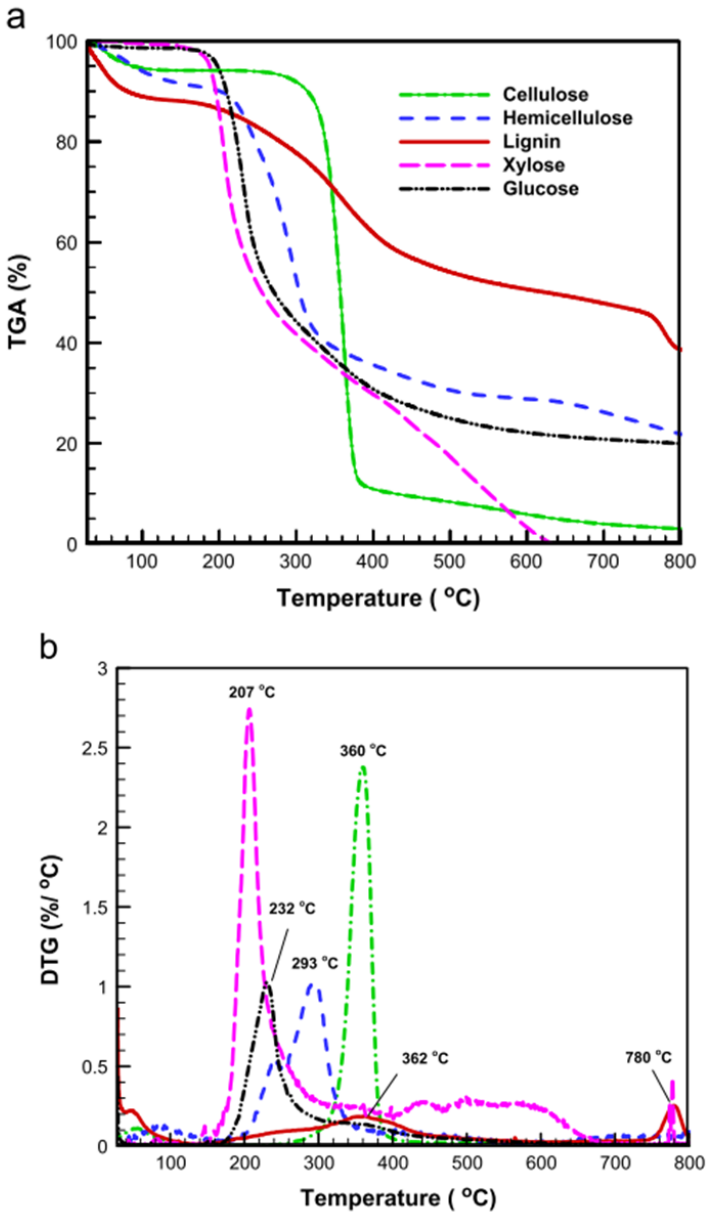


Figure 2.2: (a) Thermogravimetric (TG) and (b) Derivative thermogravimetry (DTG) thermograms of standard samples of cellulose, hemicellulose, and lignin. Sourced from literature [62].

Figure 2.2 depicts the TGA and DTG thermograms of standard samples of cellulose (Alfa Aesar, A17730), hemicellulose (SIGMA, X-4252), lignin (Tokyo Chemical Industrial Co., L0045), xylose (SIGMA, X-1500), and glucose (Panreac Quimica SA, 131341) [62]. Typical of hemicellulose which is the most reactive of the three components, decomposition below 200°C is gradual (basically due to moisture

expulsion and early pyrolysis), leading to an eventual rapid decrease in weight between 220 and 315^{o}C due to the expulsion of volatiles. This is succeeded by a final gradual decomposition to approximately 23% of its original weight up to 1000°C.

Due to its crystalline nature as previously mentioned, cellulose exhibits greater thermal stability than hemicellulose at temperatures below 300°C but rapidly degrades completely within a narrow temperature range of around 300–400°C, which is a behavior characteristic of linear polymers [66]. A practical explanation of this behaviour is the rapid ignition and burnout of dry paper which is largely made of cellulose material when exposed to high ambient temperatures in the presence of oxygen.

Lignin, in contrast, is observed to retain the largest fraction of its original weight (>40 %) after a gradual but steady decomposition process, which reflects its high thermal stability. Lignin is observed to exhibit no peaks on its thermogram, indicating its low volatility during its thermal decomposition. This is in contrast to the presence of early peaks exhibited by hemicellulose and later on by cellulose reiterating their capability to ignite at low temperatures.

The thermal stability of lignin is also evident in the thermal resistance of tree barks to heat as observed in a recent study [70]. The outer barks of trees contain the highest lignin composition than any other part. This explains the low thermal conductivity of tree barks when exposed to high forest fires. This property of tree barks delays the carbonization of the inner layers of tree trunks when exposed to forest fires by delaying the transfer of heat into its inner particles through its well-insulated pores made possible by the presence of lignin. Softwoods in contrast to hardwoods, possess thicker barks which tends to limit their rate of carbonization when exposed to high ambient temperatures and thus are most likely to survive forest fires.

As discussed in subsection 2.2.3, the contrast in the thermogravimetric behaviors of the three structural components directly affects the type and yield of the biofuel produced from wood at different stages of pyrolysis and gasification processes.

2.2.3 Contribution of biomass structural components on biofuel type and yield

Apart from describing the thermal decomposition of the individual components, the contributions of the products expelled in the course of their decomposition, which make up the three biofuels (bio-oil, char, and syngas) produced, can be predicted from their thermogravimetry conducted in previous studies. Variations in the yield of these individual biofuels can also be achieved depending on the composition of each structural component relative to each other in the lignocellulosic biomass feedstock. Other factors that affect such variation include operating parameters such as temperature, pressure, resident time, and heating rate.

In the course of a thermochemical reaction, the decomposition of the three components occurring at different rates and temperature ranges makes the whole process of lignocellulosic biomass thermal conversion complex [66]. However, by studying there individual thermograms (see Fig. 2.3), it is observed that the temperature milestones attained by the peak rates of decomposition of each component corroborate the ranges at which char, bio-oil, and syngas are produced in an actual wood pyrolysis or gasification process. The pyrolysis phase from which char and bio-oil is produced takes place approximately between the temperature range of 350 – 550°C [71], coinciding with the peak decomposition temperatures of hemicellulose and cellulose. Meanwhile, with the aid of a gasifying agent in the presence of char, syngas production coincides with the temperatures at which lignin decomposition progresses above 550°C.

The rapid decomposition of cellulose to about 10% of its original weight between 315 and 400°C [62] and the more gradual decomposition of hemicellulose to approximately 40% of its original weight from 200–350°C (as shown in Fig. 2.2a), indicate their greater contribution to the production of condensable tars which

make up the bio-oil formed in the active pyrolysis stage. On the contrary, lignin contributes the most to char residue formed after the decomposition of cellulose and hemicellulose, considering that at least >60% of its original weight remains intact beyond the pyrolysis temperature of 400°C. Meanwhile, syngas production becomes prevalent with the decomposition of the char (made up of lignin) at higher temperatures. However, according to previous studies highlighted below, the hemicellulose (alongside lignin), has also been described to be part of the char residue formed. This is due to a significant fraction of its original weight also remaining after pyrolysis has taken place.

Anukam *et al.* [72] report that higher proportions of cellulose in a biomass feedstock increases both gasification rate, gas and tar yields. They also likened the thermal reaction kinetics of hemicellulose to that of cellulose. However, several corroborating and contradicting conclusions have been drawn from various studies as it pertains the contribution of each component to individual biofuels produced.

Branca *et al.* [73] in their study, agreed that bio-oil/tar production was mainly a function of cellulose and hemicellulose decomposition. They, however, described lignin as a major contributor to char formation and its decomposition as the main contributing factor to syngas production – with less emphasis on hemicellulose. Søren & Birk [74] also reiterated this fact by describing a competition between bio-oil formation and char formation during pyrolysis which is triggered by cellulose/hemicellulose and lignin decomposition respectively. In their description, the bio-oil formation becomes more prevalent than char formation during the decomposition of cellulose and hemicellulose (expelling volatiles) at lower temperatures. Char, therefore, is formed as a residue after the expulsion of volatiles resulting from the decomposition of cellulose and hemicellulose. Meanwhile, gas generation was observed to thrive more at higher temperatures (gasification temperatures) due to the increased rate of lignin decomposition at higher temperatures.

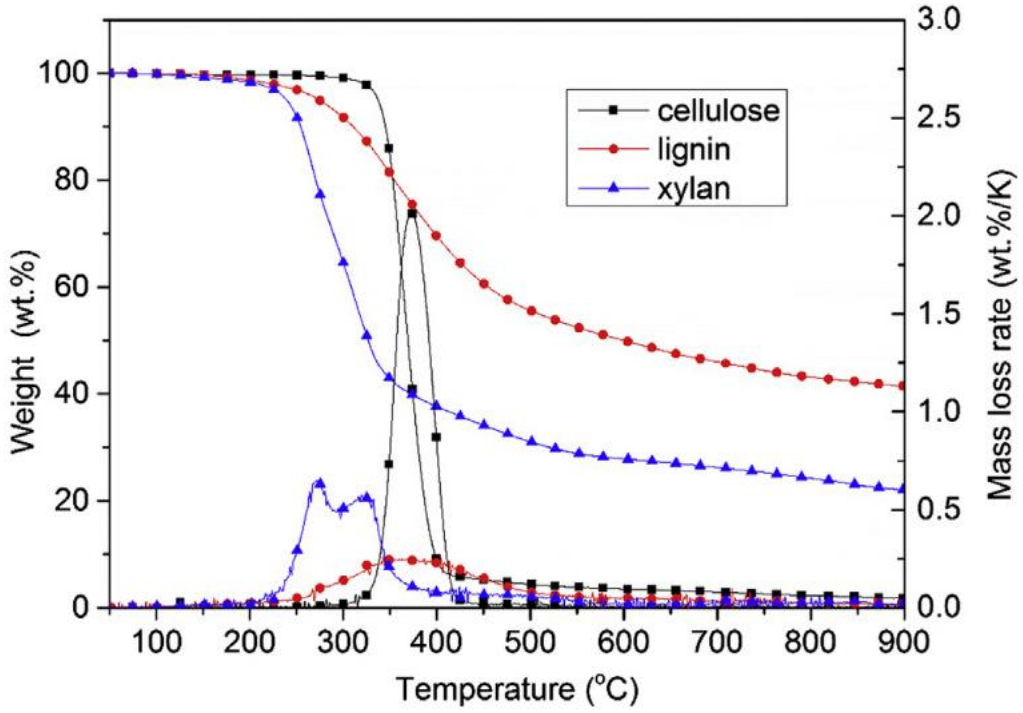


Figure 2.3: TGA and DTG thermograms of cellulose, xylan (hemicellulose) and lignin. Sourced from literature [66].

On the other hand, Yu *et al.* [66] in their study described hemicellulose alongside lignin as the main contributors to char yield (and not just lignin alone), due to the duo's ability to decompose gradually over a wide temperature range, characteristic of solid fuels. This is because from the degradation patterns on the thermograms, hemicellulose and lignin still retained a substantial percentage of their original mass beyond the pyrolysis threshold of 400°C.

In the same context, a study by Chen *et al.* [75] on the nature and type of the pyrolysis reactions of each structural component, identified hemicellulose and lignin pyrolysis reactions as naturally exothermic while that of cellulose is largely endothermic (see Fig. 2.4). In corroboration to this, Ball *et al.* [76] recognized the product of the exothermal reactions as char and those of the endothermal reaction as volatiles. These volatiles are a mixture of condensable and

incondensable pyrolysis gases. The condensable pyrolysis gases in-turn condense below room temperature to form tars/bio-oil.

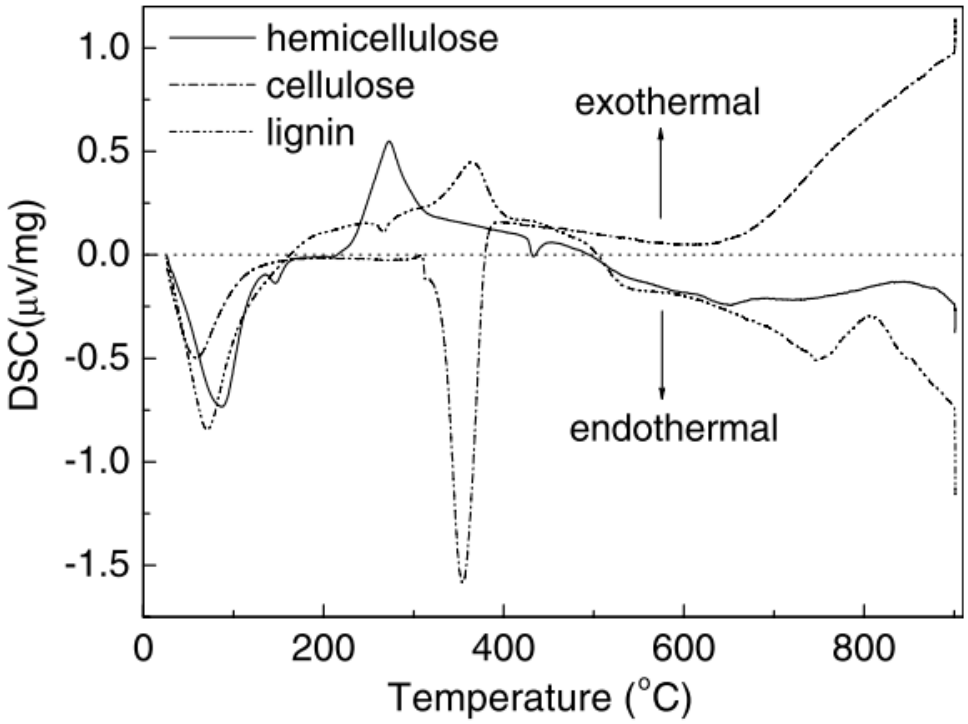


Figure 2.4: DSC thermograms of hemicellulose, cellulose and lignin thermal decomposition. Sourced from literature [65].

Differential scanning calorimetry (DSC) is one of the standard techniques adopted for the study of heat flow into and out of a sample when thermally threated. As a confirmation of the contribution of each component to the formation of each pyrolysis product, Yang [65] with Fig 2.4, analyzed their individual DSC peak values. It was observed that the exothermal DSC peaks attained by hemicellulose and lignin within the pyrolysis temperature range of 200–400°C, were approximately 0.5 μv/mg. This was much lower than that of the single endothermal peak exhibited by cellulose, -1.5 μv/mg at 350°C. This high peak exhibited by cellulose can be attributed to the generation of volatiles which corroborates the conclusion made by Ball *et al.* [76]. Meanwhile, the exothermal peak exhibited by hemicellulose alongside lignin indicates the contribution of hemicellulose as part of char

formation, in addition to its contribution to the formation of bio-oil at lower temperatures.

With regards to the influence of heating rate on the contribution of each structural component to the relative yield of each pyrolysis product, Pattanotai *et al.* [77], described the char mass reduction as a function of an increased heating rate (see Fig. 2.5). This accelerates the rate of decomposition of the biomass within a short residence time, thus giving rise to an increased rate of production of condensable gaseous matter which form bio-oil. This increased rate of decomposition can thus be likened to that of the early and rapid decomposition of hemicellulose and cellulose leading to the early formation of tars/bio-oil.

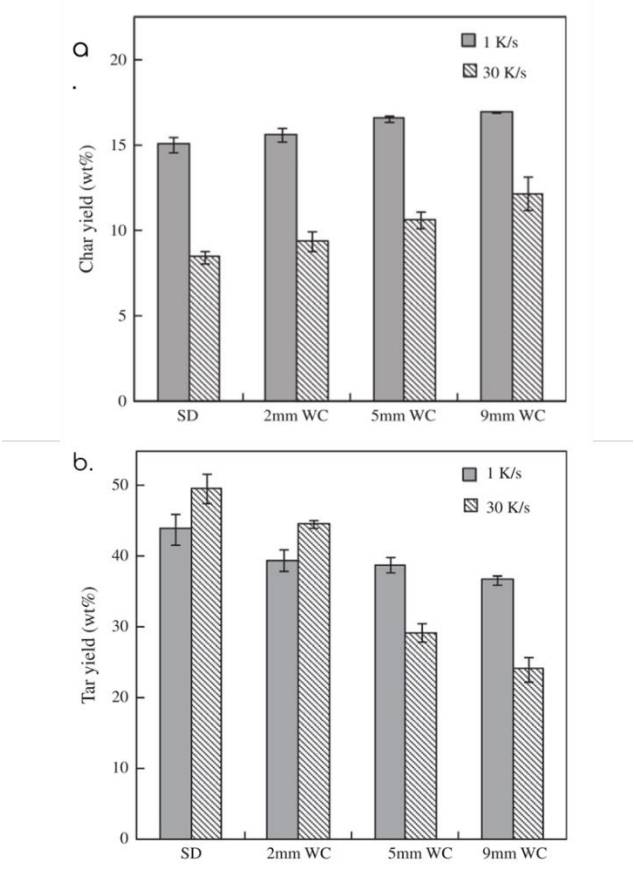


Figure 2.5: Effect of heating rate on (a) char yield and (b) Tar (bio-oil) yield, of different wood sizes – sawdust (SD), 2, 5- and 9-mm cylindrical wood pellets. Sourced from literature [77].

2.3 Biomass Thermochemical Conversion

The thermochemical conversion of biomass into gaseous, liquid and solid fuels remains a broad research area that has garnered increasing interest in recent years despite the long-term existence of thermochemical conversion technologies dating back to the 1800s. This renewed interest has largely been influenced by the present global environmental and energy crises leading to an increased pressure for the adoption of renewable energy technologies. There is an urgent need to reduce the global carbon footprint, minimize the dependence on the depleting fossil fuels as well as foster energy independence. This can be actualized by creating localized access to a variety of available energy resources, to checkmate the instability in the supply and rise in the price of crude oil and natural gas.

Among other renewable energy technologies, biomass thermochemical conversion remains one of the most attractive options due to the following advantages:

a. The global availability, accessibility and sustainable supply of the biomass feedstock thus eliminating the issue of energy security;
b. The maturity of the conversion technologies applied;
c. The energy storage capabilities of biomass as feedstock;
d. The low net carbon emission resulting from the conversion of biomass to heat, power and transport fuels; and
e. The relatively cheaper capital involved in constructing bioenergy plants as compared to other renewable energy technologies.

Gasification, pyrolysis, liquefaction, and combustion are four key thermochemical technologies utilized for the conversion of low grade solid carbonaceous materials such as wood into useful energy. While gasification, pyrolysis, and liquefaction convert these carbonaceous materials into more useful, versatile fuels and chemical feedstock – convenient for a wide range of applications, combustion is mostly confined to the production of heat energy from such materials. Moreover,

the oxidation of the carbonaceous material during combustion to release its energy, also produces very harmful and undesirable gaseous products with no useful energy value. This is contrary to the more environmentally benign pyrolysis, liquefaction and gasification processes that transform the energy stored in biomass into cleaner, more suitable liquid, solid and gaseous energy carriers for several downstream applications (see Fig. 2.6).

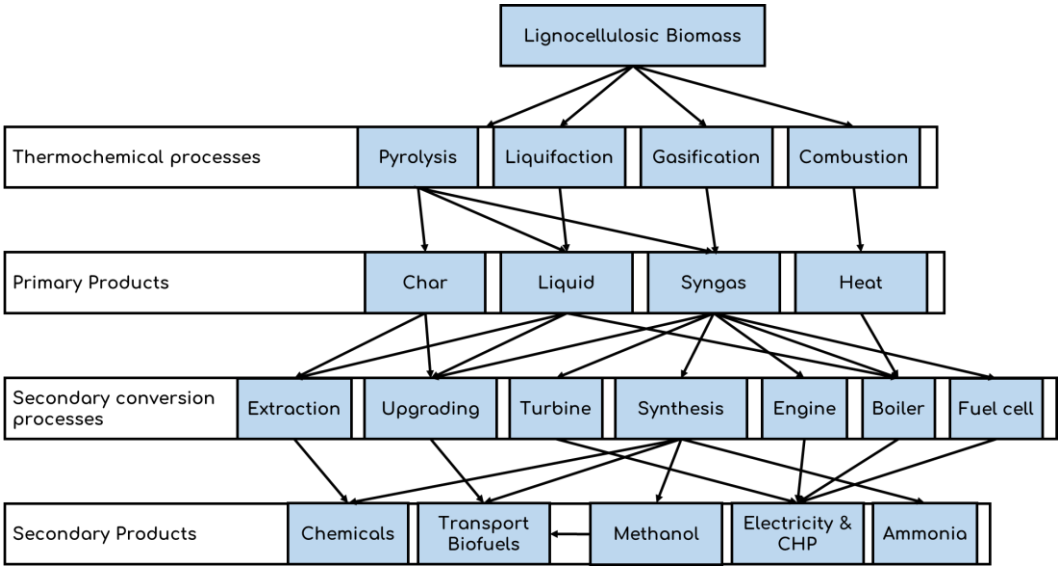


Figure 2.6: Lignocellulosic biomass and their thermochemical conversion processes for biofuel products. Adapted from literature [31].

As depicted in Fig. 2.6, the importance of syngas as a primary product can also not be overemphasized. Syngas is the single most important bio-energy carrier for the production of electricity, liquid transport biofuels, chemicals, methanol, pharmaceuticals, and other commercial products. The use of lignocellulosic biomass as feedstock provides the option for the production of these several end-products through a wide variety of primary and secondary conversion processes which makes it one of the most versatile renewable energy resources closest to fossils. Finally, Fig. 2.6 also depicts the importance of Pyrolysis and Gasification as very vital to the transition of the global energy market to Bioenergy. Through both processes, more intermediate and final bio-products can be produced from lignocellulosic biomass.

Therefore, within the context of pyro-gasification in this study, more emphasis was placed on pyrolysis and gasification processes.

2.3.1 Pyrolysis

As earlier defined, biomass pyrolysis is the thermal decomposition of solid biomass, ideally carried out in an absolute inert atmosphere. This inert condition prevents the oxidation/combustion of the biomass as temperature increases. It is made possible by passing an inert gas such as nitrogen, helium or argon through the reactor at low to medium temperatures and atmospheric pressure. It is worthy to note that pyrolysis is a completely independent thermochemical process from gasification – which on its own also incorporates a pyrolysis or decomposition phase. It is most times difficult to give a straightforward detailed description of the process of pyrolysis due to the complexity of the overlapping thermal decompositions of the structural components of the biomass feedstock as well as the variations in its physical and chemical properties. However, a general overview of the reactions involved in biomass pyrolysis is presented as follows.

2.3.1.1 Stages and reactions in biomass Pyrolysis

Biomass pyrolysis incorporates the transition from drying of the feedstock to its volatilization as described below [33]:

a. *Drying*: Wet Biomass + Heat → Dry Biomass + $H_2O(g)$ (2.1)

b. *Volatilization:* Dry Biomass ↔ H_2 + CO + CO_2 + CH_4 + $H_2O(g)$ + TAR + CHAR (2.2)

Drying involves the expulsion or evaporation of moisture from the fresh biomass feedstock, represented by small peaks occurring around 105 – 110°C on the derivative thermogravimetry thermogram of the biomass thermal decomposition process. This is gradually succeeded by its volatilization or expulsion of volatiles as the gasifier temperature is increased. This second stage is usually characterized by the sharp peaks of its hemicellulose and cellulose thermograms occurring

between 250 – 450°C, depicting their peak rates of volatilization. Depending on the physical properties of the biomass material and on the relative proportions of its structural components, this process can extend up to 700 °C. During this volatilization stage, tars generated together with the light hydrocarbons in the gaseous mixture are expelled by the thermal decomposition of the holocellulose leaving behind a solid char residue, as previously discussed.

2.3.1.2 Pyrolysis Products

The products of pyrolysis are categorized into a gaseous fraction (i.e. the non-condensable pyrolysis gases), liquid fraction (bio-oil or tar) and a solid fraction (char).

The gaseous product also known as *pyrolysis gas*, is a mix of H_2, CO, CO_2, light hydrocarbons like CH_4 and inert gases which are not condensable at room temperatures. These are released together with heavy condensable tars of which when passed through a gas condenser, condense to form part of the liquid product known as bio-oil. This gaseous fraction sometimes makes up 70–90% of the original weight of the feedstock [31]. The release of these gaseous and liquid products leaves behind the char which represents the solid residue, basically made of carbon and ash particles with little or no tar. The pyrolysis gas may exhibit low ignition and poor combustion due to the dilution of the inert carrier gas used for the pyrolysis process. Moreover, the higher concentrations of carbon and hydrocarbons are stored in the char residue and bio-oil than in the pyrolysis gas, and thus may contribute to the low energy density of the latter. In essence, pyrolysis as an independent thermochemical conversion process is commonly carried out specifically for the production of two useful products – bio-oil and char as described below.

Bio-oil also known as pyrolysis oil or aerosol, is a dark, thick viscous, low-value liquid. Despite containing about 350 compounds, the basic constituents of bio-oil are water (previously evaporated from biomass during drying) and Tar (heavy hydrocarbons condensed from the pyrolysis gas) which constitute the insoluble

particles. Tar is a dark greasy liquid made up of several organic and inorganic compounds, nitrogen, sulfur, acids, and some ash and char fragments, which contribute to its distinct dark-brown appearance [35]. Due to variations in feedstock type and reactor operating conditions, the constituents and volume of bio-oil vary significantly. Moreover, the proportions of these constituents in the bio-oil depend on the physical and chemical properties of the biomass feedstock, the presence of impurities, its pre-treatment, conversion operating conditions as well as post-treatment and storage [78].

Bio-oil is commonly obtained through fast pyrolysis of biomass, which involves the condensation of the gaseous matter generated from biomass subjected to high heating rates at a very short resident time [78]. Alternatively, it can be obtained by liquefaction, whereby biomass is treated in a solvent and pressurized to high values of up to 200 atm in the presence of a catalyst at low-temperature environments [78]. Bio-oil by liquefaction though more expensive exhibits more calorific value than the former and shares similar characteristics with conventional liquid fossil fuels.

Bio-oil serves as a raw material for the production of higher quality liquid chemicals and bio-fuel when preserved for a period of time in controlled conditions. This depends on the aqueous and the organic stages in which the bio-oil passes through during this storage period. The high presence of soluble chemical compounds in the aqueous phase of the bio-oil makes it suitable for the production of chemicals while its use for biofuels production is largely possible in the organic stage [35].

Bio-oils when unrefined are generally of lower quality when compared to their fossil counterpart – crude oil, due to their lower calorific value, high instability, acidity, and higher viscosity when exposed to prolonged heating [78,79]. These properties make them less suitable for direct use in automobiles, thus often requiring further up-gradation to high-quality biofuels [36]. Other significant issues associated with bio-oil use include:

a. Poor engine ignition (as a result of high moisture content) when used in conventional diesel engines;
b. The current high cost of production leading to high market prices when compared to fossil fuels;
c. Widespread unavailability of handling and storage facilities designed specifically for bio-oil;
d. Poor blending with conventional fossil fuels
e. Unavailability of established international specifications to ensure quality;
f. Lack of widespread availability; and
g. Negative market perception of bio-oil [36].

Currently, more research on bio-oil has been focused on its up-gradation and reduction in the cost of feedstock and production to accelerate its full commercialization.

Meanwhile, the solid fraction*, Char,* widely known as charcoal or biochar, is the solid mass of carbon and ash particles obtained from controlled pyrolysis of lignocellulosic biomass materials, such as wood, fruit shells, corn cobs, and husks. The ratio of carbon to ash in char is largely a factor of the feedstock properties.

Char is widely used in the domestic sector as a traditional fuel for cooking and space heating, as a soil fertility additive in agriculture and for industrial process heating and production of chemicals [80]. Recent studies on the application of char include its use as activated carbon, its use as a catalyst for gasification, a solid sorbent for several chemical processes such as water purification, and CO_2 capture [81,82].

Traditionally, charcoal is commercially produced from wood lumps harvested either by illegal felling of trees from forests or legally from plantations grown specifically for charcoal production. These wood lumps or offcuts are gradually

carbonized for weeks by heating them to medium temperatures within 450-600°C either when buried in soil, or placed in conventional kilns in the absence of air [83]. These methods are common in rural Sub-Sahara Africa and Asia. The charcoal industry in these regions though largely informal is huge; providing substantial revenue for the government and employment to a large number of skilled and unskilled personnel across its supply-chain [84].

In general, char is hydrophobic and light-weight in nature, promoting long-term storage and ease of transportation respectively [77,83]. It burns steadily and releases fewer toxic pollutants than raw wood when combusted thus making it a more reliable and popular cooking fuel in households across urban and rural areas in developing countries [83]. These properties are largely due to the massive expulsion of moisture and volatile matters originally present in the virgin biomass, leaving behind the solid carbon mass [77].

Most chars exhibit high calorific values of up to 31 MJ/kg [85], which is also comparatively much higher than those of their parent raw woods and within the range of some grades of coals used for power generation [39,86]. Previous studies [39,70,77,85,87], reveal that char CV, reactivity and yield are, however, largely dependent on the properties such as burning rate (BR) and mass loss ratio (MLR), type and specie of raw wood used as feedstock and also on the operating parameters of the pyrolysis process. The chief operating parameter with the most effect on char yield is the pyrolysis heating rate [66]. Other properties of wood that affect charcoal quality such as apparent density, moisture content, volatile compounds, ash, and fixed carbon also vary significantly across different wood species [85,87]. However, the fixed carbon content does not differ considerably across trees of the same genus [87]. Raw wood is known to generally contain carbon approximately half its original weight while charcoal exhibits a carbon content of about 90 percent its weight [41].

One major downside in the production of charcoal is its production efficiency and yield. It is estimated that about 40% of the original weight of wood is obtainable

as char after conversion. This is largely dependent on the efficiency of the production process, properties and particle size of the wood and set process parameters such as final pyrolysis temperature and heating rate. However, the issue of the balance between yield and reactivity of char arises when it is being produced for application in chemical processes as reported by Pattanotai *et al.* [77]. During a fast pyrolysis of biomass for bio-production, the char produced as a by-product is of minimum yield but is very reactive if gasified. Meanwhile, slow pyrolysis to maximize char yield produces char which is less reactive than the former. Other issues related to char production include the by-production of tars and other acidic materials as well as the emission of particulates, volatile compounds and some greenhouse gases which need to be managed during char production [84]. However, these emissions can be minimized if the pyrolysis gaseous product is condensed to bio-oil and treated further when passed through other post-production gas cleaning units.

2.3.1.3 Modes of Pyrolysis

As previously discussed, the yields of either of the aforementioned pyrolysis products have been attributed to the structural composition of the biomass feedstock and most especially to the operating conditions such as the heating rate and the final temperature of the pyrolysis process. Based on these two operating parameters mentioned, pyrolysis can, therefore, be classified into three modes, namely—fast pyrolysis, intermediate pyrolysis, and slow pyrolysis. Table 2.3 compares the estimated product yields from three pyrolysis modes with those obtained from gasification [88]:

In the study on the effect of heating rate on the yield of biomass pyrolysis products reported by Pattanotai *et al.* [77], the char yields and tar yields of a Japanese cypress sawdust and pellets were analysed after pyrolysis at a low heating rate of 1 K/s and a high heating rate of 30 K/s. Figure 2.5 depicts a switch in char and tar yields across all wood sizes at the different heating rates. By increasing the pyrolysis heating rate from 1 to 30 K/s, the tar yields (see Fig. 2.5 b) were observed to be increase by approximately 5%.

Table 2.3: *Three modes of pyrolysis and their products in comparison to gasification* [88]*.*

Pyrolysis mode	Liquid (bio-oil)	Solid (bio-char)	Gas (syngas)
Fast pyrolysis: Moderate pyrolysis temperature (~500 °C), short hot vapour residence time (<2s) (high heating rate)	75% tar (25% water)	12%	13%
Intermediate pyrolysis: Low to moderate pyrolysis temperature, moderate hot vapour residence time (moderate heating rate)	50% tar (50% water)	25%	25%
Slow pyrolysis: Low to moderate temperature, long residence time	30% tar (70% water)	35%	35%
Gasification: High temperature (>800 °C), long vapour residence time.	5% tar (5% water)	10%	85%

Conversely, char yield (Fig. 2.5 a) was drastically reduced by as much as 7% as a result of this increase in heating rate. However, as depicted in Fig. 2.7, it was observed that the char produced at a higher heating rate, 30 K/s, though at a lesser yield, was generally more reactive across all samples and vice-versa. This can be attributed to the fact that for the wood pellet, there was a more complete and rapid expulsion of volatiles during the pyrolysis at the higher heating rate of 30 K/s. This thereby created wider pore diameters leading to the exposure of the inner particles for a more complete conversion of the pellet to char. Therefore, the 30 K/s char becomes more likely to be very reactive during gasification since

due to its increased surface area, its inner carbon particles are better exposed to reaction with the gasifying agent. This reaction process is, however, straightforward for the sawdust sample since the particles are already loose and occupy a larger surface area.

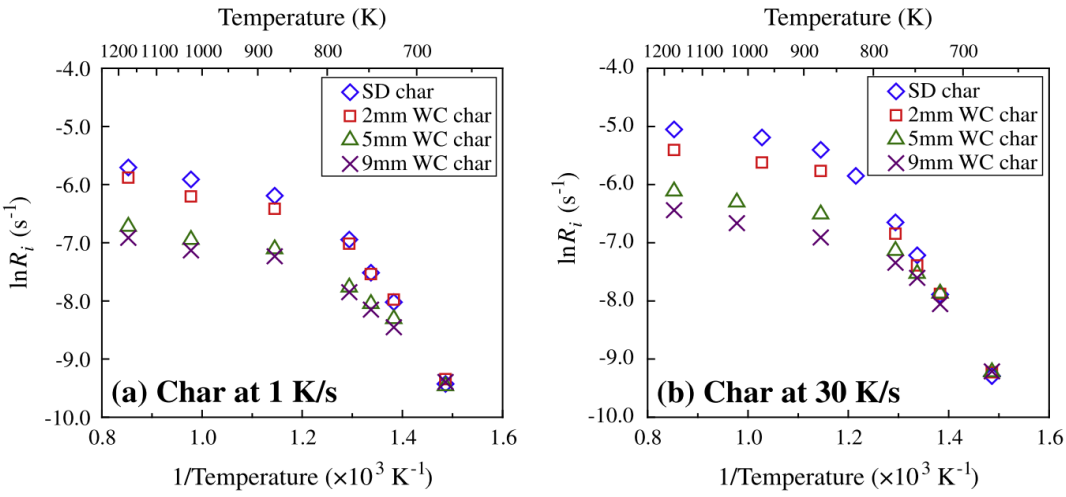


Figure 2.7: Effect of increase in heating rate from 1 K/s to 30 K/s to the char reactivity of the same sample in different sizes – Sawdust (SD), 2, 5- and 9-mm diameter cylindrical wood pellets. Sourced from literature [77].

One important feature of the pyrolysis technology is the capability of separating and extracting the condensed tar produced from the biomass. This, therefore, leaves behind a relatively tar-free and carbon-rich char residue. This volatiles-free char residue formed can then be gasified separately for the production of syngas with much-reduced tar content. This is the basis on which pyro-gasification is being developed as discussed in Section 2.4.

2.3.2 Gasification

Gasification is the thermochemical conversion of a raw or pre-processed carbonaceous feedstock like biomass (or coal) at high temperatures in the presence of an oxidizing agent, for the sole production of a product gas mixture containing synthesis gas. The product gas consists of a mixture of combustible gases comprising of 0 – 5% CH_4, 5 – 15% CO_2, other gaseous compounds and most

importantly, a clean gaseous fuel mixture known as Synthesis gas or Syngas (comprising of 30 – 60% CO and 25 – 30% H_2) [89].

2.3.2.1 Stages and reactions in biomass gasification

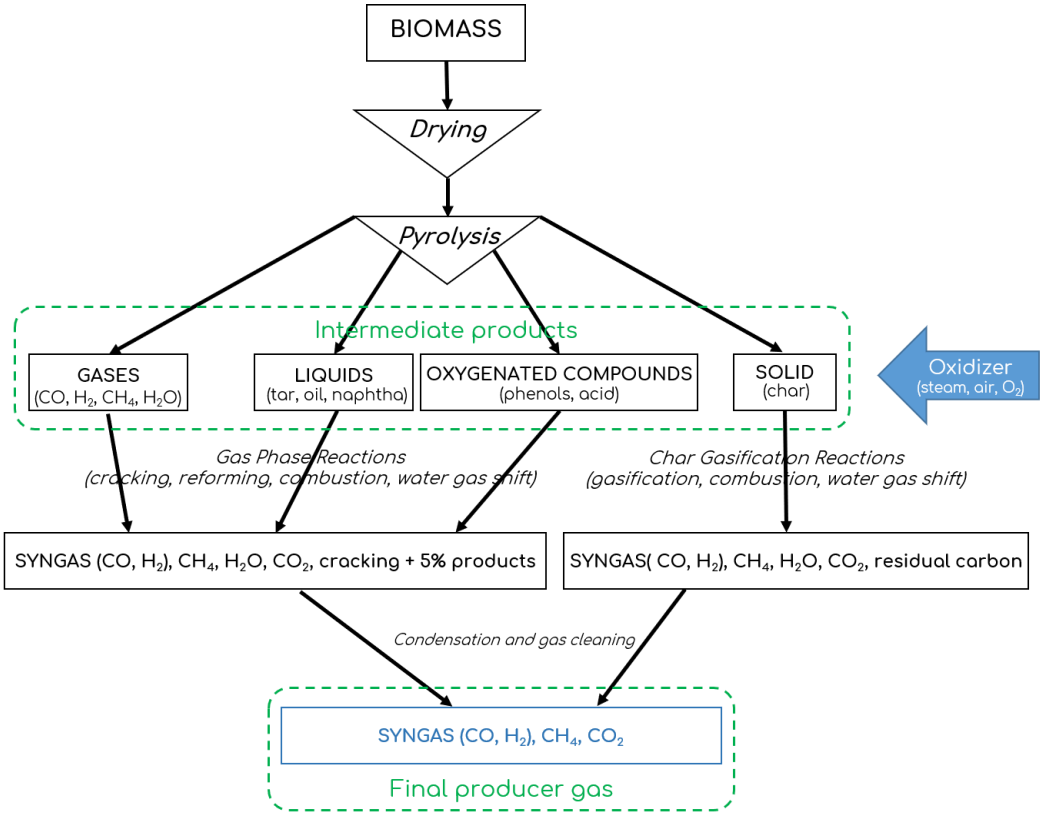


Figure 2.8: Stages, processes, and products of the biomass gasification. Adapted from literature [89].

Biomass exhibits high thermochemical reactivity and ignition stability, which make them more suitable than coals for conversion to gaseous fuels with minimal combustion propensity [90]. Gasification of biomass for the production of syngas is a complex process involving a series of chemical reactions occurring at different stages of the process as shown in Fig. 2.8. However, there are four stages leading to the production of the final product gas during biomass gasification. They include the:

a. *Drying stage*; which involves an endothermic reactions of water expulsion from the raw biomass feedstock;

b. *Pyrolysis stage*; which also involves endothermic reactions of decomposing the dry biomass feedstock into liquid, gaseous and solid components;

c. *Partial oxidation stage*; which involves exothermic reactions of partially combusting the liquid, gaseous and solid pyrolysis components to generate heat and some useful gaseous compounds; and the

d. *Reduction stage*; involving endothermic reactions of converting the unreacted products of pyrolysis and partial oxidation to produce syngas.

The gasification process also includes an additional stage due to the need to eliminate the tars generated in the pyrolysis stage. Undesirable tar compounds are thermally broken down to useful gaseous products in high-temperature tar-cracking reactions which are energy-intensive, requiring heat supply from an external source.

a. Drying stage:

Drying occurs as the first phase of a biomass gasification process. It involves an endothermic reaction occurring from room temperature up to 150 °C, whereby moisture is expelled from the biomass in form of steam as represented by Eq. 2.3. The heat required for this reaction is supplied either externally from a furnace or internally from the recycled hot gases generated during the partial combustion of char, tars and pyrolysis gases at the partial combustion stage of the gasification process.

$$\text{Wet Biomass} + \text{Heat} \rightarrow \text{Dry Biomass} + H_2O\,(g) \qquad (2.3)$$

Depending on the biomass type, specie, and storage conditions, the biomass feedstock can contain moisture of up to 31% of its total weight [90]. High amounts of moisture in the biomass feedstock lowers gasification efficiency by decreasing the internal temperature in the gasification zone of the gasifier. For optimum efficiency of the gasification process, moisture contents below 15% have been reported suitable for biomass feedstock [90]. This can be achieved by drying the

feedstock separately as a pre-treatment process to upgrade the fresh biomass before the gasification process.

b. Pyrolysis stage:

Also known as the thermo-decomposition or volatilization stage, this stage of the gasification process is critical to the quality of the final syngas product as well as the kinetics of the gasification process as a whole. During a wood gasification process, the formation of the primary products which serve as precursors to the production of the final product gas commences from this pyrolysis stage. The pyrolysis phase occurs by a series of complex reactions governed by the gasifier pressure and temperature, heating rate, feedstock residence time, feedstock moisture content, the structural composition of the feedstock and feedstock particle size [69]. At this pyrolysis stage, complex polymers in the biomass are broken-down, generating volatiles that contain both condensable and non-condensable gases. The condensable gases, when condensed, form tar or bio-oil. Meanwhile, the un-volatilized solid part of the biomass remains as the char residue. These primary products formed are similar to do those generated from biomass pyrolysis when carried out as an independent process as previously described.

However, contrary to biomass pyrolysis (as a separate process) – whereby these primary products formed are extracted and used for downstream applications, the products of the pyrolysis stage of a gasification process remain trapped in the reactor. The combination of the carbon-rich char (the desirable component) and tar (the undesirable component) trapped in the reactor, progress as reactants for the reactions in the advanced stages of gasification. Due to difficulties of decomposing tar at low to medium gasification temperatures, it remains as part of the final product gas, thereby undermining the syngas quality.

$$\text{Dry biomass} + \text{Heat} \rightarrow H_2(g) + CO(g) + CO_2(g) + CH_4(g) + H_2O(g) + \text{TAR} + \text{CHAR} \quad \text{(Endothermic)} \qquad (2.4)$$

Similar to drying, the thermal decomposition phase comprises an endothermic decomposition reaction. This reaction involves the thermal treatment of the moisture-free biomass to pyrolysis temperatures between 250 ℃ and 500 ℃ in an oxygen-deficient atmosphere [31].

Equation 2.4 shows a list of products obtainable from biomass pyrolysis. The yields of these individual products relative to each other at this stage is mostly affected by the structural composition of the biomass feedstock. Unlike is obtainable in the pyrolysis thermochemical process whereby the heating rate is set to maximize either char or bio-oil yield, the heating rate in this pyrolysis stage of a gasification process is of less significance to the yield of the final syngas produced. This is because as previously mentioned, all individual intermediates produced remain in the reactor without separation and progress together as reactants for the succeeding stages of the gasification process irrespective of their yields.

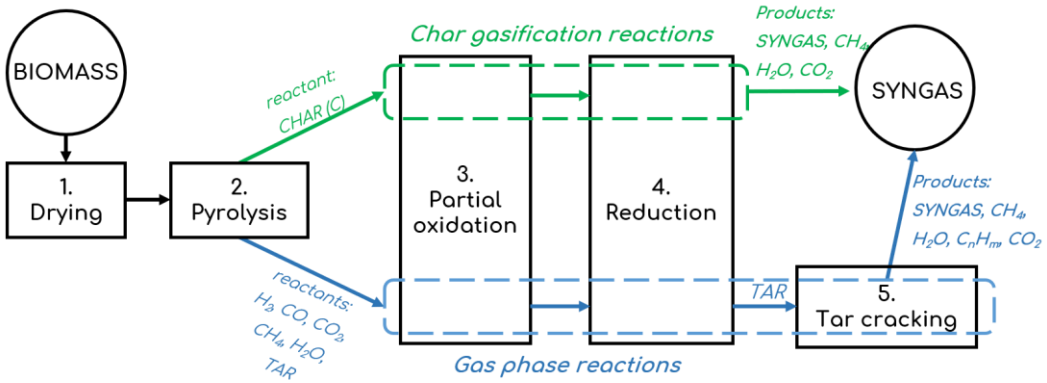


Figure 2.9: Pathways for char-phase reactions and gas-phase reactions of biomass gasification.

As depicted in Fig. 2.9, the reactions involved in stages three and four of the gasification processes – can be categorized into char-phase gasification reactions (depicted in green) and gas-phase reactions (depicted in blue). The carbon particles C, present in the char residue serve as the sole reactant for the char phase reactions in both stages. Meanwhile, the gaseous pyrolysis products which include tar serve as reactants to the gas phase reactions in stages three and four. However,

since the tar remains difficult to decompose in stages three and four operating at normal temperatures (600°C – 1000°C), the gas phase reactions may extend to stage five. This fifth stage occurring at ultra-high temperatures therefore enables the cracking of the tar in the gaseous mix. This furthers the production of syngas and other combustible gases (see Eq. 2.13). Alternatively, the use of a catalyst during tar cracking lowers the temperature at which tar cracking reaction is enabled.

For this study, however, more emphasis was placed on the char gasification phase reactions in describing the partial oxidation and reduction stages. Steam was considered as the preferred oxidizing agent and carbon as the main reactant in describing the partial oxidation and reduction reactions of the gasification process. This was so because in the pyro-gasification technique adopted in this study, tar was extracted during the pyrolysis stage. Therefore, the char gasification phase reactions were more prevalent for syngas production in biomass pyro-gasification.

c. Partial Oxidation / Combustion stage:

This phase involves the partial oxidation or combustion of the char and other combustible pyrolysis products in limited oxidizer concentrations to produce CO, other gaseous products and most importantly heat. The heat generated is important to supply the much-needed thermal energy to maintain gasifier temperature and enable the endothermic reactions involved in the drying, pyrolysis and reduction stages.

In order to partially oxidize the intermediate products to generate not just heat but also CO and other useful gaseous products in the process, it is expected that the equivalence ratio (ER), is greater than 1 to ensure partial oxidation/combustion. This translates to a limited supply of oxygen as represented by Eq. 2.5.

However, with a stoichiometric ratio greater than 1 (i.e. in excess oxidizer concentration), the exothermic reaction becomes a complete

oxidation/combustion, which releases higher thermal energy and CO_2, other than CO (see Eq. 2.7).

The partial oxidation of char at low oxygen concentration is represented by Eq. 2.5 and 2.6 [31,91]:

$$C + \frac{1}{2}O_2 \rightarrow CO \qquad \Delta H = -111 \text{ kJ/kg.mol} \tag{2.5}$$

At low oxygen concentrations, the hydrogen present in the pyrolysis gas is also combusted to releasing heat and moisture:

$$H_2 + \frac{1}{2}O_2 \rightarrow H_2O \qquad \Delta H = -242 \text{ kJ/kg.mol} \tag{2.6}$$

Meanwhile, the complete oxidation/combustion of the carbon in char in a higher oxygen concentration is represented as:

$$C + O_2 \leftrightarrow CO_2 \qquad \Delta H = -394 \text{ MJ/kg.mole} \tag{2.7}$$

The use of steam as an oxidizing agent particularly in high concentrations is most effective for the formation of hydrogen molecules during char oxidation reactions as described with Eq. 2.6. This in turn contributes to the production of a hydrogen-rich syngas. Therefore, steam was adopted as the preferred oxidizer for the partial oxidation of char in this study.

$$C(s) + 2H_2O(g) \leftrightarrow CO_2(g) + 2H_2(g) \tag{2.8}$$

d. Reduction stage:

This stage involves the final formation of syngas from a series of endothermic and exothermic reactions (see Eqns. 2.9 and 2.10) between steam (i.e. the oxidizing agent) and carbon which is the most important reactant in the gasifier. Other intermediates produced from the previous reactions in the earlier stages, also serve as reactants at this stage and contribute to the composition of the final product gas as a whole.

The main reactions occurring at this stage, progress at higher gasifier temperatures of up to 1000°C. They include Boudouard reaction, Water-gas

reaction, Water-gas shift reaction, and Methane formation reaction, as represented by Eqns 2.9–2.11 below [31]. The heat energy required for these reactions may be generated internally during the combustion reactions or supplied from an external source.

Boudouard reaction:

$$C(s) + CO_2(g) \leftrightarrow 2CO(g) \qquad \Delta H = 172 \text{ MJ/kg.mol} \qquad (2.9)$$

Water-gas reaction:

$$C(s) + H_2O(g) \leftrightarrow CO(g) + H_2(g) \qquad \Delta H = 131 \text{ MJ/kg.mol} \qquad (2.10)$$

Water-gas shift reaction:

$$CO(g) + H_2O(g) \leftrightarrow CO_2(g) + H_2(g) \qquad \Delta H = -41 \text{ MJ/kg.mol} \qquad (2.11)$$

The Boudouard reaction represents the reaction between the char and the CO_2 generated from the combustion reactions of the previous stage. The Boudouard reaction generates excess CO which further reacts with steam in the water-gas shift reaction to produce more hydrogen molecules. Equation 2.10 describes the water-gas reaction (also known as the char reformation reaction) of the carbon in the char with superheated steam. This generates a mixture of carbon monoxide and hydrogen molecules, known as syngas or “water gas” from which the name is derived. Meanwhile, the carbon monoxide produced in Eqn. 2.5, 2.9 and 2.10, may further be oxidized to carbon dioxide with the production of more hydrogen molecules in a water-gas shift reaction (Eqn. 2.9).

Furthermore, a methane formation reaction may also occur at this stage, between carbon monoxide and excess hydrogen molecules produced from Eqns 2.8, 2.10 and 2.11 to form methane and steam which are part of the product gas mixture:

Methane formation: $CO(g) + 3H_2(g) \leftrightarrow CH_4(g) + H_2O(g) \; -88 \text{ MJ/kg mole}$ (2.12)

Among all exothermic reactions, the complete combustion of carbon with oxygen (Eqn. 2.6) gives off the most energy. As earlier stated, the heat released in this

phase can be transferred for the endothermic reactions in the biomass drying, decomposition, and reduction stages.

e. Tar Cracking:

Tar is an undesirable product of a biomass pyrolysis and its thermal decomposition is virtually unachievable under normal gasification conditions. Therefore, it remains part of the product gas generated and lowers the quality of the syngas to be used for downstream applications. However, when gasification processes can progress to elevated temperatures above 1000°C, with an external heat input, the tar formed during the pyrolysis stage is cracked to further release useful gaseous compounds as shown below:

$$TAR \rightarrow CO_2(g) + CO(g) + H_2(g) + CH_4(g) + C_nH_m(g) \quad (2.13)$$

This stage of gasification is also regarded as a syngas pre-production tar cleaning method, which is a highly energy-intensive method. This reaction can also be aided by a catalyst. A description of this method and other tar cleaning methods have been presented in section 2.4.

2.3.2.2 Gasification Product

Syngas (H_2 and CO) is the most essential product of gasification which makes up a fraction of the product gas mix, also consisting of other gases such as carbon dioxide, methane, and moisture. Its yield from the gasification of biomass can range from 1 – 3 Nm^3 per kg of the biomass feedstock. Its yield, composition of its constituent gases (H_2 and CO) and calorific value can vary, depending on the type of gasifier, oxidizing agent and operating parameters adopted, amongst other factors. Syngas net calorific value has been reported to range from 4-15 MJ/Nm^3 [31].

The potentials of syngas particularly for the production of alternative transportation fuels and power and heat generation have been well documented [71,90,92,93]. For transport biofuel production, much work is being done in the conversion of syngas to synthetic liquid fuels such as biodiesel, bio-ethanol, bio-

methanol, and also gaseous fuels such as biomethane, hydrogen and synthetic natural gas (SNG) for use in automobiles [94,95]. Liquid automobile fuel production can be achieved by liquifying syngas introduced to a Fischer-Tropsch (FT) synthesis reactor in the presence of a catalyst [96]. This process, however, requires syngas particularly produced with steam/air oxidizer and the final product (biodiesel, bioethanol or methanol) depends on the catalyst employed [95].

There are specific interests in the production of ethanol from syngas due to the potentials in maximizing its production from other lignocellulosic biomass feedstocks rather than traditional food-related feedstock like sugarcane and corn. This can be achieved either through biochemical or catalytic thermochemical pathways. The former involving a low-cost fermentation of syngas in the presence of acetogens, a special kind of bacteria which act on CO_2 or CO and H_2 present in the syngas [31,97]. Meanwhile, the latter, a more energy-intensive option, involves a thermochemical reaction in the presence of Rh or Cu compounds as catalyst in temperatures of up to 858^{o}C [31,95]. Additionally, bio-methane produced from syngas is also being developed commercially as an alternative transport fuel in existing natural gas-powered automobiles in some EU countries. This is being done by subjecting compressed syngas to an exothermal type reaction in the presence of a catalyst such as nickel-alumina or copper-alumina compounds or by passing it through polymer membranes [31,98,99].

In terms of heat and power generation, syngas can be used directly in conventional gas turbines, internal combustion engines (ICEs) and in high-temperature fuel cells for power and heat generation [31,72,100–102].

As previously mentioned, high tar volumes generated alongside syngas remains a major downside to syngas production from biomass. This is primarily caused by the high levels of moisture and volatile matter originally present in the raw biomass feedstock which form tar thereby limiting syngas yield and quality [103,104]. An ideal syngas is regarded as one with high H_2: CO ratio, consisting of negligible tar content and low incombustible impurities. Tars, particulates, nitrogen and

sulfur compounds, alkali and halides present in bio-syngas as impurities reportedly damage gas turbine components, internal combustion engines and poison fuel cell catalysts [71,96,105,106]. Moreover, the high presence of tar in biomass can cause corrosion and blockages in pipes and also inhibit the optimum thermal efficiency of the pyro-gasification process [107].

2.3.2.3 Factors associated with gasification

The following are some factors which largely affect the production of syngas from LCBs, the syngas properties and relative proportions of its gaseous components (H_2 and CO):

a. Type of Gasifier:

The type of gasifier employed for a gasification process largely affects the quality, composition and fuel properties of the syngas produced. This is so because the direction of the flow of the feedstock and the oxidizer into the gasifier as well as their mode of interaction with each other is governed by the architecture of the gasifier. There are two main types of gasifiers, the fixed bed, and the fluidized bed gasifiers. However, each of these is further subdivided into other subtypes, based on the modifications made to their designs (see Fig 2.10).

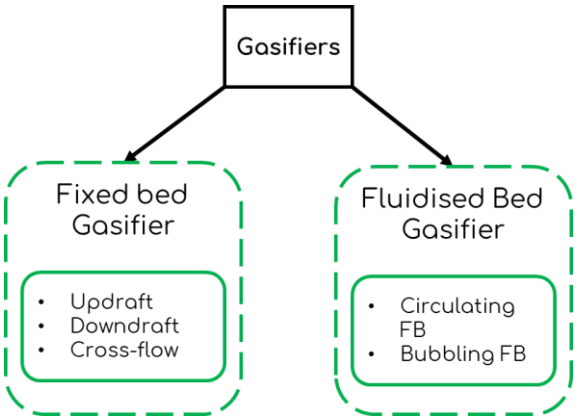


Figure 2.10: Classification of gasifiers.

Fixed bed gasifiers are the oldest and most widely used gasifiers for high-temperature gasification processes of up to 1000°C. They are characterized by their simple design and operation, high thermal efficiency and capability to

gasify a wide range of biomass with little pretreatment requirement which makes them most ideal for small-scale gasification. Their design principle is based on the direction of the flow of the gaseous oxidizing agent across the gasifier and through the biomass feedstock. Depending on the direction of gas flow they are subdivided into three types – updraft, downdraft and crossflow.

However, their main disadvantage is the production of low-quality syngas with low CV (approximately 6 MJ/Nm^3), characterized by high tar composition, low hydrogen and carbon monoxide concentrations and a dilution of high concentrations of nitrogen. A typical syngas produced by a fixed bed gasifier is reported to contain as low as 15–20% hydrogen, 10–15% carbon monoxide, 40–50% nitrogen, 10–15% carbon dioxide and 3–5% methane [91]. The high nitrogen composition can be attributed to the use of air as the preferred oxidizer for this type of gasifier.

The fixed bed gasifiers are usually built with layers through which the products of the biomass decomposition pass through as the gasification process progresses. *Updraft* gasifiers are designed for the biomass feedstock to be fed in a downward direction from the top of the gasifier while the air flows in an upward direction from its bottom. Meanwhile a mixture of the tar and gas generated exit through the top of the gasifier, thus making the gas tar-laden. Tar composition in syngas produced from updraft gasifiers can be as high as 50 g/Nm^3 [96]. The design of the *downdraft* gasifier, however, allows for a co-current flow of air and that of the feedstock. Tar content in the syngas produced from a downdraft gasifier is much lower than that from an updraft gasifier and can be as low as 1 g/Nm^3 [96]. This is because unlike the updraft gasifier, the downdraft gasifier is equipped with a narrow throat in the high-temperature combustion layer whereby the tars produced in the pyrolysis chamber is cracked as it passes through the combustion layer towards the exit point. In the *crossflow* type, the air inlet is positioned at the side of the gasifier while the biomass feedstock is fed in a downward direction from the top. Meanwhile, the product gas exits the reactor from the side exactly opposite of the air inlet. Crossflow gasifiers are, however, disadvantaged by their

low overall energy efficiency due to the high temperatures at which the product gas exits the reactor and the high tar concentration of their product gas.

Fluidized bed (FB) gasifiers, in contrast, gasify the feedstock in a fluidized state as the name implies. This is performed by introducing the gasifying agent (in most cases air) at a high velocity into the heated reactor to enable the thorough mixing of a finely grained bed material and the sawdust particles of the biomass feedstock in a fluidized state. This type of gasifier is commonly used in coal gasification. The advantage of fluidized bed gasifiers over the fixed bed gasifiers is the uniformity of the temperature distribution in the gasification zone. This ensures the fine biomass particles, the hot bed material, and the hot gasifying agent are mixed thoroughly [91]. However, operational issues such as slagging of the bed material caused by the high ash contained in the biomass is common. Syngas produced from FB gasifier is also known to contain impurities such as particulate matter (PM), NO_X, SO_X, alkali compounds, tar and particulates in different proportions [91]. Particulates produced by fluidized bed gasifiers are usually higher in concentration than that produced by a fixed bed gasifier. A post-production gas cleaning is therefore essential for fluidized bed gasifiers. The *circulating* type of fluidized bed gasifier functions by recycling the fine bed material between the reactor chamber and a cyclone separator [91]. This enables the separation and removal of ash from the reactants while the bed material and char being formed are returned into the reactor. Meanwhile, the *bubbling* FB gasifier comprises a gasification chamber equipped with an air inlet grate at the bottom and a moving bed at the top of the grate, containing the fine particles of the bed material. On this moving bed containing the bed material, the biomass feedstock in the form of sawdust is introduced to be fluidized. Its capability to generate product gas with low tar content is its greatest attribute. The low tar content is a result of the cracking of heavy condensable gaseous compounds that come in contact with the hot bed material particles thereby producing gas with a tar content of as low as 1–3 g/Nm^3 [91].

An important deduction from the above description of the various types of gasifiers is the similarity in their modes of gasification whereby the tar produced during the pyrolysis stage is allowed to progress alongside other reactants through to the later stages of the gasification process. As a result, tar is produced together with the product gas and thus would require a post-production cleaning as previously mentioned. Meanwhile, gasifiers equipped with tar cracking capabilities such as the downdraft and bubbling fluidized bed gasifiers in most cases require high energy input to carry out such tar cracking reactions. Tar cracking by such reactors is classified under pre-production tar cleaning methods which are discussed in Sect. 2.4.1.

b. Type of gasifying agent:

As previously highlighted, the type of gasifying (or oxidizing) agent employed in gasification has a great influence on the overall gasification process as well as the heating value and composition of the final product gas. This also influences the variations in the relative proportions of the H_2 and CO of the syngas present in the product gas. Three types of gasifying agents are widely employed in gasification processes namely, oxygen, air, and steam. Some studies have also investigated the use of CO_2 and hydrogen in a process called hydrogenation for biomass gasification [91,108].

The use of air is widely practiced and is the cheapest for gasification processes. However, it results in the production of syngas with low calorific value usually within the range of 4–6 MJ/Nm^3 which is much lower than that of natural gas at 36 MJ/Nm^3 [91]. This is mainly due to the influence of high nitrogen concentration in the syngas. The nitrogen present in the air as well as in the biomass dilutes the syngas thereby limiting its combustibility [96]. Moreover, the high concentration of nitrogen in the gasifier which creates an inert atmosphere may limit gasification reactions.

Meanwhile, the use of pure oxygen which is rather more expensive supports the increased production of CO rich syngas (as described by Eqn. 2.7) with net calorific

values usually within the range of 10–15 MJ/Nm^3 [91]. Besides, gasifier temperatures are maintained at high temperatures due to the combustion of the pyrolysis products by the oxygen to produce the heat required for other reactions. Syngas calorific value is also higher due to its higher CO proportion.

Steam gasification has proved most effective for the production of syngas with higher H_2 proportions than CO which makes it a much cleaner fuel. Higher hydrogen percentage in syngas ensures efficient combustion with low carbon emissions and optimum engine performance of power plants [31,33,109,110]. High net calorific values of up to 20 MJ/Nm^3 is also obtainable in syngas produced with steam [91]. However, the use of steam particularly in excess reduces gasification temperatures which affects process efficiency and thus may require heat input from an external source. In contrast to the use of air or oxygen which provide heat for gasification reactions through the full combustion of the pyrolysis products, the use of steam particularly during the water-gas reaction with char (Eqn. 2.10) occurring around 700 °C, is endothermic and thus requires an external heat input.

The use of steam as the preferred gasifying agent in this study is because in the pyro-gasification process, only the carbon-rich char residue progresses to the later stages of the gasification phase without other products formed in the pyrolysis phase. Therefore, the gasification phase reactions are strictly char-based reactions which would be more beneficial for the production of hydrogen-rich syngas if steam was used as the gasifying agent (see Eqns. 2.10 and 2.11). Moreover, the use of an infrared furnace provides the necessary external heat input to support the endothermic water-gas reaction. Steam also supports the production of hydrogen-rich syngas which is more environmentally benign, exhibits high calorific value and is relatively economical since steam is generated from water. Moreover, the hot steam produced alongside the product gas can be redirected back into the reactor to further support the endothermic reactions.

c. Temperature and Steam/Biomass Ratio:

Several studies investigating the effect of temperature on syngas composition and yield have been conducted on a variety of biomass feedstock at different steam to biomass (S/B) ratios [33,111–114].

Siyi Luo *et al.* [111], varied the bed temperature at 600°C, 700°C, 800°C and 900°C using a fixed bed reactor with sawdust from pine as feedstock. The experiment was carried out using Steam to Biomass ratios varied within 0 to 2.8 at a constant feedstock flow rate of 5 g/min. Gil *et al.* [114], conducted a similar experiment but with pine wood chips as feedstock. They investigated the effect of steam as a gasifying agent on the hydrogen content of the product gas. A research on the reactions affecting biomass gasification process on a fluidized bed was also carried out by Franco *et al.* [112], whereby it was observed that at an S/B ratio of 0.6-0.7 at a gasifier temperature of 800°C, maximum values were recorded for H_2 yield, calorific value and carbon conversion rate. Meanwhile, Subbaiah *et al.* [113] in their research, studied the effect of both varying bed temperature and S/B ratio on the resultant product gas composition, calorific value and gas yield using groundnut shells as a biomass feedstock.

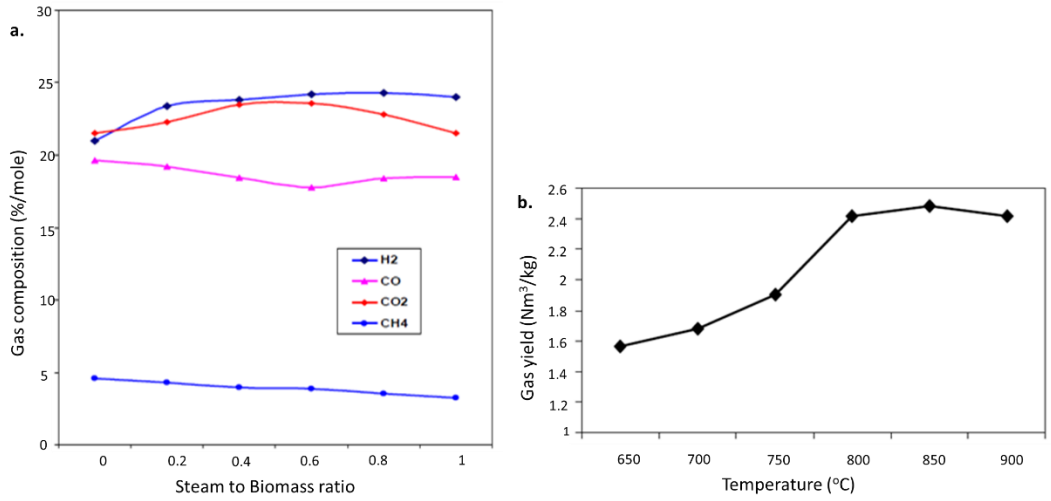


Figure 2.11: (a) Influence of S/B ratio variation on gas composition; (b) Effect of temperature variation on product gas yield. Sourced from literature [113].

According to conclusions by these researchers, bed operating temperature strongly affected gas composition. It was discovered that the syngas composition

in the product gas increased with an increase in temperature [113]. The study on the effect of operating temperature on reaction product yield also revealed an obvious increase in the total volume of gas generated in Nm^3 per kg of the biomass feedstock. This is understood to be as a result of a greater amount of char thermochemically reacting to form more gaseous products as temperature increased [33,113]. The product gas yield, however, peaked at 850°C as shown in Fig. 2.11 b.

In terms of the effect of S/B ratio influence on gas composition, it was observed that there was more hydrogen formation at higher S/B ratios which corresponds with the description on Eqn. 6. However, a significant temporary reduction in CO composition was noticed at an S/B ratio of 0.6 as represented by Fig. 2.11 a.

These aforementioned observations were contrary to that of Li *et al.* [33], who investigated the effect on hydrogen yield of gasifying wood pellets in a fixed-bed gasifier at ultra-high temperatures (800°C to 1435°C), using steam with a fixed flow rate of 9.0 g/min and varying steam to biomass ratios.

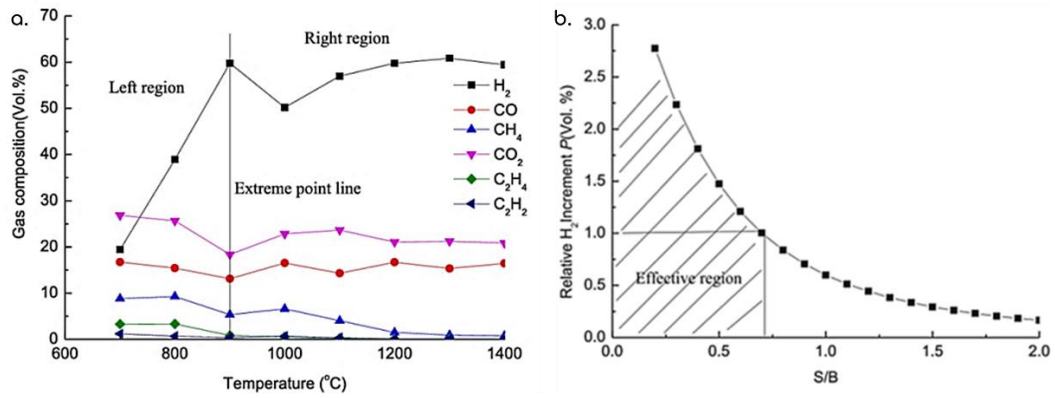


Figure 2.12: (a) Composition of products at varying temperatures (at a steam flow rate of 9.0 g/min); (b) Effect of S/B on Hydrogen increment by ASPEN simulation. Sourced from literature [33].

Interestingly, there was an increase in H_2 composition from about 20% at 617°C to a maximum of 59.76% at 917°C, succeeded by a quick drop in yield to about 50% at 1000°C as described in Fig. 2.12 a. This, however, increased afterward on a

gentle slope and again attained a value close to the previous maximum value at 1300°C. The initial jump to a maximum yield can be attributed to the endothermic reactions such as the water-gas reaction taking place at the beginning of the process.

According to Fig. 2.12 b, increasing the S/B ratio decreased hydrogen yield at different temperatures. It was observed that the ideal S/B ratios for a decent fraction of hydrogen in the product gas, was within the effective region (i.e. S/B = 0.0 to 0.7) assuming the minimum value of relative hydrogen increment P for an enhanced hydrogen yield is 1.0%.

d. Feedstock Particle size:

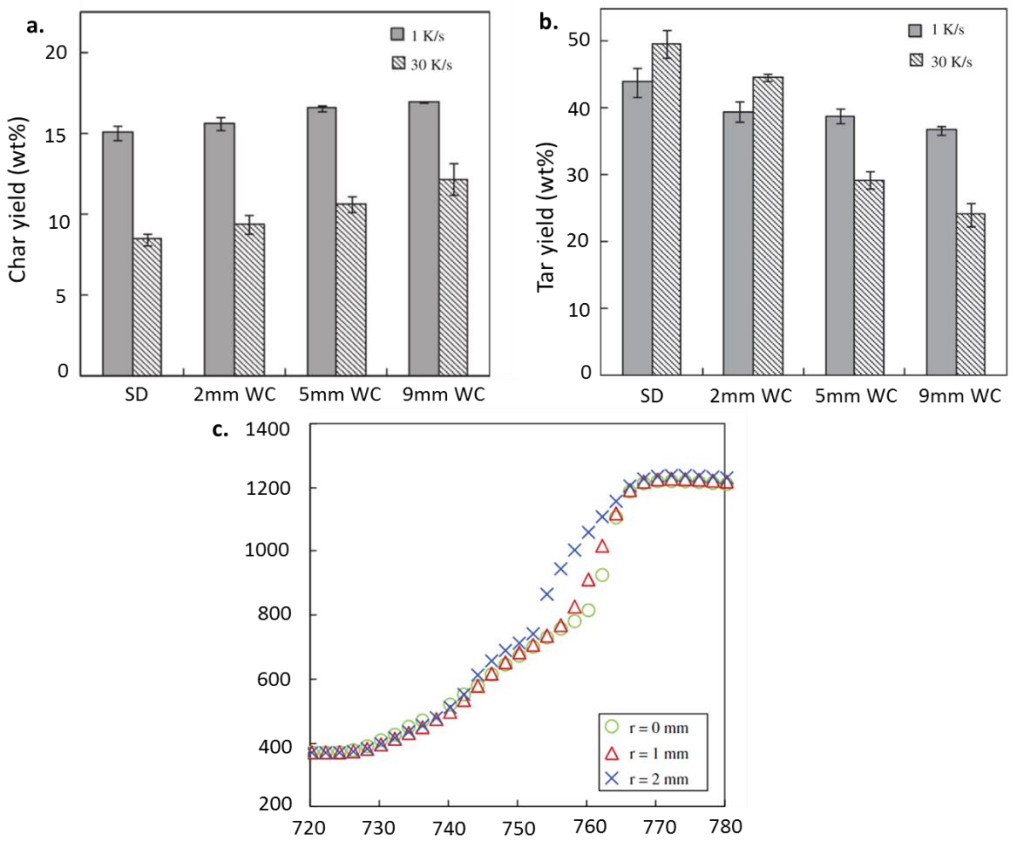


Figure 2.13: (a) Effect of wood size on tar yield; (b) Effect of wood size on char yield; (c) Temperature histories at three locations within the wood cylinder during the pyrolysis at a heating rate of 30 K/s. Sourced from literature [77].

Investigation into feedstock particle size has been an important issue in most research relating to the thermochemical conversion of wood. There seems to be a positive correlation between wood size and rate of thermochemical reaction [77,111,115]. To demonstrate this, a pyrolysis experiment was carried out by Pattanotai *et al.* [77] on the sawdust and three cylindrical wood pellets (WC) of the same tree but of varying radii – 2 mm, 5 mm and 9 mm. This was carried out at two heating rates – 1 K/s and 30 K/s increasing from 400K to 1200K. The result showed a glaring temperature gradient between the center of the wood cylinder and its outermost surface. The difference in temperature between these two points within a particular timeframe was higher than 200K. It took a longer time duration for the temperature of the inner particles to equalize with that of the outer particles – a situation that was non-existent during the pyrolysis of the sawdust sample. The smaller the radius of the wood cylinder, the shorter the time duration for its inner particle temperature to equalize with that of its outermost surface particles. The results showed that sawdust produced more volatiles (translating to more tar production) than the wood cylinder samples especially at the higher heating rate of 30 K/s while the difference in char yield was negligible. They also reported that the sawdust which is produced when the bonds between wood particles have been mechanically broken (i.e. during sawmilling), reacted faster during thermochemical conversions than the wood blocks consisting of particles stacked together by intermolecular bonds. Such intermolecular bonds require additional energy and a longer feedstock residence time to break down. This increases reaction time and limits syngas yield. Figure 2.14 describes the results.

Okoye *et al.* [38] also described some key stages in the thermochemical breakdown of bulk wood as depicted in Fig. 2.14. Considering the density and size of the wood, heat transfer into the inner particles is mostly done by diffusion through the pores and cracks on the surface acting as biological air valves with moisture as heat carriers [38,77]. This explains the fact that despite the higher heat of combustion possessed by plastic over wood, the ignition and combustion of wood is quicker

than that of plastic because unlike plastics which do not possess pores, the pores present in woods allow heat penetration into inner parts of the wood [38].

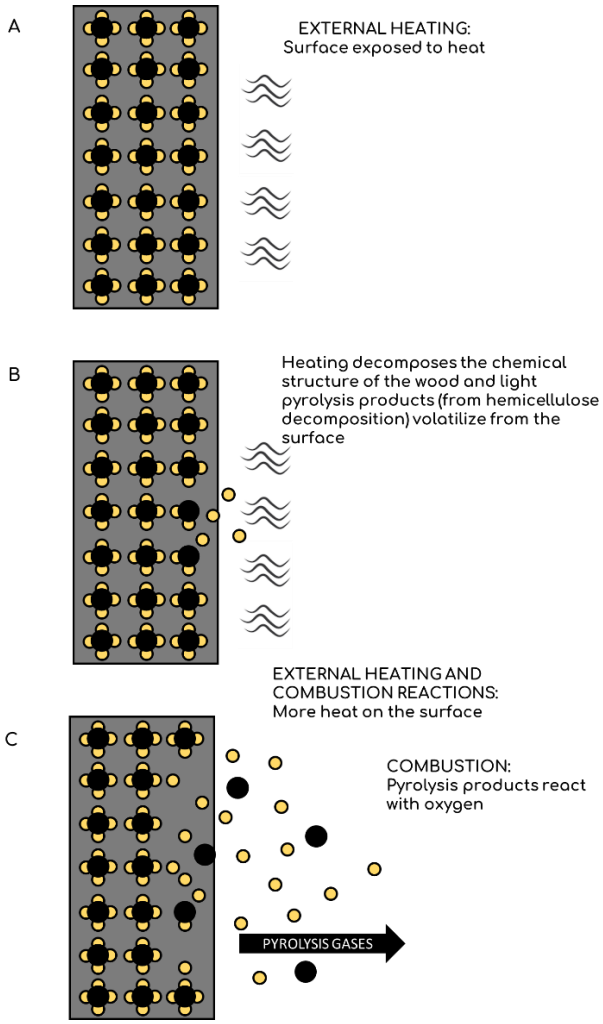


Figure 2.14: A schematic representation of the thermochemical conversion process of bulk wood. Adapted from literature [38].

They further explained that the thermochemical process (pyrolysis) follows two pathways – the *tar-forming pathway* which involves the breaking of the intermolecular bonds between wood particles to form tar, product gas, and other volatiles and the *char-forming pathway* which is the breaking of the intra-molecular bonds of particles to form charcoal.

2.4 Tar in biomass gasification

Tar, as defined by the International Energy Agency (IEA) Gasification Task meeting, is a classification of all organic compounds capable of boiling at temperatures above that of benzene [116,117]. They are the condensable compounds (condensing at <150°C) contained in products of biomass pyrolysis and gasification [118]. Tars generated from biomass usually contain a variety of aromatic compounds including benzene in varying proportions as shown in Fig. 2.15.

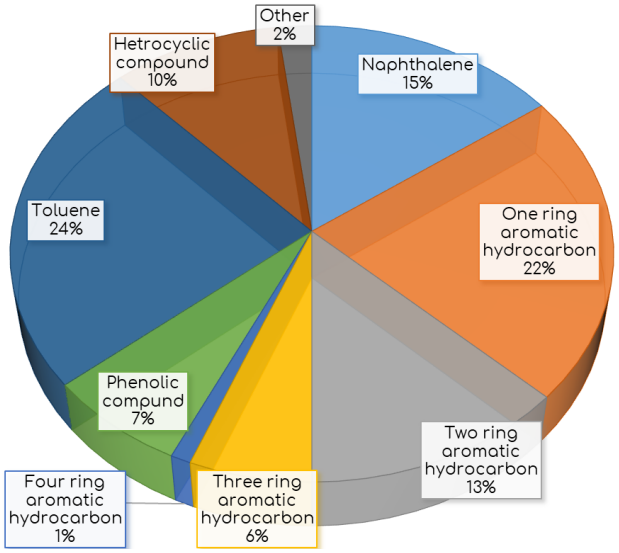


Figure 2.15: Typical composition of biomass tar. Adapted from literature [118].

Tar generation, caused by the release of volatiles during the biomass decomposition phase (or pyrolysis phase) of the gasification process, affects the purity of the syngas product and clogs fuel transfer channels of gasification reactors. Moreover, as previously mentioned several downstream applications of syngas are sensitive to and are easily compromised by the presence of tar and other impurities in syngas. The allowable impurities and tar compositions of syngas acceptable for downstream applications are as presented in Table 2.4.

Table 2.4: *Allowable amounts of tar and impurities in syngas for downstream applications as reported in literature* [119].

Syngas impurities	Application		
	Internal Combustion Engines	Gas Turbine	Fuel cell
Particles (mg/Nm^3)	<50	<30	–
Particulate matter (µm)	<100	<5	<1
Tar (mg/Nm^3)	<10	<5	<1
Alkali metals (mg/Nm)	–	<0.24	–

2.4.1 Tar cleaning techniques

Techniques for tar reduction in gasification as reported in literature can be broadly categorized into primary methods (or pre-gas production tar removal) and secondary methods (or post-gas production tar removal) as summarized in Fig. 2.16.

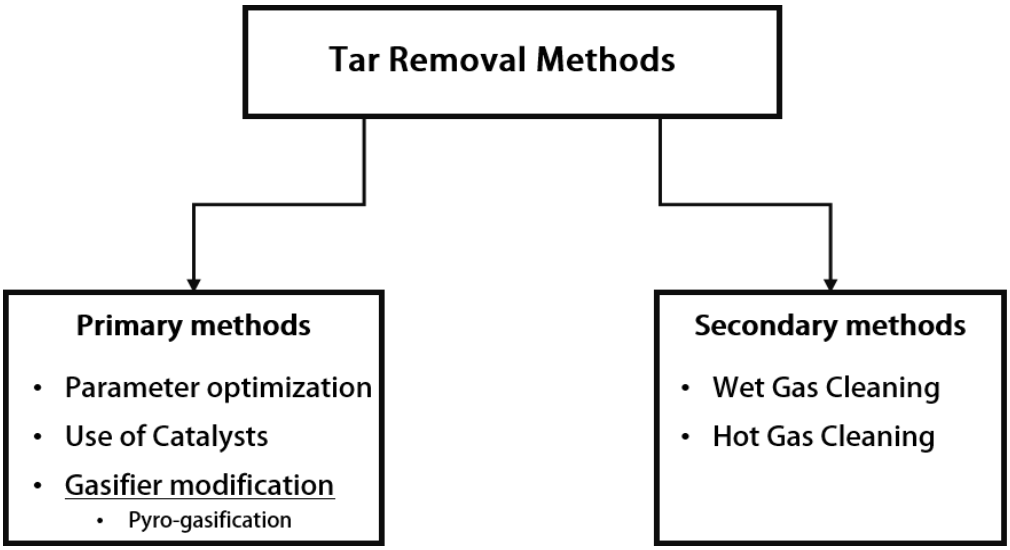


Figure 2.16: Classification of tar removal methods with a focus on pyro-gasification. Adapted from literature [118].

2.4.1.1 Secondary Tar cleaning

The secondary (or post-production) tar cleaning methods developed in literature, basically involve the transfer of the tar-laden syngas produced from a gasifier to a separate cleaning reactor for tar separation or tar cracking processes. Classified under the secondary methods is the wet gas cleaning which is based on tar condensation at low temperatures. This method involves the use of technologies like the spray tower, venturi, venturi and spray, venturi and cyclonic demister and the vortex scrubbers to condense the tar when the impure syngas is passed through it. Increasing the water flow rate of the scrubber has been reported to reduce the tar concentrations in the syngas to as low as 20–40 mg/Nm^3 after cleaning [118,120]. This is also in corroboration with a study by Surjosatyo [121], whereby an analysis was conducted on the tar composition of syngas produced from coconut shells in a downdraft gasifier connected to a venturi scrubber. Tar content in the syngas was observed to be significantly reduced to 125 mg/Nm^3 from 675 mg/m^3 with an increase in the water flow rate of the scrubber. Conversely, in hot gas cleaning, the syngas produced in a primary gasifier is transferred to a separate secondary high-temperature gasifier for further cracking of the tar contained in the presence of a catalyst at elevated temperatures. Though regarded as a very expensive procedure, the hot gas cleaning at elevated temperatures between 500 – 900°C has been found as the most effective in tar reduction and improvement of syngas heating value to date, whereby a 98% tar to hydrogen conversion efficiency was attained [118].

The use of catalyst in a secondary hot gas cleaning process to eliminate or minimize tar at low gasification temperatures has also been explored. Wang *et al.* [122] in their study observed Ni/dolomite catalyst was very effective in the removal of tar already produced from biomass. A 97% tar conversion was observed at gasification temperatures as low as 750°C. This was achieved with a minimum steam to carbon ratio of 2.5 at the said temperature which helped in preventing the coke formation on the catalyst surface. A study on the syngas and methane-rich gas production via steam gasification of from wood was carried out by Mudge

et al. [123] at optimum process conditions with a trimetallic Ni-Co-Mo catalyst on silica-alumina doped with Na. The results showed that tar production alongside the syngas was prevented as long as the catalyst remained active. Additionally, the increase to higher gasification temperatures promoted an increase in the rates of gasification reactions and supported hydrogen production.

2.4.1.2 Primary Tar cleaning

On the contrary, primary (or pre-production) tar cleaning methods involve employing the reduction of tar as gasification progresses inside a reactor before the production of syngas and may not require syngas transfer to a secondary purification reactor. These methods of tar cleaning are predominantly thermally based whereby tars are cracked at very high gasification temperatures. Tars in the gaseous state can react with gases such as hydrogen (also known as hydrogasification tar cracking); carbon dioxide; or steam (also known as gasification tar cracking) present in the product gas; or in inert conditions (also known as thermal tar cracking) [124].

Primary tar cleaning can be achieved by adopting either or all of the following techniques:

a. A selection of ideal reactor operating parameters such as temperature, equivalence ratio, oxidizing agent/biomass ratio, steam/biomass ratio and feedstock residence time;
b. The use of catalysts and additives for tar cracking; and
c. Modifications in Gasifier design; whereby conventional designs of gasifiers are altered to minimize tar mixing with syngas during gasification [118].

a. Primary Tar cleaning by selection of ideal reactor operating parameters

Several notable research within the context of tar cleaning by selection of ideal operating parameters have been reported in literature. Subject to the type of tar and residence time, thermal cracking reactions occur at temperatures greater than 1200°C. However, the reaction rate has largely been attributed to the kind of

tar involved. Zwart [124] reports that tars and oils generated from biomass pyrolysis are usually more reactive than those generated from coals, thus making them easier to crack. Tar reaction rates are also dependent on the type of gasifying agent involved in the thermal reaction with the tar. The use of steam and carbon dioxide (in a gasification tar cracking process) reportedly increase the rate of tar cracking. Conversely, the use of hydrogen at high pressures (in a hydrogasification process) tends to reduce the reaction rates of tar cracking reactions. This is due to the additional hydrogenation of aromatic rings which result in high concentrations of methane as tar cracking reactions progress [124]. Sun *et al.* [125], investigated the influence of equivalence ratio (ER) and the introduction of secondary air in a gasification reactor. Besides other improvements observed on the fuel qualities of the syngas produced and the overall process efficiency, the increase in the ER from 0.20–0.26 in a secondary air process led to a 59.9% reduction in the syngas tar composition. The influence of temperature on the yield of tar and other pyrolysis products from the pyrolysis of wood, coconut shell, and straw, was also a subject of study by Fagbemi *et al.* [126]. The effect of temperature was evident as the quantity of tar produced from the three samples attained its maximum at 500°C, after which it dropped increasingly as the temperature rose above 500°C. The maximum tar yield from a variety of biomass materials at 500°C have also been confirmed in another study [127]. A physical evidence of this can be observed in the lab-scale pyrolysis of the eight LCB materials conducted in this study, whereby thick brownish-yellow clouds were visible in the gas condenser at 500°C. A possible explanation to this is that at lower pyrolysis temperatures, the heavy proportions of volatiles do not initially evolve from the biomass feedstock as gases but as viscous oil mixed with moisture. This oil is later evaporated to condensable gaseous compounds as temperature rises to 500°C and then exits the reactor alongside other lighter pyrolysis gases (easily generated at lower temperatures). Therefore, at 500°C, thick clouds of condensing gaseous tar compounds were observed to build up in the condenser. By varying gasification parameters such as temperature, pressure, and S/B ratio, Mayerhofer *et al.* [128], were able to vary the

syngas composition and tar content in the syngas generated from a steam allothermal BFB gasifier. Among the observations made, was the reduction in the composition of some compounds present in the tar (such as the heterocyclic and light aromatic compounds), with an increase in temperature. Moreover, at elevated temperatures, tar reduction was more significant with an increase in the S/B ratio. Meanwhile, at atmospheric pressure, it was observed that the composition of some other tar components such as naphthalene increased moderately with a rise in gasification temperature.

b. Primary tar cleaning with the use of catalysts and additives

Amongst a variety of additives and catalysts, the dolomite bed additive and catalysts such as nickel, activated carbon, palladium have been used extensively for the catalytic cracking of tar at low gasification temperatures. A lab-scale fluidized bed gasifier was used to investigate the influence of temperature varied from 400 – 600°C on the catalytic gasification of bamboo by Wongsiriamnuay *et al.* [110]. Alongside other observations made such as improvements in syngas yield, heating value and carbon conversion efficiency, 80% tar conversion was attained with an air/steam gasification at a low temperature of 400°C. This was attributed to the presence of the dolomite bed additive used. A catalytic hot gas clean-up using a variety of nickel-based catalysts with and without calcined dolomite as the bed additive was conducted by Corella *et al.* [129]. The results show that tar conversions between 97% and 99.5% were attained. Tar proportion in the gas was reduced to 1.3 wt% when the catalysts were used alongside the calcined dolomite bed additive, as opposed to a 6.6 wt% tar proportion without the additive. In a study conducted by Jin-Won Kim *et al.* [81], the air gasification of plastic wastes was carried out to investigate the influence of activated carbon and dolomite for tar removal and hydrogen production. In their conclusion, activated carbon was found more effective in tar clean up than dolomite. An increase in the amount of activated carbon of up to 640 g resulted in higher efficiencies in tar removal and twice the production of H_2. In another study, a catalytic tar hydrocracking technique employing a palladium catalyst in a pilot-scale updraft gasifier was

conducted by Huang *et al.* [106]. The aim was to catalytically convert the tar to useful hydrocarbons to minimize its concentration in the syngas generated from wood chips. At a constant gas flow rate of 20 Nm^3/h, the tar conversion rates attained, increased from 44.9% to 78.1% and then to 92.3%, as temperature increased across three regimes – 500°C, 600°C, and 700°C respectively. Higher conversion rates of up to 98.6% were also attained at lower gas flow rates. However, a low syngas composition consisting of higher CO proportions (18-23%) than H_2 (8-10%), was observed in the product gas mix. It was also reported that at some point, the heat loss of the catalyst led to a significant deactivation of the catalyst due to inconsistencies in the heat and mass transfers occurring in the catalytic bed. This further led to a reduction in tar conversion efficiency.

c. Tar reduction by gasifier design modification

Research has also focused on the re-design or modification of conventional gasifiers for tar clean-up of syngas. Schmid *et al.* [130] in a recent study, developed a customized dual fluidized bed reactor separated into an air/combustion chamber and a fuel/gasification chamber connected by upper and lower fluidized loop seals (see Fig. 2.17).

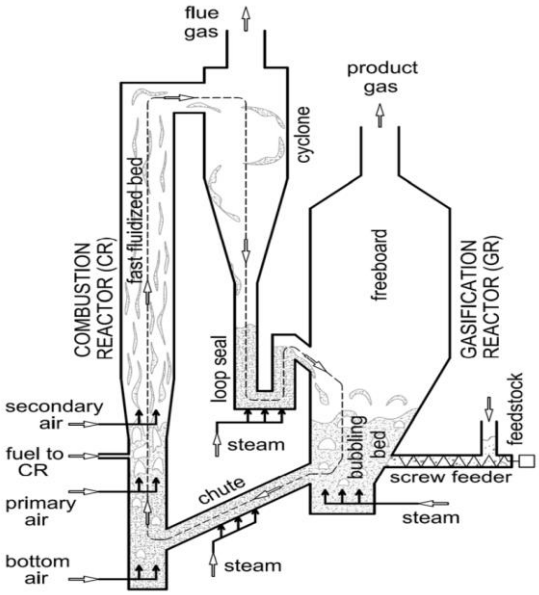


Figure 2.17: Schematic diagram of a typical dual fluidized bed gasifier. Sourced from literature [130].

The system was designed to generate syngas with low tar concentrations and completely free of nitrogen by dispersing the solid biomass particles in a downward direction, thereby restricting the generation of volatiles in the top parts of the reactors. It was observed that by increasing the fluidization velocity of the hydrocarbon, the conversion was improved. This was made possible through a rapid and continuous exchange of the fluidized solid particles between the two chambers, which in-turn minimized tar concentration in the syngas produced.

The use of catalysts and the modification of gasification parameters particularly in hot gas tar cleaning are the most common methods employed for the tar reduction. High tar removal efficiencies have been achieved by employing the aforementioned methods. However, high costs of operation associated with hot gas tar cleaning and the use of expensive catalysts make these methods commercially unattractive for scale-up.

2.5 Pyro-gasification

Conventional biomass gasification is comprised of various superimposing chemical reactions which make each phase difficult to control and optimize independently in a conventional single-stage reactor. This also makes it difficult to prevent the mixing of tars and char produced during the biomass decomposition phase. The mixing of tar-forming volatiles and char negatively affects the gasification phase process and contaminates the syngas produced from char gasification [89]. Ideally, the gasification of char alone in a volatile-free atmosphere would enhance the rate of char reaction with the gasification agent, improve syngas purity and the overall efficiency of the process as well as minimize tar formation.

Pyro-gasification may be categorized under the primary tar removal method by reactor modification. It is a systematic separation of the pyrolysis stage and the gasification stages (partial oxidation and reduction) of a gasification process, to eliminate the unwanted pyrolysis product (tar). This thereby leaves only the carbon-rich char residue behind, to progress to the gasification stages. It may be described from a different perspective, as a hybrid or multi-stage thermochemical

process, primarily involving a combination of pyrolysis and gasification as one continuous process, but controlled independently to restrict tar from advancing alongside char to the critical stages of syngas production.

It thereby ensures that only a carbon-rich char residue with negligible tar composition is left to react with the gasifying agent in the partial-oxidation and reduction stages. The aim of adopting this technique in this study is to gain some independent control of the type of pyrolysis products advancing as reactants for the gasification phase reactions. It also ensures the biomass conversion at each phase is carried out under optimized conditions to enhance syngas production.

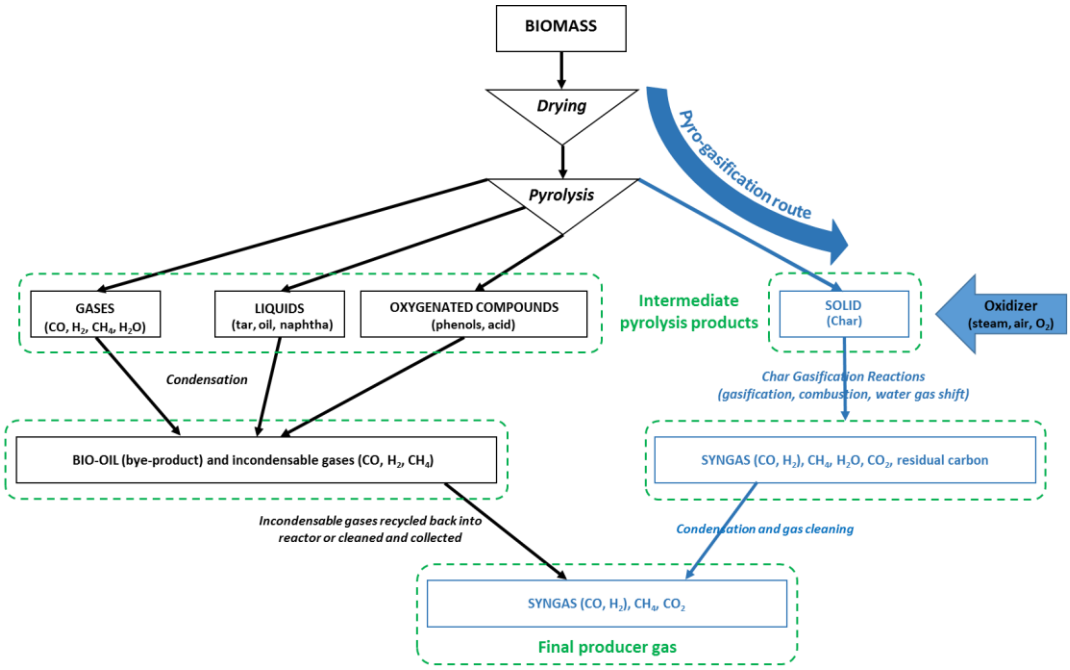


Figure 2.18: The pyro-gasification pathway. Adapted from literature [89].

In comparison to conventional gasification, pyro-gasification as depicted in Fig. 2.18 is seen to differ in the description from Fig. 2.6, beyond the pyrolysis stage. In Fig. 2.18 char is isolated from other pyrolysis products after being formed at the pyrolysis stage. It is the only pyrolysis product allowed to react with steam (the gasifying agent oxidizer). This is in contrast to conventional gasification whereby the char, tar, and other pyrolysis products all react with the gasifying agent in the partial combustion and reduction stages of the process.

The pyro-gasification technology may not have been extensively reported in literature, however, pilot studies relating to it are under investigation by the Asian Institute of Technology (AIT), Thailand [118], the Danish Technical University (DTU), Denmark [131], and Karlsruhe Institute of Technology, Germany [89].

The combined heat and power (CHP) system design developed by the Danish Technical University named the *Viking* (Figs. 2.19 and 2.20), involves an integrated two-stage type of pyro-gasification process consisting of a modified down-draft gasifier [89,132]. The gasifier is equipped with independently controlled biomass pyrolysis and gasification chambers, with a narrow partial oxidation channel, all merged into a single overall unit as described on its schematic process diagram (Fig. 2.20). It was designed to first dry and pyrolyze the biomass feedstock in the cylindrical pyrolysis chamber of the system in an absolute inert atmosphere. A rotating screw conveyor was installed in this cylindrical chamber to transfer the biomass feedstock at controlled speeds across the cylinder as it pyrolyzes to form char and tar. The feedstock inlet end of the cylindrical pyrolysis chamber is heated to around 50°C for drying the feedstock as it is fed into the pyrolysis chamber. Meanwhile, temperature increases as the feedstock moves across the pyrolysis cylinder towards the char and tar products outlet point at the other end of the pyrolysis cylinder, where the pyrolysis temperature gets to about 600°C. The heating rate is controlled by the speed of the screw conveyor transferring the feedstock from the low-temperature end to the high-temperature end of the cylindrical pyrolysis chamber. Meanwhile, beyond this point of exiting the pyrolysis chamber, the mixture of char and tar is allowed to pass through a narrow partial oxidation corridor supplied by an airflow. This allows for oxidation of the tar by air, resulting in a considerable reduction of up to 500 mg/Nm^3 in tar volume. This exothermic oxidation reaction also provides the heat required for the endothermic gasification reaction of the char when it is eventually deposited in the gasification chamber. Steam may be used as the oxidizer in the gasification chamber. With this system, the operating conditions of each phase can be controlled independently and optimized to minimize tar. The product gas exiting

the system has been observed to contain about 32% hydrogen and 16% carbon monoxide with negligible tar and methane composition. Currently, the system capacity is rated at about 200 kW_e with a *potential scale-up to about 500 kW_e* [89,132].



Figure 2.19: The Viking pyro-gasification combined heat and power (CHP) demonstration and research plant. Sourced from literature [131].

McKendry [91], also reported on a previously proposed process with a similar principle to pyro-gasification, which entails a two-stage, two-reactor hybrid process for the improvement of syngas quality. Its process involves an initial pyrolysis of the biomass feedstock in the first reactor heated externally at temperatures of up to 600 °C, thereby forming char and releasing tar-laden gases which further react with steam fed into the reactor to crack the tars. Meanwhile, in the second phase gasification reactor, only char transferred from the pyrolysis reactor is gasified to produce syngas which is suitable for use in spark-ignition gas engines. Another recent study similar to pyro-gasification which involves a simultaneous production of syngas and biochar from hazelnut pruning using a downdraft gasifier, has also been reported to improve syngas LHV from 3.84 MJ/Nm^3 to 4.45 MJ/Nm^3 [133].

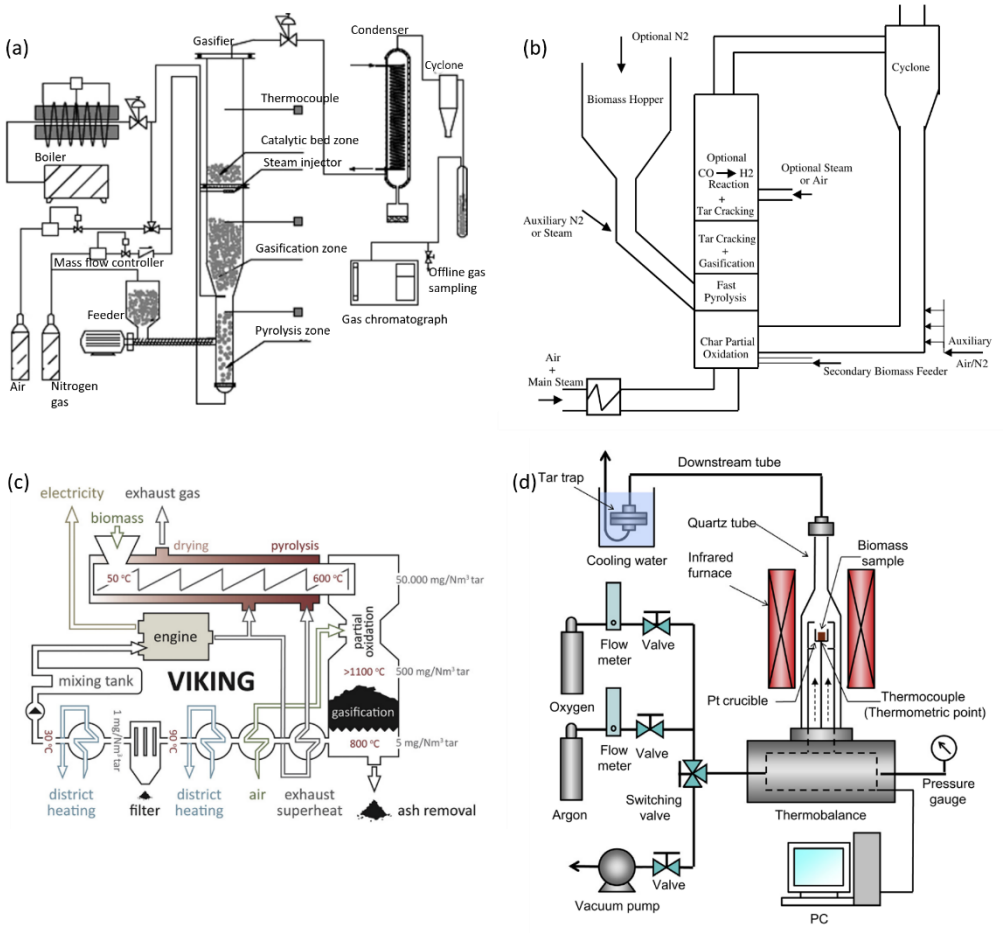


Figure 2.20: Schematic diagrams of pyro-gasification reactor designs reported in literature by (a) Alipour et al.[134]*; (b) Chen et al.* [135]*; (c) Ahrenfeldt et al.* [131]*; (d) Pattanotai et al.* [77].

Other literature on pyro-gasification and similar processes have been reported by Alipour *et al.*[134], Chen *et al.* [135], and Pattanotai *et al.* [77] (Fig. 2.20 a, b, and d). In their study, Alipour *et al.* investigated the production of syngas from coconut shell by integrating pyrolysis and air-steam gasification processes on a lab-scale fixed fluidized bed gasifier. Amongst the parameters investigated were the reaction temperature equivalence ratio, and steam/biomass ratio. A hydrogen and syngas yield of 83.3 and 485.9 g/kg of feedstock were attained respectively under optimized conditions, with a syngas LHV of 12.5 MJ/N m^3. However, this was attained by incorporating a catalytic tar cracking reaction by passing the tar-laden syngas produced in the char gasification zone through a dolomite catalyst on the

catalytic bed zone of the reactor. A similar method (Fig. 2.20 b) was adopted by Chen *et al.*[135] in the production of syngas from miscanthus pellets. However, their study was carried out on a circulating fluidized bed and involved a high temperature tar cracking process and not a catalytic tar cracking reaction. The concept integrated partial oxidation, fast pyrolysis, gasification and tar cracking reactions occurring in different zones of the reactor. Results from this study show that gas yields of up to 2 Nm^3/kg was obtainable with tar concentration of 75 mg/N m^3. An insufficient reactor temperature, low efficiency of the cyclone, rigid biomass feeding point and poor biomass feedstock particle size, were some of the constraints reported in their study [135]. Meanwhile, Pattanotai *et al.* [77] in their study of the gasification characteristics of a Japanese cypress char of different wood cylinder sizes and sawdust, adopted a different reactor design (Fig. 2.20 d) and approach but not for the purpose of syngas production. It involved a variation of the reactor temperature between 673 and 1173 K, incorporating both the pyrolysis and gasification phases with that temperature bracket. However, to differentiate both phases, a 20% oxygen was introduced to the existing inert atmosphere previously initiated with aid of an argon flow.

An investigation into the strengths and limitations of these pyro-gasification systems over the conventional single-stage reactors was also carried out by simulation [89]. The results reveal a significant reduction in syngas tar concentration to 10 mg/Nm^3, a high char thermal conversion efficiency of 98% and an equally high gasification efficiency of about 81% [89].

Meanwhile, for this research, a lab-scale pyro-gasification rig was developed for investigating the pyro-gasification of sawdust blends of various wood species. Data collated from this exercise have been presented and discussed in detail in Chapter 6.

Due to a lack of open reports on extensive operation and study of existing pyro-gasification pilot plants, there is insufficient information to truly ascertain the challenges of scaling-up the systems to commercial status. However, based on

aforementioned investigations reported so far [74,89,131,132,134,135], some possible bottlenecks which may hinder its development are discussed below:

a. System Complexity

So far, existing pyro-gasification systems are very complex, consisting of several interconnected units and processes. A notable instance is the Viking, which requires the recycling of heat expelled for the partial oxidation channel, char gasifier and engine exhaust channelled for use in the pyrolysis zone and district heating. In as much as this is economically very attractive, the complex piping connections and moving parts of the screw conveyer in the pyrolysis chamber will require periodic rigorous and expensive maintenance operations to maintain the overall system efficiency. The removal of ash deposits also proved to be problematic, as the Viking required regular removal of ash deposits from the grate which often resulted in a pressure drop across the system [131].

b. Oil Blockage in Pipes

Blockages in the pipes channelling bio-oil released during the pyrolysis phase of a pyro-gasification process is usually expected. This, however, depends on the viscosity of the bio-oil. For instance, after some tests were conducted with the pyro-gasification experimental set-up (Fig. 3.4), it was observed that the bio-oil extraction pipe connected to the exit at point C of the reactor was often blocked by very viscous bio-oil residue. Such blockages occurred when the bio-oil flowing through the pipe flowed from the hot section of the pipe inserted in the cylindrical furnace to the cooler section of the pipe away from the heat of the furnace. This oil, coming in contact with the colder surface of the pipe increasingly became more viscous before reaching the condenser 1, thereby reducing its flow and subsequently causing blockages. This required the passing of compressed air through the pipe to blow-off the trapped bio-oil in the pipe after each run. However, a more permanent solution would be, to increase the diameter of the bio-oil pipe, and wrap it with heating coils to maintain high temperatures along

the pipe. This is expected to preserve the high temperature of the oil and maintain a low viscosity as it flows towards the *Gas condenser 1*.

c. Feedstock Compatibility

One common problem with biomass thermochemical conversion is the wide variation in feedstock properties. As previously mentioned, biomass feedstock properties vary widely, based on type, specie, geographical, geological and climatic conditions of their source. This limits the use of pyro-gasification systems for the conversion of a wide variety of biomass feedstock. Pyro-gasification may be best suited for feedstock with moderate to high fixed carbon contents capable of forming a carbon-rich char mass sufficient for gasification in the gasification phase of the process. Thus, a feedstock with high moisture and volatile matter composition may be difficult to utilize unless pre-treated adequately to meet standards. The pyrolysis chamber of the Viking reactor was, however, reported to handle feedstock with moisture contents as high as 45%. In the case of woody biomass feedstock, milling to a suitable particle size may be required. It was observed that blockages occurred in the feedstock conveyor of the Viking by larger wood particles stuck in the conveyor, which led to unplanned shutdowns. Also, feedstock agglomeration may occur frequently during the transfer of biomass particles from the inlet point (*i.e.* drying point) through to the char and tar exit point in the pyrolysis chamber. This could result in a reduction in the overall system efficiency.

d. Syngas suitability for downstream application

Syngas produced from pyro-gasification systems may require additional cleaning before use as feedstock for downstream processes or applications like in fuel cells, gas turbines, internal combustion engines with slim tar and particulates tolerance thresholds (see Table 2.4). This may result in additional installation and operational costs asides that incurred in setting up the pyro-gasification plant. However, within the scope of this study, the purity of the syngas produced through the pyro-gasification experiments conducted was not tested by standard

procedures to ascertain its suitability for direct use in some downstream applications. The ignition of the three-cylinder spark-ignition engine connected to the Viking proved difficult and thus required the use of natural gas to start-up before switching to the syngas supply. Moreover, engine power was observed to have dropped, while a conversion efficiency of 28% from syngas to mechanical energy was attained [131].

2.6 Concluding remark

In this section, understanding the role of the structural components of an LCB and the individual thermal decomposition behaviours as they affect the yield and fuel properties of the final biofuel product was vital to this research. Moreover, the influence of the biomass properties, particle size and process parameters on its thermochemical conversion are also of utmost importance. In addition, the principles of conventional pyrolysis and gasification of lignocellulosic biomass and associated factors, as well as various tar removal techniques reported in literature were extensively reviewed. Finally, an introduction to pyro-gasification, its working principles and a review of recent literature on related studies was also carried out.

The principle of pyro-gasification is primarily based on the contribution of hemicellulose, cellulose and lignin to the production of char and tar/bio-oil in the pyrolysis phase, and the controlled progression of char to the gasification phase. The expulsion of tar-forming volatiles was attributed to the thermal decomposition of hemicellulose and cellulose, while, the formation of char was as a result of residues of lignin and hemicellulose after volatilization. Tar extraction after volatilization is therefore key to minimizing its presence in the product gas after char gasification.

Tar presence in syngas impact on its yield and undermines its quality for use in several downstream applications. As reported elsewhere, several techniques have been adopted to minimize tar in the final syngas product. Most of these involve high-temperature input from external sources which are rather expensive, while

others involve the installation of additional post-gas cleaning components. Between both categories of techniques, the high-temperature tar cleaning above 1000°C has proved more effective. The use of catalysts and their mixtures with bed materials, which is also thermally based have also been reported to prove effective as well. However, catalyst deactivation is inevitable due to the continuous poisoning of the catalyst as a result of its excessive contact with Tar which form a layer of coating on the catalysts. This could prove to be a very expensive option during extended use in large-scale operations.

This research therefore, adopts the use of pyro-gasification for the conversion of wood wastes to syngas. Primarily, this is classified as a pre-syngas production cleaning technique. However, contrary to other pre-syngas cleaning techniques, which require high temperature input or/and use of catalysts, tar extraction from the reactor is carried out mid-way through the pyro-gasification process at low pyrolysis phase temperatures of 400–600°C. Therefore, literature on the dynamics of the pyrolysis of biomass and the contribution of the decomposition of its components to the yield of its pyrolysis products was extensively reviewed. The pyro-gasification technique in this study allows for the independent control of the pyrolysis phase parameters and gasification phase parameters of the whole conversion process. This makes it more flexible than other techniques discussed above. Moreover, the outright removal of tar/bio-oil within pyrolysis temperatures makes it less energy-intensive than the high temperature tar cleaning methods reported in literature. In pyro-gasification, only the carbon-rich char residue progresses to the later stages of the gasification process without other products formed in the pyrolysis stage. Therefore, the gasification phase reactions are strictly char-based reactions which would be more beneficial for the production of hydrogen-rich syngas if steam was used as the gasifying agent. Moreover, the gasification phase reactions of steam with the carbon-rich char would be more efficient due to the early extraction of tar from the reactor. Tar is known to inhibit gasification reactions, therefore its prevention from progressing

to the gasification phase would improve syngas yield, heating value and purity for downstream applications.

By the independent control of the pyrolysis phase parameters, high tar removal can be promoted by adopting suitable heating rates. The adoption of high heating rates in the fast pyrolysis of biomass was reported to support high tar generation and produce char with very high reactivity which is ideal for gasification reactions in the gasification phase of the process. Meanwhile, with regards to sample size, sawdust particle sizes are understood to be most ideal for maximum tar removal.

Chapter 3

Materials and Methods

3.1 Introduction

This chapter presents the materials and equipment used, as well as the methods employed in carrying out the experiments required for each objective. Descriptive details and discussions of the experimental results for each objective have been presented in subsequent chapters.

3.2 Wood sampling

3.2.1 *Identification and harvesting of wood species*

In this research, eight wood species were utilized. They include four IAPs namely – Eucalyptus, Jacaranda, Bugweed and Poplar, and four tropical hardwoods – the African mesquite, African mahogany, African oilbean and Opepe.

The IAP wood samples were selected for investigation, primarily due to their severe environmental impacts in Southern Africa and classification as category 1 and 2 invaders [136]. The identification of these species was made possible by consultations with botanists in the School of Animal, Plant and Environmental Sciences (APES) of the University of the Witwatersrand. Assisted by a qualified field botanist from Servest Pty Johannesburg, the samples were harvested from a heavily invaded location in the Gauteng province of South Africa. Likewise, the tropical hardwoods were selected primarily due to their popular use as raw material from which enormous amounts of wastes are generated in the sawmill and allied industry in West and Central Africa. This selection was further supported by useful information on their fuel properties as reported in literature [38,39]. The identification and harvesting of these tropical samples were carried out in an approved government-owned forest reserve located in Enugu State, South-Eastern Nigeria, and aided by a qualified botanist in the Ministry of Environment and Mineral Resources. Furthermore, evidence of their historic use as raw material for commercial charcoal production and fuel for blacksmithing was gathered from rural householders in the host community.

For uniformity, all wood samples were harvested from the trunks of the trees, and the main stem of the shrub, in the case of the Bugweed. Both sets of samples were transported to the University of the Witwatersrand laboratories for pre-treatment.

3.2.2 Wood sample pre-treatment

In preparation for the experiments, some wood lumps due to their hardness were first sawn into smaller blocks using a vertical band saw (Mössner Rekord SSF 520), from which sawdust produced during sawing was carefully collected in plastic sampling bags to avoid contamination. Some of the wood blocks were also sun-dried and size reduced to sawdust particles using Restec SM 200 biomass sawmill. The collected sawdust was then sieved through a Sigma-Aldrich no. 40 mesh sieve with a nominal opening of 0.420 mm as used and described elsewhere [39], air-dried and stored in a desiccator to keep the samples dehydrated.

For the bulk density, however, wood blocks of each sample were cut into regular shapes of known dimensions.

3.3 Experimental

3.3.1 Structural Analysis

The procedures adopted below for the determination of the structural and non-structural components of the samples were as described in literature [64,137,138]. Soxhlet extraction of extractives was performed at 70°C for 4 h on 2.5 g of sawdust of each raw sample using 300 mL acetone solvent. The extracted samples were first air-dried and then oven-dried to constant weight at 105^{o}C. The percentage weight of extractives was calculated by subtracting the weight of the extracted sample from that of the raw sample dried at 105^{o}C.

Sample treatment for the hemicellulose composition was performed by adding 150 mL of 500 mol/m^3 NaOH into an Erlenmeyer flask containing 1 g of the extractive-free sawdust and boiling the mixture for 3.5 h in a hot water bath. Vacuum filtration and washing of the residue using deionized water was

performed until Na+ was undetectable (i.e. at pH approximately 7) and the residue was allowed to oven-dry to constant weight at 105°C (see Fig. 3.1). The oven-dried residue was cooled in a desiccator to room temperature and weighed using a Mettler Toledo PB1502-S weighing balance.

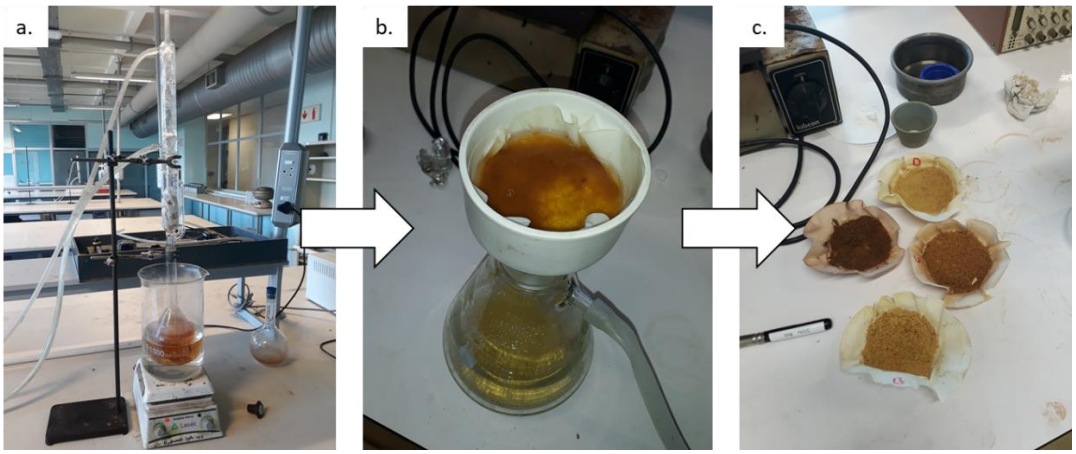


Figure 3.1: (a) The soxhlet extraction process, (b) the vacuum filtration of the NaOH and extractive-free sample mixture after boiling for 3.5 h, and (c) the oven-dried sample residue.

In determining the lignin composition, 0.3 g of the extractive-free sawdust of each sample was hydrolysed for 2 h in a test tube by adding 3 mL of 72% H_2SO_4 and performing a subtle agitation of the mixture at 30 min intervals. Afterward, the mixture was diluted with 84 mL of distilled water and run in an autoclave at 121°C for 1 h. The autoclaved solution was vacuum-filtered and the residue oven-dried at 105°C. The acid-insoluble lignin (AIL) was then determined by weighing the ash left over after incinerating the oven-dried residue (constituting of ash and AIL particles) in a furnace at 575°C for 6 h. Whereas, the acid-soluble lignin (ASL) composition was ascertained by measuring the absorbance of the hydrolysate at 205 nm (recommended for woods) [139].

3.3.2 Proximate and Ultimate Analysis

Proximate analysis is the estimation of the mass percentages of the moisture content (MC), volatile matter (VM), fixed carbon (FC) and ash contained in a

carbonaceous material. Meanwhile, ultimate analysis is used to measure the percentage elemental (C, H, N, O, S) composition of such materials [140].

Proximate and ultimate analyses are important in the evaluation of the conversion efficiency and emissions potentials of combustible materials [141]. They also are good indicators of a fuel's quality and can be used to predict the final chemical composition of the syngas [31]. Ultimate analysis has also been employed in literature for the empirical determination of the HHV of solid, liquid and gaseous fuels [35,141,142]. Sahito & Siddiqui [140] also reported on the use of the proximate composition of biomass for HHV determination.

In this study, the proximate analysis was carried out on the samples by adopting standard procedures as described in ASTM E1756-08, ASTM E872-82 and ASTM E1755-01 [143–145]. The FC composition was then obtained using Equation 3.1:

$$\%FC = 100 - \%(MC + VM + Ash) \quad (3.1)$$

3.3.3 Ultimate analysis

In conducting the ultimate analysis, a Flash 2000 analyzer (Thermofisher Scientific, USA) connected to a source of oxygen gas (for combustion) and a source of helium gas (as a carrier gas), was used to determine the percentage composition of C, H, N, and S, while the percentage oxygen composition was calculated using Equation (3.2):

$$\%O = 100 - \%(C + H + N + S) \quad (3.2)$$

3.3.4 Fuel Ratio

The fuel ratio (FR) of a solid fuel is a factor of its fixed carbon and volatile matter compositions. It is expressed as the ratio of its fixed carbon (FC) to its volatile matter (VM) content obtained from the outcome of the proximate analysis.

3.3.5 Higher Heating Value

The gross calorific value (GCV) or higher heating value (HHV) refers to the quantitative energy content of a combustible material. The HHVs of the raw wood

samples were determined experimentally using a Drycal Modular Oxygen Bomb Calorimeter. The experimental procedure was carried out in triplicate of each sample for accuracy of results.

3.3.6 Bulk and Energy Density

To determine the bulk density, $\boldsymbol{\varrho_B}$ of the samples, the wood lumps were first cut into cubes and cuboids of known shapes. To calculate their volumes, the dimensions of the wood blocks were first measured using an Absolute Digmatic electronic vernier caliper. The samples of known volume were then weighed to determine their masses with the aid of a Radwag PS 750.R2 weighing scale (see Fig. 3.2). $\boldsymbol{\varrho_B}$ was then calculated using Equation (3.3) [39,146]:

$$\varrho_B = \frac{Mass\ of\ wood\ block\ (g)}{Volume\ of\ wood\ block\ (cm^3)} \tag{3.3}$$

Where $\boldsymbol{\varrho_B}$ = Bulk density (g cm^{-3})

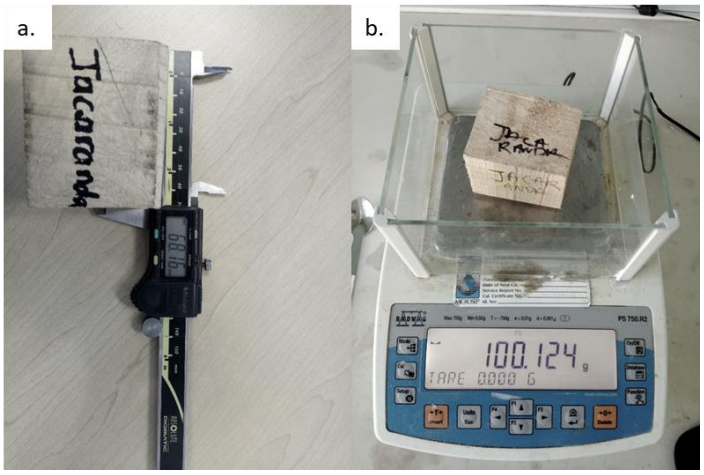


Figure 3.2: Measurement of dimensions and mass for the bulk density of the Jacaranda wood sample.

Meanwhile, the energy density (ED) is the energy contained in a unit volume of a combustible material. This was calculated for each wood sample using Equation (3.4) [147]:

$$ED = \varrho_B \times HHV \tag{3.4}$$

Where ED = Energy density (GJ/m^3);

ϱ_B = Bulk density (g/cm^3);

HHV = Higher Heating Value (MJ/kg)

3.3.7 Char yield and reactivity

The values of the char yield and reactivity of the individuals were determined with the aid of their TGA and DTG results. The TGA procedure is described in Sub-section 3.4.1. The char reactivity of the samples is regarded as the peak rate of thermal decomposition of the samples observed in the char degradation part of their DTG thermograms after volatilization [77]. Meanwhile, equation 3.5 was employed in determining the char mass yields of the individual samples.

$$\text{Yield}_{\text{char}} = \frac{\text{m}_{\text{char}}}{\text{m}_{\text{raw}}} \times 100\ \% \qquad (3.5)$$

Where:

$\text{Yield}_{\text{char}}$ = mass yield of char (%);

m_{char} = mass of char (mg);

m_{raw} = mass of raw wood samples (mg).

Other useful information like the *initial decomposition temperature (IDT)* was also derived from the derivative thermogravimetry (DTG) profiles of the wood samples. Meanwhile, the *maximum char yield temperature* and *final char decomposition temperature* were estimated from the weight loss profiles of the wood samples.

3.3.8 Fuel evaluation exercise

As part of the characterisation exercise, experimental results in Tables 4.1 and 4.5 were used to inform the six key evaluators used for this study namely – char yield, char reactivity, fuel ratio, energy density, Nitrogen content, and ash content. These evaluators were classified as either desirable and undesirable to pyro-gasification, for simplicity (see Fig. 3.3).

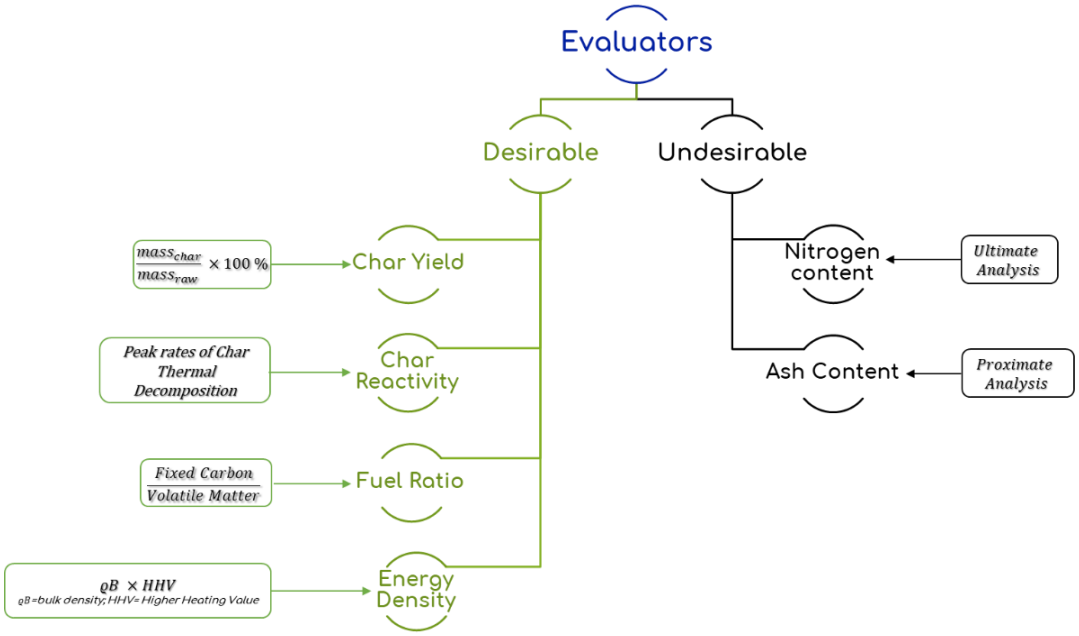


Figure 3.3: Classification of fuel evaluators.

In the fuel evaluation as shown in Table 3.1, the following rules were employed:

a. Firstly, the desirable evaluators were assigned a *relevance factor (RF)* with numbers 1 (least relevant factor) to 2 (most relevance factor) based on their relevance to pyro-gasification and the syngas composition. Meanwhile, the undesirable evaluators were assigned negative relevance factors -1 (least severe) and -2 (most severe).

b. Furthermore, to score a particular wood sample's quality against a particular evaluator, a *primary fuel quality ranking (PFQR)* ranging from 1 (worst rank) to 8 (best rank) was assigned to each of the eight samples based on their experimental result relating to that evaluator. Each sample was ranked accordingly, depending on their superiority over each other. For instance, if wood *sample A* gives the highest char yield of 40 wt% out of the lot, and wood *sample B* gives the least char yield of 20 wt%, *sample A* may be assigned a PFQR of 8 out of eight, while *sample B* may be primarily ranked 1 out of eight samples.

Table 3.1: A sample of fuel evaluation table.

PARAMETER	Relevance Factor (RF)	Biomass Sample A	
		Primary Fuel Quality Rank (PFQR)	*Secondary Fuel Quality Score (SFQS)*
Char Yield	2	4	8
Char Reactivity	2	8	16
Fuel Ratio	2	6	12
Energy Density	2	2	4
Nitrogen content	1	-8	-8
Ash content	2	-7	-14
Total Fuel Superiority Score (TFSS)			18

c. A *secondary fuel quality score (SFQS)* was then calculated for the individual samples under each evaluator. This was derived by multiplying the primary fuel quality ranking of a particular sample with the factor assigned to that particular evaluator (see Eqn. 3.6).

Wood sample A SFQS for char yield evaluation:

$$SFQS_{\text{sample A}} = PFQR_{\text{sample A}} * RF_{\text{char yield}} \quad (3.6)$$

d. Finally, the *total fuel superiority score (TFSS)* of the individual samples was generated by summing up their secondary fuel quality scores for the various evaluators.

The total fuel superiority score (TFSS) of *sample A* relative to other samples is the summation of the secondary fuel quality scores (∑ SFQS) of sample A across all parameters tested.

3.4 Thermo-decomposition Analysis (TGA) and Kinetic Study

3.4.1 Thermo-decomposition Analysis (TGA)

By subjecting the individual wood samples to a thermal treatment, the thermogravimetric analysis (TGA) was conducted and used to obtain key information about their thermal decomposition and the Derivative Thermogravimetry (DTG).

The procedure was carried out by loading 10 mg of each sample onto an alumina sampling cup, placed onto the furnace of a Q600 SDT thermal analyser (TA Instruments, USA). For each run, the equipment, purged with nitrogen flowing at 10 mL/min, was set at a heating rate of 10 ^{o}C/min. The process was set to run from an initial temperature of 25^{o}C to a final temperature of 800°C at which it was held for 30 minutes. The results obtained from the thermal analyser was plotted and analysed using the Universal V4.5A TA Instruments Data Analysis software.

3.4.2 Kinetic Analysis

The kinetic parameters were determined using data from the thermogravimetric analysis of the individual samples. The Friedman method [148], which incorporates an iso-conversional technique was employed in determining the activation energies of the non-isothermal decomposition of the wood samples. A derivation of the Friedman's method is presented as follows.

Friedman method [148]:

The rate of decomposition of biomass may be expressed by the Arrhenius Equation:

$$k = A\, e^{-\frac{Ea}{RT}} \qquad 3.7$$

Where *A* = Pre-exponential Factor;

E_a = Activation Energy; *R* is the Universal Gas Constant; and

T = Temperature.

In describing the decomposition process of biomass, the rate of the chemical reaction and the Arrhenius law are recognized. For simplicity, this decomposition process may be classified as a one-stage chemical reaction.

Therefore, the rate of decomposition of biomass determined by the temperature *T*, and the undecomposed quantity of the biomass ***f(α),*** is expressed as:

$$\frac{d\alpha}{dt} = k(T) \, . f(\alpha) \qquad 3.8$$

Where α = conversion of the decomposing or the decomposed fraction of the biomass material with respect to temperature;

k(T) also known as *k* = the rate constant which depends on the temperature *T*;

f(α) = the conversion function which represents the undecomposed fraction of the biomass. It is an effect of the mass of the biomass on the rate of reaction.

Meanwhile, this function *f(α)* may be expressed as:

$$f(\alpha) = (1- \alpha)^n \;\; = \;\; f(\alpha) = (1- \alpha) \qquad 3.9$$

where *n* = reaction order assumed to be 1.

Recall, the rate constant *k* (i.e. *k(T))* as earlier mentioned is also expressed by the Arrhenius equation 3.7.

In a thermolysis process at a constant heating rate, the heating rate meanwhile, can be represented by β, which is also defined as the change in temperature with time t, and expressed as:

$$\beta = \frac{dT}{dt} \qquad 3.10$$

The biomass rate of decomposition with respect to time can also be expressed by multiplying its rate of decomposition with respect to temperature with the set heating rate:

$$\frac{d\alpha}{dt} = \frac{d\alpha}{dT} \, . \frac{dT}{dt} \qquad 3.11$$

However, substituting $\frac{dT}{dt}$ with equation 3.10, the biomass rate of decomposition may, therefore, be expressed as:

$$\frac{d\alpha}{dt} = \frac{d\alpha}{dT} \, . \, \beta \qquad 3.12$$

Furthermore, recalling equation 3.8 and combining with equation 3.12, the biomass rate of decomposition may be further expressed as:

$$\frac{d\alpha}{dt} = \beta \, . \, \frac{d\alpha}{dT} = k \, . f(\alpha) \qquad 3.13$$

Where *k* represents *k(T)*

In substituting *k* with the Arrhenius equation, the above equation 3.13 is expressed as:

$$\frac{d\alpha}{dt} = \beta \, . \, \frac{d\alpha}{dT} = A \, e^{-\frac{Ea}{RT}} \, . \, f(\alpha) \qquad 3.14$$

Taking the natural log of equation 3.14:

$$\ln\left(\frac{d\alpha}{dt}\right) = \ln\left[\beta\left(\frac{d\alpha}{dT}\right)\right] = \ln\left[A \, e^{-\frac{Ea}{RT}} \, . \, f(\alpha)\right] \qquad 3.15$$

Recalling the Law of Log:

$$\ln[A * B] = \ln A + \ln B$$

and applying it to equation 3.15:

$$\ln\left(\frac{d\alpha}{dt}\right) = \ln\left[\beta\left(\frac{d\alpha}{dT}\right)\right] = \ln[A \, . f(\alpha)] + \ln\left[e^{-\frac{Ea}{RT}}\right] \qquad 3.16$$

Also recalling the Law of Log:

$$\ln e^{x} = x$$

and applying it to equation 3.16:

$$\ln\left(\frac{d\alpha}{dt}\right) = \ln\left[\beta\left(\frac{d\alpha}{dT}\right)\right] = \ln[A \, . f(\alpha)] - \frac{E_a}{R} * \frac{1}{T} \qquad 3.17$$

Comparing equation 3.17 to the equation of a straight line graph:

$$\ln\left[\beta\left(\frac{d\alpha}{dT}\right)\right] = \ln[A\,.\,f(\alpha)] - \frac{E_a}{R} * \frac{1}{T} \quad \equiv \quad y = C + Mx$$

Therefore, the kinetic parameters E_a and A can be determined graphically by:

Plotting $\ln\left[\beta\left(\frac{d\alpha}{dT}\right)\right]$ as the Y-axis; while $\frac{1}{\boldsymbol{T}}$ is plotted as the X-axis;

$$\text{Slope M} = -\frac{E_a}{R} \qquad 3.18$$

Intercept C = $\ln[A\,.\,f(\alpha)]$;

Where the universal gas constant, R = 8.314 J/mol.K

In generating the kinetic parameters, the above equation was split into parts and tabulated to plot a corresponding straight-graph across the temperature range from 30°C to 800°C. From the straight-line equation generated from the graph, the value of the slope M, was obtained and substituted into equation 3.18 to determine the Activation Energy of that sample.

3.5 Pyro-gasification experiment

In conducting the pyro-gasification of the wood samples, a bench-scale pyro-gasification rig was designed and fabricated. Details of this set-up are as follows.

3.5.1 Description of the Pyro-gasification reactor

The reactor which is the core component of the rig was fabricated in the workshop of the School of Chemical and Metallurgical Engineering, with the aid of drawings and specifications developed by the researcher. A detailed blueprint and picture of the pyro-gasification reactor are presented in Figs. 3.4 and 3.5.

The reactor was fabricated with a cylindrical shell made of a 3.4 mm thick brushed-steel material, with an outer diameter of 50.4 mm, an inner diameter of 43.6 mm and a longitudinal length is 230.3 mm. This was to enable the reactor to contain sizeable volumes of biomass of varied particle sizes. Halfway through this length, a steal mesh of 212 µm aperture was installed to retain unreacted tiny biomass and char particles. This would prevent the particles from exiting reactor with the

product gases and volatiles, and causing blockages in the outlet pipes. The outlet end of the reactor was enclosed in the form of a dome shape with a 13.5 mm diameter cavity (*outlet point C*) which serves as the exit for tar/oil and volatiles. With the tube furnace inclined at an angle of 35°, the dome shape of the reactor ensures the free-flow of liquid in form of moisture (during drying) and oils (at low pyrolysis temperatures) under gravity, out of the reactor through the *outlet point C*. Meanwhile, attached to the curved side of the reactor shell is another pipe of 4 mm in diameter, which serves as the *outlet point B* through which product gas is allowed to flow out of the reactor in the gasification phase.

At the other end of the reactor, is a 22 mm thick steel cover with an outer diameter of 43.6 mm and an 11.4 mm diameter gas inlet hole (*inlet point A*). This cover is also threaded from the base to the midpoint of its longitudinal section, to be fastened when closing the reactor. When open, this end of the reactor serves as the biomass feeder and when closed with the cover, the *inlet point A* on the cover serves as the nitrogen/steam inlet channel into the reactor. The thickness of the cover and that of the reactor shell ensures the reactor is prevented from rupturing under severe pressure and extreme temperatures.

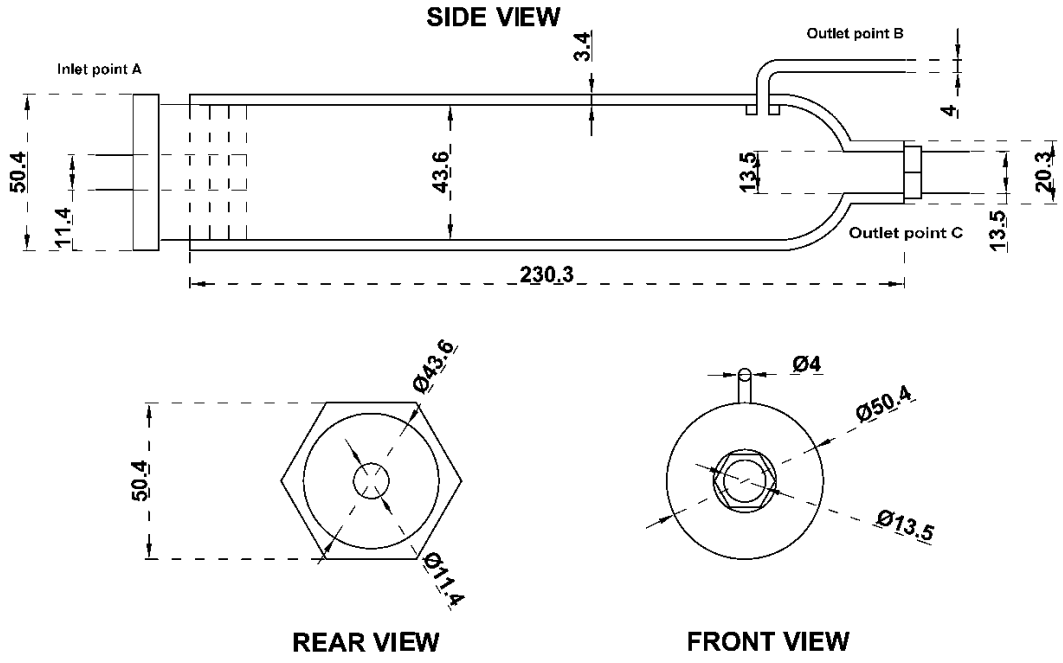


Figure 3.4: Blueprint of the pyro-gasification reactor.

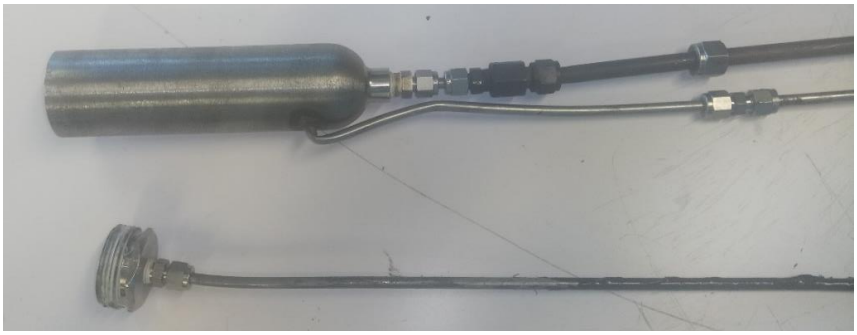


Figure 3.5: Reactor after fabrication.

3.5.2 Description of the Pyro-gasification Rig

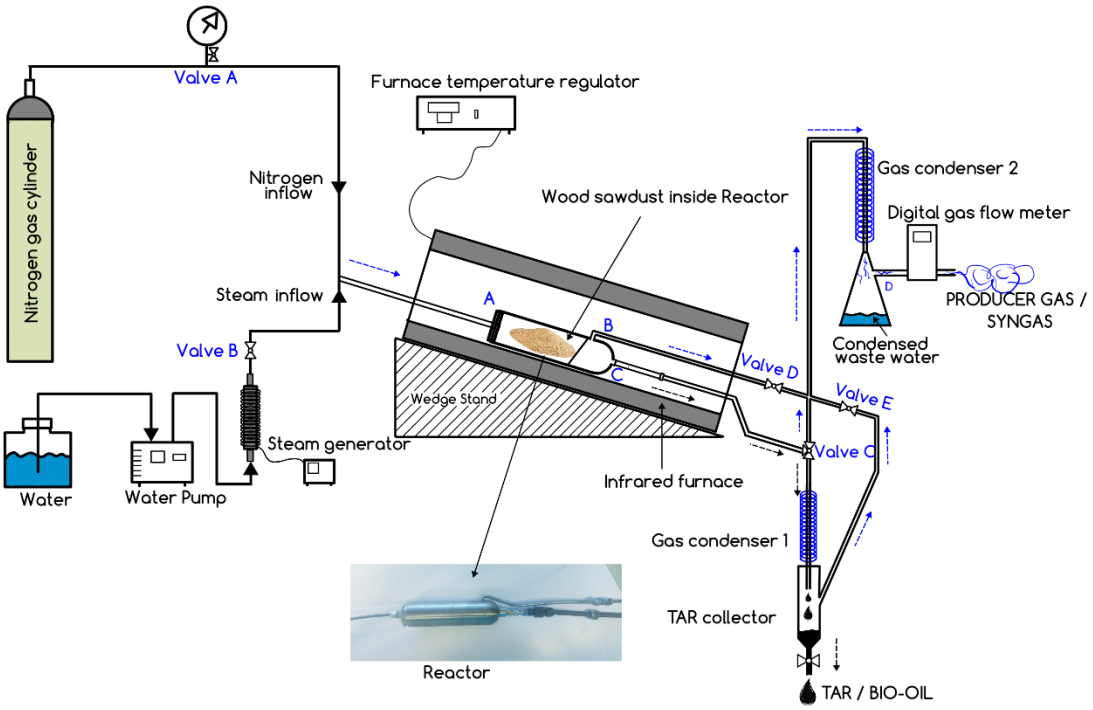


Figure 3.6: Schematic diagram of the pyro-gasification rig.



Figure 3.7: The pyro-gasification rig.

Figure 3.7 shows a picture of a simple lab-scale experimental rig developed for the pyro-gasification of sawdust samples of the eight wood species.

The rig as a whole consists of the following components:

a. A cylindrical stainless-steel reactor;

b. A high-temperature capacity infrared cylindrical tube furnace with a dedicated temperature and heating rate regulator;

c. A 35^{o} furnace wedge stand;

d. An electronic water pump;

e. A steam generator with temperature regulator;

f. An electronic gas flow meter;

g. Gas condensers 1 and 2;

h. Oil collectors 1 and 2;

i. A condensed wastewater collector;

j. Valves – A, B, C, D, and E;

k. An Omega FMA3300 Series electronic gas flowmeter;

l. A nitrogen gas cylinder; and

m. A fresh water container

Studies on the above set-up are still on-going to identify areas for future improvement and optimization.

3.5.3 Operation of the Rig

The rig is operated by feeding small-sized wood chips or sawdust of known volume through the feeder into the cylindrical reactor. The reactor is then closed by fastening the feeder bolt to ensure it is air-tight. It is then placed inside the tube furnace inclined at an angle of about 35^{o} to the horizontal with the aid of a wedge stand. This inclination ensures maximum oil flow through the pipe from the reactor's outlet *C* to the *Valve C*. Meanwhile, gas *inlet A* of the reactor was then connected to a two-way input line at *T-junction 1*. This *T-junction 1* was connected to both the nitrogen cylinder and the steam generator channels. Fluid flow through these lines to the reactor is regulated by *Valves A* for nitrogen and *B* for steam inflows respectively. The super-heated steam is generated by pumping water from the water container with the aid of the electronic water pump at set flow rates. This water flows through the pre-heated steam generator for the onward flow of the generated steam towards the reactor.

Meanwhile, at the production section of the rig, the two exit channels from outlets *C* and *B* of the reactor are connected to *Valves C* and *D* respectively. While *valve C* controls the flow of the pyrolysis phase liquid and gaseous products towards the *Gas condenser 1*, the *valve D* controls the flow of just the wet product gas. The *valve D* is, however, directly connected to the *Gas condenser 2,* which condenses the wet gas, thereby allowing the exit of dry syngas out of the rig. On the other hand, the flow of condensed oils/tar through the *Gas condenser 1* directly leads to the oil/tar collector equipped with a tap for easy collection of the bio-oil. Through

this condenser, the incondensable pyrolysis gas is allowed to exit and flow-through (via the *T-junction 2*) to the *Gas condenser 2.* This allows for further condensation of the pyrolysis gas before exiting the system through the outlet *D*. Across this channel is the *Valve E* which when closed, ensures a backflow of the wet product gas into the oil/tar collector is prevented during the gasification phase of the process. Finally, the dry product gas exiting the system at the outlet *D* is passed through the gas flow meter connected across the outlet channel and collected for analysis.

The rig was designed to separately drain out the condensed liquid tar being released during the biomass pyrolysis phase from the reactor, at low to medium temperatures. One advantage of this design is the possibility of extracting and collecting the bio-oil for further downstream processing, while char is left to be gasified. Moreover, the process parameters such as heating rate and temperature in the initial pyrolysis phase may be optimized to either improve char or tar/bio-oil yield (i.e. by slow or fast pyrolysis) before the char gasification phase. The process also offers the flexibility of switching between a variety of gases during either the pyrolysis and gasification phases. An inert gas is utilized during the pyrolysis phase to ensure the pyrolysis phase is carried out in an absolute inert atmosphere whilst heating rate and pyrolysis temperature are optimized. Meanwhile, in the gasification phase, individual oxidizers such as steam, air, and oxygen, or a mixture of any two may be introduced into the reactor for the char gasification reactions. For this study, however, only steam was utilized to support hydrogen production.

3.5.4 Description of the pyro-gasification process

In carrying out the pyro-gasification procedure, the wood sample in the form of sawdust was fed into the reactor. The reactor was then placed in the cylindrical tube furnace as depicted in Fig. 3.6.

To activate the first phase of the process – the pyrolysis (which also involves feedstock drying), the furnace was set to a final pyrolysis temperature of 800°C.

At the same time, *valve A* was opened (while *valve B* remained closed), to allow the inert gas (nitrogen) flow directly into the reactor through the inlet point *A*. The nitrogen gas was set to flow with a pressure of 50 kPa to ensure a completely inert atmosphere in the reactor for this phase. Meanwhile, a constant heating rate of 30 ^{o}C/min was set for the pyro-gasification process. A thick brownish-yellow cloud of volatiles and oils were observed to flow out of the reactor, and through to the *gas condenser 1* between 500°C and 700°C depending on the wood specie. For some species (the hardwoods in particular), this release of this volatiles continued up until about 800°C. The condensed oil was collected in the tar collector while the incondensable fraction of the volatiles exited the tar collector. As the pyrolysis temperature was increased to 850°C, the thick cloud of volatiles was observed to have cleared almost completely, leaving a flow of colourless gas through the *Gas condenser 1*. This marked the end of the pyrolysis phase.

At the 850°C temperature point, the process was held for 10 minutes as nitrogen flow was withdrawn. The temperature was then increased to the first gasification phase temperature of 900°C. Simultaneously, super-heated steam was introduced into the reactor, flowing through the layer of char particles in the reactor and exiting through its outlet point *B*. Steam to Biomass Ratio (SBR) for all runs was 0.6. The initial gasification phase temperature of 900°C was chosen after several observations from preliminary runs at varied temperatures. During the preliminary test runs, higher concentrations of syngas were observed from 900°C and above. The syngas flow rate was measured at 900°C, 950°C and 1000°C using the gas flowmeter and collected for analysis with an offline Bruker 430C TCD Gas Chromatograph equipment. Meanwhile, to observe their flame colour and propagation, the syngas for each sample was safely ignited for five minutes.

3.5.4.1 Pyro-gasification of individual samples

Firstly, the pyro-gasification of individual wood samples was conducted to ascertain their syngas yields at the three temperature points – 900°C, 950°C and 1000°C. The aim was to ascertain the gas yields of the individual samples at the three temperature points when pyro-gasified separately. Moreover, this provided

some knowledge of what to expect when two samples are blended. 20 g of sawdust of each wood sample was weighed and fed into the reactor and the pyro-gasification process was carried out.

3.5.4.2 Pyro-gasification of the blended samples

In blending the samples for pyro-gasification, the IAP wood samples sourced from within South Africa were blended separately with each other, likewise the tropical wood samples from Nigeria. This was in consideration of the economic feasibility of sourcing biomass wastes locally from where they are being generated. Thus, blending samples from the same region was thought to be logical than blending samples from two regions geographically far apart.

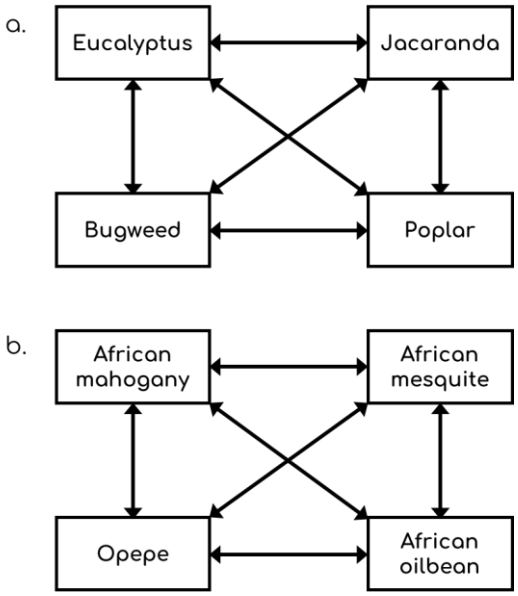


Figure 3.8: Blending pattern of (a) IAP samples and (b) Tropical hardwood samples, in blend ratios: 50/50, 70/30, 30/70.

The sawdust of two samples A and B were blended in the following ratios with a total feedstock mass of 20g:

30/70 (i.e. sample A= 6 g; sample B = 14 g);

50/50 (i.e. sample A = 10 g; sample B = 10 g) and;

70/30 (i.e. sample A = 14 g; sample B = 6 g).

The pyro-gasification procedure then commenced.

3.5.5 Novelty of this pyro-gasification method and rig design

The basic principle of the pyro-gasification method used for this research is similar to the experimental process adopted by Alipour *et al.* [134] and Pattanotai *et al.* [77]. However, the major differences and novelty of this research in terms of the method, reactor design and process conditions are highlighted as follows.

3.5.5.1 Similarity

One basic principle of pyro-gasification adopted in this research and similar to those adopted by both aforementioned researchers is the switching from pyrolysis to gasification in a single reactor. Most similar to this study, Alipour *et al.* ensured an independent control of the pyrolysis phase and gasification phase conditions of the pyro-gasification process. However, this could only be achieved by adopting a reactor design with separate zones installed with two separate electric heaters. One heater supplied about 400–650°C to the pyrolysis zone and the other supplied 750–1100°C to the gasification zone and tar catalytic bed the of the reactor. Meanwhile in the process adopted by Pattanotai *et al.*, an inert gas (argon) was passed through the reactor while the pyrolysis process progressed from 673K to 1173K. However, with no further increase or change in this final temperature of 1173K, the gasification process was enabled by allowing 20% oxygen into the inert reactor chamber.

3.5.5.2 Differences and Novelty of this research

a. *Contrasts in reactor temperature:* In this study, the pyro-gasification process was carried out by enabling a consecutive but defined switch from the pyrolysis phase to the gasification phase with an absolute control of the reactor temperature in each phase to maximize process efficiency. During the pyro-gasification process, the reactor temperature ran from 30°C to 850°C in the pyrolysis phase which incorporated feedstock drying. This was subsequently switched to the higher gasification phase temperatures from 900°C – 1000°C after tar was completely extracted. Moreover, the pyrolysis

and gasification phase temperatures were separated by a 50°C temperature gap allowed within a holding time of 10 mins to allow for a complete switch from an inert to an oxidized reactor atmosphere. This is in contrast to the method by Pattanotai *et al.* whereby the temperature switch from the pyrolysis and gasification phases was seamless with no defined holding time, with both phases only varied within the same low temperature range of 673 – 1173K. Meanwhile due to the design of the reactor used by Alipour *et al.* as earlier described, the temperatures of both zones were controlled by two independent heaters.

b. *Contrasts in reactor atmosphere:* Asides switching the reactor temperature to suite both phases of the pyro-gasification process in this study, particular emphasis was placed on ensuring the reactor atmosphere was well suited for each phase. This was necessary to maximize the process efficiency of both phases. To actualize this, nitrogen gas was purged into the reactor to create an absolutely inert atmosphere for the pyrolysis phase, and was subsequently withdrawn and displaced with a super-heated steam to ensure an absolutely oxidized reactor atmosphere for the char gasification phase reactions. This is in contrast to the introduction of a 20% oxygen and 80% argon flow into the reactor to enable the gasification phase as reported by Pattanotai *et al.* This method was also in contrast to that adopted by Alipour *et al.* which involved a separate supply of nitrogen to the pyrolysis zone, and a mixture of steam and air to the gasification zone.

c. *Reactor design:* One major novelty of this research lies in the reactor design. Although it basically can be classified as a cross-flow fixed bed (CFB) reactor, its design principle is different from those reported in literature. The reactor and rig were designed and fabricated to drain out tars and impurities (which are undesirable for gasification) for recovery as bio-oil midway into the process. This is to ensure that tars and impurities are restricted from progressing to the gasification phase. This allows for the presence of a carbon-rich char residue as the only reactant with steam in gasification phase, thereby

ensuring the production of syngas with low tar impurities and high yield. In contrast to this, previously reported models have allowed the progression of all three pyrolysis products to the gasification phase. These have inevitably incorporated an additional catalytic and/or high temperature tar cracking zone syngas purification and improved yield. Figures 2.20 a, b, c, and d, are examples of reactor designs used in pyro-gasification processes as reported in literature.

3.5.6 Determination of yield and production rate of syngas, H_2 and CO

For each wood sample and each mix ratio of two blended samples, the production rate and yield of each syngas component (H_2 and CO) as well as that of the syngas in total at 900, 950 and 1000°C respectively were derived using the following mathematical expressions [108].

a. Production rate of each syngas component (H_2 or CO):

$$r_i = \frac{\Upsilon_i * f_t}{m} \quad \text{(mL/min/gram of feedstock)} \qquad 3.19$$

Where:

f_t = volumetric gas flow rate at a temperature of sampling of syngas;

Υ_i = volume fraction of the gas component (H_2 or CO) at sampling temperature of syngas;

m = initial mass of biomass feedstock.

b. Gas yield of each gas component (H_2 or CO), Y_i:

$$Y_i = \frac{\Upsilon_i * Q_{total}}{m} \quad \text{(mL/gram of feedstock)} \qquad 3.20$$

Where:

Υ_i = volume fraction of the gas component (where i = H_2 or CO) at sampling temperature of syngas;

Q_{tot} = Total syngas product volume collected;

m = initial mass of biomass feedstock.

The total syngas yield:

$$Y_{syngas} = \sum Y_i \qquad 3.21$$

Chapter 4

Fuel examination of Invasive Alien Plants and Tropical hardwoods as feedstock in pyro-gasification

4.1 Introduction

Woods are versatile types of LCBs which can be used as feedstock for both thermochemical and biochemical conversion processes. As previously described, they are composite materials generally comprising of approximately 40-60% cellulose, 20-40% hemicellulose and 10-25% lignin. The fraction of each of these structural components in any biomass plays a key role in determining its suitability as feedstock for either biochemical or thermochemical conversion processes. Fibrous biomass materials with high holocellulose composition are usually most suitable for biochemical conversion processes. This is due to the ease of a biochemical breakdown of the holocellulose components as opposed to lignin. Meanwhile, dense, non-fibrous LCB materials such as wood, comprising of significant amounts of lignin exhibit qualities most suitable for thermochemical conversion processes.

In the thermochemical context, these structural components of biomass also serve as precursors to the yield and quality of its thermochemically generated products. In pyrolysis, for instance, the decomposition of its hemicellulose and cellulose components contributes to the volume of tar-forming volatiles which form the bio-oil when condensed. Likewise, the decomposition of lignin, and to some extent, that of hemicellulose have a direct influence on the yield and reactivity of the char residue formed during pyrolysis. These two components form the fixed carbon and ash particles which primarily make up the char residue.

In pyro-gasification however, the outcomes of the pyrolysis phase such as the yield and reactivity of the char produced, are vital for the efficiency of the gasification phase of the process. High char yield translates to longer residence time of the char, while high char reactivity translates to lower activation energy for the gasification reactions. This translates to a high production of syngas at lower

temperatures. Other fuel properties of biomass which either strengthen or undermine the quality of the syngas produced from pyro-gasification or gasification include its heating value, fuel ratio, energy density, nitrogen, sulphur and ash compositions [31,149,150]. These parameters were determined from a series of experimental results such as the ultimate and proximate analysis, calorimetric test, bulk density, and thermogravimetric analysis of the biomass samples [71].

Some of the wood samples adopted for this research such as the tropical West African species have previously been characterised in literature [39] specifically as feedstock for combustion purposes. However, such results remain inadequate to determine their suitability as feedstock for pyro-gasification, since the reaction kinetics of combustion and pyro-gasification differ. Therefore, an investigation into additional properties relevant for pyro-gasification is required to determine feedstock suitability for syngas production. Furthermore, the use IAPs for syngas production has seldom been reported, despite the recent literature [30,45,47] supporting the economic viability, and sustainability of using biomass wastes derived from IAPs control as feedstock for biofuel conversion. Therefore, there exists a gap in the knowledge of their suitability for syngas production via pyro-gasification and other thermochemical processes.

Against this background, this chapter presents and discusses the experimental data collated from the characterisation of eight wood samples. They include four IAP wood samples common in Southern Africa – Jacaranda, Eucalyptus, Bugweed and Poplar, and four tropical hardwoods common in Central and West Africa – African oilbean, African mesquite, African Mahogany and Opepe. The samples were characterised based on their – structural compositions, proximate compositions, ultimate compositions, Higher heating value, bulk density, char yields and char reactivity. Other fuel properties such as their fuel ratios and energy densities were, however, derived from calculations using the results of the analyses conducted. Finally, the results of a fuel evaluation of the eight wood samples based on the following evaluators – Char yield, Char reactivity, Fuel ratio, Energy density, Nitrogen emission and Ash deposition were presented and

discussed in this chapter.

4.2 Results and Discussion

4.2.1 Structural analysis

The lignocellulosic composition of wood, as well as its secondary cell wall structure, are the basic contributors to its physical and chemical characteristics which distinguishes it as ideal feedstock for conversion to specific biofuels either by biochemical or thermochemical methods [151].

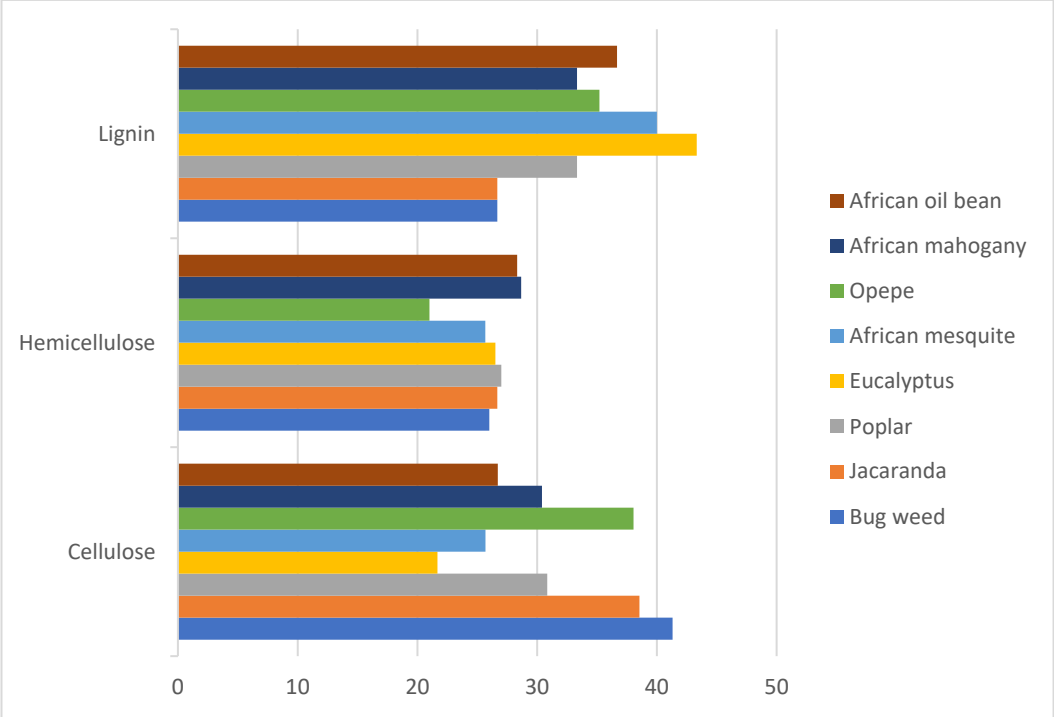


Figure 4.1: A comparison of the Structural compositions of the eight wood samples.

Figure 4.1 compares the lignocellulosic compositions of the wood species investigated. The Bugweed exhibited the highest cellulose composition of 31.31 wt % and a total holocellulose (cellulose + hemicellulose) composition of 67.31 wt % which can be attributed to its fibrous nature. This was closely followed by the jacaranda (65.21 wt % holocellulose), a softwood. In general, the lignin composition of the samples tested ranged from 26.67 % to 43.33 %. Considering their high holocellulose and lower lignin composition, such wood species as the Bugweed and Jacaranda were expected to exhibit higher rates of thermal

decomposition. This is due to the high rates of thermal decomposition normally exhibited by holocellulose. However, the higher holocellulose composition (than lignin) of Bugweed may also qualify it for use as feedstock for biochemical conversion processes.

Conversely, the lignin values were generally higher in the hardwoods. These include the hardwoods in the list of IAPs such as the Eucalyptus and Poplar species. Lignin promotes mechanical strength and also contributes to wood hydrophobicity and resistance to pest and microbial attack [54,55,151,152]. This corroborated with the rigidity and high-density physical properties exhibited by the hardwoods during milling. In some instances, high lignin composition can also be found in softwoods, and in particular, those with thicker barks. This is due to the high amounts of lignin contained in barks of trees. In this study, however, the sawdust samples were sourced from the sapwood and heartwood of the tree trunk.

Lignin has also been reported to exhibit higher heating values than those of hollocellulose due to its lower rate of oxidation or decomposition [56,57]. In most cases, the average difference between the HHV of hardwoods and softwoods is basically due to the difference in their lignin composition [150]. This corroborated with the results of the samples investigated as observed in Sect. 4.2.4. In general, the results of the samples tested were consistent with values for similar woods reported in literature [57,60].

Table 4.1: Experimental data of the eight wood samples.

Analysis		BIOMASS								Recommendations for wood fuels	
		Eucalyptus	Bugweed	Poplar	Jacaranda	African mesquite	Opepe	African mahogany	African oil bean	Austria ONORM M7135[153]	German DIN51731 /DINplus[153]
Lignocellulosic analysis %	Cellulose	21.68	41.31	30.84	38.54	25.69	38.05	30.4	26.71	-	-
	Hemicellulose	26.51	26	27.01	26.67	25.67	21	28.67	28.33	-	-
	Lignin	43.33	26.67	33.33	26.67	40	35.2	33.33	36.67	-	-
	Extractives	8.48	6.02	8.82	8.12	8.64	5.75	7.6	8.29	-	-
Proximate analysis %	MC	9.13	8.93	12.21	9.12	9.61	7.16	7.21	8.56	-	-
	VM	49.88	54.92	56.56	57.91	43.29	58.65	52.12	51.01	-	-
	FC*	39.98	34.44	30.2	30.76	47.11	33.17	40.36	39.86	-	-
	Ash	1.01	1.74	1.04	2.21	0	1.02	0	0.58	≤0.5	<1.5/<0.5
Ultimate analysis %	C	47.82	43.33	42.34	44.23	50.49	48.62	48.42	45.64	-	-
	H	5.37	5.66	5.82	5.73	5.63	6.02	5.81	5.81	-	-
	N	0.08	0.4	0.27	0.18	0.26	0.37	0.19	0.4	<0.3	<0.3
	S	0	0	0	0	0.01	0	0	0	<0.04	<0.08/0.04
	O*	46.73	50.75	51.58	49.87	43.61	44.99	45.59	48.16	-	-
HHV (MJ/kg)		18.84	17.58	18.8	18.43	20.72	18.9	19.34	19.15	>18.0	17.5 - 19.5/ >18
Bulk density (g/cm^3)	ϱB	1.01	0.4	0.5	0.51	1.05	0.67	0.66	0.95	-	-
Energy density (GJ/m^3)	ED	19.03	7.03	9.4	9.4	21.76	12.66	12.76	18.19	-	-
Fuel Ratio FC/VM	FR	0.8	0.63	0.53	0.53	1.08	0.6	0.8	0.8	-	-

***** by difference

With regards to the influence of the structural components on the type and yield of the pyrolysis product formed, higher char yields (see Table 4.5) were expected from tree species such as the Eucalyptus and the African mesquite, exhibiting relatively higher amounts of lignin – 43.33% and 40% respectively (see Table 4.1). Conversely, low char yields were expected from species such as the Bugweed and Jacaranda exhibiting the lowest lignin compositions of 26.67%. However, this may not necessarily be the case. As mentioned in section 2.1.3, Fig. 2.4 [66] depicts the complexity of the biomass pyrolysis process, whereby the three components (cellulose, xylan (hemicellulose), and lignin) show overlapping decomposition thermograms. Despite the lignin decomposition contributing primarily to char formation, hemicellulose also acts as a secondary contributor to char formation. This is so because while hemicellulose attains its peak rate of decomposition at a much lower temperature than the other components, it is observed to attain some thermal stability around 400°C (see Figs 2.1, 2.2, 2.4 and 2.5). Hemicellulose decomposition is therefore extended beyond that of cellulose and above the normal pyrolysis threshold temperature of 600°C, following a decomposition trend similar to that of lignin. This occurrence was also corroborated by Branca *et al.* [73]. In this current study, a typical instance was observed with the significant char yield obtained in the pyrolysis of Bugweed despite its low lignin composition (see Tables 4.1 and 4.5). However, it was concluded that, due to the highly reactive nature of hemicellulose, its significant contribution to the Bugweed char formation was one of the factors responsible for the high decomposition rate of the Bugweed char mass (see Fig. 5.1). This explains its high syngas production at lower temperatures in comparison to other wood samples, as would be discussed in Chapter 6. Meanwhile, the presence of high amounts of hemicellulose by the Bugweed, Poplar and Jacaranda also indicates their potential to produce high amounts of tar-forming volatiles during pyro-gasification.

On the contrary, the charred mass produced from the African mesquite and Eucalyptus were observed to exhibit low reactivity as would be discussed in Section 4.4.1. This was attributed to the much significant contribution of their

lignin component (present in higher proportions) to their char formation. This was also complemented by the minimal contribution of their decomposing hemicellulose component (present in lower proportions) to char formation. The char produced by these hardwood samples – African mesquite, African Mahogany, Opepe, Eucalyptus, however, exhibited lower decomposition rates (see Sect. 5.2) as a result of the greater contribution of the less reactive lignin component to the formation of the char.

Extractives are vital non-structural components of trees, largely responsible for preventing them from attacks by insects and biotic organisms and thus, contributing to their physical attributes such as colour, scent and hydrophobicity. In addition, they act as energy storages [35,58,154,155]. Extractives are also known to have a positive influence on the HHV of wood [59,60], and in most trees, are known to contain carbon-rich triterpenes which augment the total carbon composition [61]. A study by Peng [63], reveals high heating values of up to 38 GJ/t possessed by extractives, which were higher than those of cellulose, hemicellulose and lignin.

In agreement with Nguyen *et al.* [58], the sample test results showed extractives were within the range of 5.75 – 8.82 %. Opepe (5.75 %) recorded the lowest composition of extractives while higher amounts of 8.82% and 8.64% were observed in Poplar and the African mesquite respectively. A trend was observed whereby most samples exhibiting relatively high extractive compositions possessed higher lignin content. In corroboration with Demirbas [59] and Telmo [60] & Lousada [60], this observation could be related to the fact that higher amounts of extractives were observed for hardwoods which coincidentally exhibited higher heating values.

4.2.2 Proximate analysis

4.2.2.1 Moisture content

The proximate analysis showed substantial, but below 10 % moisture content (MC) for all samples tested, except for Poplar exhibiting a higher MC of up to 12.21 %. This is expected of biomass which generally possess high moisture content. The

relatively high MC values recorded across all samples in this study could also be as a result of the samples being subjected to air-drying rather than oven-drying before the test. The poor hydrophobicity of raw wood, which makes it susceptible to moisture absorption, remains one of the major drawbacks to its use as feedstock for thermochemical processes, due to the negative impact it has on its calorific value, combustion efficiency or conversion to secondary biofuels [39]. This justifies the need for pre-treatment processes such as wood torrefaction, or pyrolysis to form char, which is very hydrophobic.

4.2.2.2 Volatile Matter and Fixed Carbon

Volatile matter (VM) and fixed carbon (FC) content of biomass, indicate the amounts of tar-forming volatiles and char mass expected from its pyrolysis. These volatiles and char mass serve as prerequisites for the succeeding thermochemical reactions leading to syngas production such as oxidation, Boudouard, methanation, water-gas shift and steam reforming reactions [112]. Hence, VM and FC contents are important for a preliminary evaluation of feedstock with potential for high tar, char and syngas yield when subjected to a thermochemical process. Unlike coal, biomass is known to generally possess higher amounts of VM and lesser amounts of FC [156]. This was evident in the wood samples tested. The results reveal high volatile matter (VM) content across the board. However, samples such as the Bugweed (54.94% VM), poplar (56.56% VM), Jacaranda (57.91% VM) and Opepe (58.65% VM), exhibited the most volatile matter composition. This can be attributed to their high holocellulose compositions – Bugweed (67.31% holocellulose), Poplar (57.85% holocellulose), Jacaranda (65.21% holocellulose) and Opepe (59.05% holocellulose), as observed in Sect. 4.2.1. Meanwhile, the FC content in the hardwood species – Eucalyptus (39.98% FC), African mahogany (40.36% FC), African mesquite (47.11% FC) and African oil bean (39.86% FC), corresponded with their high lignin compositions – 43.33% lignin (Eucalyptus), 33.33% lignin (African mahogany), 40% lignin (African mesquite) and 36.67% lignin (African oil bean). This underlines the influence of lignin on FC composition.

4.2.2.3 Ash composition

The results obtained in this study, show generally low ash compositions among all wood samples, with 0.00% value observed for the African mesquite and African mahogany. However, most samples exceeded the recommended ash content of 0.5% for wood fuels set by the Austrian National Standard for Pellets and Briquettes (Austrian ONORM M7135) and the German National Standard for fuel pellet (German DINplus) [153]. Most significant among these were the Jacaranda (2.21%), Bugweed (1.74%) and Poplar (1.04%) which are incidentally the IAP samples. Geographical differences, as well as storage conditions and differences in test procedures, could be possible factors affecting the ash content of the samples when compared to literature. This was evident as the ash content of the four tropical hardwood samples tested in this study were significantly lower than those of the same specie reported by Duruaku *et al.* [39]. However, the higher ash content similarly observed with the Jacaranda, Bugweed and Poplar could be attributed to the fact that they were harvested from the same grassland biome. This biome is characterized by dense alien plant invasion, limited groundwater supply and low mean annual rainfall. These factors lead to a decreased soil dilution capacity and consequently, high concentration of mineral matter absorbed by the trees [22,44,157].

In comparison to most other wood species reported in literature (see Table 4.2), the ash contents in the wood samples tested in this study were observed to be significantly lower.

Table 4.2: Comparison of ash composition of woods in this study with others in literature.

WOOD AND WOODY BIOMASS	ASH COMPOSITION	LITERATURE
	wt%	
Bugweed	1.74	This study
Eucalyptus	1.01	This study
Poplar	1.04	This study
Jacaranda	2.21	This study
African mesquite	0.01	This study
Opepe	1.02	This study
African mahogany	0.08	This study
African oilbean	0.58	This study
Poplar bark	2.0	[49,158]
Tamarack bark	3.8	[49,158]
Spruce bark	2.9	[49,158]
Pine bark	1.8	[49,158]
Elm bark	7.4	[49,158]
Maple bark	3.7	[49,158]
Balsam bark	2.4	[49,158]
Beech bark	7.1	[49,158]
Birch bark	1.9	[49,158]
Eucalyptus bark	4.2	[159]
Hemlock bark	2.3	[49,158]
Oak wood	0.5	[49,160]
Olive wood	3.0	[49,161]
Pine wood	5.5	[49,162]
Spruce wood	0.5	[49,162]
Willow wood	1.4	[49,163]
Alder-fir wood	2.0	[49,164]
Poplar wood	2.0	[49,164]
Hybrid Poplar wood	0.04	[164]
Christmas tree wood	0.3	[49,164]
Red oak wood	0.3	[164]
Beech wood	0.5	[160]

4.2.3 Ultimate analysis

In addition to providing valuable information about the energy output of any combustible material, an ultimate analysis is essential as a preliminary evaluation of the potential emissions expected during the thermochemical conversion of such material [35]. This also provides vital data for the reactor design and operation [141].

With effect to their energy output, the elemental carbon and hydrogen contents of solid fuels have a positive influence on their calorific values [150]. Meanwhile, the higher oxygen content normally exhibited by biomass (when compared to coal) is undesirable as it results in smoking during its thermochemical conversion [165]. This is due to the combustion of oxygen with carbon during the conversion process. Higher elemental carbon was observed in the hardwood samples – Eucalyptus (47.82%), African mesquite (50.59%), Opepe (48.62%), African mahogany (48.42%), and African oil bean (45.64%). Such higher values in carbon can be attributed to their high lignin and fixed carbon compositions. These corroborate their superior heating values over those of the Bugweed, Poplar and Jacaranda. Similar values in hydrogen contents within the range of 4.91–6.02% were however observed across the board. Higher amounts of oxygen were also observed mostly in the IAPs as shown in Table 1.

In predicting potential fuel emissions, such as NO_X and SO_X compounds formed during syngas production, the nitrogen and sulfur composition of the biomass is considered in its ultimate analysis. High nitrogen composition in solid fuels makes them less desirable for pyro-gasification and other thermochemical processes, as incombustible N_2, NH_3, HCN, NO_X (NO, NO_2), N_2O, SO_X (SO_2, SO_3) compounds may be formed during their conversion. For instance, during the partial combustion reactions, the nitrogen present in the feedstock is oxidized to form NO and NO_2 which when released to the atmosphere dissolve in rainwater to cause acid rain. Acid rain is known to be toxic to soil and aquatic organisms as it increases the soil and water acidity and consequent decline in the population of soil and aquatic organisms [8,162,166–169]. Furthermore, nitrogen can be partially converted to

ammonia (NH_3) and hydrogen cyanide (HCN) which if contained in the syngas can poison the catalysts used for downstream applications [170]. Likewise, sulfur compounds SO_2 and SO_4 formed during thermochemical processes can result in acid rain formation, if found in the feedstock. Therefore, in this study, the nitrogen and sulphur compositions of the samples were compared to the maximum allowable composition for briquettes and pellets (by the Austrian ONORM M7135 and German DIN 51731/DINplus) [153]. The nitrogen compositions of most wood samples tested were observed to be within the allowable limits of <0.3%, except for those of Bugweed (0.4% N), Opepe (0.37 % N) and the African oilbean (0.4% N). As shown in Table 4.1, the sulfur composition for all samples were however observed to be of negligible values and below the Austrian ONORM M7135 (0.04%) and the German DIN 51731/DINplus (0.08% / 0.04%) maximum allowable sulphur content. This is in corroboration with the fact that high sulfur concentrations are more commonly found in coals and mostly negligible in biomass.

In general, most wood samples evaluated in this study exhibited relatively lower nitrogen values than those reported in literature as listed in Table 4.3.

Table 4.3: Comparison of nitrogen composition of wood samples in this study with others in literature.

WOOD AND WOODY BIOMASS	NITROGEN COMPOSITION %	LITERATURE
Bugweed	0.4	This study
Eucalyptus	0.08	This study
Poplar	0.27	This study
Jacaranda	0.18	This study
African mesquite	0.26	This study
Opepe	0.37	This study
African mahogany	0.19	This study
African oilbean	0.40	This study
Poplar bark	0.6	[49,158]
Tamarack bark	0.7	[49,158]
Spruce bark	0.1	[49,158]
Pine bark	0.3	[49,158]
Elm bark	0.7	[49,158]
Maple bark	0.4	[49,158]
Balsam bark	0.2	[49,158]
Beech bark	0.7	[49,158]
Birch bark	0.5	[49,158]
Eucalyptus bark	0.3	[159]
Hemlock bark	0.2	[49,158]
Oak wood	0.3	[49,160]
Olive wood	0.7	[49,161]
Pine wood	0.5	[49,161]
Spruce wood	0.3	[49,161]
Willow wood	0.6	[49,163]
Alder-fir wood	0.5	[49,164]
Poplar wood	0.6	[49,164]
Hybrid Poplar wood	0.04	[164]
Christmas tree wood	0.3	[49,164]
Red oak wood	0.03	[164]
Beech wood	0.4	[160]

4.2.4 Higher heating value

Table 4.4 compares the HHVs of samples tested in this study with those of the same specie reported in literature. The desirability of a feedstock for biofuel production is to a significant extent, a function of its calorific value. This can be obtained experimentally and has also been calculated empirically in literature by applying the results of elemental composition of a sample reported elsewhere [35,141,142].

Among samples tested in this study, the tropical hardwoods in comparison with the IAPs, generally exhibited superior HHVs which can be attributed to their earlier observed higher lignin, fixed carbon and elemental carbon content. The African mesquite (20.72 MJ/kg) was highest while Bugweed (17.58 MJ/kg) exhibited the lowest calorific value. Compared with the minimum allowable calorific value for briquettes and pellets, the value for Bugweed (17.58 MJ/kg) was close but not up to the Austrian ONORM M7135 set minimum value of 18.0 MJ/kg. The wood samples also exhibited superior HHV when compared to other types of biomass wastes reported in literature such as Bamboo (17.13 MJ/kg) and sugarcane bagasse (15.79 MJ/kg) [171], the South African sweet corn ear husks (16.61 MJ/kg) etc. [172]. The Olive kernel [173] with a value of 20.39 MJ/kg, however, exhibited similar high heating values to those of the tropical hardwoods such as the African mesquite (20.72 MJ/kg) reported in this study. The high heating value exhibited by the olive kernel can be attributed to its high lignin composition which is responsible for the hardness observed in fruit shells. This can be related to the physical and structural properties also observed in the hardwood species tested.

Table 4.4: Comparison of Higher heating values of wood samples in this study with literature.

BIOMASS	HHV	Reference
	(MJ/kg)	
Bug weed	**17.58***±0.70*	This study
	16.9	[162]
Jacaranda	**18.43***±0.10*	This study
	-	
Poplar	**18.80***±1.10*	This study
	19.38	[56]
	18.57	[174]
Eucalyptus	**18.84***±0.04*	This study
	18.64	[142]
Opepe	**18.90***±0.50*	This study
	21.44	[39]
African oil bean	**19.15***±0.10*	This study
	20.06	[39]
African mahogany	**19.34***±1.13*	This study
	20.79	[39]
African mesquite	**20.72***±0.20*	This study
	22.41	[39]
Hog wood	*20.95*	[164]
Hybrid Poplar	*18.95*	[164]
Willow tree	*18.79*	[174]
Pine tree	*19.38*	[174]
Birch tree	*19.34*	[174]

4.2.5 Bulk density

The bulk density of a solid material reflects its porosity and how loosely packed its particles are in its original state. This is mathematically expressed as the mass of its particles divided by the volume occupied by those particles. Therefore, the

higher the number of particles occupied in a fixed volume of solid, the denser and harder that solid would be.

Due to their physical hardness, the bulk densities of the hardwoods were also observed to be higher than those of softwoods like the Bugweed and Jacaranda. This was attributed to the dense packing of the fibres contained in the hardwoods as opposed to the loosely packed softwood fibres. The Poplar, despite being classified as a hardwood, exhibits significantly lower bulk density than its hardwood counterparts due to the loose nature of its fibres. This reinstates the fact that not all species classified as hardwoods are physically hard. As reported in Table 1, the bulk densities of six out of eight wood samples investigated in this study were within the range of 400 – 950 kg/m^3, similar to the range reported for other woods [39,156,175]. However, the bulk densities for the African mesquite (1050 kg/m^3) and eucalyptus (1010 kg/m^3), exceeded this range. Solid fuels with such high densities may exhibit delayed ignition time and slow-burning rate during combustion [38], or require higher temperatures to enhance their rate of reaction during gasification. This is usually as a result of bottlenecks in the penetration of hot oxidizing gases through the surface of the densely packed solid fuel into its inner particles.

4.2.6 Char yield and reactivity

Results of the char yield of each sample was derived from Eqn. 3.5 (Sect. 3.3.7), and used to assess the wood samples. Meanwhile, the rate of char reactivity (also known as the char rate of decomposition), was derived from the peak rates of decomposition of the chars of the individual wood samples as observed on their DTG thermograms (see Sect. 5.2). These peaks occurred at temperatures ranging from 400 to 800°C.

Table 4.5 shows the results of the char yields and char reactivities of the wood samples. Asides the results of the maximum obtainable char yield and char reactivity, other related parameters also listed include the initial decomposition temperatures (IDTs) of the raw wood samples as well as the temperatures at

maximum char yield and final char decomposition. The maximum char yield temperature is regarded as the approximated temperature mark at which the volatiles in the biomass were observed to have been expelled, leaving behind a carbon-rich char mass. This marked the end of the volatilization phase of the wood samples and the beginning of the char decomposition phase as observed on the TGA thermograms.

Table 4.5: Char properties of wood samples.

Biomass	Initial Decomposition Temp.	Maximum char yield	Maximum char yield temp.	Char reactivity	Char burnout temp.
	℃	%	℃	%/min	℃
Bug weed	179	36.18	320	3.13	475
Jacaranda	170	32.97	355	0.95	785
Poplar	185	31.24	355	2.87	510
Eucalyptus	171	40.99	360	1.19	795
Opepe	180	34.19	370	1.37	660
African oil bean	198	40.44	345	3.07	515
African mahogany	202	40.36	355	1.70	640
African mesquite	183	47.11	375	0.87	>800

As depicted in Table 4.5, the maximum char yield temperatures for most samples were observed to be approximately between 350 – 400°C. These are similar to the maximum char yield temperatures reported in literature [77,176,177]. However, the temperature at which the maximum char yield for Bugweed was observed, was lowest at 320°C when compared to those of other samples tested. This was due to the decomposition of its hemicellulose and cellulose components (which are in greater proportions) peaking at much lower temperatures before attaining the 320°C temperature point. The decomposition of these holocellulose components at lower temperatures can also be attributed to the high porosity of the Bugweed

which is evident of its low bulk density. High porosity in wood creates more reaction active sites in the wood, as hot gaseous reactants are easily transferred into the inner particles through the pores. Therefore, the highly porous nature of the Bugweed allows for a rapid transfer of heat into its inner particles thereby encouraging an easier and low-temperature breakdown of the intermolecular chains of its holocellulose components. The variation in the temperature at which these intermolecular chains breakdown in the different wood species is the reason for the differences in their initial decomposition temperatures as presented in Table 4.5. Conversely, the African mesquite attained the highest temperature at maximum char yield of 375^{o}C, which can be attributed to its much lower porosity resulting in its high bulk density. This higher temperature required by the African mesquite also translates to the high energy input required to penetrate and completely breakdown its holocellulose components. The variations in the maximum char yield temperatures of the samples are in corroboration with literature [178], where a study of the pyrolysis of cotton cocoon shell, tea factory waste and olive husks reported unique maximum char yields at different temperatures.

With the variations in the maximum char yield temperatures of the samples though attributed to their unique properties, further increases in the pyrolysis temperature and heating rate would further reduce char yield [178,179]. The maximum char yield observed was highest from the African mesquite (47.11% wt.), Eucalyptus (40.99% wt.), the African mahogany (40.36% wt.) and the African oil bean (40.44% wt.). This was due to their high fixed carbon composition as observed in Sect. 4.2.2. Char yield was however fairly lower from the Poplar (31.24% wt.), Jacaranda (32.97% wt.) and Bugweed (36.18% wt.) samples.

For the Bugweed sample, its final char decomposition temperature was at the lowest of 503^{o}C. This was as a result of its high char reactivity which was highest amongst all samples, with a maximum peak of 3.13 %/min at 413.91^{o}C as depicted in Fig. 5.1. Generally, char obtained from biomass is known to be very reactive mainly due to its high porosity [96]. Furthermore, char reactivity is affected by

factors like the type of parent biomass feedstock and reactor variables such as the heating rate, final pyrolysis temperature and pressure [77].

Low char reactivity (or low rates of char decomposition), can lead to poor, inadequate or incomplete conversion of the carbon particularly at low temperatures in the gasification phase of the pyro-gasification process. This can result in low syngas yield and can affect the syngas composition and heating value. Most importantly, this translates to the fact that a higher activation energy is required to trigger a complete conversion of the char to syngas. In other words, a sample with higher char reactivity is expected to have converted a larger proportion of its carbon at a lower temperature than those of lower char reactivity. This corroborated the syngas yields collected from the pyro-gasification experiments of the samples at 900°C, 950°C and 1000°C, reported in Chapter 6. The results reveal that higher syngas yields and dry gas flow rates were observed at a lower temperature of 900°C for samples with higher char reactivity. Meanwhile, those with low char reactivity produced higher syngas yields and dry gas flow rates mostly at higher temperatures of 950°C and 1000°C. Therefore, wood samples with high char yield and high char reactivity proved more suitable as feedstock for the production of syngas at lower temperatures in the gasification phase. However, as would be discussed in Chapter 6, high char reactivity may limit char residence time in the gasification phase.

4.2.7 Fuel Quality Evaluation

Table 4.6 shows the results of the fuel quality evaluation of the eight wood samples derived from their experimental results presented in Sect. 4.2. The evaluation was carried out based on six relevant fuel evaluators and presented in Table 4.6.

Table 4.6: Fuel evaluation scores of wood samples

PARAMETER	RF	BIOMASS															
		Bug weed		Eucalyptus		Jacaranda		Poplar		African mesquite		African oil bean		African mahogany		Opepe	
		PFQR	*SFQS*	*PFQR*	*SFQS*	*PFQR*	*SFQS*	*PFQR*	*SFQS*	*PFQR*	*SFQS*	*PFQR*	*SFQS*	*PFQR*	*SFQS*	*PFQR*	*SFQS*
Char Yield	2	4	8	7	14	2	4	1	2	8	16	6	12	5	10	3	6
Char Reactivity	2	8	16	3	6	2	4	6	12	1	2	7	14	5	10	4	8
Fuel Ratio	2	6	12	7	14	4	8	4	8	8	16	7	14	7	14	5	10
Energy Density	2	2	4	7	14	3	6	3	6	8	16	6	12	5	10	4	8
Nitrogen content	1	-8	-8	-2	-2	-3	-3	-6	-6	-5	-5	-8	-8	-4	-4	-7	-7
Ash content	2	-7	-14	-4	-8	-8	-16	-6	-12	-1	-2	-3	-6	-2	-4	-5	-10
TFSS			**18**		**38**		**3**		**10**		**43**		**38**		**36**		**15**

RF (Relevance Factor of evaluator); PFQR (Primary Fuel Quality Rank); SFQS (Secondary Fuel Quality Score); TFSS (Total Fuel Superiority Score).

4.2.7.1 Char yield and Char reactivity evaluators

The char yield and char reactivity of the wood samples were considered as yardsticks for the feedstock evaluation of the wood samples for pyro-gasification, due to their direct influence on the gasification phase reactions as earlier highlighted. Therefore, given the importance of char yield and char reactivity to pyro-gasification, both evaluators were individually assigned a relevance factor of 2 (see Table 3.1).

Considering its moderate char yield and its highest rate of char reactivity relative to those of other samples, the Bugweed was assigned an intermediate PFQR of 4 for char yield and the highest PFQR of 8 for the char reactivity evaluation. In contrast to the Bugweed, the African mesquite, exhibited a rather gradual char decomposition extending beyond 800°C. This was as a resulting of its very low char reactivity averaging 0.87 %/min with no apparent peak. Its char gasification reactions, therefore, would require a higher activation energy, triggered by high gasification temperature inputs, or lowered by the presence of a suitable catalyst. Therefore the A. mesquite was assigned the highest PFQR of 8 for its high char yield and the lowest PFQR of 1 for its very low char reactivity relative to the other seven samples. The PFQR for Char yield of the samples is presented in the following order:

African mesquite (8) > Eucalyptus (7) > African oilbean (6) > African mahogany (5) > Bugweed (4) > Opepe (3) > Jacaranda (2) > Poplar (1)

For the Char reactivity, the samples were ranked in the following order:

Bugweed (8) > African oilbean (7) > Poplar (6) > African mahogany (5) > Opepe (4) > Eucalyptus (3) > Jacaranda (2) > African mesquite (1)

The effect of the highly porous nature and low bulk density of most softwoods on their char yield was also evident in the results of the TGA tests conducted (see Chapter 5). It was observed that the initial decomposition temperatures (IDTs) were mostly lower for the softwoods due to their lower bulk densities which is a factor of their higher porosity.

4.2.7.2 Fuel ratio evaluator

The data for the fuel ratio evaluation was obtained from the fuel ratio results of the samples in Table 4.6. In conducting this evaluation, the fuel ratio evaluator was also assigned a relevance factor of 2. This is due to the influence of the volatile matter and fixed carbon contents of the biomass feedstock on the type and yield of the pyrolysis phase products, which in turn affect the quality, composition and yield of the final syngas produced [103,104]. The high amounts of VM and relatively low FC of biomass solid fuels makes them more reactive and less energy-dense than coal [156]. In as much as high volatile matter content in biomass is a desirable property for the quick ignition when blended with coal for combustion, in the gasification phase, higher amounts of fixed carbon are most desired to promote syngas yield. Moreover, as previously mentioned, the presence of these tar-forming volatiles generated by biomass affect syngas quality and limit its end use for downstream applications [71]. Therefore, samples with higher fuel ratios (i.e. Higher FC and lower VM) were considered most desirable for pyro-gasification.

The derived fuel ratios of the samples tested, revealed lower values for Opepe (0.6), Poplar (0.53) and Jacaranda (0.53). Therefore, low PFQRs were assigned to these samples to satisfy their low fuel ratios. Meanwhile, the FC content were observed to be slightly higher than the VM content in hardwood species like the African mesquite, and as such, it exhibited a higher fuel ratio of 1.08 and the highest PFQR of 8. Three hardwoods – the Eucalyptus, African mahogany and African oil bean, all exhibited an equally high FR of 0.80 and hence were equally assigned a PFQR of 7. The combination of a very high MC and VM exhibited by Poplar (12.21% MC; 56.56% VM) and Jacaranda (9.12% MC; 57.91% VM), may have had a significant impact on their fuel ratios which were lowest at 0.53. High moisture content is known to limit the fuel quality of solid fuels. Therefore, both species were also equally assigned the least PFQR of 4.

Despite the samples in this study exhibiting high volatile matter contents comparable to those of other woody biomass samples reported in literature (see Table 4.7), their fixed carbon contents were, however, observed to be higher than

those of most other biomass. This disparity may be attributed to variations in moisture contents and ash contents common with biomass as a result of growth conditions, storage and handling. Moreover, as previously mentioned, moisture and ash content may vary between wood samples of the same species. This is possible if both samples were harvested in different geographical and climatic locations or harvested from different parts of the same tree. The wood samples evaluated in this study were harvested from the trunks of trees and stem in the case of the Bugweed. As reported in a study by Duruaku *et al.* [39], comparing the fuel properties of the main branches and trunks of 11 tropical trees, wood samples harvested from the trunks exhibited better fuel properties than their counterparts sourced from the main branches of the same tree. The PQFR and corresponding SFQS for the fuel ratio evaluator are summarised in the following order:

African mesquite (8) > (Eucalyptus = African mahogany = African oil bean (7)) > Bugweed (6) > Opepe (5) > (Jacaranda = Poplar (4))

In comparison to fuel ratios of other wood and woody biomass reported in literature, Table 4.7 presents VM, FC and corresponding fuel ratios of the wood samples used for this study.

Table 4.7: Comparison of proximate properties of wood samples in this study with literature

WOOD AND WOODY BIOMASS	VM %	FC %	FUEL RATIO	REFERENCE
Eucalyptus	48.88	39.98	0.8	This study
Bugweed	54.92	34.44	0.63	This study
Poplar	56.56	30.2	0.53	This study
Jacaranda	57.91	30.76	0.53	This study
African mesquite	43.29	47.11	1.08	This study
Opepe	58.65	33.17	0.60	This study
African mahogany	52.12	40.36	0.80	This study
African oilbean	51.01	39.86	0.80	This study
Poplar bark	73.6	16	0.22	[49,158]
Tamarack bark	63.7	24.1	0.38	[49,158]
Spruce bark	67.3	21.4	0.32	[49,158]
Pine bark	70.2	23.3	0.33	[49,158]
Elm bark	67	17.2	0.26	[49,158]
Maple bark	70.1	17.8	0.25	[49,158]
Balsam bark	70.9	18.3	0.26	[49,158]
Beech bark	65	23.9	0.25	[49,158]
Birch bark	71.7	17.8	0.25	[49,158]
Eucalyptus bark	68.7	15.1	0.22	[159]
Hemlock bark	65.9	23.4	0.36	[49,158]
Oak wood	77.6	21.9	0.28	[49,160]
Olive wood	74.3	16.1	0.22	[49,161]
Pine wood	76.50	14.45	0.19	[174]
Spruce wood	71.0	14.4	0.20	[174]
Willow wood	74.2	14.3	0.19	[49,163]
Alder-fir wood	36.3	9.1	0.25	[49,164]
Poplar wood	79.7	11.5	0.14	[49,164]
Hybrid Poplar wood	78.97	11.63	0.15	[164]
Christmas tree wood	46.02	12.93	0.28	[49,164]
Red oak wood	76.35	11.92	0.16	[164]
Beech wood	82.5	17.0	0.21	[160]

4.2.7.3 Energy density evaluator

The energy density of a combustible material is a function of its HHV and its bulk density $\boldsymbol{\varrho_B}$ (which largely influences the rate at which hot gases penetrate its inner particles as well as its burning/flame duration) [156,175]. It is defined as the amount of energy obtainable from a unit volume of fuel. In this study, the energy density evaluator was assigned an RF of 2 to justify its influence on the fuel conversion efficiency and heating value of the final syngas product. Classified as a desirable evaluator to pyro-gasification, the sample with the highest energy density was assigned the best PFQR of 8 out of eight and vice-versa.

Low values of biomass bulk density and HHV impact severely on its overall utility as feedstock particularly, in its pre-treatment, storage and handling. Most especially, it affects its thermochemical conversion efficiency of the biomass and the HHV of the final syngas product. The bulk density of raw biomass is approximated to be about one fifth and its heating value at about half that of coal [180]. This low bulk density of biomass results to its poor grindability, high hydrophobicity, low resistance to weathering and biological attack; and most importantly the high agglomeration of its particles during feeding onto a gasifier. Expensive improvement practices such as thermal pre-treatments like torrefaction alongside storage and handling preparations are often required before their thermochemical conversion. Also, the desirability of a biomass feedstock for biofuel production is to a large extent, a function of its calorific value.

Due to their high bulk densities and HHVs as previously highlighted, the calculated energy density, therefore, was highest for the African mesquite (21.76 GJ/m^3) and eucalyptus (19.03 GJ/m^3). Hence, they were assigned a PFQRs of 8 and 7 in the energy density evaluation. Meanwhile, the Bugweed with its very low energy density (7.03 GJ/m^3) (resulting from its low bulk density and HHV), was assigned the lowest PFQR of 1 in this category. The PFQR of the wood samples under the Energy density evaluation are summarised in the following order:

African mesquite (8) > eucalyptus (7) > African oil bean (6) > African mahogany (5) Opepe (4) > (Poplar = Jacaranda (3)) > Bugweed (2)

In general, the energy densities of the hardwoods such as the African mesquite, African mahogany, Opepe and African oil bean, were comparable to those reported in literature [39]. They were also observed to be higher than those of their softwood counterparts in this study. This can be attributed particularly to their superior bulk densities since the difference between their HHVs were minimal.

4.2.7.4 Nitrogen emissions evaluator

Biomass containing low values of elemental nitrogen and sulfur contents are desirable for pyro-gasification and other thermochemical conversion processes [75]. As earlier mentioned, the incombustible nitrogen compounds – N_2, NO_X (NO, NO_2), N_2O, formed during thermochemical processes into the atmosphere while NH_3 and HCN are undesirable for syngas downstream applications. However, due to the small quantity of sawdust tested, the effects of the nitrogen composition of the samples was not significant. Within the scope of this study, any gaseous nitrogen compounds present in the syngas was not detected. Meanwhile, as earlier observed, the sulfur content of the samples evaluated were negligible and therefore sulfur composition was not considered as part of the evaluation.

Asides the negative impacts caused by its emission, nitrogen on the other hand, was more important in this study as plant biomass most times is known to contain significant amounts of nitrogen, particularly when growing on agricultural active soils. Naturally, soils contain an adequate amount of nitrogen, supplied naturally by a nitrogen fixation process in a nitrogen cycle. However, in most cases, the increased use of fertilizers for soil rehabilitation in agriculture increases soil nitrogen concentration which exceeds the usable nitrogen composition of the soil. While the extra nitrogen concentration in the soil is attractive for agriculture, it impacts on the nitrogen balance of the ecosystem. Therefore, plants are left to take up and store the excess soil nitrogen thereby making them less ideal biomass feedstock for energy production.

In this study, the nitrogen compounds evaluator was assigned a factor of 1. This was because the nitrogen compositions of most wood samples evaluated were also below the maximum allowable limits of 0.3%, except for those of the Bugweed (0.4% N), Opepe (0.37 % N) and the African oil bean (0.4% N). Despite the slightly greater composition of nitrogen in these samples, their nitrogen compositions were still comparably much lower than those of coals. As one of the two classified undesirable evaluators, the sample with the least nitrogen content was assigned the best PFRQ of -1 out of eight and vice-versa. Informed by the nitrogen composition of the samples, the PFRQ ranking was in the order of:

Eucalyptus (-2) > Jacaranda (-3) > African mahogany (-4) > African mesquite (-5) > Poplar (-6) > Opepe (-7) > (African oilbean = Bugweed (-8))

4.2.7.5 Ash deposition evaluator

The ash content is a key factor in selecting any combustible material as a feedstock because its deposition is known to accelerate the corrosion of internal reactor components. Moreover, a common occurrence in combustion and gasification of biomass which is also expected in pyro-gasification is the deposition of layers of ash residues containing reaction-inhibiting silicone particles on the char surface. These ash layers block char pores and inhibit the free transfer of hot oxidizing gases into its inner carbon particles. This thereby minimizes the rate of char partial oxidation and conversion of the inner carbon particles [90,91,181]. This occurrence greatly reduces char oxidation rates and consequently lowers the optimum gasifier temperature [182]. Problems such as poor energy conversion efficiency, catalyst deactivation due to ash fouling, agglomeration due to the low melting point of biomass ash, sintering, aggregation, deposition and eventual corrosion of the gasifier, can arise as a result of high amounts of ash in the feedstock. Moreover, ash in high amounts reduces the calorific value of the feedstock and thus result in a reduced syngas calorific value. It is worthy of note that high char yield does not necessarily translate to a high concentration of fixed carbon present in the char. High ash composition in the raw biomass contributes to high char yield since char is primarily made up of fixed carbon and ash particles. In such a

situation, the gasification phase reactions will be greatly hindered by the huge presence of ash residue.

The ash evaluator was assigned an RF of 2 due to the generally greater ash compositions exhibited by most samples in comparison to the Austrian and German recommended maximum values of 0.5% and 1.5%. Unlike with coal, the lower ash composition of woody biomass may be insignificant if used for combustion. However, this may not be the case if considerable deposits of ash are formed during pyro-gasification.

Out of the eight samples, the jacaranda exhibited the highest ash content of (2.21%) and hence was assigned a PFQR of -8. Meanwhile, the least PFQR of -1 was assigned to the African mesquite for its negligible ash composition of 0.01%. With respect to the experimental results, the PFQR for ash deposition evaluation of the samples were summarised in the following sequence:

African mesquite (-1) > African mahogany (-2) > African oilbean (-3) > Eucalyptus (-4) > Opepe (-5) > Poplar (-6) > Bugweed (-7) > Jacaranda (-8)

4.3 Concluding remark

In this chapter, the results of the characterization of the eight wood samples were presented and discussed. Finally, a fuel quality evaluation of the individual samples based on the experimental results of their characterization was conducted. Below is a summary of the findings from these results.

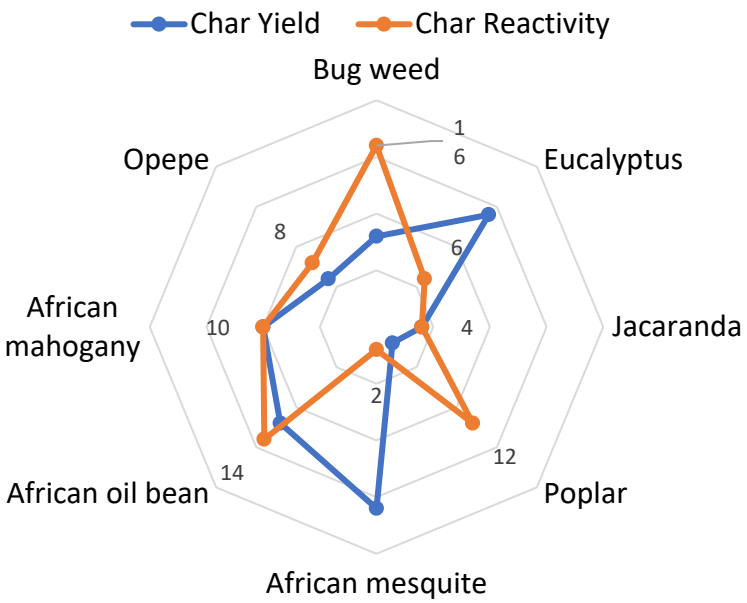


Figure 4.2: Chart depicting a comparison of the Char yield and Char reactivity fuel evaluation ranks of the wood samples relative to each other.

The structural analysis of the samples shows a generally higher lignin composition in the hardwoods than the softwoods. This reflected on the higher HHV, elemental carbon and fixed carbon composition of the hardwoods, which are largely dependent on the amount of lignin present in a feedstock.

Volatile matter composition was observed to be slightly higher in the Bugweed, Poplar, Jacaranda and Opepe. This was attributed to their relatively high holocellulose compositions. Such high amounts of VM contribute to high tar generation in the pyrolysis of biomass. Ash composition was insignificant while FC was relatively higher in the African mesquite and African mahogany, thus resulting in the production of char with high carbon concentrations.

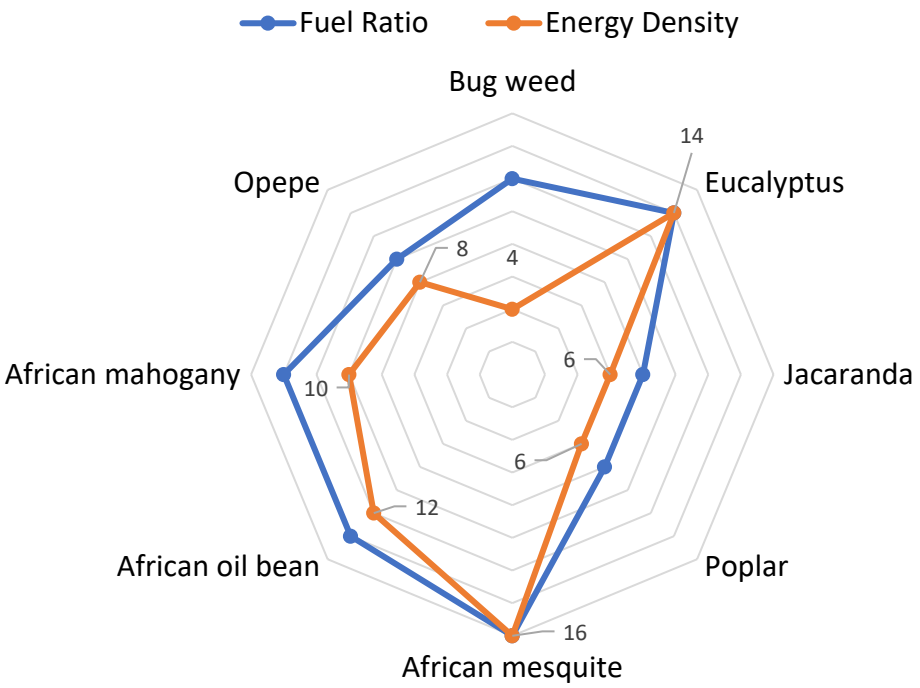


Figure 4.3: Chart depicting the Fuel ratio and Energy density fuel evaluation ranking of the wood samples relative to each other.

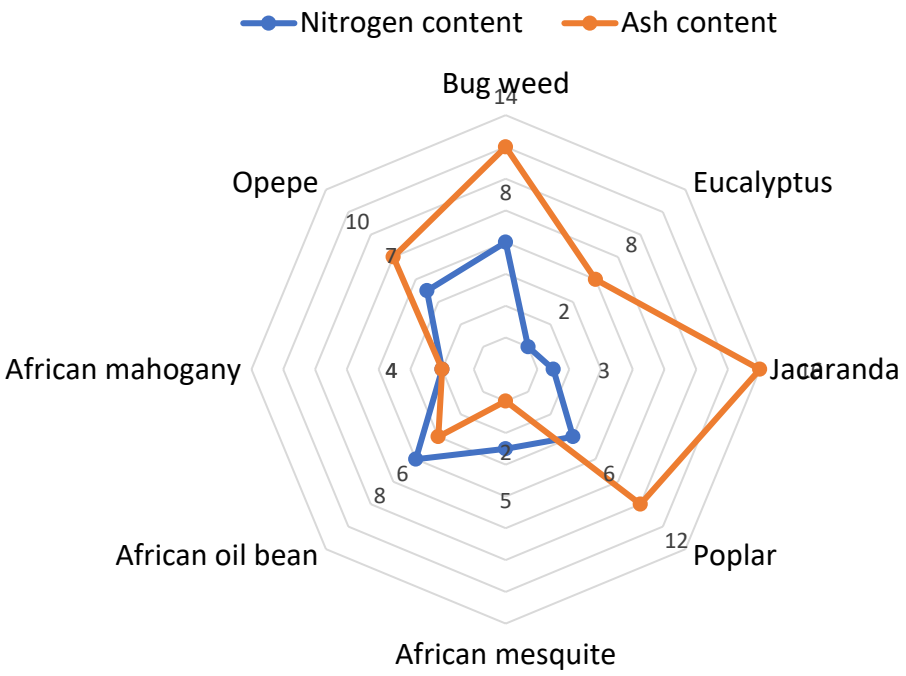


Figure 4.4: Chart depicting the Nitrogen content and Ash content fuel evaluation ranking of the wood samples relative to each other.

Results of the ultimate analysis reveal no traces of sulfur in any of the wood samples. However, nitrogen concentrations in the Bugweed, Opepe and the African oilbean were observed to exceed the recommended limits for wood fuels. As expected, high elemental carbon was observed in the hardwood samples – Eucalyptus, African mesquite, African mahogany, African oil-bean and Opepe, which exhibited higher lignin and FC compositions. As a result, their HHVs were observed to be higher than those of the softwoods – Jacaranda, Bugweed and Poplar.

A summary of the total fuel superiority of the samples relative to each other across all evaluators is depicted in Fig. 4.5. The very low overall score of 3 for the jacaranda can be attributed mostly to its tendency to deposit high amounts of ash. Moreover, due to the significant effect of ash deposition which could inhibit the gasification phase reactions, the ash evaluator was given a high RF of 2. The Jacaranda also scored relatively low SFQS under important evaluators such as the char yield, char reactivity, fuel ratio and energy density. These would also reflect

on the dry gas flow rate of the syngas produced during its pyro-gasification, thus, reinstating the need for its blending with other samples as presented in Chapter 6.

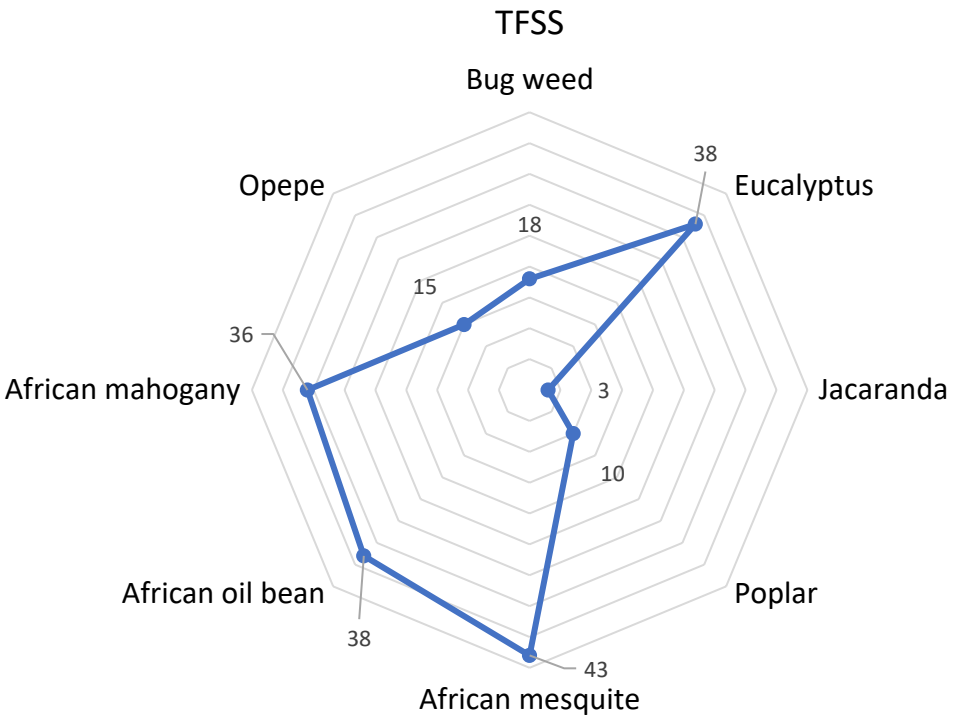


Figure 4.5: Chart depicting the Total fuel superiority ranking of the wood samples relative to each other.

Conversely, the African mesquite scored the highest TFSS of 43, due to its overall superior SFQS across all evaluators except for the char reactivity evaluator. This very low char reactivity of the African mesquite was also evident in the very low gas flow rate of the syngas observed during its pyro-gasification as presented in Chapter 6.

As depicted in the Figure 4.5, all hardwood species asides the Opepe, generally recorded much higher TFSS than the softwoods – Jacaranda, Poplar and Bugweed. However, it is worthy of note that the TFSS results of the woods samples do not necessarily classify them as either the most ideal or least ideal for pyro-gasification. Most importantly, their PFQR under each evaluator offers a clearer insight into their strengths and weaknesses under each evaluator. It also informs

the exploration of blending two wood species of contrasting properties. For instance, the outstanding PFQR exhibited by the Bugweed under the char reactivity evaluator creates an opportunity to explore its blending with the African mesquite which exhibits a very low char reactivity PFQR. Meanwhile, the African mesquite, on the other hand, exhibits exceptional fuel ratio and energy density observed to be low on the Bugweed.

Chapter 5

Thermogravimetric Analysis (TGA) and Kinetic Study of the wood samples

5.1 Introduction

This chapter presents and discusses the following:

i. The Thermogravimetric Analysis; and

ii. Kinetic study of the samples' thermal decomposition.

The aim of conducting these analyses was to provide information for the selection of suitable parameters for the pyro-gasification experiment. This also provided an idea on what wood species would provide the best possible blend for maximum syngas production at the lowest set gasification-phase temperature.

5.1.1 Thermogravimetric Analysis (TGA) / Derivative Thermogravimetry (DTG)

In analysing the TG and DTG data of the samples, more emphasis was placed on comparing the decomposition patterns of the individual sample thermograms with each other. A side by side comparison of the these DTG thermograms as well as peaks in the rate of volatilization and char thermal decomposition observed at particular temperatures were noted. From the thermograms, the thermal decomposition data such as the start, midpoint and end of volatilization, and burn out temperature of each sample were also collated and presented in Table 5.1.

5.1.2 Kinetic study

In this section, the parameters of the derived kinetic equation developed by Friedman (Sect. 3.4.2), were used to develop a straight-line graph and a corresponding straight-line equation. From the intercept C and slope M, of the generated straight-line graph equation, the activation energies E_a of the samples were derived.

The activation energy of a combustible material is the least amount of energy required to kick-start any reaction in which it participates in as a reactant. In this case, the activation energy of the wood samples is the least energy required to

commence its thermal decomposition. However, as earlier discussed, lignocellulosic biomass is known to be a natural composite material comprising of its three structural components – hemicellulose, cellulose and lignin, which are in most cases, thermally non-monolithic. Individually, these components thermally decompose at different rates with peaks occurring at varying temperatures. An evidence of this can be observed by plotting a graph of conversion **α** of the Jacaranda against temperature **T**, as shown in Fig. 5.1.

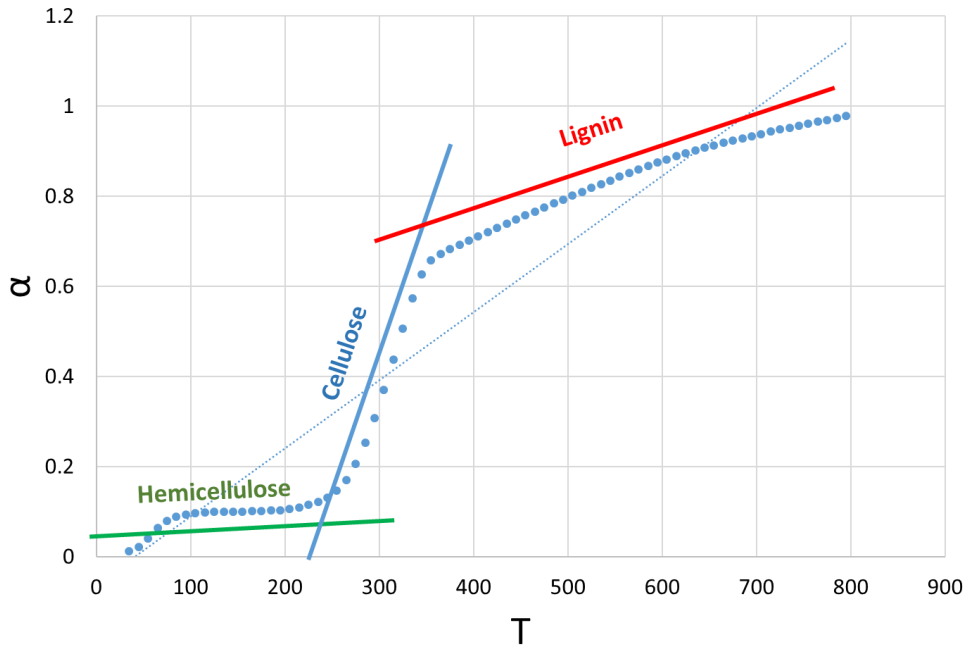


Figure 5.1: Typical non-monolithic decomposition patterns of biomass structural components.

The graph shows a non-monolithic decomposition of the biomass structural components. This is represented by the three different slopes with tangents intercepting each other at the beginning of three temperature ranges which correspond to the start of the thermal decomposition of each structural component.

Therefore, the kinetic study of each wood sample was conducted, by independently analysing and deriving the kinetic parameters of each structural component – hemicellulose, Cellulose and Lignin.

5.2 Results and Discussion

5.2.1 TGA and DTG of wood samples

Figures 5.2 – 5.9, depict the thermogravimetric decomposition patterns of the individual samples, while Figs. 5.10 and 5.11 are overlays of the derivative thermogravimetry thermograms of the samples. Data extracted from these graphs are summarized in Table 5.1. The wide variations in the decomposition patterns of the thermograms provide a clearer perspective of the distinctiveness in the thermal properties of the individual wood samples. These results also reflect the properties of these samples as previously observed in their characterisations, presented in Chapter 4. The thermograms depicted, give an insight into the potential behaviours of the samples when subjected to the actual pyro-gasification process. They further inform the need to explore the blending of the individual samples with each other.

5.2.1.1 Volatilization phase

In predicting the temperature regime for the pyrolysis phase of the pyro-gasification process, the volatilization temperature points – T_{start}, $T_{mid\text{-}point}$, T_{end}, T_{peak}, as well as the volatilization time interval of the potential feedstock are of utmost importance. The volatilization phases of the individual samples were, however, observed to collectively occur roughly between 200°C and 400°C – which is common with most woody biomass. Considering its bulk density which permit the quicker transfer of heat through to its inner particles, the T_{start} of the Bugweed was observed to be lowest compared to those of other samples. However, a sample's bulk density (and pore size) which directly influence the heat transfer rate into its inner particles, can be considered as a major factor only if the wood, in its lump size, was subjected to the thermal treatment. This was also observed in the study by Pattanotai *et al.* [77]. Therefore, the low-temperature volatilization of the Bugweed in this study was attributed mostly to the high reactivity of its particles (see Chapter 4) and particle density since its particles tested were milled to sawdust. These high reactivity and particle density were also evident in its much higher peak rate of volatilization (11.36 %/min) and much lower volatilization time

interval of 4.84 min. It highlights the suitability of the Bugweed for blending with the less reactive wood species. Conversely, more energy input was required to commence the volatilization of the African mesquite. Its higher T_{start} (304^{o}C) and corresponding high $T_{mid\text{-}point}$ (329.66^{o}C), creates a wide temperature shift from those of other samples. This was attributed to its much higher particle density, lower reactivity and partly to its high lignin composition as previously characterised. It, however, highlights its poor ignition at lower temperatures and low burning rate which are similar to those of coals. More insight into the activation energies has been presented in Sect. 5.3. It is also worthy of note that, despite its low rate of volatilization, the African mesquite was observed to exhibit an equally low volatilization residence time of 6.05 mins. Such low residence time is typical of those samples exhibiting higher rates of volatilization. Such occurrence can be attributed to the very low holocellulose proportion of the African mesquite, thus resulting to an early depletion of holocellulose structural components.

a. Bugweed:

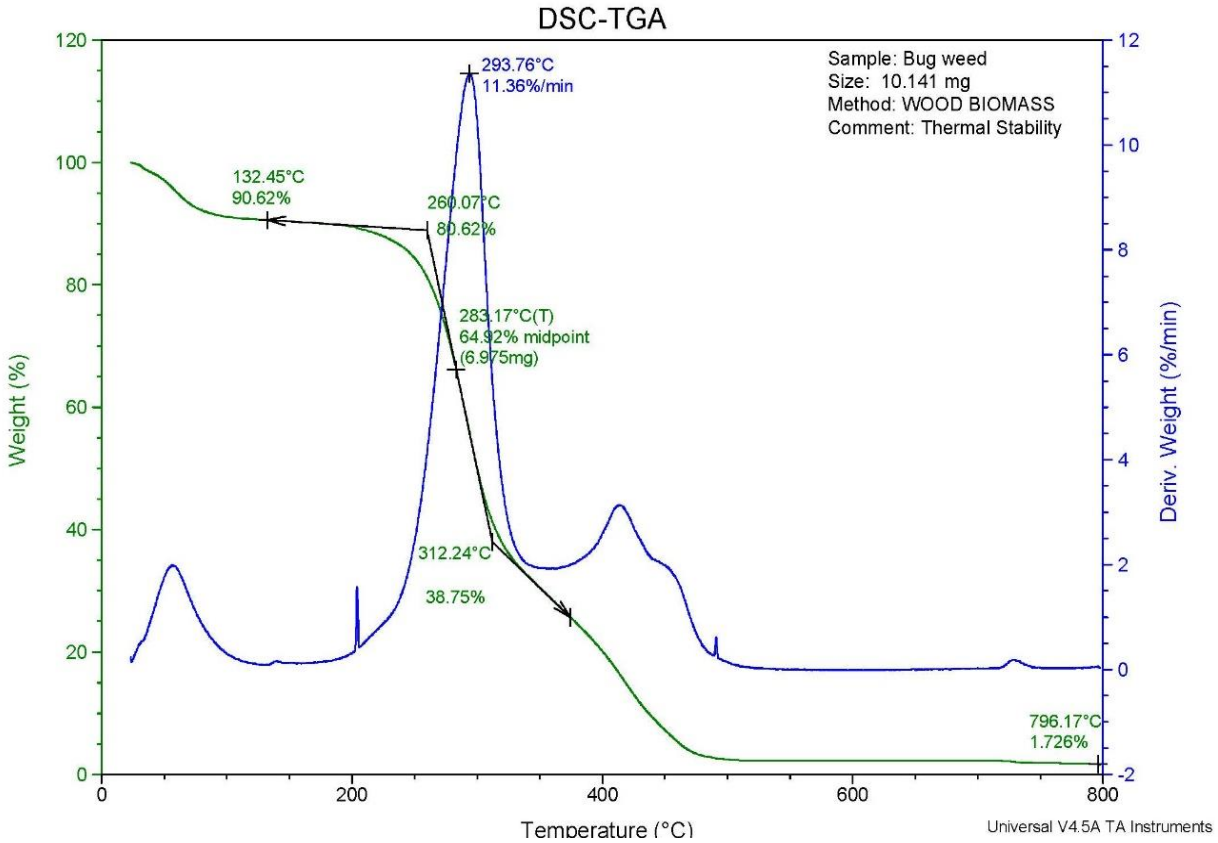


Figure 5.2: TGA and DTG thermograms of Bugweed.

b. Eucalyptus:

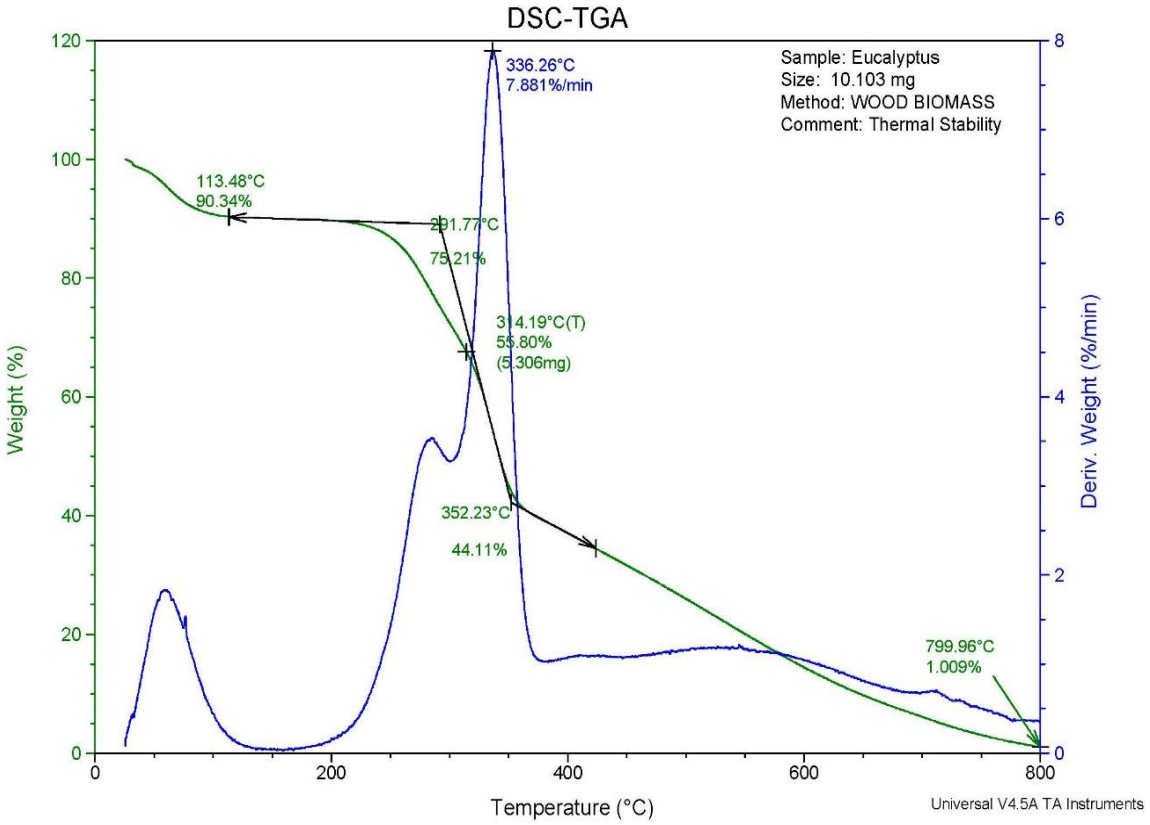


Figure 5.3: TGA and DTG thermograms of Eucalyptus.

c. Jacaranda:

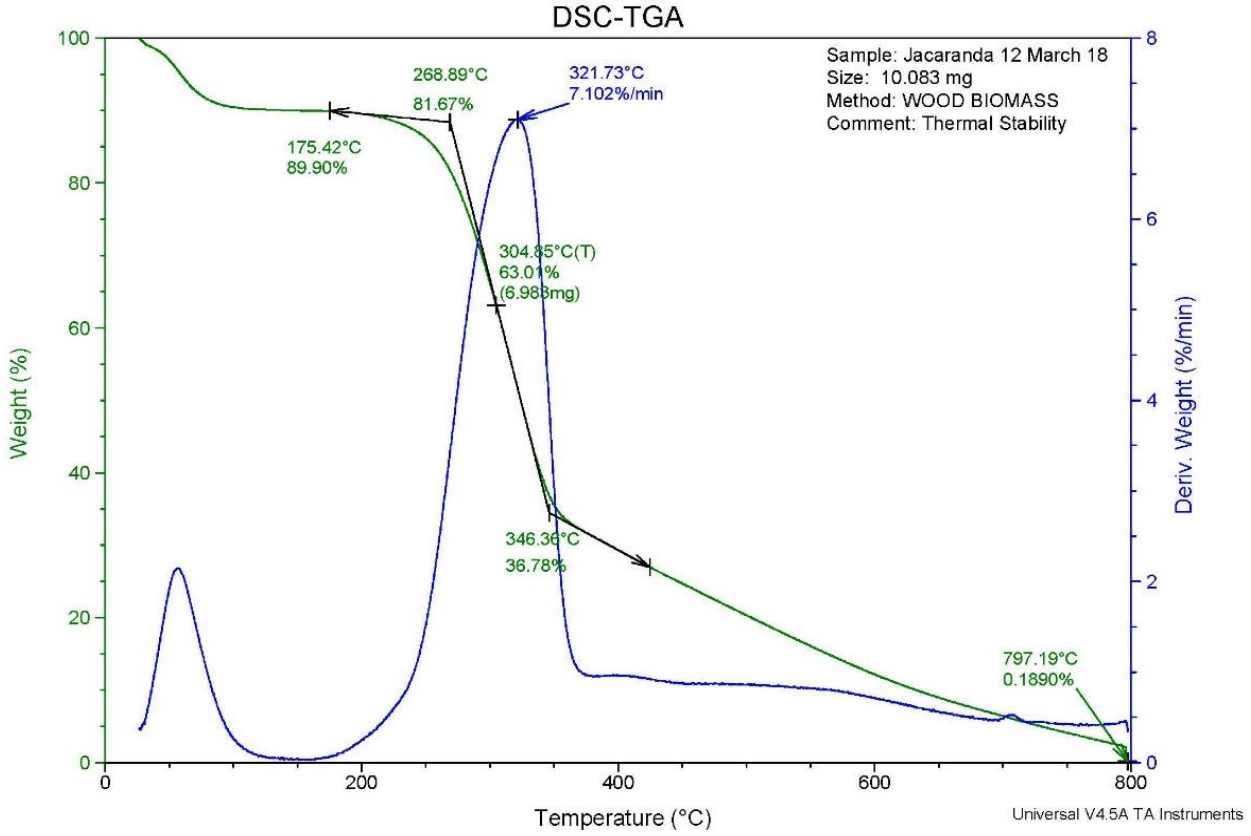


Figure 5.4: TGA and DTG thermograms of Jacaranda.

d. Poplar:

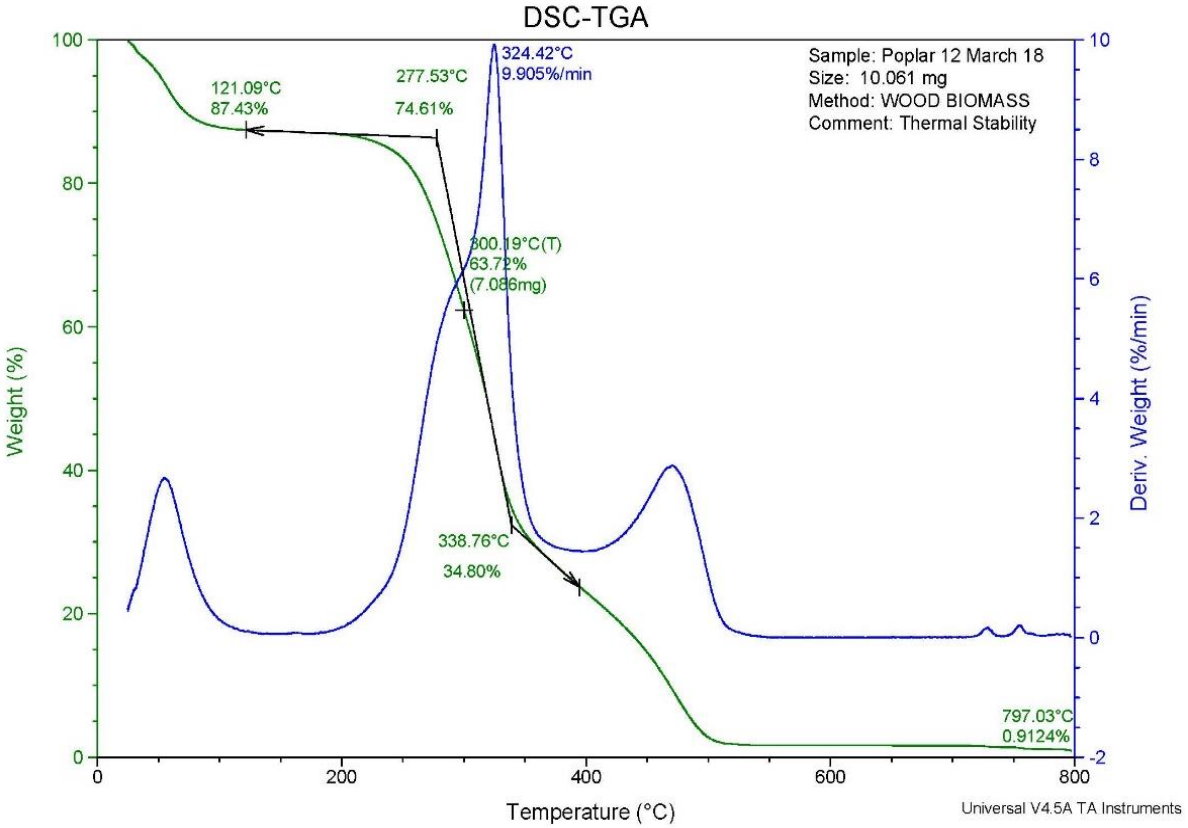


Figure 5.5: TGA and DTG thermograms of Poplar.

e. African mesquite

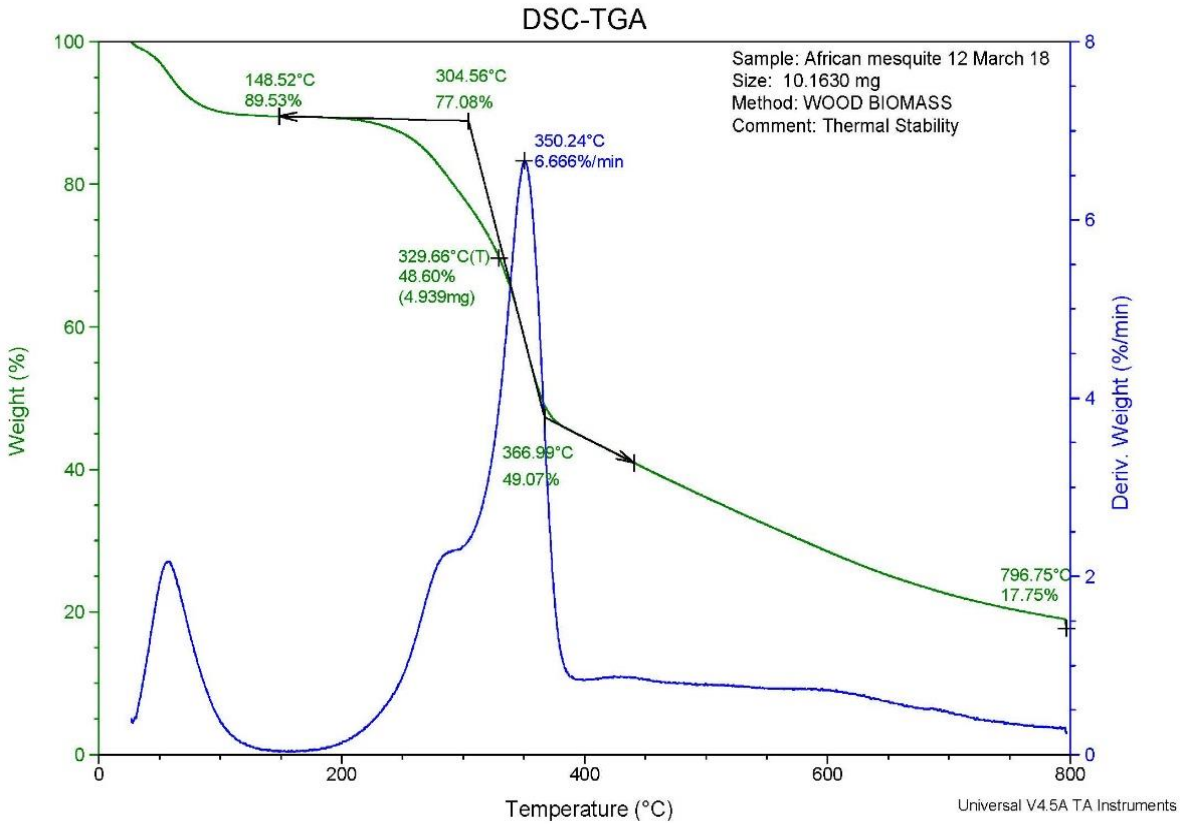


Figure 5.6: TGA and DTG thermograms of the African mesquite.

f. African mahogany:

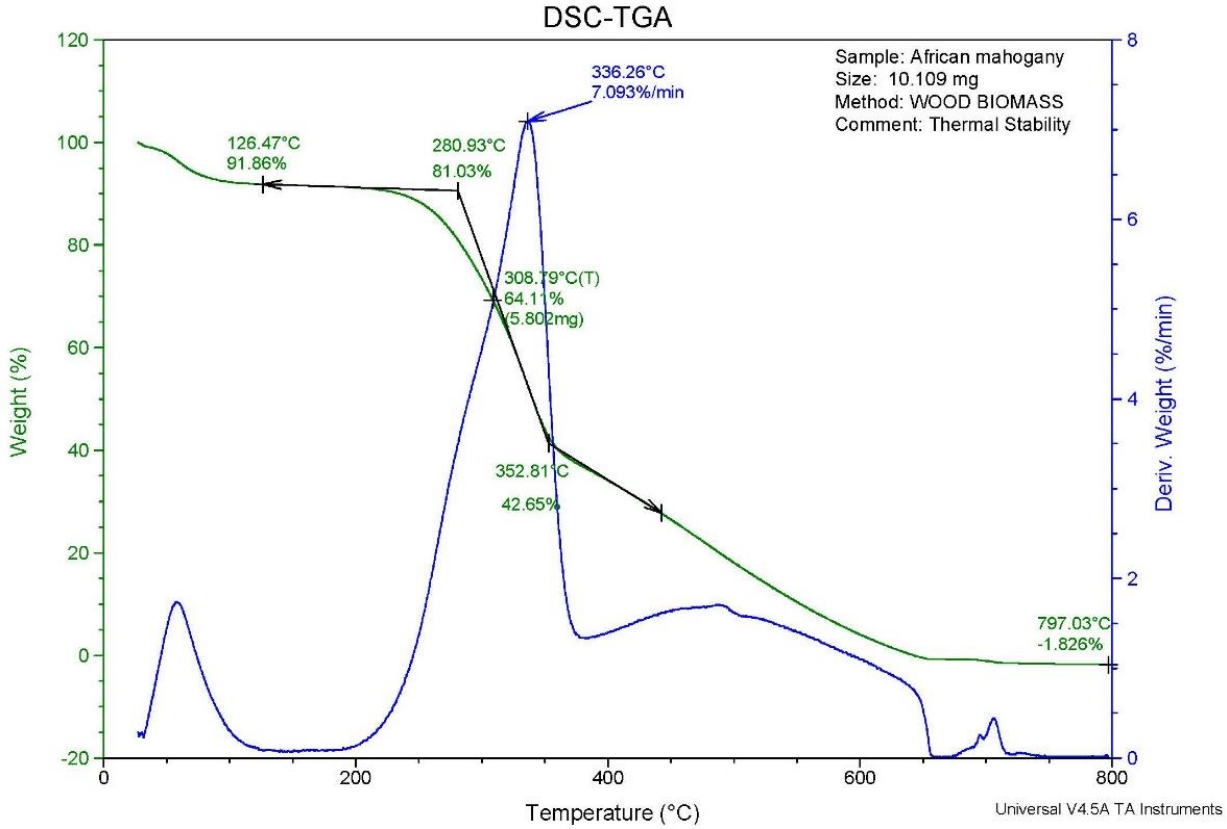


Figure 5.7: TGA and DTG thermograms of the African mahogany.

g. African oil-bean:

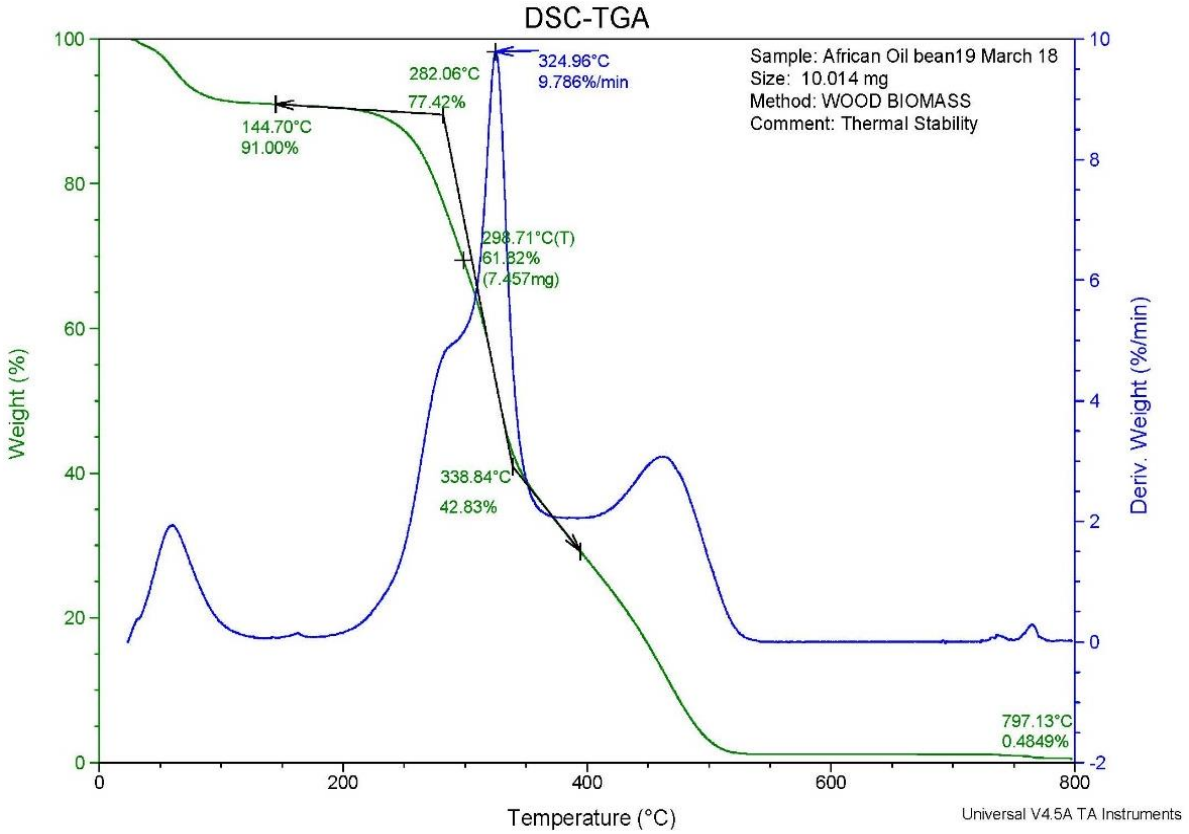


Figure 5.8: TGA and DTG thermograms of the African oilbean.

h. Opepe:

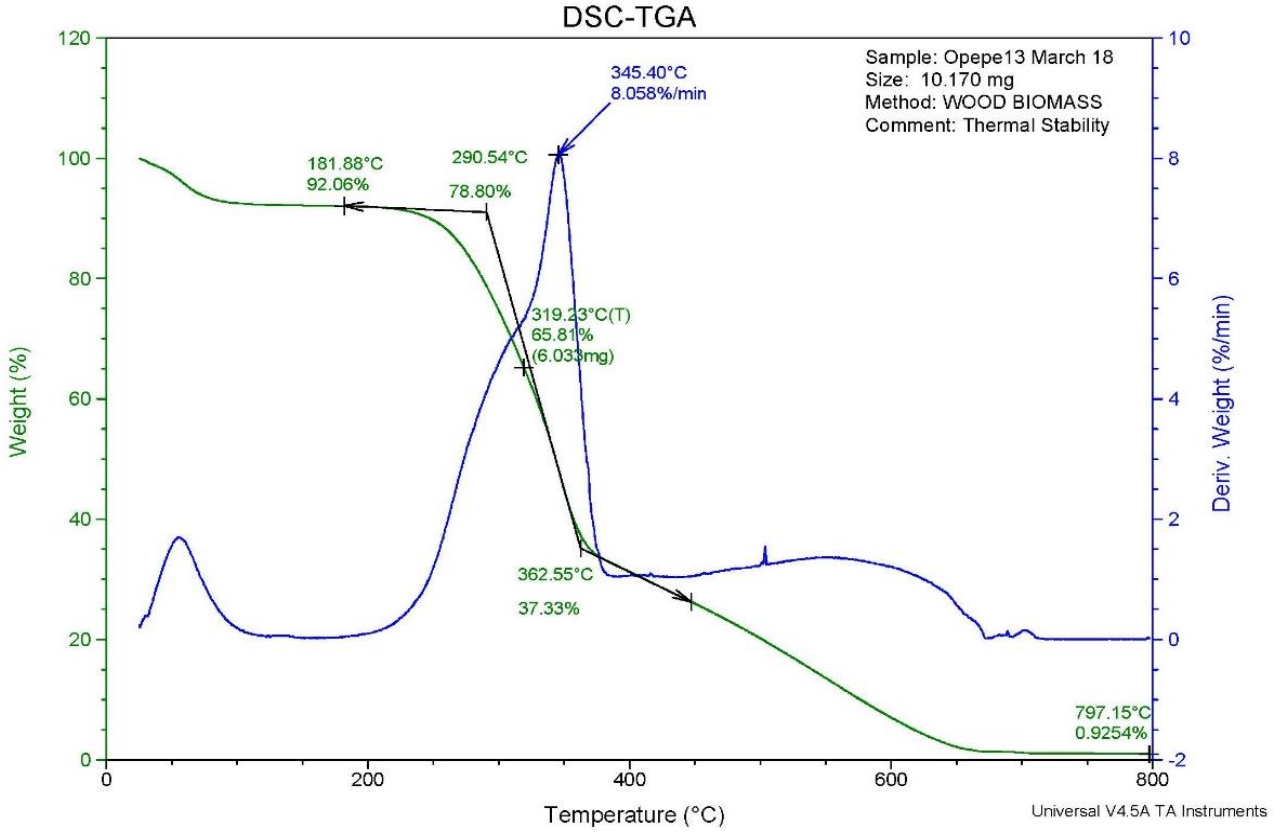


Figure 5.9: TGA and DTG thermograms of Opepe.

i. Overlay of IAP samples DTG thermograms:

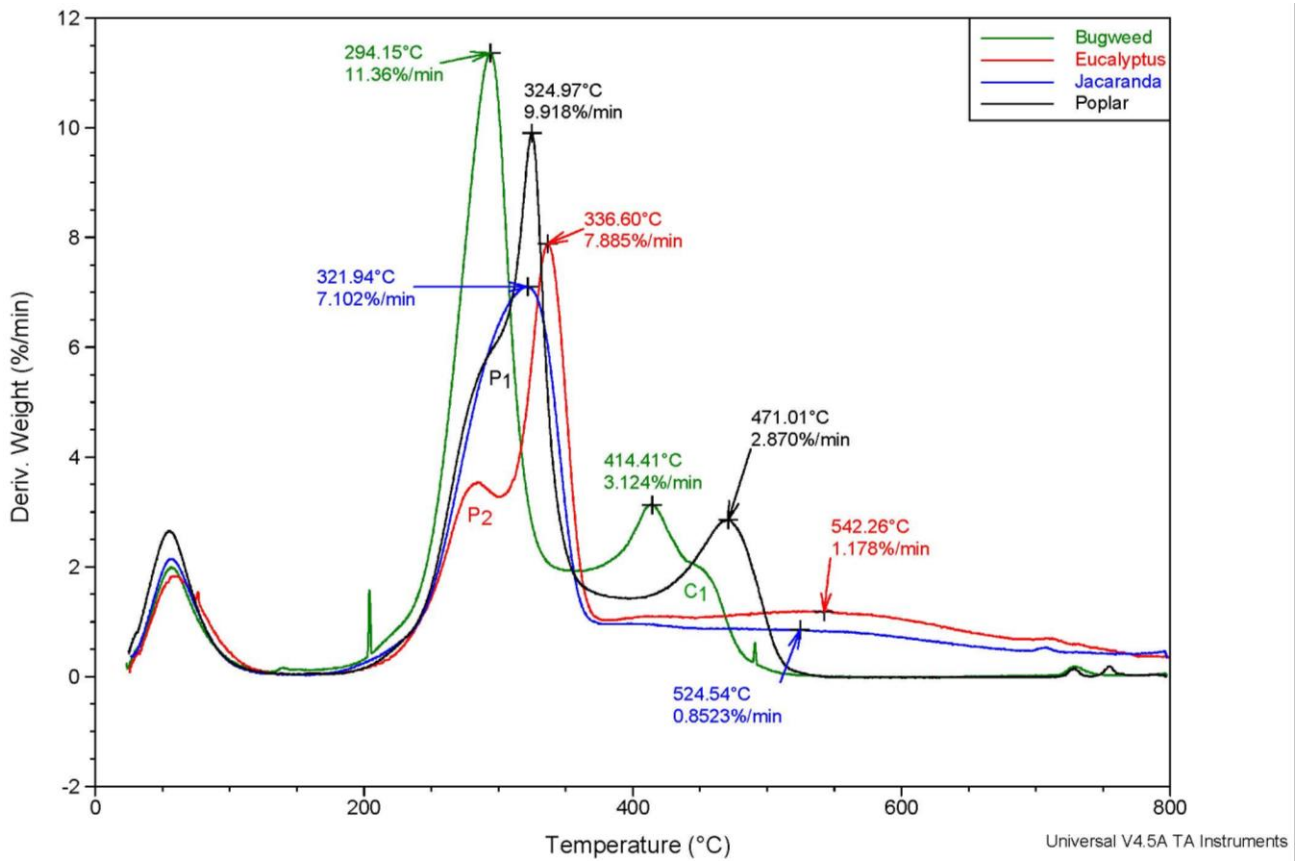


Figure 5.10: An overlay of the DTG thermograms of the IAP wood samples depicting their peak rates of volatilization and char decomposition.

j. Overlay of Tropical samples DTG thermograms:

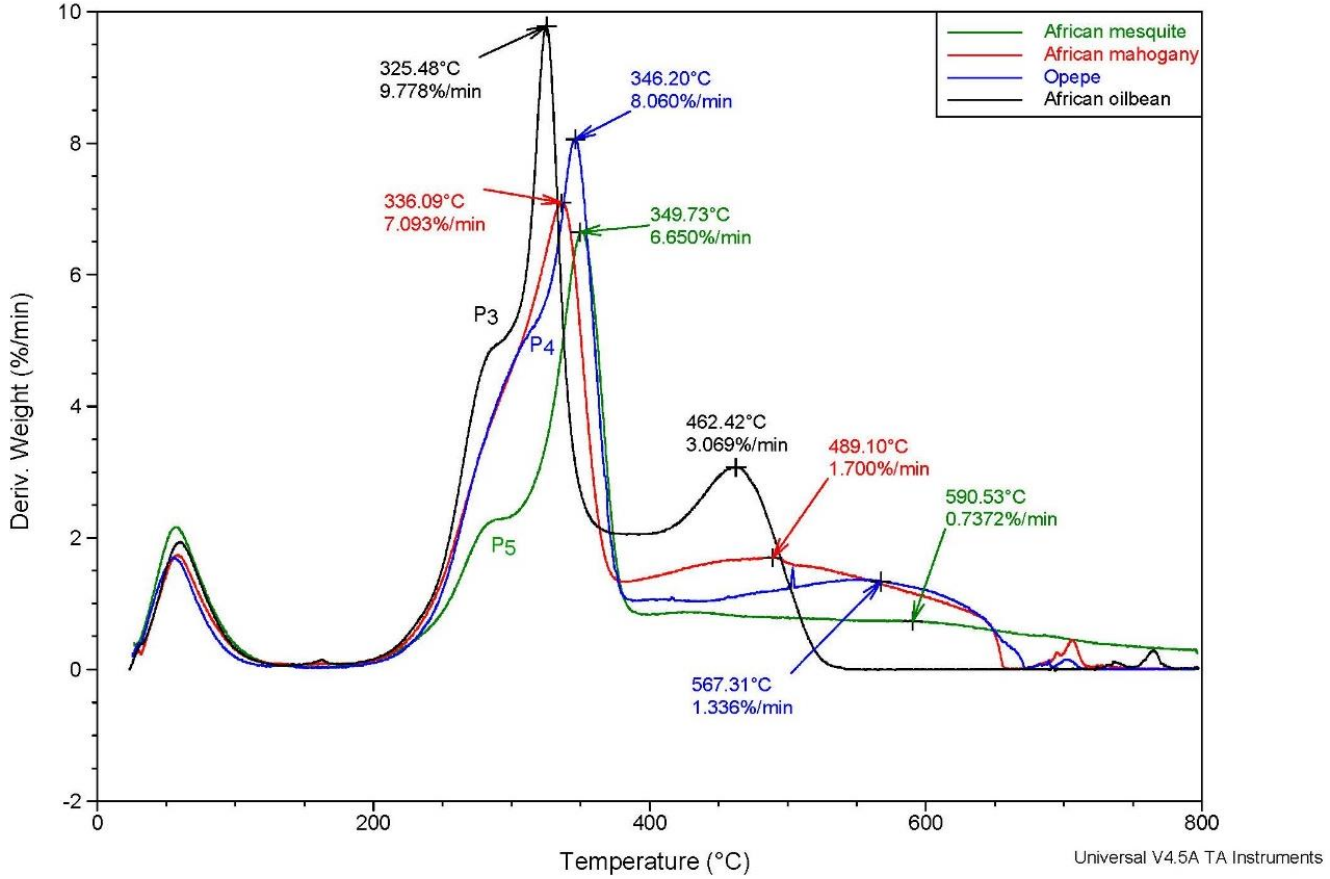


Figure 5.11: An overlay of the DTG thermograms of the Tropical hardwood samples depicting their peak rates of volatilization and char decomposition.

Table 5.1: TGA data of the wood samples.

Heating Rate: *10 °C/min*	**Volatilization**						**Char decomposition**			**Wt. of residue at 800°C**
Sample	**T_{start}**	**$T_{mid-point}$**	**T_{end}**	**T_{peak}**	**Resident time**	**Peak rate**	**$T_{char-end}$**	**$T_{char-peak}$**	**Peak rate**	
	°C	***°C***	***°C***	***°C***	***min***	***%/min***	***°C***	***°C***	***%/min***	**%**
Bugweed	260.07	283.17	312.24	293.76	4.84	11.360	503.34	414.41	3.12	1.726
Eucalyptus	291.77	314.19	352.23	336.26	6.03	7.881	>800	542.26	1.18	1.009
Jacaranda	268.89	304.85	346.36	321.73	9.60	7.102	~800	524.54	0.85	0.1890
Poplar	277.53	300.19	338.76	324.42	8.82	9.905	520.26	471.01	2.87	0.9124
African mesquite	304.56	329.66	366.99	350.24	6.05	6.666	>800	590.53	0.74	17.75
African mahogany	280.93	308.79	352.81	336.26	7.11	7.093	654.31	489.10	1.70	0
African oil bean	282.06	298.71	338.84	324.96	5.35	9.786	527.52	462.42	3.70	0.4849
Opepe	290.54	319.23	362.55	345.40	7.13	8.058	670.33	567.31	1.34	0.9254
Mean Temperature	***282.04***	***307.35***	***333.85***	***329.12***	-	-	***670.47***	***507.70***		

5.2.1.2 Char decomposition

As depicted in Figs. 5.9 and 5.10, the DTG thermograms reflect the uniqueness of each sample with regards to their peak rates of volatilization and char decomposition. As expected, the peak rates of char decompositions of the samples were generally much lower and occurred at higher temperatures than those of the volatilization. This was as a result of the much gradual breakdown of the lignin component at higher temperatures as previously discussed. Besides the African oil bean (3.069 %/min) and Poplar (2.87 %/min), the peak rates of char decomposition of other hardwood samples – African mesquite (0.74 %/min), African mahogany (1.70 %/min), Opepe (1.34 %/min), Eucalyptus (1.18 %/min) occurred at much lower values. This was attributed mainly to their superior energy densities. Understandably, the Poplar exhibited a lower energy density (see Table 4.1) which serves as a major contributing factor to rate of decomposition of any feedstock. Its peak rate of volatilization was also considerably high at 9.905 %/min. Similar to the Poplar, and despite its high energy density (18.19 GJ/m^3), the African oil bean also exhibited a corresponding high rate of volatilization (9.786 %/min). This highlights the unique highly reactive nature of its particles and serves as an indication of a rich syngas production at lower gasification temperatures. Similar to the hardwoods, the Jacaranda (a softwood) however, exhibited a very low peak of 0.85 %/min, despite its much lower energy density (9.4 GJ/m^3). It is also worthy to note its much higher ash composition (2.21%). As earlier described (Sect. 4.3.5), ash inhibits carbon reaction due to its highly inert nature which prevents heat absorption. Moreover, its tendency to form thick layers of ash coating the carbon particles may greatly decrease the decomposition rate of the Jacaranda char and be responsible for its prolonged volatilization time duration of 9.6 min.

The poor reactivity exhibited by the African mesquite led to the presence of a very high char residue of 17.75% at 800°C. This also translates to an incomplete reaction of char during pyro-gasification and a presence of an unreacted char residue after the process. Figure 5.11 is an evidence of a significant mass of unreacted carbon residue (4.22 g) of the African mesquite found in the reactor

after 20 g of its sawdust was subjected to an actual pyro-gasification process as reported in detail in Chapter 6. Thus, with respect to its thermal behaviour, relatively long volatilization residence time (6.05 min) and high energy density, the African mesquite can be considered as feedstock most suitable for combustion.

5.2.1.3 Influence of structural components on thermal decomposition

In addition to the aforementioned observations made from the thermal decomposition of the wood samples, further observations on the influence of the structural compositions of the individual samples on their DTG thermogram patterns (Figs. 5.9 and 5.10) were made and presented as follows.

a. In the volatilization phase, the DTG thermograms of the all hardwood samples – Poplar, Eucalyptus, African oil bean, Opepe and African mesquite, exhibited shoulders – P_1, P_2, P_3, P_4 and P_5 respectively, before attaining their peaks. The only exception being that of the African mahogany.

b. Similarly, a shoulder – C_1 was observed on the Bugweed thermogram after attaining its peak in the char decomposition phase.

In the volatilization phase, the Bugweed attained its peak rate of decomposition at a similar temperature (294.15^{o}C) to those of the shoulders P_1, P_2, P_3, P_4 and P_5. This peak temperature also corresponds to approximately 293^{o}C at which hemicellulose reportedly attains its peak rate of decomposition (see Figs. 2.1, 2.2, 2.3 and 2.4) [65,66,171]. Therefore, the shoulders P_1, P_2, P_3, P_4 and P_5 represent the early decomposition of the hemicellulose fraction of the wood samples. With respect to the aforementioned description, the main peaks of volatilization of the samples can be said to represent the thermal decomposition of the cellulose fraction occurring after that of hemicellulose. Meanwhile, the char peak rates of decomposition represent the decomposition of the lignin fraction of the samples.

In the case of the African mahogany, the absence of any apparent hemicellulose shoulder before attaining its peak maybe as a result of the thermally monolithic behaviour of its holocellulose components whereby the peak rate of decomposition of its cellulose fraction occurred at a similar temperature with that

of its hemicellulose fraction. The softwoods–Bugweed and Jacaranda also appear to share this condition.

In the char decomposition phase, a similar shoulder effect (C_1) was also observed on the Bugweed just after attaining its peak rate of char decomposition. This was attributed to the highly reactive nature of its hemicellulose fraction. As previously explained in Sect. 2.1.3, hemicellulose in most cases form part of the char mass formed after wood pyrolysis. Despite attaining its peak rate of volatilization at a much lower pyrolysis temperature than that of cellulose, the hemicellulose is observed to still retain a considerable mass than the cellulose (see Figs. 2.1, 2.2, 2.4 and 2.5). Due to its crystalline structure, the cellulose is observed to completely decompose (at approximately 390°C) immediately after attaining its peak rate of volatilization. Meanwhile, hemicellulose exhibits a continuous and gradual thermal decomposition of its remaining mass which extends together with lignin to the char decompositions phase. Therefore, due to the highly reactive nature of the Bugweed's hemicellulose in the char fraction, it is observed to exhibit a greater peak rate of decomposition of 3.124 %/min than its lignin counterpart. Moreover, unlike other samples, the peak rate of decomposition attained by the hemicellulose of the Bugweed in this char decomposition phase is also observed to occur at a lower temperature (414.41^{o}C) than that of the its lignin (which peaked at C_1).

5.2.2 Determination of Activation energies:

The calculations for the derivation of the activation energies of the individual structural components of each wood sample was conducted using the straight-line equation generated from their graphs (Figs. 5.12 – 5.19).

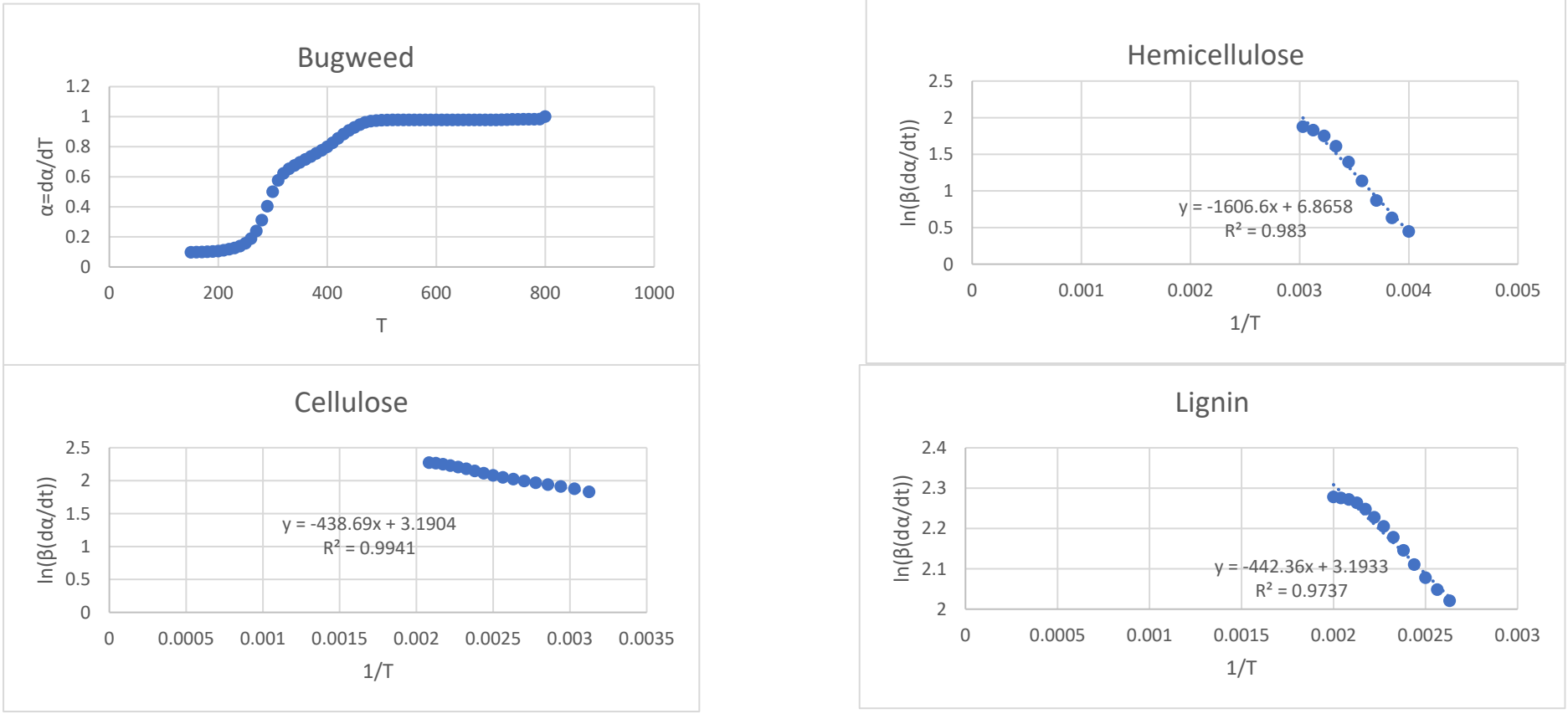


Figure 5.12: Separate decomposition patterns of Bugweed structural components.

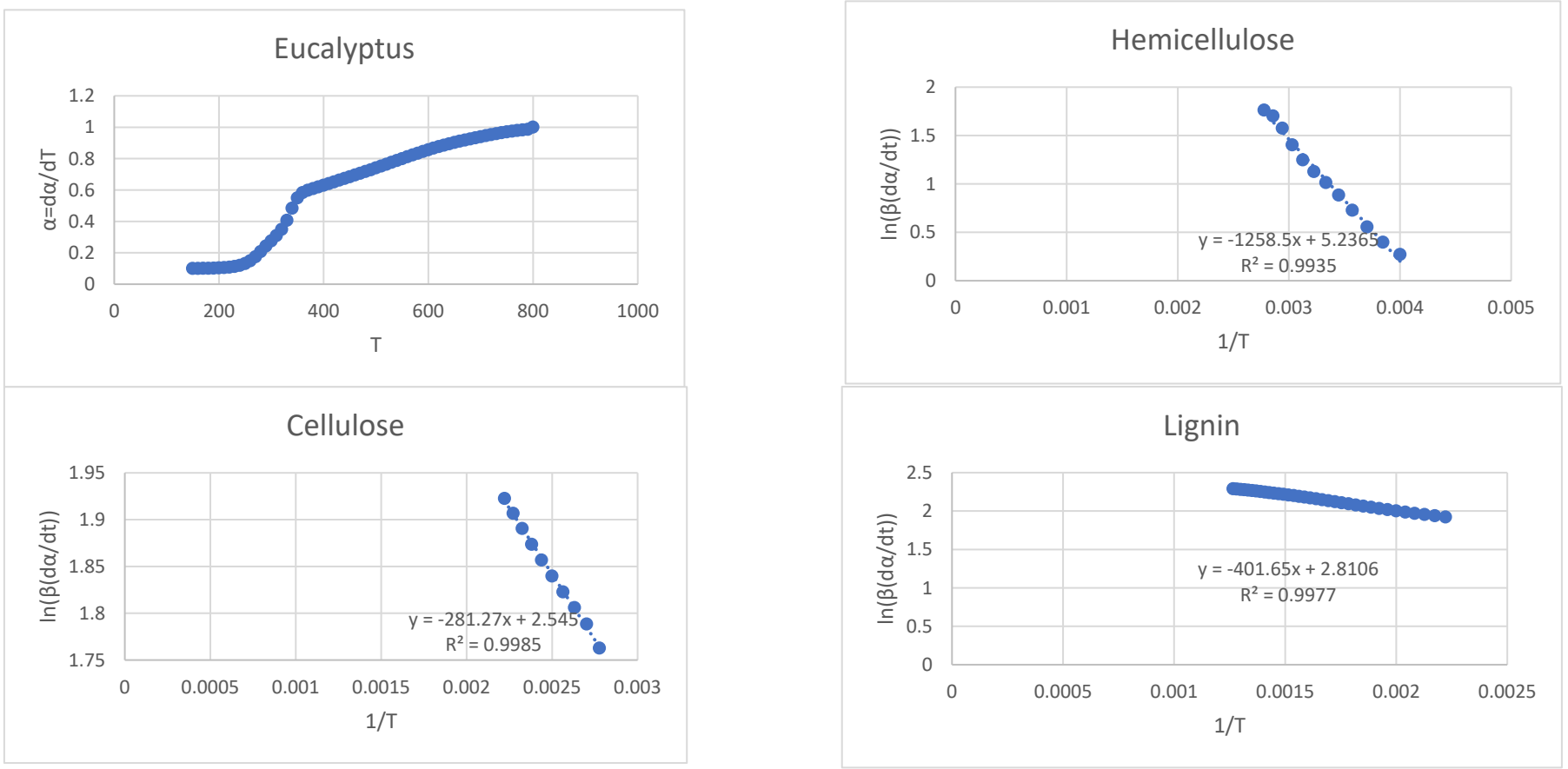


Figure 5.13: Separate decomposition patterns of Eucalyptus structural components.

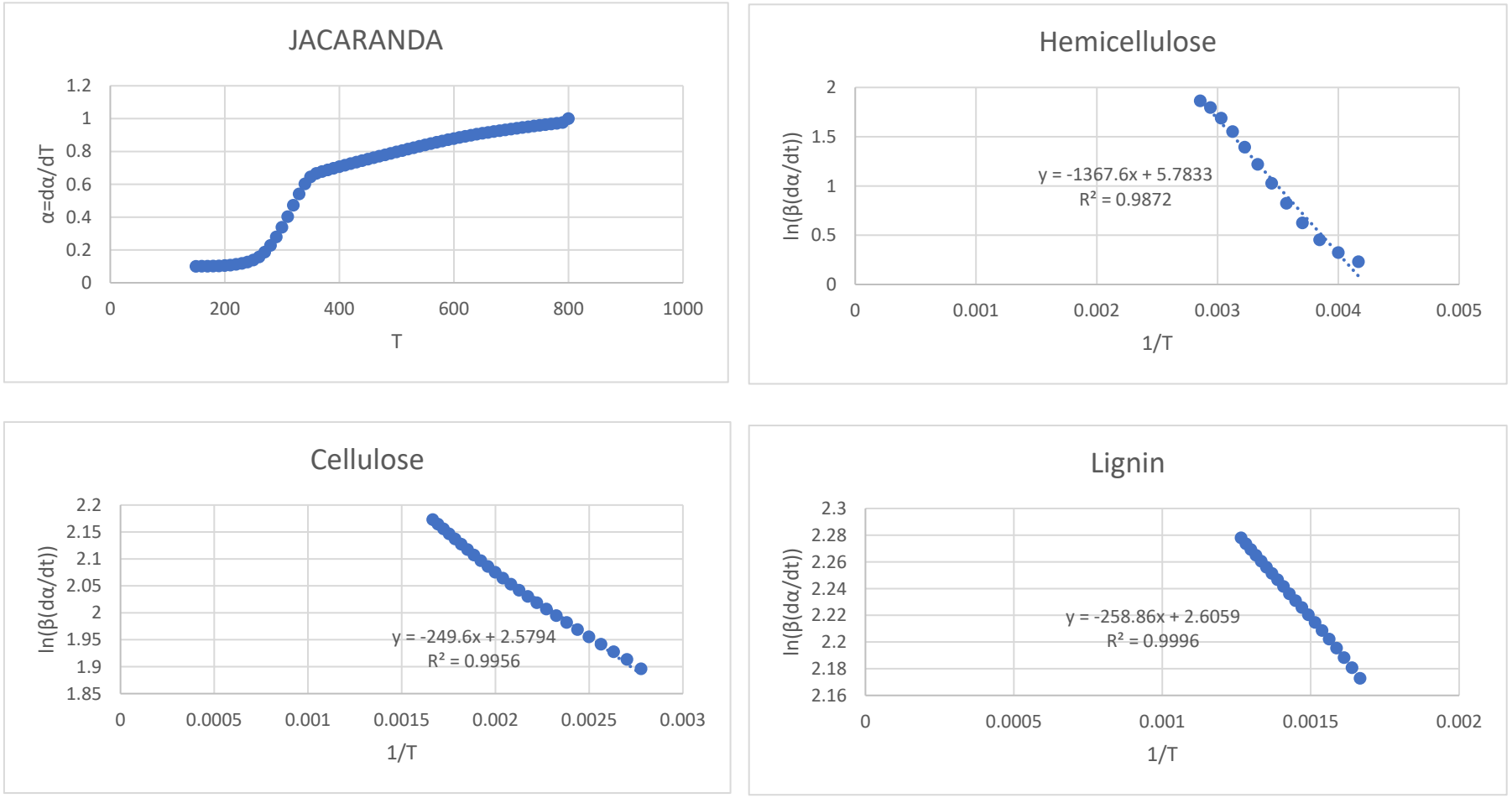


Figure 5.14: Separate decomposition patterns of Jacaranda structural components.

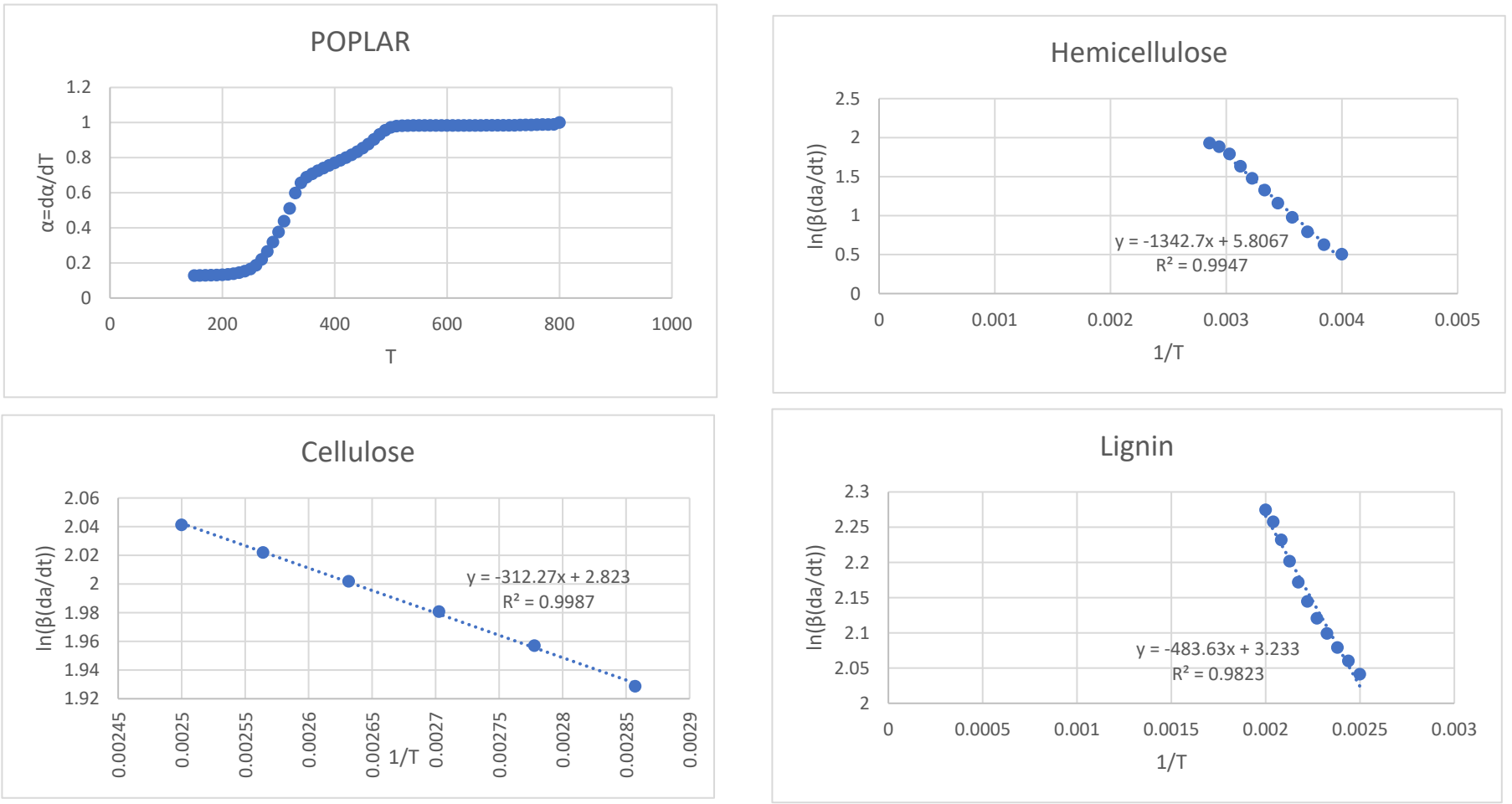


Figure 5.15: Separate decomposition patterns of Poplar structural components.

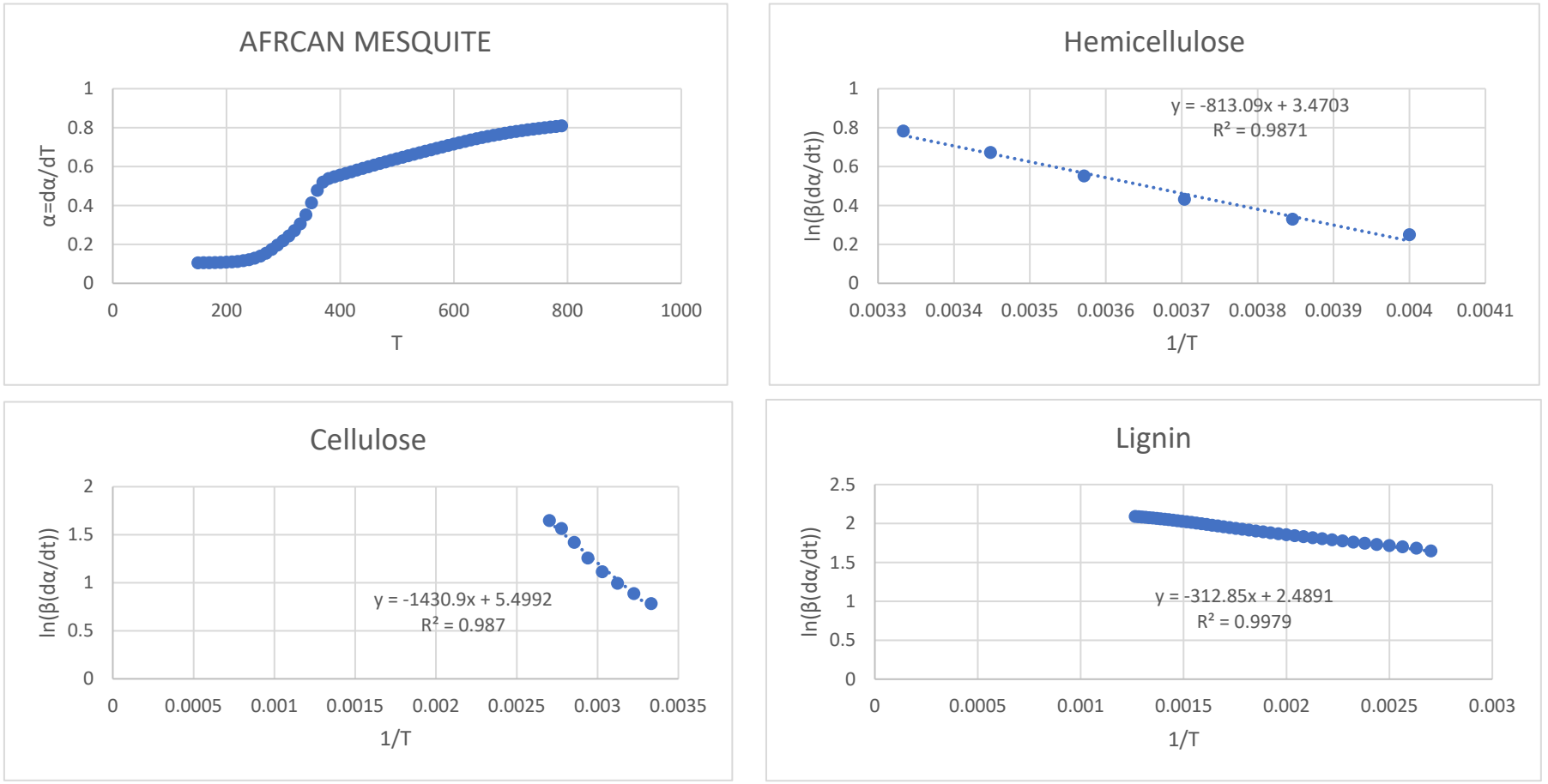


Figure 5.16: Separate decomposition patterns of African mesquite structural component.

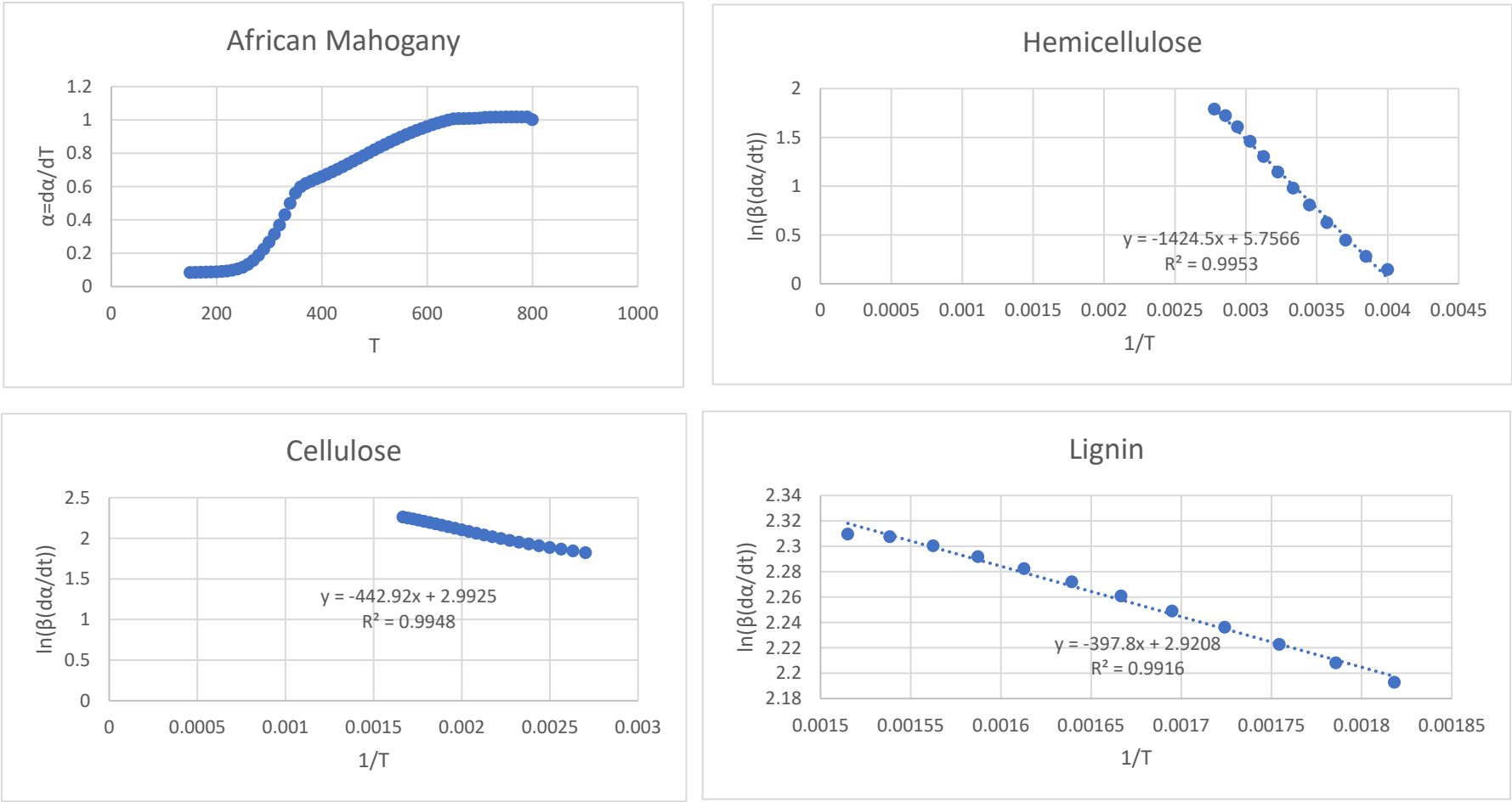


Figure 5.17: Separate decomposition patterns of African mahogany structural components.

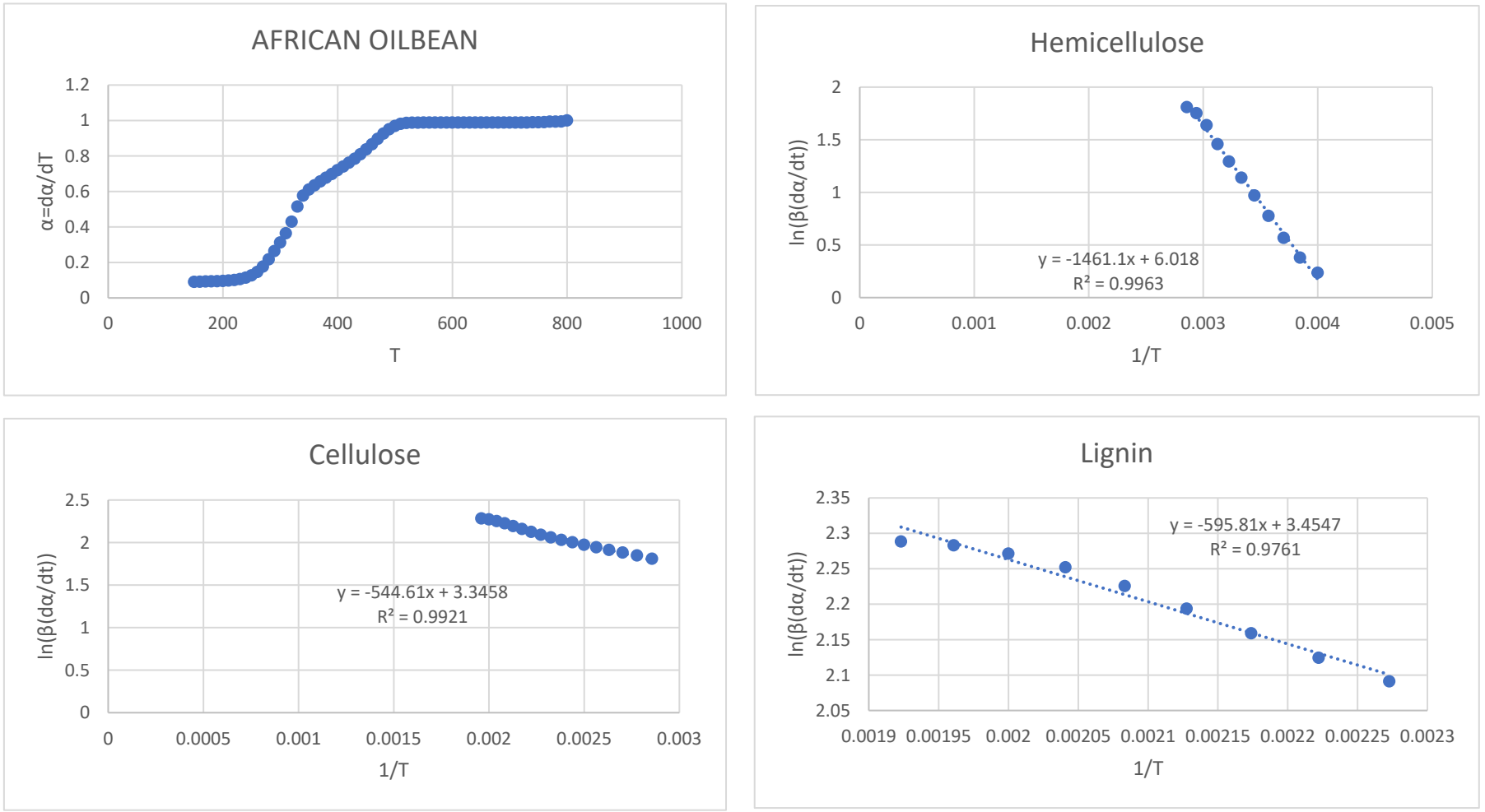


Figure 5.18: Separate decomposition patterns of African oilbean structural components.

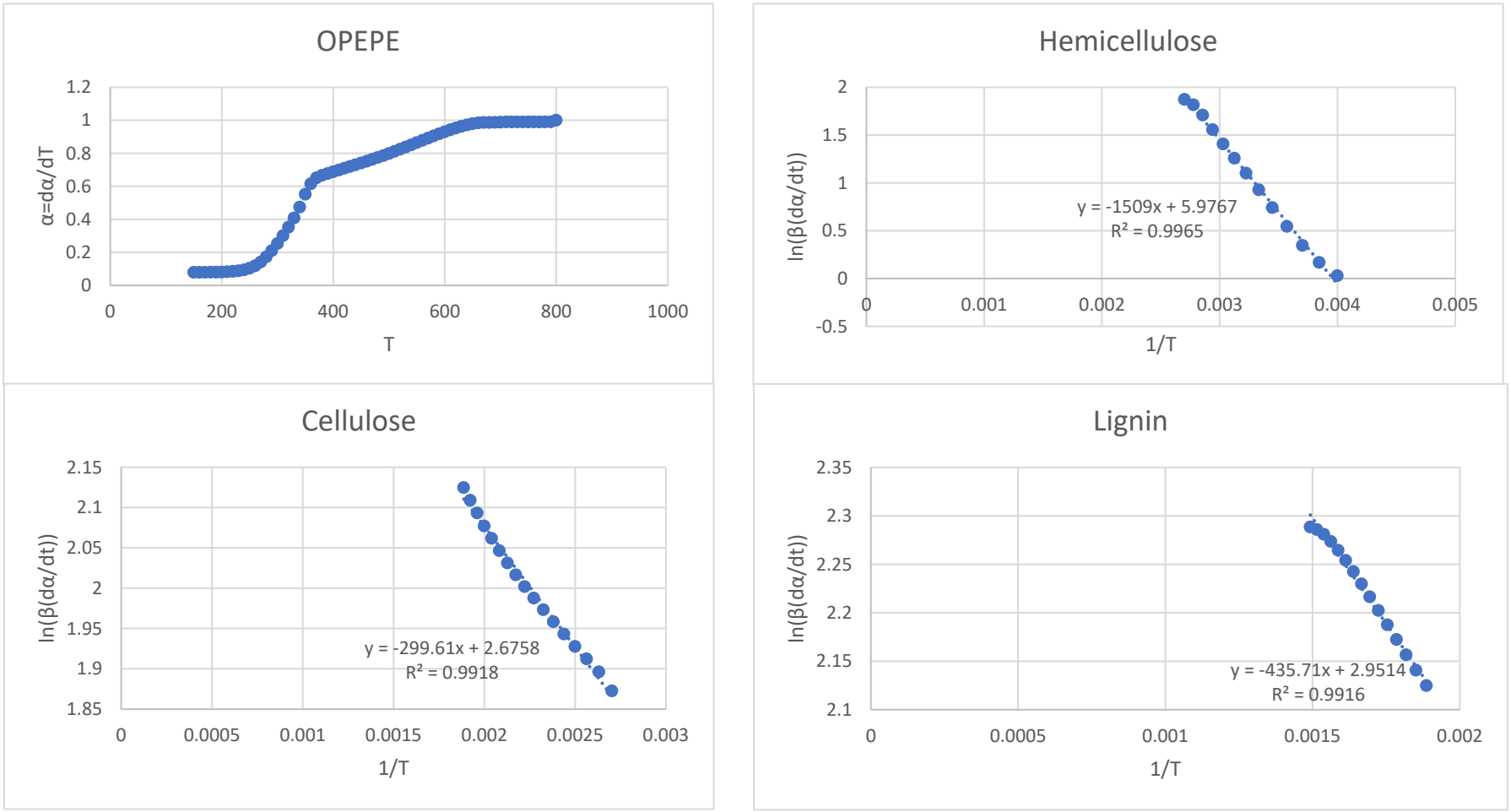


Figure 5.19: Separate decomposition patterns of Opepe structural components.

Table 5.2: Activation energies of the wood samples.

Wood sample	Activation Energies (kJ/mol)				Class of biomass
	Hemicellulose	Cellulose	Lignin	Sample activation energy	
Bugweed	13.36	3.65	3.68	3.65	CLH
Eucalyptus	10.50	2.34	3.34	2.34	CLH
Jacaranda	11.40	2.08	2.15	2.08	CLH
Poplar	11.20	2.60	4.02	2.60	CLH
African mesquite	6.76	11.90	2.60	2.60	LHC
African mahogany	6.76	3.68	3.31	3.31	LCH
African oil bean	12.10	4.53	4.95	4.53	CLH
Opepe	12.50	2.49	3.62	2.49	CLH

Note: CLH – Cellulose < Lignin < Hemicellulose

The calculations are as presented in Appendix A. A summary of the activation energies of the hemicellulose, cellulose and lignin of each wood sample is presented in Table 5.2. The activation energy, which is the minimum amount of energy required by either of the hemicellulose, cellulose or lignin, of a particular wood sample, was regarded as the activation energy of that sample. From the structural component with the least activation energy value to that with highest, the wood samples were classified as either – HCL, HLC, CLH, CHL, LCH, and LHC.

From the data provided above, the Jacaranda exhibited the lowest activation energy of 2.08 kJ/mol, which was exhibited by its cellulose component. This was followed by its Lignin (2.15 kJ/mol) and then its hemicellulose (11.40 kJ/mol) and thus was classified as a *CLH (Cellulose-Lignin-Hemicellulose)* biomass. Likewise, for samples such as the Bugweed, Eucalyptus, Poplar, African oilbean, and Opepe, the cellulose exhibited the lowest activation energies. However, for the African

mesquite *(LHC)* and African mahogany *(LCH)*, their activation energies were exhibited by their lignin components.

For most samples, it was observed that the hemicellulose exhibited a significantly higher energy value than the cellulose and lignin. This was attributed to the fact that when an LCB is subjected to thermal treatment, the thermochemical breakdown of its structural components is not successive, but simultaneous. This goes to show that, at the same pyrolysis start temperature T_{start}, all three components commence thermal decomposition at the same time, but at varying activation energies and varying rates – whereby the hemicellulose rate of decomposition peaks at a lower temperature than those of the other two components. Despite this early peak in its rate of decomposition, the hemicellulose may not exhibit the highest activation energy as depicted in Table 5.2, but a much lower activation energy corresponding to its low energy of decomposition. For instance, the observed high activation energy of the Bugweed's hemicellulose component (13.36 kJ/mol) may be regarded as an apparent activation energy and could be due to the summation of the energy input required to also activate the breakdown of its cellulose and lignin, which add up to give such high values. The variations in the decomposition of the three components only become apparent as the decomposition process progresses, whereby different peaks on the biomass thermograms become visible at different stages and temperature points of the process. Therefore, to conduct a more accurate kinetic study of the thermal decomposition of the individual structural components, each component may have to be thermally treated independently and not as a unit in one biomass wood sample.

5.3 Concluding remark

In this chapter, the thermogravimetric data of the wood samples were generated and their energy densities derived from their kinetic study. Below is a summary of the observations made.

The volatilization phases of the wood samples mostly occurred roughly between 200°C and 400°C, which was in corroboration with those of hemicellulose and cellulose peak volatilization temperatures as reported in literature. The bulk density and pore size of a wood sample of lump size contributed to its rate of volatilization. However, in this study, the reactivity of the particles of the samples were more influential because of their sawdust form.

The Bugweed exhibited the least volatilization start temperature T_{start}, volatilization time interval and highest peak rate of volatilization. This indicates the suitability of the Bugweed as a potentially suitable additive for blending with less reactive species. Conversely, the African mesquite exhibited the highest T_{start} temperature of all samples tested due to its superior density and lower reactivity.

In the char decomposition phase, the energy density of the samples played a major role in the decomposition rates of the chars. The thermogravimetry of the hardwoods chars in general exhibited lower peak rates of char decomposition than the softwoods. Despite being classified as a softwood and exhibiting a low bulk density, the Jacaranda also exhibited a low rate of char decomposition. This was attributed to the inhibiting influence of its high ash composition on its thermal decomposition.

The influence of the structural components of the wood samples on their decomposition patterns was also observed on their thermograms. Shoulders before their peak rates of volatilization were observed and signified the early peak decomposition of hemicellulose occurring at a lower temperature than that of cellulose. These shoulders were apparent on the thermograms of most samples.

Calculations to generate the activation energies of the different samples were conducted. However, the kinetic study was not conducted on the biomass as a whole but each of its structural components. However, the activation energies derived did not corroborate with the thermogravimetric analysis data collated. For instance, the hemicellulose component whose decomposition is activated by a much lower energy input than the cellulose and lignin component was observed

to exhibit a significantly higher activation energy than the latter. The energy input required to activate the thermal breakdown of the cellulose and lignin may have contributed to this very high activation energy of the hemicellulose component. This was because thermal treatment of the three structural components commence simultaneously at the same temperature, despite decomposing at varying rates. Therefore, the activation energy of the hemicellulose component of the Bugweed, Eucalyptus, Jacaranda, Poplar, African oilbean and Opepe were regarded as apparent.

Chapter 6

Pyro-gasification of wood samples

6.1 Introduction

The actual production of syngas via the pyro-gasification of the wood samples was finally conducted at 900°C, 950°C and 1000°C to obtain and analyse the following:

i. The concentration of syngas and its components (H_2 and CO) in the product gas;
ii. The average dry gas volumetric flow rate;
iii. The calculated production rate of each syngas components and that of the syngas in total;
iv. The gas yield of the H_2 and CO components as well as that of the syngas in total;
v. The volume of tar/bio-oil extracted from each run;
vi. Mass of unreacted char residue remaining in the reactor after 1000°C of each run;
vii. Any observations in gas ignitability, flame color and flame propagation.

The experiment was conducted as described in Sect. 3.5, results and discussion as well as observations made during the experiment, have been presented in this chapter. Please refer to Appendix B for the numerical data of each run.

Every instantaneous gas flow rate reading at each of the three temperature points has been carefully collated and all readings have been averaged to give the final volumetric dry gas flow rate for the respective gas sampling temperature points.

In presenting the results, the experimental data collated from the pyro-gasification of each set of wood samples were presented alongside those of their associated blends, for a straightforward analysis.

6.2 Results and Discussion

The discussion on the data collated from the pyro-gasification of the wood samples and their blends will be based on the: (a) Dry gas volumetric flow rate; (b) Syngas production rate and those of its components; (c) Syngas yield and those of its components; (d) bio-oil extracted and char residue; and finally (e) the observed flame properties.

6.2.1 Dry product gas volumetric flow rate:

Dry gas volumetric flow rate is the time rate at which a unit volume of the product gas exits the pyro-gasification rig after the gas has been condensed through the gas condenser 2, thereby making it moisture-free. This flow rate is also a reflection of the rate at which the char reacts with the oxidizing agent (steam) in the reactor. Ideally, high gas flow rates at lower temperatures is most desired due to the need to generate maximum gas volumes with minimum energy input. The gas volumetric flow rate and concentration of syngas in the product gas directly determine the rate of production of syngas from the reactor and its flame propagation when ignited.

In general, the average volumetric flow rate of the gases produced by the individual IAP samples were moderately high, ranging from as low as 285 mL/min (for the Jacaranda) to as high as 1856 mL/min (for the Eucalyptus). However, the flow rate was observed to exhibit an increasing trend with an increase in temperature from 900°C to 1000°C. This was attributed to the fact that the rate of chemical reactions is known to increase with increase in temperature. Amongst the IAP samples tested, the Bugweed exhibited the highest gas flow rate, averaging 1714 mL/min at the lowest gas sampling temperature of 900°C. This was understandably so, considering its high reactivity as exhibited in its characterisations as presented in previous chapters. Its high gas flow rate also remained consistent at 950°C and 1000°C. Another interesting observation was made with the Jacaranda.

Figure 6.1 depicts a very low dry gas flow rate by the Jacaranda at 900°C. Though a slight increase in flow rate was observed due to an increase in temperature to 950°C and 1000°C, the flow rates still remained much lower than those of the other IAP samples. This corroborates its poor char reactivity as depicted in Figs. 4.2 and 5.9., and was attributed to its high ash content, inhibiting the conversion of its carbon particles.

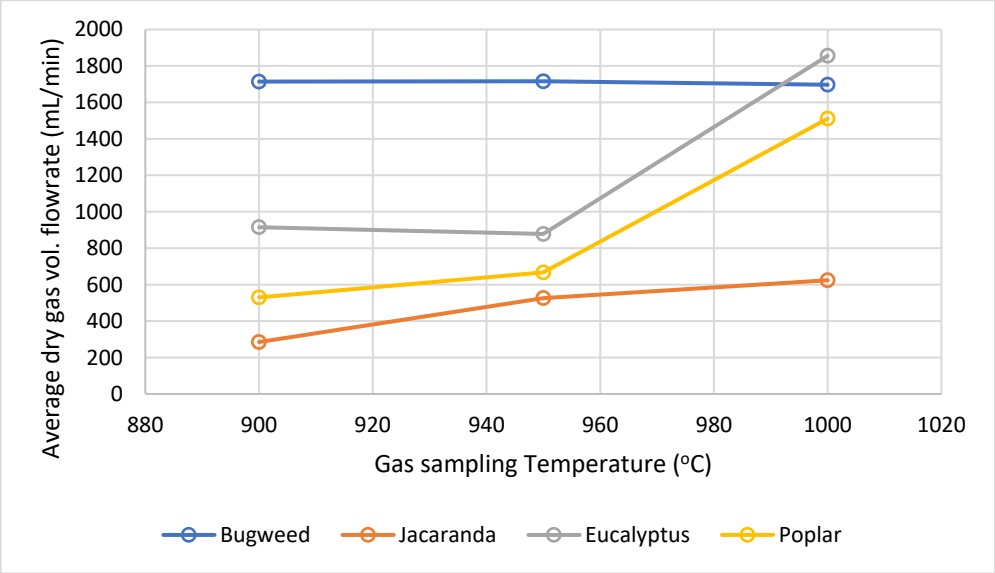


Figure 6.1: Average dry product gas volumetric flow rate of individual IAP wood samples.

The influence of the high reactivity of the Bugweed could also be observed in its associated blended samples. For instance, in Fig. 6.2, it can be observed that the high reactivity of the Bugweed greatly contributed to the high gas flow rate of the Eucalyptus-Bugweed 50/50 and 30/70 blends at the lowest temperature 900°C, while the 70/30 blend of which the Eucalyptus was of greater proportion, was observed to exhibit a lower gas flow rate at 900°C. The same scenario can also be observed for the Bugweed-Jacaranda (see Fig. 6.3) and the Bugweed-Poplar blends (see Fig. 6.4). A significant drop in the gas flow rate from 1219 mL/min (at 900°C) to 32 mL/min (at 950°C) and finally to 12 mL/min (at 1000°C) was observed for Bugweed-Jacaranda 70/30. This reduction in flow rate can be as a result of a complete conversion of the carbon at 900°C, with no carbon residue left to be

converted at the higher temperatures. This is possible, considering the much greater proportion of the Bugweed in this blend, as well as its very high reactivity.

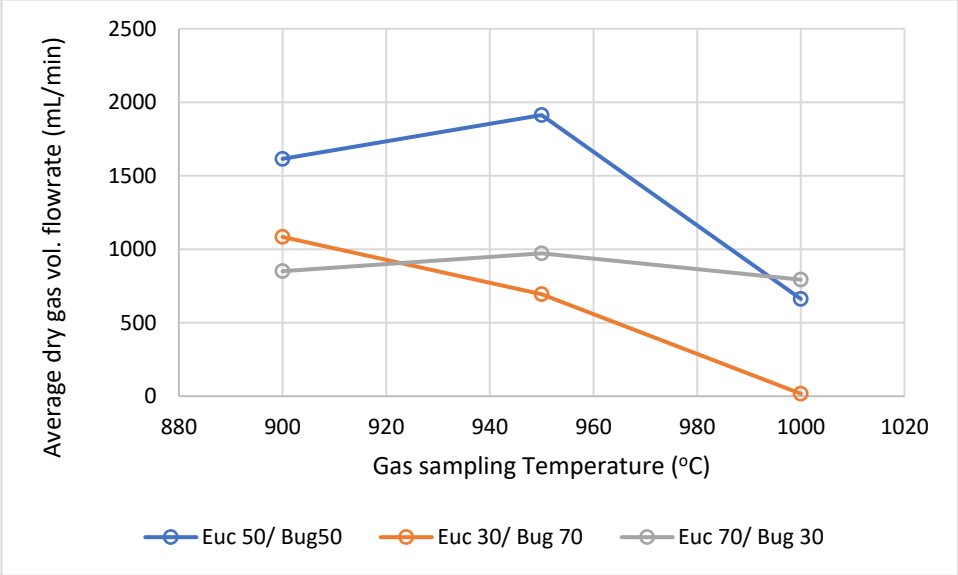


Figure 6.2: Average dry product gas volumetric flow rate of Eucalyptus-Bugweed blend.

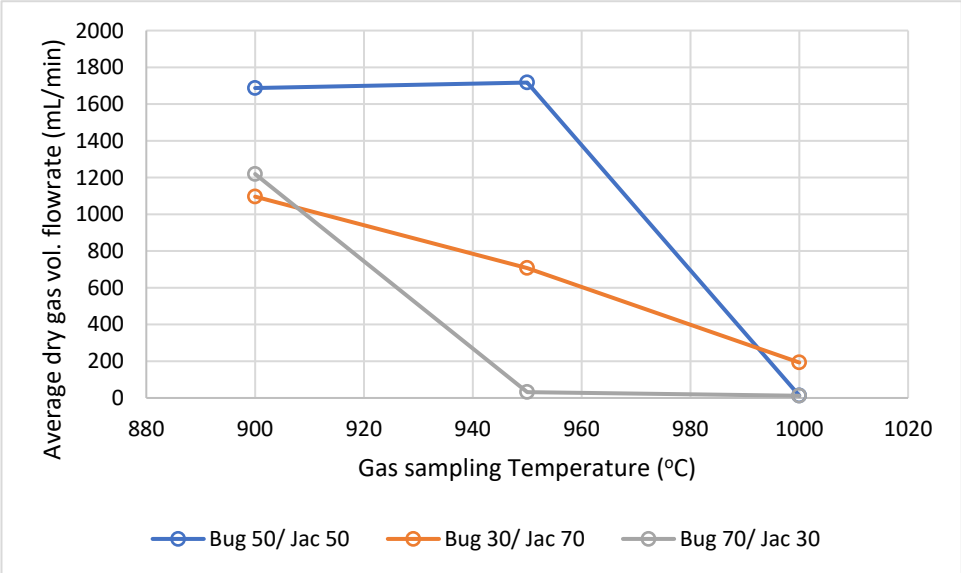


Figure 6.3: Average dry product gas volumetric flow rate of Bugweed-Jacaranda blend.

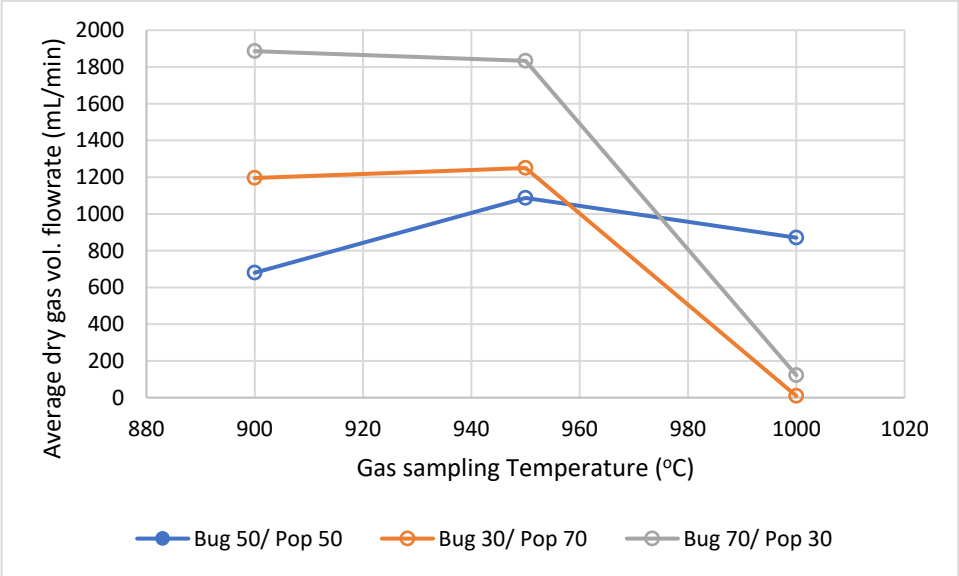


Figure 6.4: Average dry product gas volumetric flow rate of Bugweed-Poplar blend.

Amongst all the blends tested, the Jacaranda-Poplar (Fig. 6.5) exhibited the overall best gas flow rate, at 900°C, with gas flow rates averaging between 1726 mL/min and 2000 mL/min. This, however, can be attributed to the influence of the generally higher reactivity of the poplar char as observed in the fuel evaluation test (see Fig. 4.2, Sect. 4.3.1). Other factors such as the energy densities and fuel ratios of both samples may also play a greater role in improving the individual gas flow rates of both samples when blended. This high flow rates at 900°C were, however, maintained by the Jacaranda-Poplar 50/50 and 30/70 blends, as temperature increased to 950°C and 1000°C. Meanwhile, the Jacaranda-Poplar 70/30 blend exhibited a gradual reduction in its dry gas flow rate from 2000 mL/min (at 900°C) to 1650 mL/min (at 950°C) and then to 660 mL/min (at 1000°C). This was attributed to a much higher reactivity of the char at 900°C, thus leading to a gradual depletion of the carbon with an increase in temperature.

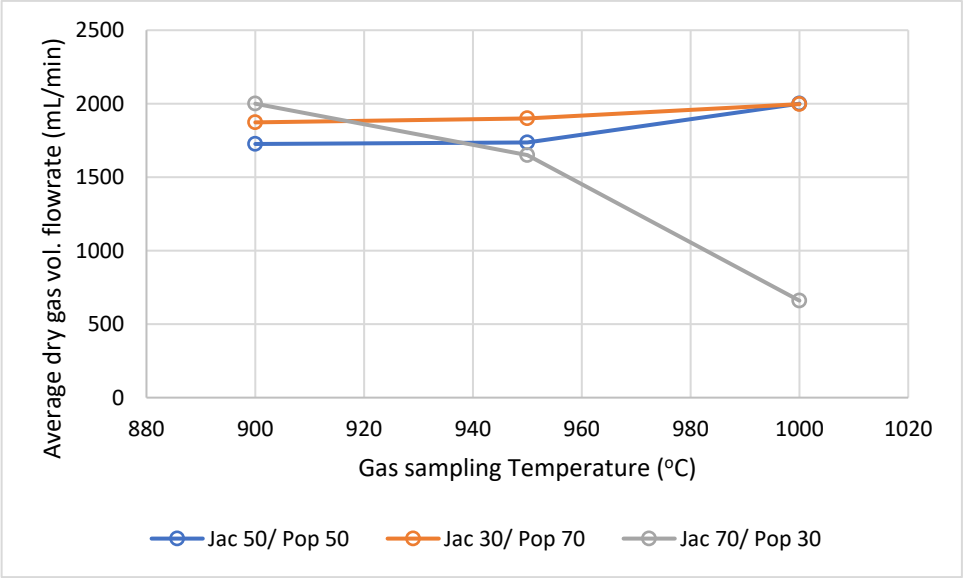


Figure 6.5: Average dry product gas volumetric flow rate of Jacaranda-Poplar blend.

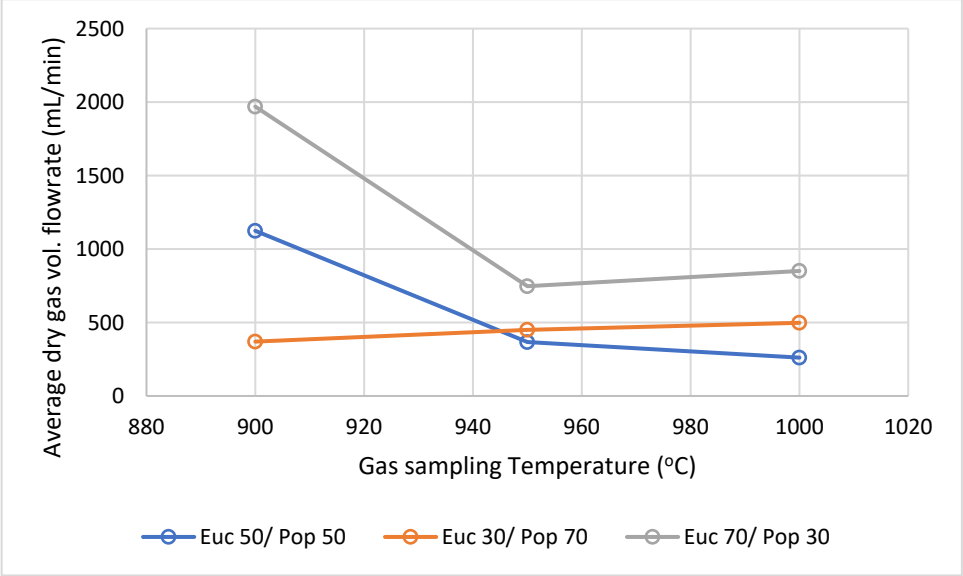


Figure 6.6: Average dry product gas volumetric flow rate of Eucalyptus-Poplar blend.

The lowest flow rate at 900°C and across other gas sampling temperature was, however, exhibited by the Eucalyptus-Poplar 30/70 (see Fig. 6.6). It was also observed that a high proportion of ash was present in the char residue found in the reactor after the pyro-gasification of the Eucalyptus-Poplar

blends (see Fig.6.6). As described in Sect. 4.3.5, ash inhibits gasification reactions and this was reflected on the gas flow rate exhibited by this blend. Therefore, the relatively high amounts of ash observed in the fuel evaluation of the Poplar (see Fig. 4.4, Sect. 4.4) may have been a contributing factor to the poor reaction of its blends with the Eucalyptus.

In comparison with those of the IAP samples, the volumetric gas flow rates of the tropical wood samples were generally much lower, with particular reference to those of the African mesquite (155 – 395 mL/min), African mahogany (172 – 417 mL/min) and Opepe (172 – 271 mL/min) (see Fig. 6.7). Amongst the four tropical hardwoods, only the African oilbean exhibited a relatively high gas flow rate at 900°C. This validates its superior char reactivity as summarized in Fig. 4.2 (Sect. 4.4). The gas flow rate was, however, observed to also increase with an increase in the reaction temperature. This occurrence can also be described by the fact that at a fixed volume (of the reactor), an increase in temperature increases pressure, thus increasing the flow rate of the gas produced.

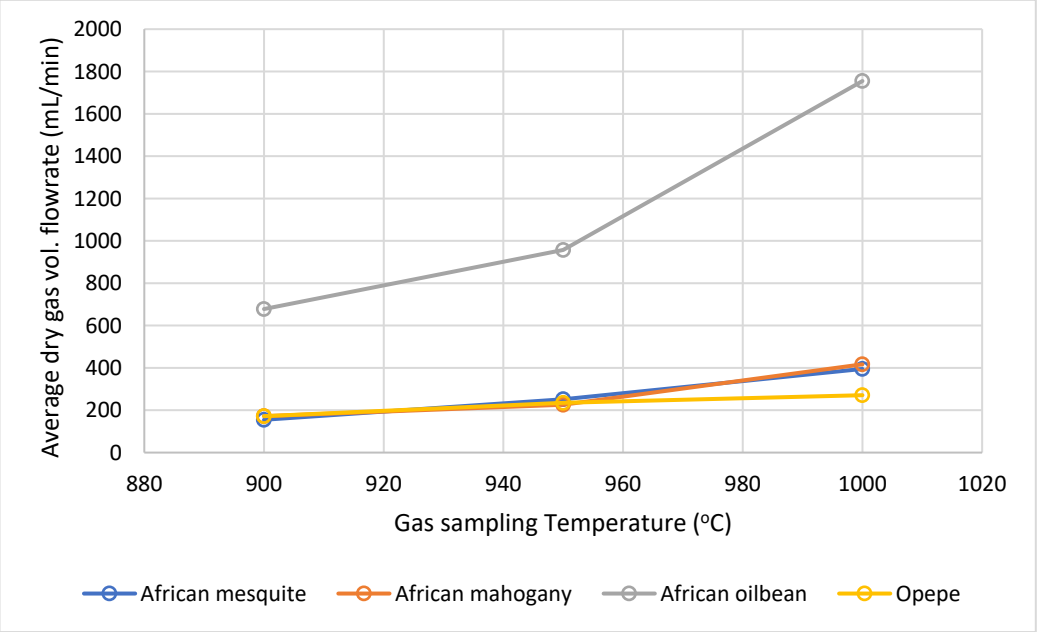


Figure 6.7: Average dry product gas volumetric flow rate of the individual Tropical hardwood samples.

The low gas flow rates of the tropical wood samples also resulted to higher amounts of char residue (with greater carbon mass) left in the reactor (See Fig. 6.7). Therefore, this reinstates the fact that the low char reactivity of the samples plays an important role in their resultant syngas flow rates, particularly at low temperatures.

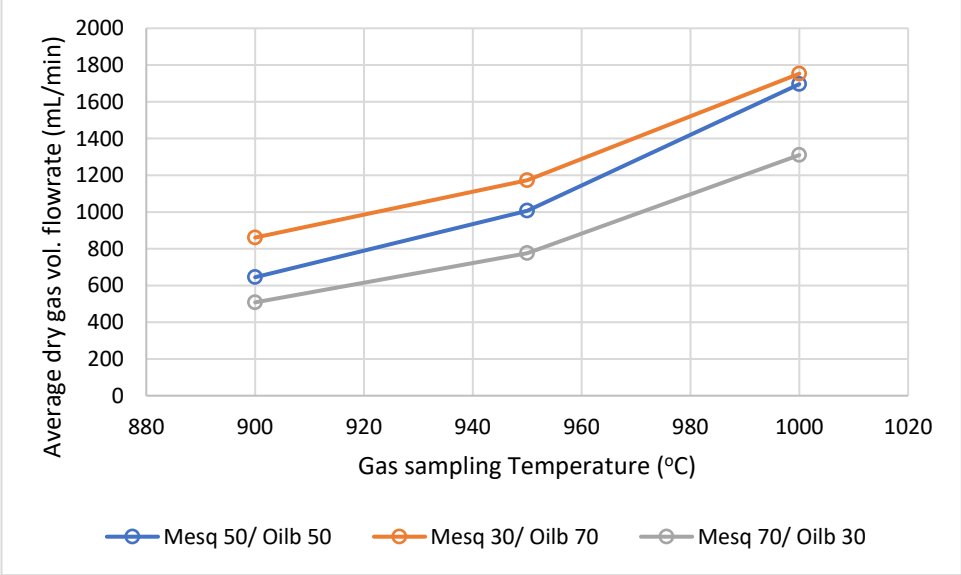


Figure 6.8: Average dry product gas volumetric flow rate of African mesquite-African oilbean blend.

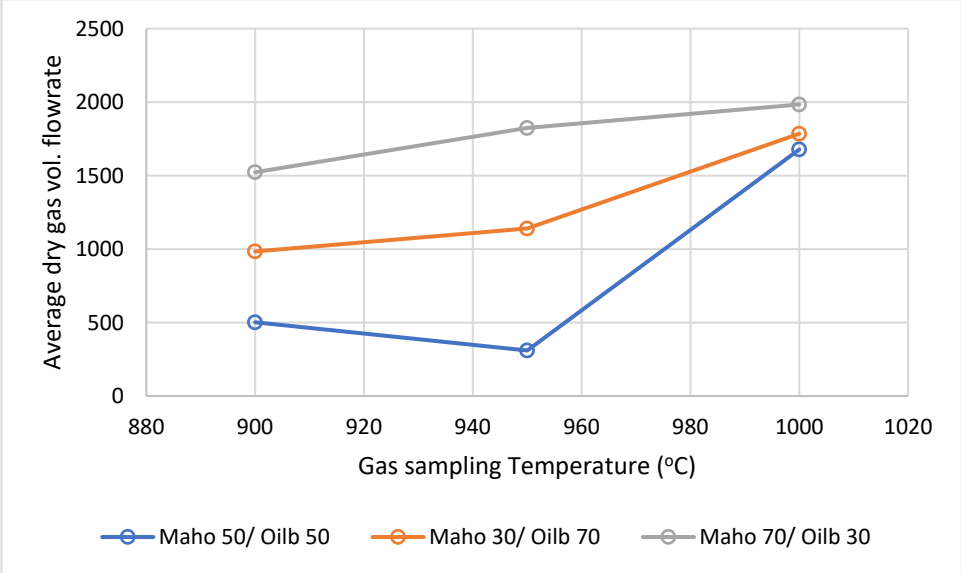


Figure 6.9: Average dry product gas volumetric flow rate of African mahogany-African oilbean blend.

With respect to the tropical wood blends, a generally improved gas flow rate was observed across the board from those of the associated individual samples. Most notably, were the gas flow rates for the African mesquite/ African oilbean (see Fig. 6.8) and those of the African mahogany/ African oilbean (see Fig. 6.9) blends. Considering the low char reactivity and resultant low gas flow rates exhibited individually by the African mesquite and African mahogany (see Figs. 4.2 and 6.7 respectively), the higher reactivity of the African oilbean was referred to as a contributing factor to the increase in the gas flow rates observed in their respective blends.

6.2.2 H_2, CO and Syngas production rate

The syngas concentration in the product gas (also comprising of CH_4 and CO_2) as well as the volumetric flow rate of the product gas are employed in determining the syngas rate of production as well as those of its components H_2 and CO. This implies that a higher product gas flow rate does not necessarily mean a higher syngas production rate if the syngas concentration in the product gas is low. However, with generally high syngas concentrations in the product gas of the wood samples tested, the syngas production rates were high for those samples exhibiting higher dry gas flow rates. In general, higher production rates of CO than H_2 were also observed across the board due to the much higher concentration of CO in the product gas.

Figure 6.10 depicts fluctuations in production rates of Syngas and its components by the individual IAP samples. However, there seemed to be a general characteristic increasing trend in the production rate of H_2 as the temperature is increased from 900°C to 1000°C. This is because H_2 formation is known to increase at higher gasification temperatures as described in Sect. 2.2.2. However, this can be altered to occur at lower temperatures with the aid of a Nickel-based catalyst. H_2 production rate was, however, observed to be highest from the Poplar (3556.14 mL/min/g of feedstock) at 1000°C. This was comparable to its CO production rate of 3636.22 mL/min/g at the same gas sampling temperature.

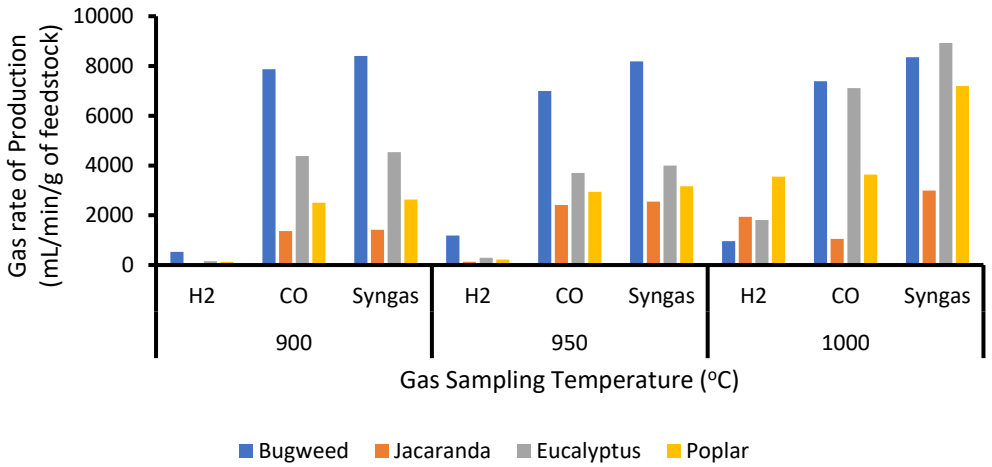


Figure 6.10: Rate of production of syngas and its components from the individual IAP samples at 900, 950 and 1000°C.

The Bugweed in particular exhibited a significantly higher syngas production rate at lower temperatures than the other samples and remained consistent up to 1000°C. This was expected, considering its much superior char reactivity. However, it was observed that similar to that of the Poplar, the syngas production rate of the Eucalyptus only peaked at 1000°C and was highest across the board only at that particular high temperature. This was attributed to their poor char reactivity and difficulty in the breakdown of their lignin structural component – which was at a greater proportion. This poor char reactivity property of the Eucalyptus and the Poplar samples was evident in Fig. 6.25, whereby high amounts of unreacted carbon particles in their char residue (weighing 3.14 g for the Eucalyptus and 0.7 g for the Poplar) were found in the reactor at the end of the process.

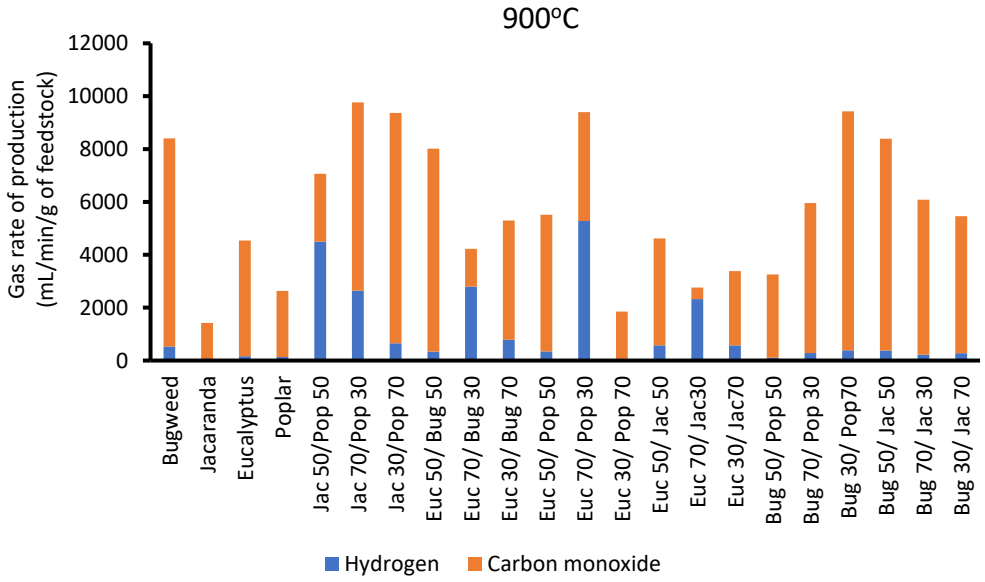


Figure 6.11: Rate of production of H_2 and CO from the individual IAP samples and their blends at 900°C.

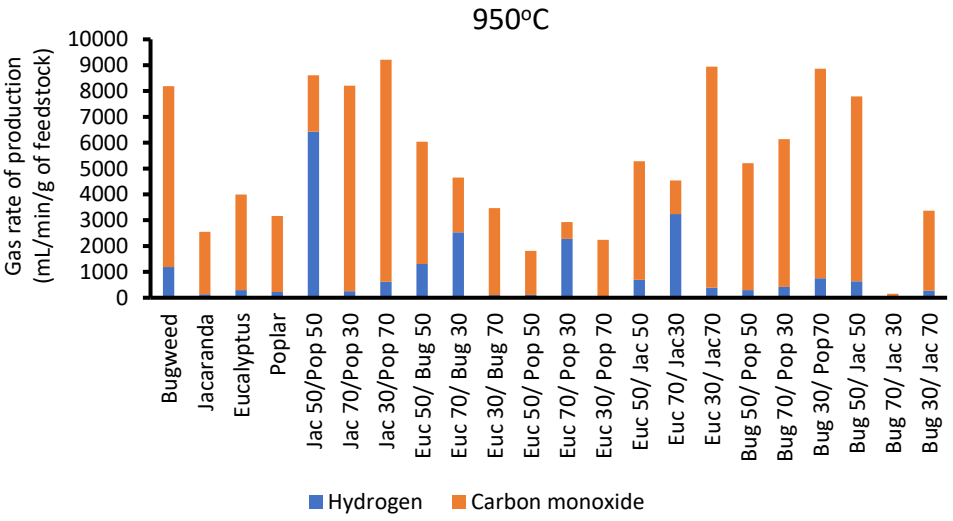


Figure 6.12: Rate of production of H_2 and CO from the individual IAP samples and their blends at 950°C.

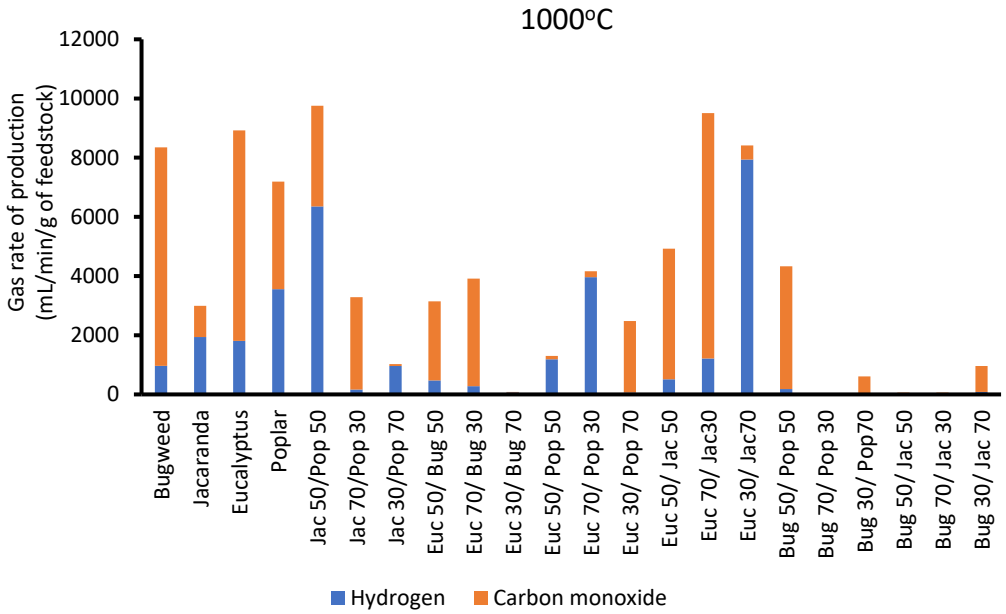


Figure 6.13: Rate of production of H_2 versus CO from the individual IAP samples and their blends at 1000°C.

Figures 6.11 – 6.13, compare the H_2 and CO rates of productions of the individual IAP wood samples with those of their respective blends at 900°C, 950°C and 1000°C. When compared to those of their associated individual samples, a general improvement in the syngas production (particularly at the lower temperature of 900°C) was observed for most of the blended samples. It is also worthy of note, that the ratio of the hydrogen production rate to that of the carbon monoxide was significantly improved particularly with the Jacaranda-Poplar 50/50, Eucalyptus-Poplar 70/30, Eucalyptus-Bugweed 70/30 blends. The highest hydrogen production rate (7937.07 mL/min/gram of feedstock) was however attained by the Eucalyptus-Jacaranda 30/70 blend. An evidence of the greater hydrogen production rate by these aforementioned blends can be observed in the predominantly blue flame produced by the gases when ignited. As shown in Fig. 6.30 d, the Eucalyptus-Jacaranda 30/70 blend can be seen to produce a blue flame with a high flame propagation, typical of hydrogen-rich gaseous fuels.

On the other hand, the syngas production rates of the Jacaranda-Poplar 30/70, Eucalyptus-Bugweed 30/70, Eucalyptus-Poplar 50/50, Bugweed-Poplar 70/30, Bugweed-Poplar 30/70, Bugweed-Jacaranda 50/50, 70/30 and 30/70 blends, were greatly reduced at 1000°C. This was attributed to a possible depletion of their carbon residue in the reactor. This is an evidence of their high reactivity at lower temperatures, thus leading to a quick depletion of their char fixed carbon.

The tropical hardwoods as depicted in Fig. 6.14 clearly exhibited lower gas production rates than their IAP counterparts. The African oilbean however, was observed to produce syngas at a significantly higher rate than the rest of the tropical samples tested.

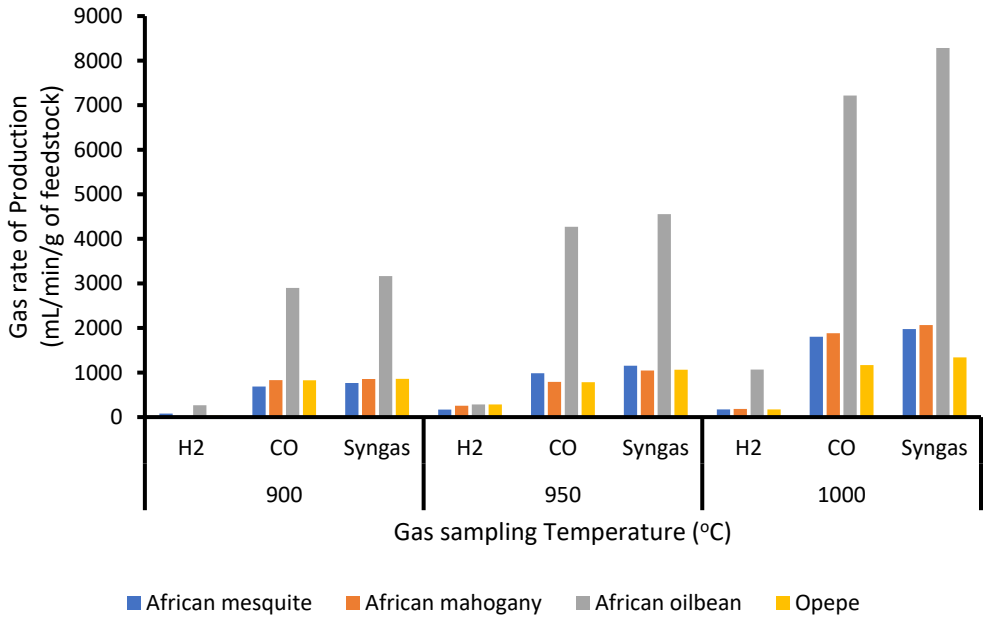


Figure 6.14: Rate of production of syngas and its components from the individual Tropical hardwood samples at 900, 950 and 1000°C.

As summarized in Fig. 4.2 of Sect 4.4, the high reactivity of the African oilbean char can be referred to as a factor for its high syngas production rate. However, it was observed that there was a higher carbon monoxide production rate than that of hydrogen, with increasing CO production rates concurrent with an increase in temperature. This can be attributed to a potential dominance of the CO formation via reactions such as the Boudouard reaction during the gasification phase. Such

high CO production rates may be caused by the presence of excess carbon reacting with the CO_2 generated from the partial oxidation of the carbon-rich char of the hardwoods. Thus, a high carbon to steam ratio played a major role in the production of such CO rich syngas by the tropical hardwoods.

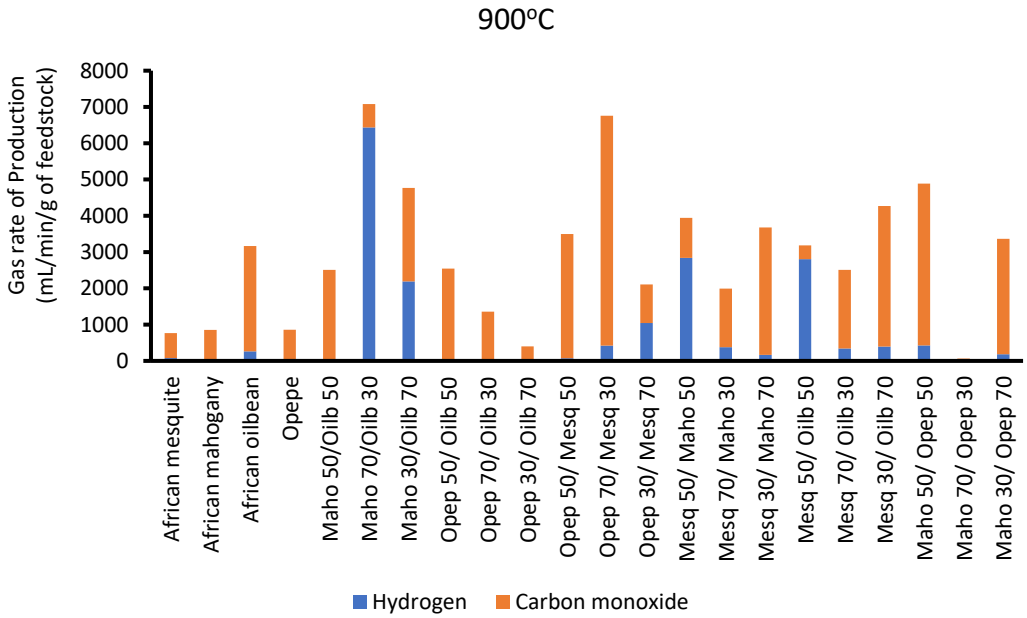


Figure 6.15: Rate of production of H_2 versus CO from the individual Tropical hardwood samples and their blends at 900°C.

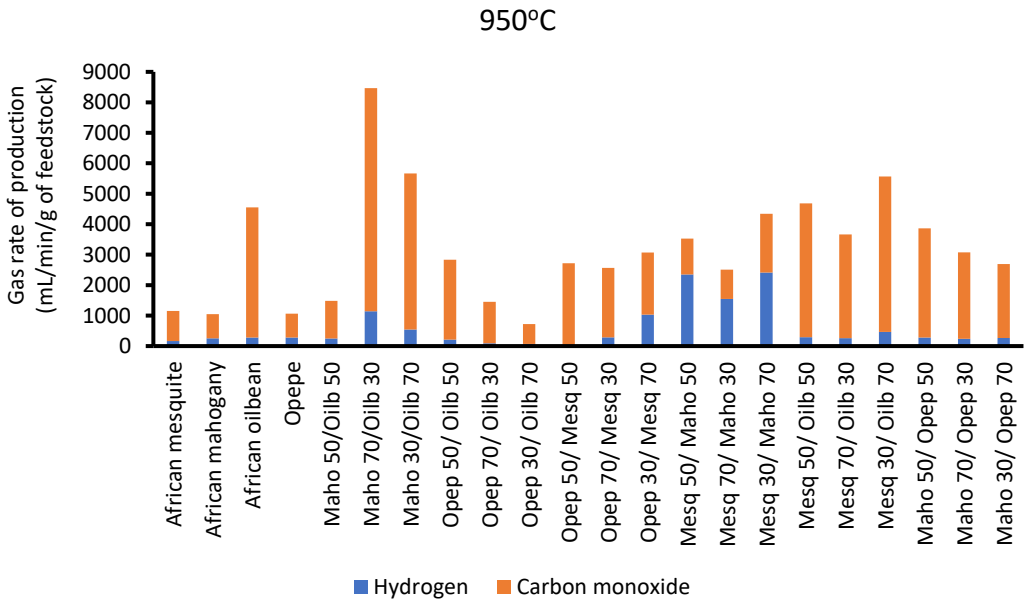


Figure 6.16: Rate of production of H_2 versus CO from the individual Tropical hardwood samples and their blends at 950°C.

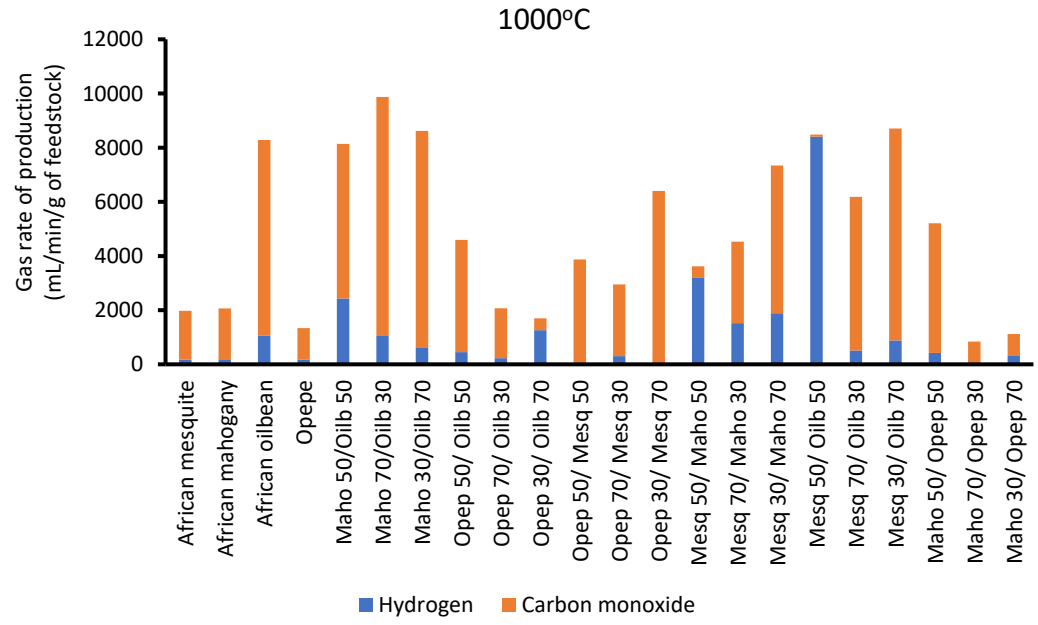


Figure 6.17: Rate of production of H_2 versus CO from the individual Tropical hardwood samples and their blends at 1000°C.

In comparison with those of their associated individual samples, some tropical wood blends such as the Mahogany-Oilbean 70/30, Mesquite-Mahogany 50/50, and the Mesquite-Oilbean 50/50 blends, were observed to produce hydrogen at significantly higher rates than carbon monoxide at 900°C (see Fig. 6.15). However, there was a 200% increase in the rate of production of hydrogen at 1000°C by the African mesquite-African oilbean 50/50 blend from its value at 900°C. This was, however, characterized by a temporary drop in H_2 rate of production at 950°C before its rise at 1000°C. This temporary drop in the H2 rate of production is similar to that reported by Li *et al.* [33] (see Fig. 2.12 a). This could be attributed to a possible temporary increase in the rate of combustion of carbon, thus producing excess CO_2 for a higher rate of production of CO (than H_2) via the Boudouard reaction. Nevertheless, a generally higher rate of production of CO-rich syngas was achieved with the tropical wood blends than with their IAP counterparts.

6.2.3 Syngas yield

The volume of syngas obtainable from the pyro-gasification of each gram of sawdust of the wood species tested reflects the efficiency of the wood as feedstock for the pyro-gasification process. It provides vital information on the economic viability of using certain wood species for syngas production based on the volume of syngas the wood can dissipate during its thermochemical decomposition process. As follows, Figs. 6.18 and 6.19 compare the syngas yields of the individual samples at the three gas sampling temperatures – 900°C, 950°C and 1000°C.

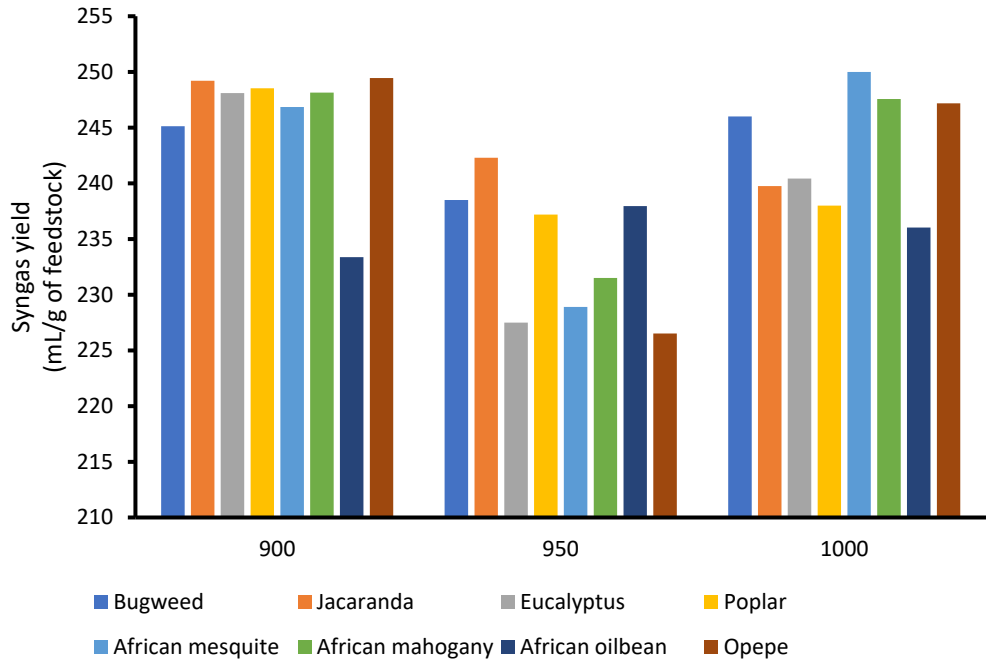


Figure 6.18: Syngas yield of all individual wood samples

Inasmuch as the African oilbean exhibits the highest syngas production rate, its yield per gram of sawdust was observed to be the lowest across the board, particularly at 900°C and 1000°C. This was as a result of the greater concentration of CH_4 and CO_2 present in its product gas at these temperatures. Most samples exhibited impressive syngas yields at lower temperatures. However, as with the case of the Jacaranda and Poplar, for instance, syngas yield dropped at higher temperatures. This was attributed to a rapid depletion of the carbon in their char mass at 1000°C – due to their high rates of reaction at lower temperatures. Conversely, such drops in syngas yield at 1000°C were not observed with the African mesquite, African mahogany and Opepe. This was due to their high char yields and lower char reactivities. This meant that a considerable amount of carbon residue was left unreacted in the reactor after the experiment. Evidence of this can be found in Fig. 6.25. Therefore, due to their higher char reactivities only attainable at higher temperatures, their syngas yields were observed to peak at 1000°C.

In comparison with the individual samples, the blended samples attained no major increases in their total syngas yield. However, at the different gas sampling temperatures, significant variations in the syngas yields of the blended samples were observed. The Jacaranda-Poplar 30/70 blend was found to have exhibited a significantly low syngas yield at 1000°C. Conversely, the Mahogany-Opepe 70/30 yielded the lowest syngas volume at 900°C, followed by significant increases in syngas yield at 950°C and 1000°C. The highest total syngas obtainable from the individual and blended IAP samples across all sampling temperatures was by the Eucalyptus-Bugweed 30/70 blend (744.42 mL/gram of feedstock). Meanwhile, amongst the Tropical hardwood samples, the Mahogany-Opepe 30/70 yielded the highest total volume of syngas (735.8 mL/gram of feedstock). On the other hand, the Jacaranda-Poplar 30/70 and the Mahogany-Opepe 70/30 yielded the lowest total syngas volume of 518.05 and 493.7 mL/gram of feedstock, respectively.

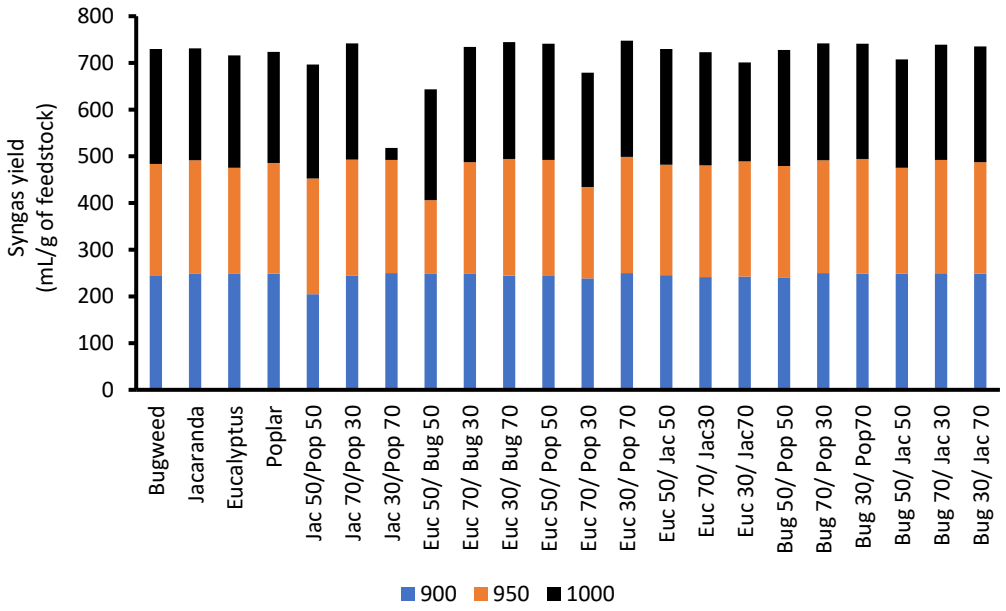


Figure 6.19: Syngas yield of individual IAP samples and their blends at 900, 950 and 1000°C

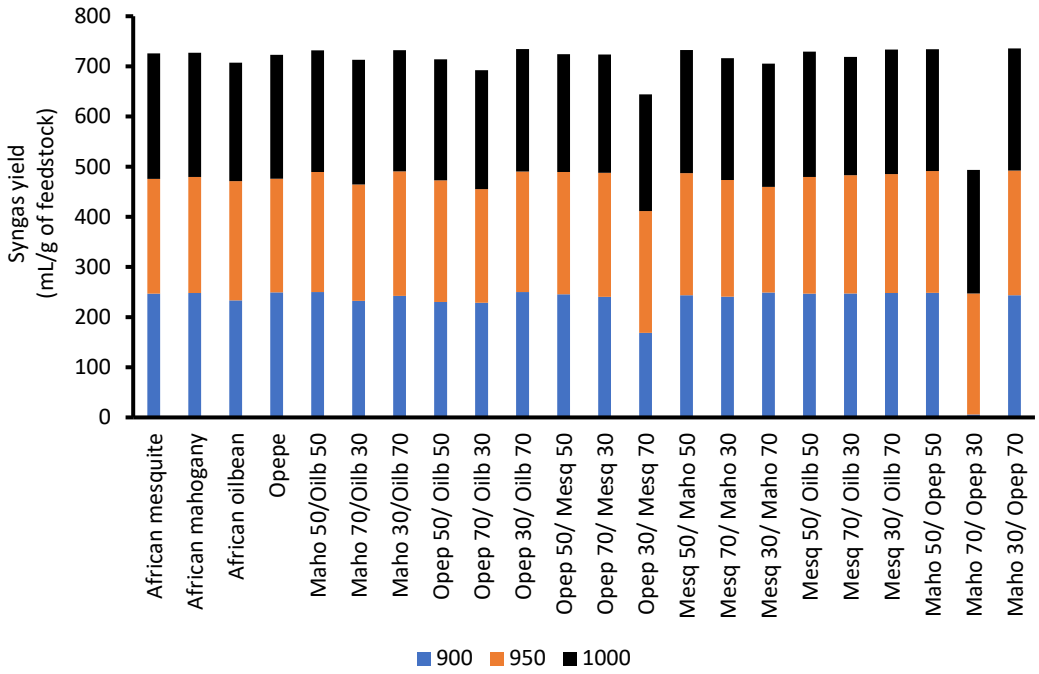


Figure 6.20: Syngas yield of individual Tropical hardwood samples and their blends at 900, 950 and 1000°C

6.2.4 Bio-oil extracted and Char residue after process

The bio-oil extracted, and the unreacted char residue left in the reactor after the pyro-gasification of the samples give better evidence of their thermochemical behaviours during the process. Figures 6.22–6.29 capture the most significant amounts of both products obtained after the process.

As shown in Figs. 6.22 and 6.23, varying volumes of bio-oil were obtained from the pyrolysis phase of the pyro-gasification of the samples. As previously mentioned, factors such as the feedstock MC at the time of this experiment, its VM, the reactor temperature and heating rate, as well as the cooling water flow rate of the condenser, affect the amount of bio-oil obtainable from the feedstock. These as well affect the water to tar ratio of the bio-oil, therefore making it impossible to predict the volume of the bio-oil collected from each sample. Moreover, during the drainage of the bio-oil, periodic blockages in the pipe were experienced due to an increase in the viscosity of the bio-oil as it flowed from the high-temperature section of the pipe to its cooler section. This, therefore, influenced the accuracy of

the bio-oil measurement. It is important to note that, the determination of the constituents of the bio-oil was beyond the scope of this study and therefore was not taken into consideration. Figure 6.21 shows the volatile matter condensation process in the gas condenser 1 leading to the deposition of the bio-oil in the oil collector.



Figure 6.21: Bio-oil deposition through condensation of heavy pyrolysis gases

From Figs. 6.22 and 6.23 below, the IAP samples produced more bio-oil volumes than their tropical counterparts. This was attributed to their superior VM and MC contents as well as their lower bulk densities as discussed in Chapter 4. The highest volume of bio-oil collected was 8.5 mL from the pyrolysis phase of the Bugweed-Jacaranda 50/50 blend (see Fig. 6.24), while the lowest was 1.7 mL from the African mahogany-Opepe 50/50 blend.

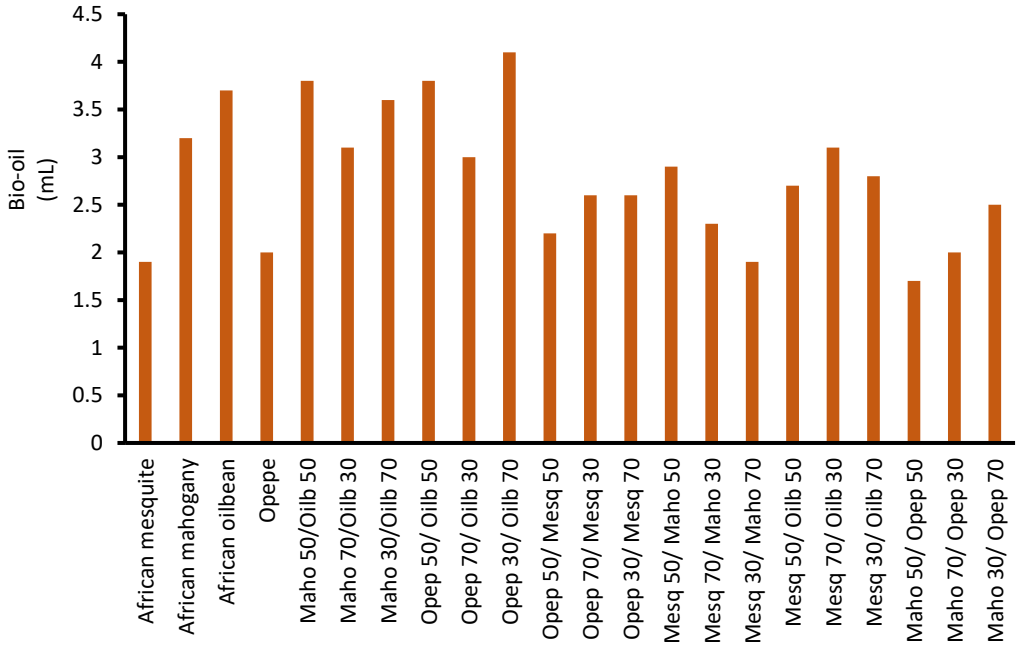


Figure 6.22: Varying volumes of Bio-oil extracted from the individual Tropical hardwoods and their blends

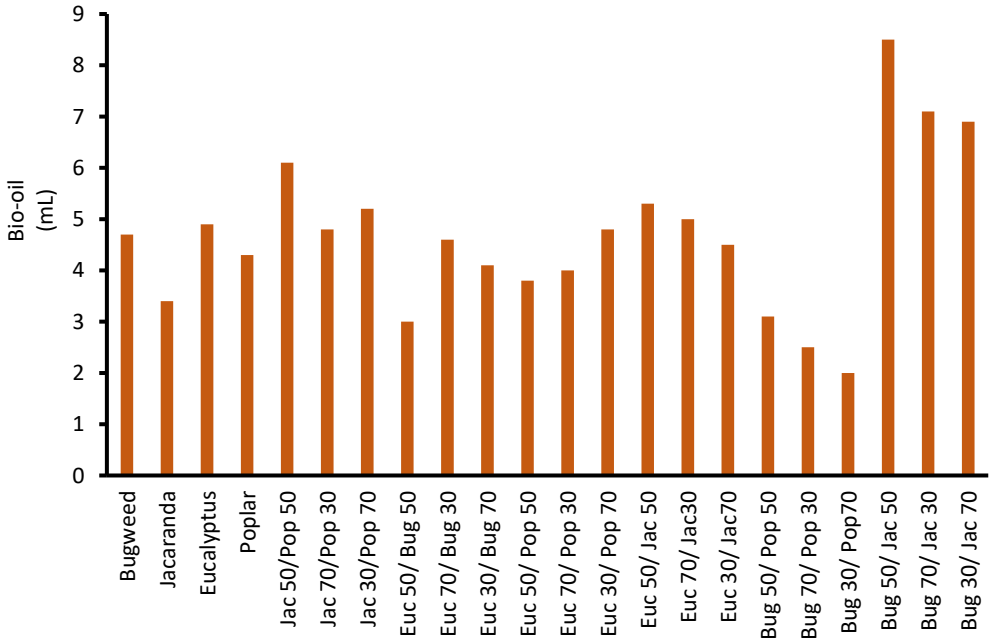


Figure 6.23: Varying volumes of Bio-oil extracted from the individual IAP samples and their blends

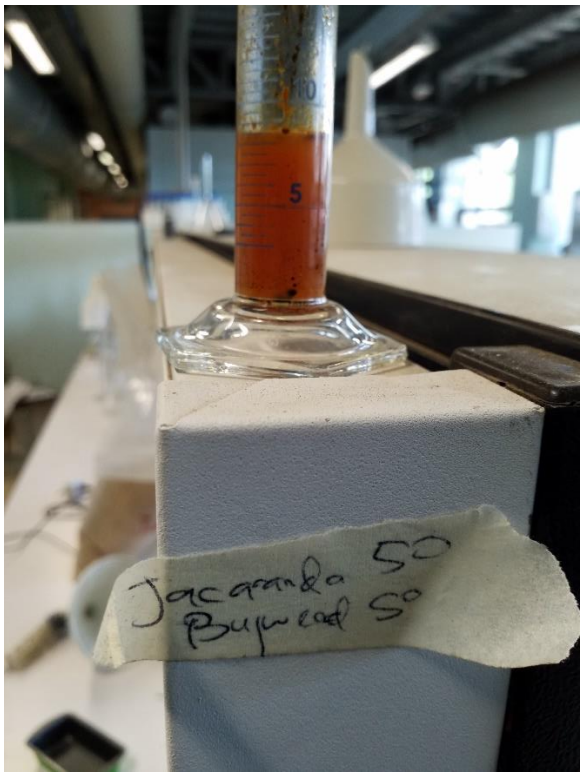


Figure 6.24: Volume of Bio-oil extracted from Jacaranda-Bugweed 50/50 blend

There were variations in the mass of the char residues recovered after the pyro-gasification of the samples. However, taking into consideration the results of their fuel evaluations (conducted in Sect. 4.3) these variations were somewhat more predictable than those of the bio-oils. For instance, hardwoods such as the Eucalyptus, African mesquite and Opepe were somewhat expected to exhibit poor reactivity during the gasification phase and thus, have higher amounts of char residue left (see Fig. 6.25). Moreover, their higher bulk densities (or particle density) reflect the high mass of the char residue recovered irrespective of their volumes.

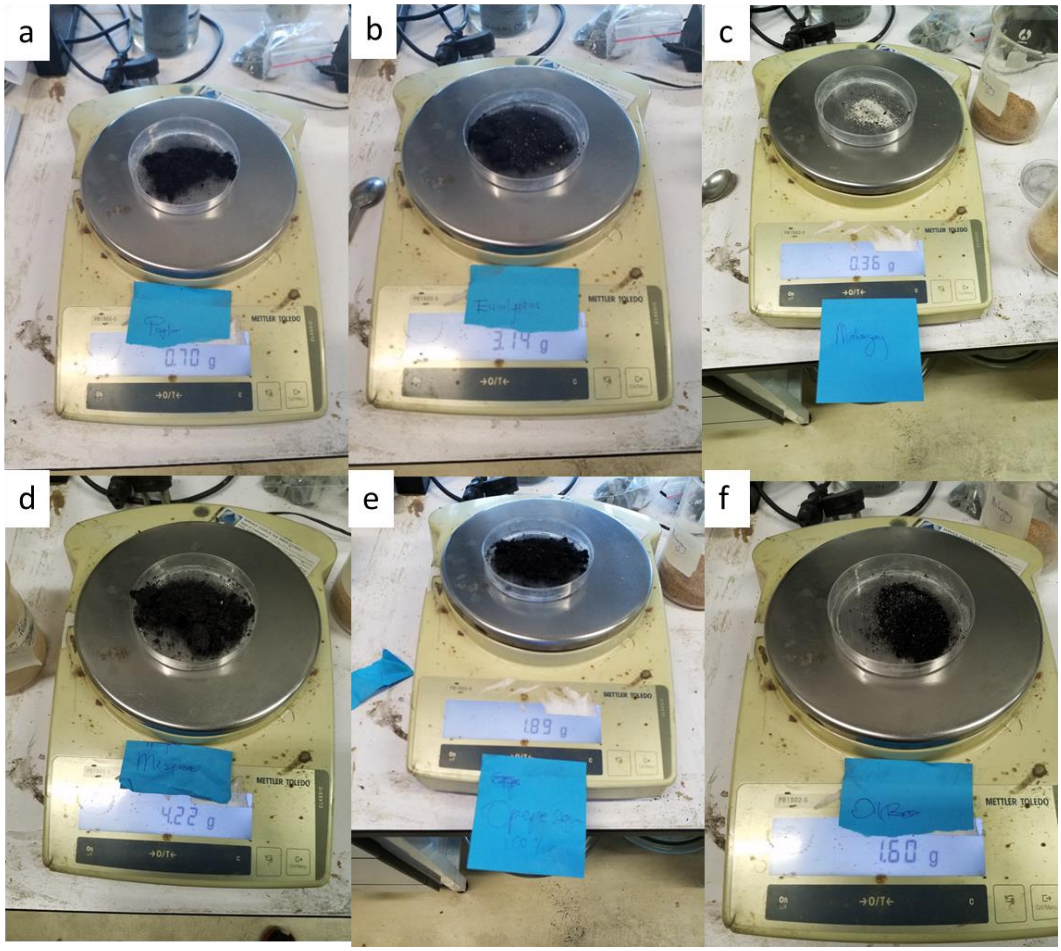


Figure 6.25: Mass of char residue recovered from the reactor after the pyro-gasification of hardwoods (a) Poplar; (b) Eucalyptus; (c) African mahogany; (d) African mesquite; (e) Opepe; (f) African oilbean.

Meanwhile, variations in the composition and mass of the char residues recovered were also observed from the pyro-gasification of the blended samples. For instance, Fig. 6.26 shows the differences in the physical properties of the char residue of Mahogany and Opepe as well as those of their blends 50/50, 70/30 and 30/70. The char residue of 0.36 g from the African mahogany (see Fig. 6.26 a) was characterised by a greater proportion of ash particles. This was an indication of a complete conversion of the carbon present in the African mahogany. This in-turn corroborates with the low char yield and moderate char reactivity of the African mahogany as depicted in Fig. 4.2 (Sect. 4.4). It also shows that its char mass produced during the pyrolysis phase was initially low before the start of the

gasification phase. Its low dry gas flow rate, syngas rate of production and syngas yield also corroborate this fact. Conversely, the Opepe exhibited its low char reactivity with a heavier carbon-rich char mass of 1.89 g left in the reactor (see Fig. 6.26b). This higher amount of a carbon-rich char residue also provides a logical explanation for its very low dry gas flow rate, syngas rate of production and syngas yield across the three gas sampling temperatures.

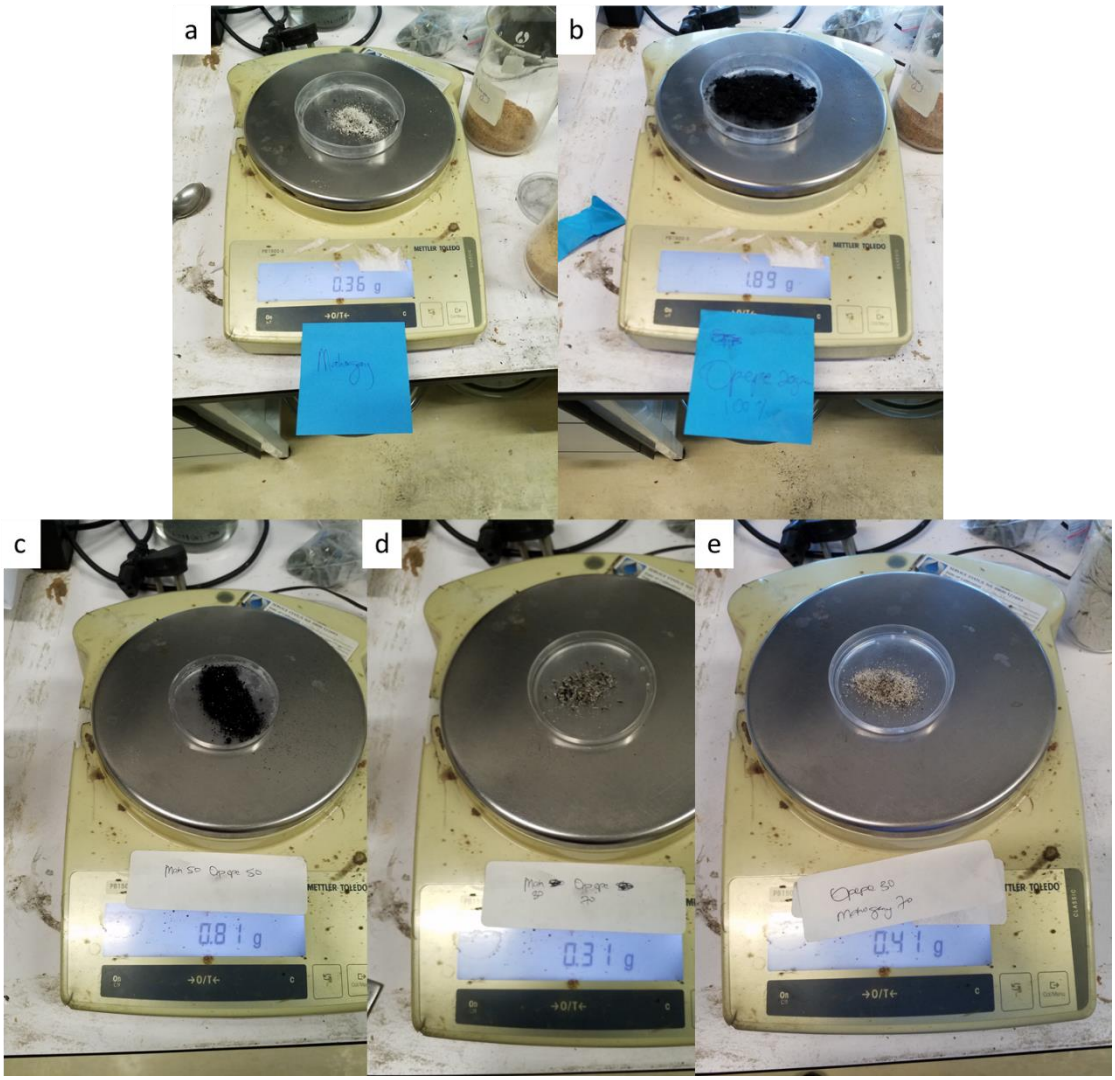


Figure 6.26: Mass of char residue recovered from the reactor after the pyro-gasification of hardwoods (a) African Mahogany and (b) Opepe; in comparison to their blends Opepe-African mahogany – (c) 50/50; (d) 30/70; (e) 70/30.

When blended with the African mahogany, however, the char residue was observed to be as low as 0.31 g for the African mahogany-Opepe 30/70 blend and as high as 0.81 g for the 50/50 blend. This 83% decrease in the char residue of the 30/70 blend from that of the individual Opepe sample is an indication of a greater conversion of the carbon in its char residue. Therefore, it can be said that the blending of the two samples greatly affected their carbon conversion efficiency. Moreover, a significant improvement in the syngas rate of production and yield of the blended samples, from those of the individual African mahogany and Opepe samples was observed (see Figs. 6.15–6.17 and 6.20), to corroborate this fact.

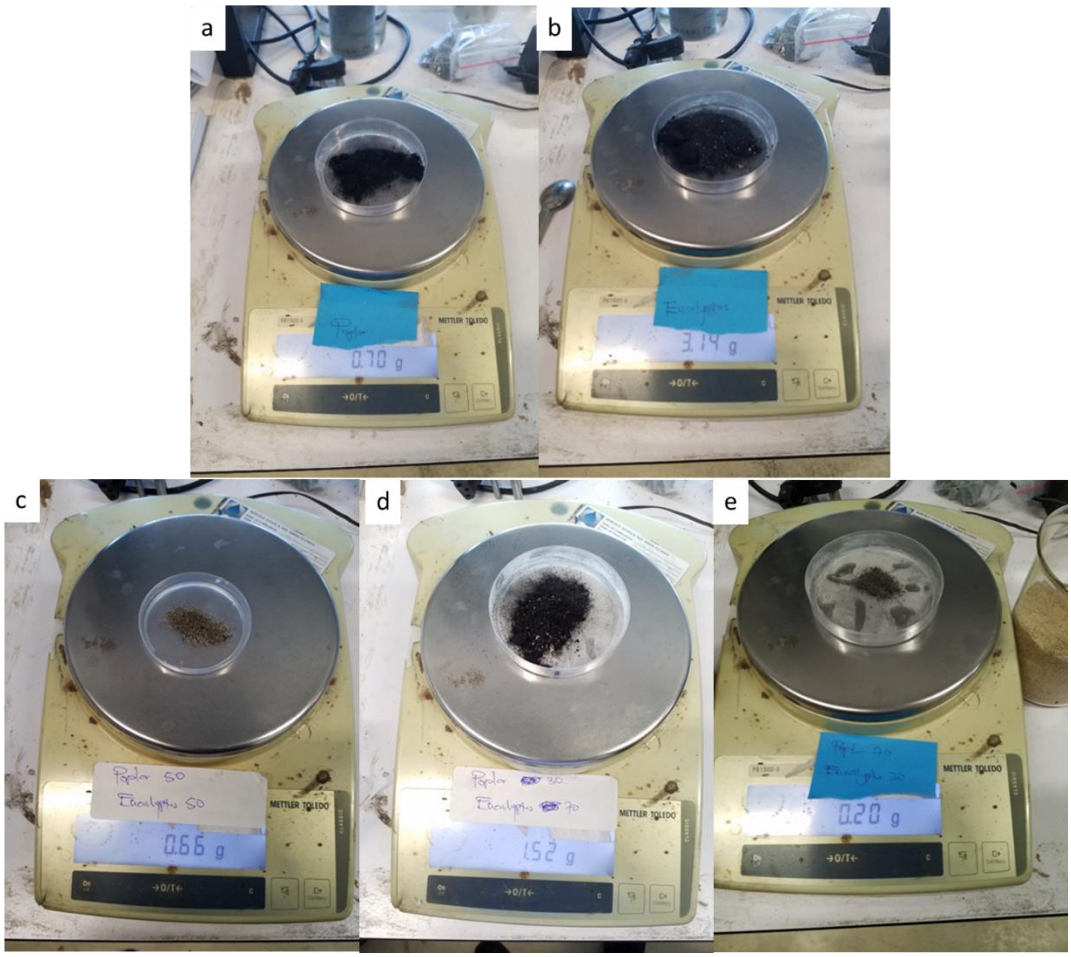


Figure 6.27: Char residue of (a) Poplar and (b) Eucalyptus chars as well as those of their blends Poplar-Eucalyptus (c) 50/50; (d) 30/70; and (e) 70/30 after pyro-gasification at 1000°C.

Another interesting observation was made by comparing the dry gas rate of production of the Eucalyptus and Poplar and their corresponding blends on Fig. 6.11, 6.12 and 6.13 with their char residues on Fig. 6.27 above. Firstly, from the dry gas rate of production graphs, it was observed that the Eucalyptus and Poplar individually exhibited low dry gas production rates at 900°C and 950°C. However, there was a 97% increase in the dry gas rate of production of the Eucalyptus and a 173% increase in the dry gas rate of production of the Poplar at 1000°C from their values at 900°C. With reference to the high carbon-rich char residue left in the reactor (see Fig. 6.27 a, b), it can be said that both samples individually attained higher reactivity at 1000°C. However, when blended, a complete conversion of the Eucalyptus-Poplar 50/50 and 30/70 chars was observed, indicated by the mass of their respective residues – 0.66 g and 0.20 g (see Fig. 6.27c and e). Also observed was the high ash contained in these char residues, which must have been as a result of the high ash composition of the Poplar as depicted in Fig. 4.4. The Eucalyptus-Poplar 70/30 blend, however, retained a greater amount of carbon in its char residue – weighing 1.52 g (see Fig. 6.27 d). This was as a result of the greater proportion of the less reactive Eucalyptus in the blend.

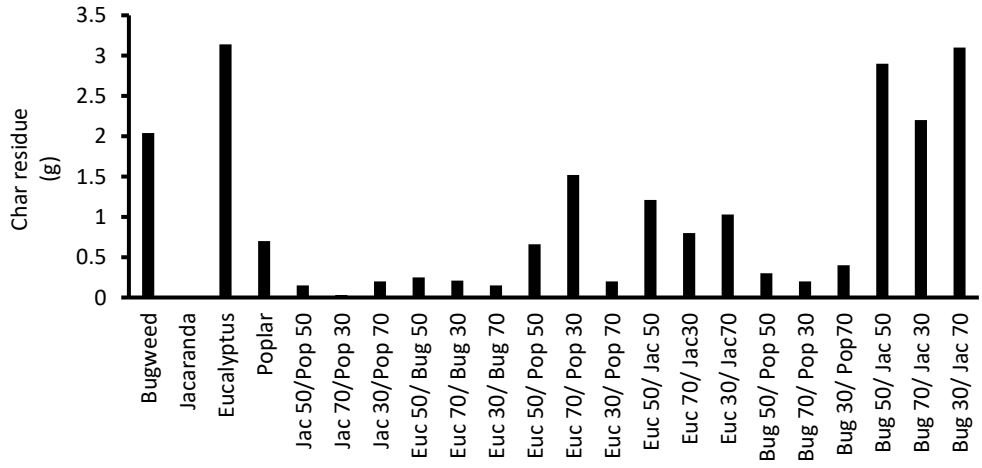


Figure 6.28: Mass of char residue recovered for the individual IAPs and their blends

A comparison of the char mass residue of all samples and their respective blends are depicted in Figs. 6.28 and 6.29. The lowest char residue was observed from the

Jacaranda-Poplar 70/30 (0.03 g), while the highest char residue recovered was from the Eucalyptus sample (3.14 g).

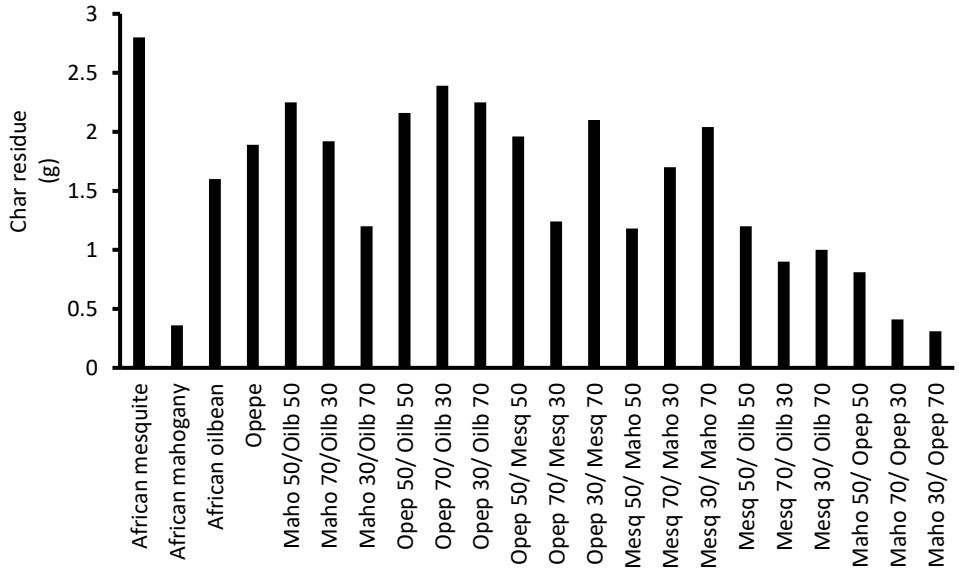


Figure 6.29: Mass of char residue recovered for the individual Tropical hardwood samples and their blends.

6.2.5 Observed flame properties

The physical properties of the flame generated when the dry product gas was ignited such as the ignitability, flame propagation and colour give a general idea of the concentration of H_2 or CO in the syngas being produced. They can also be used to predict the syngas flow rate and rate of production and most importantly, the suitability of the gas for downstream combustion applications. Simply defined, the ignitability of a gas is its 'readiness' to generate a flame when in contact with a spark or exposed to a flame in the presence of oxygen. Flame propagation, on the other hand, can be defined as the longitudinal distance travelled by the flame when ignited.

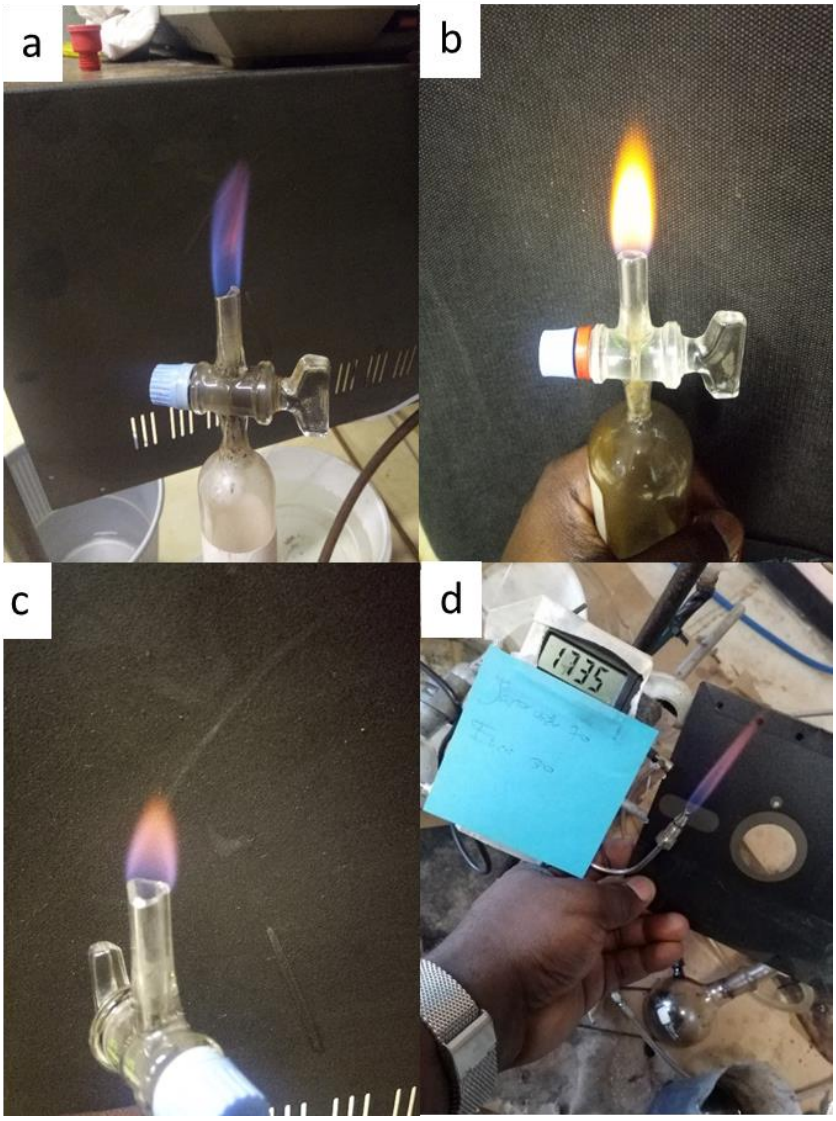


Figure 6.30: (a), (b) and (c) three types of flames generated from the syngas produced in this study; (d) flame produced from syngas of Eucalyptus-Jacaranda 30/70 blend at an instantaneous gas flow rate of 1735 mL/min

Figures 6.30 a, b and c depict the types of flames generated by the product gases in this study. In general, the pure blue flame observed in Fig. 6.30 a, is known to signify the high concentration of hydrogen in the gas ignited. Hydrogen when ignited burns with an almost invisible pale blue flame. This kind of flame does not produce smoke and is the cleanest type of flame. Conversely, Fig. 6.30 b – the pure yellow flame, signifies a very high concentration of CO than H_2 in the gas. Such flames sometimes may also depict an orange colour. Thirdly, the blue flame with

a yellow halo in Fig. 6.30 c depicts a gas with a considerable hydrogen concentration and containing some impurities or an equal concentration of CO in it. Meanwhile, in terms of flame propagation, Fig. 6.30 a, depicts a flame with high propagation, while Fig. 6.30 c depicts a flame with low propagation.

Flames with extremely low propagations were also observed in some wood samples. In most cases, flames exhibiting low ignitability and low propagation in this study were easily extinguished as they could not sustain combustion for prolonged periods. Such flames may have been diluted with Nitrogen or CO_2 which do not support combustion.

In this study, however, the ignition time and actual length covered by the flame propagation were not particularly measured due to time constraints. However, the wood samples exhibiting either high or low flame propagation, specific flame colour and ignition difficulties or ease, were identified in Tables 6.5 – 6.44. This section, therefore, highlights some samples with distinct flame properties.

Figure 6.30 d, depicts the flame property of the Jacaranda-Eucalyptus 70/30 blend at an instantaneous dry gas flow rate of 1735 mL/min. This indicates the high concentration of hydrogen with some impurities or considerable CO concentration and a high flame propagation. Table 6.45 shows a summary of the flame properties of the dry gas produced from the pyro-gasification of each sample. It was observed that the Jacaranda sample was consistent in the production of blue flames. This was evident in its capability to generate highly ignitable gas with consistent blue flame and high propagation. This also reflected on its associated blended samples, particularly, with the Jacaranda-Poplar blend.

Table 6.1: Observed flame properties of gases generated from wood samples

Sample	Dry gas ignitability		Flame colour			Flame propagation	
	Low	High	Pure blue	Blue flame with yellow halo	Pure yellow	High	Low
African mesquite	✓		✓	✓			✓
African mahogany		✓	✓				✓
African oilbean		✓	✓				✓
Opepe		✓	✓				✓
Maho 50/Oilb 50		✓	✓	✓		✓	✓
Maho 70/Oilb 30		✓	✓	✓		✓	
Maho 30/Oilb 70		✓	✓	✓	✓	✓	✓
Opep 50/ Oilb 50		✓	✓	✓		✓	✓
Opep 70/ Oilb 30		✓	✓	✓		✓	
Opep 30/ Oilb 70	✓			✓			✓
Opep 50/ Mesq 50	✓			✓	✓		✓
Opep 70/ Mesq 30		✓	✓			✓	
Opep 30/ Mesq 70		✓		✓	✓	✓	
Mesq 50/ Maho 50		✓		✓	✓		✓
Mesq 70/ Maho 30		✓		✓	✓		✓
Mesq 30/ Maho 70		✓	✓	✓		✓	
Mesq 50/ Oilb 50		✓		✓			✓
Mesq 70/ Oilb 30		✓	✓	✓			✓
Mesq 30/ Oilb 70		✓	✓	✓			✓
Maho 50/ Opep 50		✓	✓			✓	
Maho 70/ Opep 30		✓	✓			✓	✓
Maho 30/ Opep 70		✓			✓		✓
Bugweed		✓	✓				✓
Jacaranda		✓	✓				✓
Eucalyptus	✓				✓	✓	✓
Poplar		✓	✓				✓
Jac 50/Pop 50		✓	✓			✓	
Jac 70/Pop 30		✓	✓			✓	
Jac 30/Pop 70		✓	✓			✓	
Euc 50/ Bug 50		✓		✓	✓	✓	

Euc 70/ Bug 30		✓		✓	✓	✓	
Euc 30/ Bug 70		✓		✓		✓	
Euc 50/ Pop 50			✓	✓			✓
Euc 70/ Pop 30		✓		✓		✓	
Euc 30/ Pop 70		✓		✓		✓	
Euc 50/ Jac 50		✓	✓			✓	
Euc 70/ Jac30		✓		✓		✓	
Euc 30/ Jac70		✓	✓	✓		✓	✓
Bug 50/ Pop 50		✓	✓			✓	
Bug 70/ Pop 30		✓	✓	✓		✓	
Bug 30/ Pop70		✓	✓		✓	✓	
Bug 50/ Jac 50		✓	✓		✓	✓	
Bug 70/ Jac 30		✓	✓			✓	✓
Bug 30/ Jac 70		✓	✓			✓	✓

6.4 Concluding remark

The production of syngas via the pyro-gasification of the sawdust samples and their associated blends further verifies their viability and the authenticity of their characterisation results.

The sawdust char reactivity was a major factor in and is directly proportional to the gas flow rate. The Bugweed was influential in boosting the reactivity of most other samples and their resultant gas flow rate particularly at lower temperatures when blended with it. The Jacaranda-Poplar blends, however, produced syngas with the highest dry gas flow rate. This was attributed to the superior reactivity of the Poplar. In general, the gas flow rates of the tropical hardwoods were comparably much lower than those of the IAP samples. Amongst the tropical species, the African oilbean exhibited the highest flow rate at 900°C. In turn, its high char reactivity contributed to the relatively high gas flow rates of its associated blends with its counterparts.

The production rate of syngas is dependent on its concentration in the product gas and the dry product gas flow rate. Individually, the IAP samples generally showed

increases in H_2 rates of production with an increase in temperature. Among the individual samples, the Poplar exhibited the highest H_2 production rate of 3555 mL/min. g of feedstock at 1000°C (see Fig. 6.10). Meanwhile, the highest syngas production rate of 8924.6 mL/min. g of feedstock was attained by the Eucalyptus. At the lowest temperature of 900°C however, the highest syngas production rate was attained by the Bugweed, with a high production rate of its CO component being the major contributor to this high syngas production rate.

When blended, however, the IAPs exhibited much-improved syngas production rates at 900°C. In particular, the ratio of the hydrogen production rate to that of carbon monoxide of the blends was increased from those of their respective associated individual samples. In attestation to this, blue flames were observed to be predominantly generated when the gases produced from such blends were ignited. However, due to a possible depletion of the carbon in most samples, the syngas production rates were observed to largely decrease at 1000°C. A higher CO production rate was exhibited by the tropical hardwoods in comparison to their IAP counterparts. However, amongst some IAP samples, when blended, their hydrogen production rates were observed to improve particularly at 900°C. Similar increases in the hydrogen rates of production were also observed with some blends of the tropical samples. The highest increase in hydrogen production rate was the 200% increase by the African mesquite-African oilbean 50/50 blend as temperature increased from 900°C to 1000°C.

Despite its high syngas production rate, the African oilbean yielded the least syngas per gram of sawdust. Meanwhile, the syngas yield for most blended IAP samples was observed to peak at lower temperatures and greatly decrease at 1000°C. The reverse was, however, the case for their tropical counterparts, whereby syngas yield peaked at 1000°C. However, the Eucalyptus-Bugweed 30/70 blend attained the highest total syngas obtainable from the 20 g of sawdust feedstock, while the lowest was exhibited by the Jacaranda-Poplar 30/70 and the Mahogany-Opepe 70/30 blends.

Considerable amounts of bio-oils were extracted from the samples tested but the volumes measured were varied and unpredictable. Variations in moisture contents and volatile matter of the samples contributed to the variations in oil volumes. Moreover, the condensation of oil droplets in the pipe greatly affected the accuracy of the oil readings. However, in corroboration with their higher MC and VM, the bio-oil produced were predominantly higher with the individual IAP samples and their blends in comparison with those of their Tropical hardwood counterparts. The highest volume of bio-oil extracted was from the Bugweed-Jacaranda 50/50 blend while the lowest was extracted from the African mahogany-Opepe 50/50 blend.

Char residue after the process was considerably higher for the hardwoods samples which were predominantly less reactive. Char yield was also a contributing factor to the char mass leftover in the reactor. The blending of two individual samples also affected the quantity and mass of char residue recovered. The highest char mass recovered was from the Eucalyptus sample, while the lowest was recovered from the Jacaranda-Poplar 70/30 blend.

In most cases, the physical properties of the resultant flame generated from the syngas produced, corroborated with the data collated from the pyro-gasification of the various samples. Most IAP samples produced gases with predominantly blue flames when ignited, thus, indicating higher hydrogen concentration in the gases. Individually as well as in some of its blends with other samples, the Jacaranda produced the greatest number of blue flames. Conversely, higher numbers of yellow flames were observed with the Tropical samples, thus indicating a greater concentration of carbon monoxide in the gas.

Chapter 7

Conclusions and Recommendations

7.1 Conclusions

The localized utilization of the renewable energy resources of any region ensures its energy security and socio-economic development remain uncompromised as the global energy market tends towards a clean and sustainable energy future. Gasification is a proven technology for the thermochemical conversion of low-grade lignocellulosic biomass materials such as wood wastes to syngas. Through gasification, huge potentials abound with the production of syngas from LCBs. This is so since syngas can be utilised as feedstock for further conversion into secondary liquid biofuels and chemicals and as fuel for several other downstream applications such as power generation.

Feasibility studies have been conducted in literature on the utilization of wood wastes sourced from invasive alien plants and commercial tropical tree species for syngas production. However, there still exist limited knowledge of the actual performance of the variety of wood wastes with regards to yield and production rates of syngas at selected gasifier conditions. Also limited is the knowledge of any possible improvements on syngas production when wood wastes sourced from different tree species are blended in different ratios. Moreover, in the thermochemical conversion of LCB materials such as wood, high tar generation is known to compromise the quality and yield of the syngas produced. By adopting a variety of techniques, research interests have thus, been drawn towards improving the efficiency of the conversion process as well as minimizing tar generation in syngas production.

With such potentials in the sustainable production of syngas from waste, this study, therefore, was focused on investigating its production from the abundant wood wastes generated in South Africa and Nigeria. Eight wood waste samples sourced from the environmental control programme of four highly invasive IAPs and from the industrial sawmilling of four popular commercial tropical tree species

were used to conduct this research. They include IAPs namely – Eucalyptus, Poplar, Bugweed and Jacaranda and commercial tropical woods namely the African mesquite, African mahogany, African oilbean and Opepe.

Firstly, characterisations of the fuel properties of the abovementioned individual samples were conducted. Secondly, a fuel evaluation exercise was carried out on each sample to rate them according to their performance under certain fuel evaluators which influence their conversion to syngas via pyro-gasification. This evaluation was based on data collated from the experimental characterisation of the samples.

Finally, a comparative investigation of the syngas production from the individual wood samples against those of their respective blends with each other (in ratios of 50/50, 30/70, and 70/30) was conducted. In the production of syngas, an alternative tar reduction technique known as Pyro-gasification was employed, to minimize tar generation during syngas production. Data which includes the syngas composition of the product gas generated, the dry gas flow rate, the rate of production and yield of the syngas and its components (H_2 and CO) at three gas sampling temperatures - 900°C, 950°C and 1000°C was collated and analysed. In addition, the volume of tar/bio-oil extracted from each run was measured as well as the mass of unconverted char residue found in the reactor after each run. Observations on the physical properties of the flames generated by igniting the syngas produced from each run were also made.

The findings in this study established the potentials of blending certain wood species in specific ratios in the improvement of syngas production and highlighted the adoption of the pyro-gasification technology in maximizing the production of clean-burning syngas.

The following are conclusions garnered from each study conducted in this research.

a. Fuel examination and evaluation of the wood samples:

The structural analysis conducted on the individual wood samples reinstated the influence of the structural components of LCBs as the precursors to their elemental composition, proximate composition, thermochemical reactivity and biofuel yields when subjected to thermochemical treatment. In general, higher lignin compositions of up to 43.33 % were exhibited by the hardwoods such as the Eucalyptus, Poplar, African mesquite, African mahogany, African oilbean and Opepe. This in-turn was observed to influence their high FC and elemental carbon compositions. However, due to their superior holocellulose compositions, the Bugweed and Jacaranda were expected to exhibit higher reactivities than their hardwood counterparts when subjected to thermochemical treatment. In corroboration with their higher holocellulose compositions, the VM and the ash compositions of the Bugweed and Jacaranda were also observed to be of higher values than those of their hardwood counterparts.

In terms of potential emissions expected from the formation of nitrogen and sulfur compounds during biomass thermochemical conversion, the ultimate analysis revealed negligible sulfur compositions across the board. However, all samples exhibited considerable amounts of elemental nitrogen. In particular were the Bugweed (0.4%, N), Opepe (0.37%, N) and African oilbean (0.4%, N) whose nitrogen compositions exceeded the recommended European (Austria ONORM M7135 and German DIN51731/DINplus) nitrogen composition of 0.3% for wood fuels. The elemental carbon composition of the samples ranged between 42.34 – 50.49%. Higher C values were however exhibited by the hardwood samples which was attributed to their superior FC values as previously mentioned.

The above-mentioned superior C values of the hardwoods were also in effect, as they exhibited higher HHV values of up to 20.72 MJ/kg. Due to their densely packed particles, the bulk densities of the hardwoods were also observed to

be higher than those of their softwood counterparts – Bugweed and Jacaranda. As expected, the Bugweed and Jacaranda exhibited the lowest bulk densities of 0.5 g/cm^3 and 0.51 g/cm^3 respectively, which was attributed to their fibrous nature and loosely packed particles. Therefore, due to the higher HHVs as well as bulk densities of these hardwoods, their calculated energy densities were higher than those of the softwoods. Therefore, as a function of the higher HHVs and bulk densities of the hardwoods, their calculated energy densities were significantly higher than of the softwood samples. The energy densities ranged from as low as 7.03 GJ/m^3 for the Bugweed to as high as 21.76 GJ/m^3 for the African mesquite.

In comparison with most wood fuels reported in literature, the calculated fuel ratios of the samples investigated in this study were observed to be predominantly higher, ranging from as low as 0.53 for the Poplar and Jacaranda samples to as high as 1.08 for the African mesquite. This was attributed to the lower volatile matter composition of the samples which could be a result of their relatively low holocellulose composition. As reported in literature, the holocellulose structural components are known to contribute mostly to the volatile matter composition of LCBs.

From the analysis of the TGA and DTG conducted on the individual wood samples, char yield was observed to be highest from the African mesquite (47.11 % wt.). However, the reactivity of the African mesquite char was observed to be the lowest (0.87 %/min), thereby resulting in a char burnout temperature exceeding the final TGA temperature of 800°C. This was attributed to its superior fuel ratio and energy density. On the contrary, the highest char reactivity of 3.13 %/min was exhibited by the Bugweed sample, resulting to the lowest char burnout temperature of 475^{o}C. The influence of high ash presence as an inhibiting factor in char thermal decomposition was highlighted in the case of the Jacaranda sample. Its high ash composition was observed to inhibit its char decomposition as observed on its very low char

decomposition rate of 0.99 %/min, thus resulting to a delay in char decomposition and high char burnout temperature of 785^{o}C.

Therefore, with reference to the aforementioned experimental data, the primary fuel quality ratings (PFQR) of the samples under six fuel evaluators are summarised as follows:

i. Char yield: *African mesquite (8) > Eucalyptus (7) > African oilbean (6) > African mahogany (5) > Bugweed (4) > Opepe (3) > Jacaranda (2) > Poplar (1)*

ii. Char reactivity: *Bugweed (8) > African oilbean (7) > Poplar (6) > African mahogany (5) > Opepe (4) > Eucalyptus (3) > Jacaranda (2) > African mesquite (1)*

iii. Fuel ratio: *African mesquite (8) > (Eucalyptus = African mahogany = African oil bean (7)) > Bugweed (6) > Opepe (5) > (Jacaranda = Poplar (4))*

iv. Energy density: *African mesquite (8) > eucalyptus (7) > African oil bean (6) > African mahogany (5) Opepe (4) > (Poplar = Jacaranda (3)) > Bugweed (2)*

v. Nitrogen compound emissions: *Eucalyptus (-2) > Jacaranda (-3) > African mahogany (-4) > African mesquite (-5) > Poplar (-6) > Opepe (-7) > (African oilbean = Bugweed (-8))*

vi. Ash deposition: *African mesquite (-1) > African mahogany (-2) > African oilbean (-3) > Eucalyptus (-4) > Opepe (-5) > Poplar (-6) > Bugweed (-7) > Jacaranda (-8)*

b. *Thermo-decomposition Analysis (TGA) and Kinetic study of the wood samples:*

The thermogravimetric analysis of the wood samples was carried out by partitioning their thermograms into the volatilisation phase and the char decomposition phase. By so doing, the peaks generated on the thermograms

in either phase were used to describe the influence of structural components of the wood samples on their thermal decomposition behaviours.

In the volatilization phase, the wood samples were observed to volatilize roughly between 200°C and 400°C. This phase was characterised by the thermal decomposition of hemicellulose at a lower temperature, succeeded by the cellulose decomposition. In corroboration to this, it was observed that relatively higher volatilization rates were exhibited by samples composing of predominantly higher holocellulose compositions. Meanwhile, hardwoods, composing more of lignin were observed to volatilize at lower rates. Across the board, the Bugweed volatilized at the highest rate of 11.36 %/min while the African mesquite exhibited the lowest rate of volatilization of 6.66 %/min. The Bugweed, in correspondence to its high rate of volatilization, had the lowest volatilization residence time of 4.84 mins. However, despite exhibiting the lowest rate of volatilization, the African mesquite also had a relatively low volatilization residence time of 6.05 mins.

In the char decomposition phase, however, the low decomposition rate, which is typical of a high molecular-weight polymer material such as lignin was more prevalent. The char decomposition rates of the samples were observed to be generally much lower than the volatilization rates despite occurring at higher temperatures. Asides that of the African oilbean, the chars of the hardwood samples composing of higher lignin were observed to decompose at much lower rates than their softwood counterparts. This exceptionally high reactivity of the African oilbean among its hardwood counterparts was also exhibited in its volatilization phase. This was evident in its high syngas production at low temperatures when used as feedstock for the pyro-gasification experiment.

The kinetics data on the thermal decomposition of the wood samples were derived by adopting the Friedman method, using data generated from the thermal decomposition of each individual structural component. Data on the

activation energy, which is the minimum amount of energy required to activate the decomposition of the hemicellulose, cellulose or lignin, was derived for each wood sample. Therefore, the lowest activation energy of either of these three components of a wood sample was regarded as the activation energy of that sample. The Jacaranda exhibited the lowest value of 2.08 kJ/mol represented by that of its cellulose component. It was observed that in six out of the eight samples, the hemicellulose exhibited a significantly higher activation energy than the cellulose and lignin components. This was regarded as an apparent activation energy, considering that the decomposition of the hemicellulose component peaks at a much lower temperature input than those of its cellulose and lignin counterparts. This was attributed to the fact that when an LCB is subjected to thermal decomposition, its three structural components are subjected to the same thermal treatment at the same start temperature. However, their rates of thermal decomposition differ, as the hemicellulose decomposition becomes more prevalent and peaks at lower temperatures than those of the cellulose and lignin. Therefore, it was concluded that this apparent higher activation energy exhibited by the hemicellulose could be as a result of a summation of the energy input required to activate the decomposition of the cellulose and lignin.

c. *Pyro-gasification and syngas production from wood samples and their respective blends.*

In the production of syngas from the individual samples and their associated blends, their char reactivity was observed to be very influential to the outcome of their gas volumetric flow rates, yields and rates of production of their syngas. Gas flow rates exceeding 2000 mL/min were exhibited by samples with higher char reactivity such as the Bugweed and African oilbean. Conversely, lower gas flow rates as low as 172 mL/min were exhibited by samples with low char reactivity like the African mesquite, African mahogany and Opepe. Moreover, unlike with the Bugweed, high amounts of unreacted char residue from these three hardwoods were found in the reactor at the completion of

the pyro-gasification experiment at 1000°C. These low gas flow rates also resulted to the low flame propagation of the syngas when ignited. In most cases the flames were inconsistent, burning with very low intensity and were extinguished due to the intermittent reduction in the concentration of combustible gases in the product gas (from the hardwood species) to support combustion. However, variations in the H_2 and CO components of the syngas produced were observed, due to possible variations in the steam to carbon ratio of the reaction. The higher FC composition observed in the hardwoods, may have contributed to a lower steam to carbon ratio of the reactants, thereby producing syngas with lower H_2 than CO composition. An evidence of this was observed in the yellow flame of the syngas when ignited, indicating a high CO concentration in the syngas. Conversely, softwoods like the Bugweed exhibiting lower FC composition were observed to generate syngas, rich with hydrogen. This was evident in the clean-burning, high intensity, pale blue flame of the hydrogen-rich syngas generated from such species.

According to the data collated from the pyro-gasification experiment, the Bugweed (as earlier observed in its fuel characterisation) was observed to be very influential in boosting the reactivity of most other low-reactive samples blended with it. The highest dry gas volumetric flow rate of 2000 mL/min was, however, exhibited by the Jacaranda-Poplar blends. Asides the Jacaranda-Poplar 70/30 which decreased in gas flow rate with an increase in temperature, other two blend ratios maintained consistently high gas flow rates across the three sampling temperatures. It was concluded that the high reactivity of the Poplar char may have contributed to this high dry gas flow rate due to the very low reactivity consistently being exhibited by the Jacaranda sample. Meanwhile, amongst the tropical samples tested, the gas flow rate of the African oilbean was the highest at 900°C, attaining 678 mL/min. An increase in its flow rate to 1755 mL/min was also observed as the temperature increased to 1000°C. In general, the syngas flow rate from the tropical wood samples were much lower than those from their IAP counterparts.

The production rate of the syngas and those of its gaseous components – H_2 and CO, was mostly affected by the increase in temperature. Increases in the rates of production of H_2 were observed as the temperature was increased from 900°C to 1000°C. In general, the IAPs showed the highest increase in H_2 rate of production, attaining significant increases with the rise in temperature from 900°C to 1000°C. In particular, was the Poplar, exhibiting an increase in H_2 rate of production from 130.12 mL/min/gram of feedstock at 900°C to 3556.14 mL/min/gram of feedstock at 1000°C. The highest hydrogen production rate of 7937.07 mL/min/gram of feedstock was exhibited by the Eucalyptus-Jacaranda 30/70 blend. Fluctuations in the syngas rate of production was observed across the board but that of the Bugweed was consistently high across all three set temperatures. Such variations were also observed with the IAP blended samples, whereby most blended samples exhibited higher syngas production rates than their associated individual samples at a lower temperature of 900°C. However, with an increase in temperature to 1000°C, the syngas rate of production from most of these blended samples declined significantly. This was attributed to an improved rate of reaction which contributed to higher syngas production at 900°C, thus resulting in a depletion of the reactants as temperatures rose to 1000°C. Asides the African oilbean, all other tropical samples exhibited much lower syngas rate of production than their IAP counterparts. Their H_2 rates of production were also significantly lower and remained consistently low across the three sampling temperatures. However, the rate of production of CO was observed to increase with a rise in temperature, and thus mostly contributed to the increase in the syngas rate of production.

In terms of yield, the syngas produced from most samples was impressive, particularly at 900°C. This, however, was observed to drop temporarily across the board at 950°C, with a subsequent increase at 1000°C. The highest syngas yield of 744.42 mL/gram of feedstock was obtainable from the Eucalyptus-Bugweed 30/70 blend, while the lowest yield of 518.05 mL/gram of feedstock

was obtainable from the Jacaranda-Poplar 30/70 amongst all IAP samples and their blends. Meanwhile, among the tropical samples and their blends, the highest syngas yield of 735.8 mL/gram of feedstock was obtainable from the Mahogany-Opepe 30/70 blend, while the lowest yield of 493.7 mL/gram of feedstock was obtainable from the African mahogany-Opepe 70/30 blend.

Variations in the volumes of bio-oil extracted were observed across the board. The inconsistency in the bio-oil volumes was attributed to the technical issues such as the early condensation of bio-oil during its flow along the exit channel of the reactor before reaching the gas condenser. Other factors such as variations in the MC and VM of the feedstock as well as reactor temperature, heating rate and cooling water flow rate of the gas condenser may have contributed to the inconsistency of the bio-oil volumes. The highest bio-oil volume of 8.5 mL was extracted from the Bugweed-Jacaranda 50/50 blend while the lowest of 1.7 mL was obtainable from the African mahogany-Opepe 50/50 blend.

Conversely, the char residues recovered from the reactor at the end of the pyro-gasification process were more predictable and corroborated with the results of the characterization of the samples. For instance, samples which were observed to exhibit low char reactivity when characterized had greater mass of char residues left in the reactor after the process. In particular, were samples such as the Eucalyptus (3.14 g of char residue), African mesquite (4.22 g of char residue), and Opepe (1.89 g of char residue), which correspondingly exhibited low char reactivities and high bulk densities. It was also observed that by blending some samples, the mass of the char residue was significantly declined, signifying an improvement in reactivity and syngas production. This mostly occurred when wood samples with high char reactivity, were blended with those of low char reactivities. It was important to note that, for some samples, the high mass of their char residue was as a result of the high amounts of ash residue found in their chars. Therefore, in such cases, the high char residue did not necessarily translate to a high unreacted carbon residue.

In general, however, higher masses of char residues were found to be more prevalent with the tropical species and their blends than with the IAP species.

As observed, the properties of the flames produced by igniting the syngas exiting the pyro-gasification rig were consistent with the behaviours of the samples as observed during their pyro-gasification. Acknowledged, were physical properties of the flames such as colour, flame propagation and flame intensity. As earlier mentioned, samples which exhibited higher H_2 concentration were observed to produce pale blue flames when igniting their syngas. Yellow flames were however observed for the hardwoods in most cases. This signified high CO concentration in the syngas. In terms of flame propagation, the samples with poor char reactivities (also resulting to poor syngas rates of production), produced flames which were either difficult to ignite or if ignited, burned with very low propagation and extinguished with ease. However, it was observed that this poor flame propagation mostly occurred at lower temperatures and increased only with an increase in temperature to 1000°C. This observation was consistent with the results collated, whereby the low reactive samples such as the African mesquite and African mahogany for instance, only increased their char reactivity at higher temperatures thereby increasing the syngas rate of production.

7.2 Recommendations

The outcomes of this research bring to light grey areas, thus providing opportunities for further investigation into the following subject areas:

1. *Life-cycle assessment of a pyro-gasification plant:* The life-cycle analysis of a pyro-gasification pilot plant just as that of any other process plant is of utmost importance to ascertain its sustainable utilization and techno-economic viability. Analysis such as the Total Life-Cycle Cost (TLCC), and if attached to a gas-powered plant, its Levelized Cost of Energy in comparison with fossil-fueled power plants, Revenue Requirements etc., would fast-track its scale-up to full

commercialization. Moreover, the sustainability of the supply of biomass feedstock, environmental and socio-economic impact associated with the commissioning and operation of the plant should be considered and investigated.

2. *Technical improvements and scale-up of the pyro-gasification rig:* As highlighted in this report, the pyro-gasification rig as well as the pilot plants reported in literature, were observed to develop some operational faults. Research could be conducted to investigate and proffer solutions to these technical problems which limit its energy efficiency and maximizes its operational costs. Such problems include the drop in temperature and pressure of the reactors during operation, rupture of the reactor due to high temperature, blockage of the exit pipes due to early condensation of the bio-oil/tars during flow through the pipe towards the gas condenser. By wrapping these tar exit pipes with heating coils, and increasing their diameters, such occurrences of condensation can be minimized. In addition to these, the recycling of the hot flue gas by channeling it back into the reactor or for district heating could minimize energy input and improve the energy efficiency of the unit.

3. *Identification and utilization of suitable Invasive tree species for biomass-coal or biomass-biomass blending:* This research investigated the fuel properties of some IAPs and their performance when blended with each other in different ratios. By so doing, it was observed that some samples though initially perceived to be less suitable for pyro-gasification, performed well when pyro-gasified. Moreover, when blended with other samples, they were influential in improving the syngas production of other less reactive samples at lower gasification phase temperatures. A typical example is the Bugweed, which due to its high reactivity and resultant high product gas flow rate, was observed to improve the gas flow rate of species such as the Jacaranda

and the Eucalyptus. The Jacaranda and Eucalyptus were earlier observed to exhibit low gas flow rates when pyro-gasified individually. Another typical example was with the exceptional case of the Jacaranda and Poplar, whereby both species exhibited very low product gas flow rates (285 and 530 mL/min respectively), particularly at low temperatures. However, when blended with each other in different ratios, attained high gas flow rates of up to 2000 mL/min at 900°C. Such wood samples may also be utilized for blending with coal for combustion or gasification purposes.

4. *Socio-economic assessment of sustainable wood waste to bioenergy production from commercial wood processing and control of IAPs:* In the commissioning of pyro-gasification rigs as well as any process unit, the socio-economic impact cannot be overemphasized. Deliverables such as job creation across the supply chain, reduction in wildfires and pollution caused by the indiscriminate dumping and burning of wood wastes, as well as the maximum utilization of wood can be investigated to highlight the potentials of the pyro-gasification technology.

5. *The kinetics of conversion of wood blends of different ratios during a pyro-gasification process:* An in-depth investigation into the kinetics of the thermochemical behaviors of the individual wood species and their blends in this study when pyro-gasified, is needed. This is necessary to gain a better knowledge of why most wood samples were observed to perform better when blended than when pyro-gasified individually. At fixed process conditions, further investigations into their physical, chemical and fuel properties as well as their influence on the pyro-gasification reactions should be conducted.

References

1. Mohammed, YS, Mustafa, MW & Bashir, N. (2013) "Status of renewable energy consumption and developmental challenges in Sub-Sahara Africa." Renew. Sustain. Energy Rev. Vol. 27, pp 453–463.
2. The World Bank. (2016) "Access to electricity (% of population)." [Available online] http://data.worldbank.org/indicator/EG.ELC.ACCS.ZS?end=2012&name_desc=false&start=2012&view=map&year=2012 (2016).
3. The World Bank. (2015) "GDP (current US$)." [Available online] https://data.worldbank.org/indicator/NY.GDP.MKTP.CD?end=2012&namedesc=false&start=2012&view=map&year=2015.
4. Chamber of Mines of South Africa. (2018) "National Coal Strategy for South Africa 2018". National Coal Strategy.
5. Statistics South Africa. (2012) "National Accounts: Mineral Accounts for South Africa: 1980 - 2009". Vol. 67.
6. OPEC. (2018) "OPEC share of world crude oil reserves, 2017." [Available online] https://www.opec.org/opec_web/en/data_graphs/330.htm.
7. NREL. (2013) "International trade of wood pellets." [Available online] https://www.nrel.gov/docs/fy13osti/56791.pdf.
8. Remedio, E M. (2009) "An analysis of sustainable fuelwood and charcoal production systems in The Philippines : A Case Study. in Criteria and indicators for sustainable woodfuels: Case studies from Brazil, Guyana, Nepal, Philippines and Tanzania" (ed. Trossero, M.) Food and Agricultural Organization of the United Nations.
9. FAO Forestry. (2010) "What woodfuels can do to mitigate climate change." Management. Vol. 162 [Available online] http://www.fao.org/docrep/013/i1756e/i1756e00.pdf.

10. GEF. (2013) "Africa will import — not export — wood." [Available online] http://www.criterionafrica.com/wp-content/uploads/2017/06/Africa-will- Import-not-Export-Wood.pdf.

11. Smeets Ã, EM, Faaij, P, Lewandowski, IM & Turkenburg, WC. (2007) "A bottom-up assessment and review of global bio-energy potentials to 2050." Prog. Energy Combust. Sci. Vol. 33, pp 56–106.

12. Oluoti, K, Megwai, G, Pettersson, A & Richards, T. (2014) "Nigerian Wood Waste : A Dependable and Renewable Fuel Option for Power Production." World J. Eng. Technol. Vol. 2, pp 234–248.

13. Fuwape, JA. (1998) "Developments in wood-based industries in Nigeria." Foresea. Vol. 2, pp 575–585.

14. Arimoro, FO & Osakwe, EI. (2006) "The influence of sawmill wood wastes on the distribution and population of macroinvertebrates at Benin River, Niger Delta Area, Nigeria." Chem. Biodivers. Vol. 3, pp 578–592.

15. United Nations Development Programme-Nigeria. (2020) "Turning a 'burning mountain' of sawdust into briquettes." [Available online] https://www.ng.undp.org/content/nigeria/en/home/ourwork/environmentandenergy/successstories/sawdust/.

16. Matthews, E. (2017) "Fire destroys BKB Cedar Mill." Rocky Moutain Goat. [Available online] https://www.therockymountaingoat.com/2017/04/fire-destroys-bkb-cedar-mill/.

17. Food and Agricultural Organization. [2019] "Status of Invasive Tree Species in Southern Africa - South Africa." [Available online] http://www.fao.org/3/ac846e/ac846e06.htm.

18. Van Wilgen, BW *et al.* (2012) "An assessment of the effectiveness of a large, national-scale invasive alien plant control strategy in South Africa." Biol. Conserv. Vol. 148, pp 28–38.

19. Olckers, T. (2011) "Biological Control of Solanum mauritianum Scop. (Solanaceae) in South Africa: Will Perseverance Pay off?" African Entomol. Vol. 19, pp 416–426.

20. Aar, D & Cape, N. (2014) "Alien Invasive Plant Management Plan - Longyuan Mulilo Maanhaarberg Wind Energy Facility."

21. Department of Environmental Affairs South Africa. (2015) "Assessment of the potential to produce biochar and its application to South African soils as a mitigation measure." Vol. 84.

22. Enright, W. (2000) "The Effect of Terrestrial Invasive Alien Plants on Water Scarcity in South Africa." Phys. Chem. Earth (B), Vol. 25, pp 237–242.

23. Cape Nature, (2019) "Alien Vegetation Management." [Available online] https://www.capenature.co.za/care-for-nature/conservation-in-action/integrated-catchment-management/alien-vegetation-management/.

24. Colvin, C, Muruven, D, Lindley, D, Gorden, H & Schachtscheneider, K. (2016) "Water : Facts and futures rethinking South Africa's water future." World Wildl. Fund-South Africa. pp 1–100.

25. Bildirici, M & Özaksoy, F. (2016) "Woody Biomass Energy Consumption and Economic Growth in Sub-Saharan Africa." Procedia Economics and Finance. Vol. 38, 287–293.

26. Chamberlain, D, Essop, H, Hougaard, C, Malherbe, S & Walker, R. (2005) "SA forestry industry market analysis 2005." [Available online] http://www.daff.gov.za/doaDev/sideMenu/ForestryWeb/dwaf/cmsdocs/E lsa/Docs/FED/SA Forestry Industry Market Analysis 2005.pdf.

27. Food and Agricultural Organisation of the United Nations FAO. (2001) "Global forest resources assessment 2000: main report." [Available online] http://www.fao.org/tempref/docrep/fao/003/Y1997E/FRA 2000 Main report.pdf.

28. Aina, OM, Adetogun, AC, Adedokun, MO, Onilude, MA. (2005) "ALTERNATIVE COOKING FUELS FROM SAWMILL WASTES." Farm Management Association of Nigeria Conference, Asaba.

29. UMassAmherst - The Centre for Agriculture. (2017) "Fact sheet: Bedding options for livestock and equine." [Available online] https://ag.umass.edu/crops-dairy-livestock-equine/fact-sheets/bedding- options-for-livestock-equine.

30. Mugido, W. *et al.* (2014) "Determining the feasibility of harvesting invasive alien plant species for energy." S Afr J Sci. Vol. 110, pp 1–6.

31. Molino, A, Chianese, S & Musmarra, D. (2016) "Biomass gasification technology: The state-of-the-art overview." J. Energy Chem. Vol. 25, pp 10–25.

32. Li, QH, Zhang, YG, Meng, AH, Li, L & Li, GX. (2013) "Study on ash fusion temperature using original and simulated biomass ashes." Fuel Process. Technol. Vol. 107, pp 107–112.

33. Li, W, Li, Q, Chen, R, Wu, Y & Zhang, Y. (2014) "Investigation of hydrogen production using wood pellets gasification with steam at high temperature over 800 C to 1435 C." Int. J. Hydrogen Energy. Vol. 39, pp 5580–5588.

34. Ruoppolo, G, Miccio, F, Brachi, P, Picarelli, A & Chirone, R. "Fluidized Bed Gasification of Biomass and Biomass / Coal Pellets in Oxygen and Steam Atmosphere." Chemical Engineering Transactions. Vol. 32, pp 595–600.

35. Dhyani, V & Bhaskar, T. (2018) "A comprehensive review on the pyrolysis of lignocellulosic biomass." Renew. Energy. Vol. 129, pp 695–716.

36. Huber, G. W., Iborra, S. & Corma, A. Synthesis of Transportation Fuels from Biomass : Chemistry , Catalysts , and Engineering. 2, 4044–4098 (2006).

37. Vassilev, S, Vassilieva, C & Vassilev, V. (2015) "Advantages and disadvantages of Composition and properties of biomass in comparison with: An overview." Fuel. Vol. 158, pp 330–350.

38. Okoye, NH *et al.* "Effect of Density on Flame Characteristics of Some Tropical Timbers." J. Appl. Chem. Vol. 7, pp 104–111.

39. Duruaku, JI, Ajiwe, VIE, Okoye, NH & Arinze, RU. (2016) "An Evaluation of the Calorific Values of the Branches and Stems of 11 Tropical Trees." J. Sustain. Bioenergy Syst. Vol. 6, pp 44–54.

40. Akhator, P, Obanor, A & Ugege, A. (2017) "Nigerian Wood Waste: A Potential Resource for Economic Development." J. Appl. Sci. Environ. Manag. Vol. 21, pp 246.

41. Girard, P. (2002) "Charcoal production and use in Africa: what future?" International Cooperation Centre of Agricultural Research for Development. Vol. 53, pp 30–35.

42. Ogunwusi, AA. (2014) "Wood Waste Generation in the Forest Industry in Nigeria and Prospects for Its Industrial Utilization." Civ. Environ. Res. Vol. 6, pp 62–70.

43. Sjølie, HK. (2012) "Reducing greenhouse gas emissions from households and industry by the use of charcoal from sawmill residues in Tanzania." J. Clean. Prod. Vol. 27, pp 109–117.

44. Chamier, J. *et al.* (2012) "Impacts of invasive alien plants on water quality, with particular emphasis on South Africa." Water SA. Vol. 38, pp 345–356.

45. De Lange, W. (2012) "Incorporating stakeholder preferences in the selection of technologies for using invasive alien plants as a bio-energy feedstock: applying the analytical hierarchy process." J. Environ. Manage. Vol. 99, pp 76–83.

46. Early, R. *et al.* (2016) "Global threats from invasive alien species in the twenty-first century and national response capacities." Nat. Commun. Vol. 7, no1, pp 123485.

47. Mandlakazi, M. (2016) "Evaluation of the potential of non-woody invasive plant biomass for electricity generation." PhD thesis, Stellenbosch University, South Africa.

48. Environmental and Energy Study Institute. “Bioenergy (Biofuels and Biomass).” [Available Online] https://www.eesi.org/topics/bioenergy-biofuels-biomass/description.

49. Vassilev, SV, Baxter, D, Andersen, LK & Vassileva, CG. (2010) "An overview of the chemical composition of biomass." Fuel. Vol. 89, pp 913–933.

50. McKendry, P. (2001) "Energy production from biomass (part 1): Overview of biomass." Biosource Technol. Vol. 83, 37–46 (2001).

51. Bajpai, P. (2018) "Wood and Fiber Fundamentals." Biermann’s Handbook of Pulp and Paper. Elsevier.

52. Brunner, G. (2014) "Processing of Biomass with Hydrothermal and Supercritical Water." Hydrothermal and Supercritical Water Processes. Vol. 5, pp 395–509. Elsevier.

53. Asif, M. (2009) "Sustainability of timber, wood and bamboo in construction." Sustainability of Construction Materials. Woodhead Publishing Limited.

54. Bhuiyan, NH, Selvaraj, G, Wei, Y & King, J. (2009) "Role of lignification in plant defense." Plant Biotechnol. Vol. 4, pp 158–159.

55. Koch, GW, Sillett, SC, Jennings, GM & Davis, SD. (2004) "The limits to tree height." Nature. Vol. 428, pp 851–854.

56. Saidur, R, Abdelaziz, EA, Demirbas, A, Hossain, MS & Mekhilef, S. (2011) "A review on biomass as a fuel for boilers." Renew. Sustain. Energy Rev. Vol. 15, pp 2262–2289.

57. Wang, P & Howard, BH. (2018) "Impact of thermal pretreatment temperatures on woody biomass chemical composition, physical properties and microstructure." Energies. Vol. 11, pp 1–20.

58. Nguyen, QN, Cloutier, A, Achim, A & Stevanovic, T. (2016) "Fuel properties of sugar maple and yellow birch wood in relation with tree vigor." BioResources. Vol. 11, pp 3275–3288.

59. Demirbas, A. (2002) "Relationships between Heating Value and Lignin, Moisture, Ash and Extractive Contents of Biomass Fuels." Energy Explor. Exploit. Vol. 20, pp 105–111.

60. Telmo, C & Lousada, J. (2011) "The explained variation by lignin and extractive contents on higher heating value of wood." Biomass and Bioenergy. Vol. 35, pp 1663–1667.

61. St-Pierre, F, Achim, A & Stevanovic, T. (2013) "Composition of ethanolic extracts of wood and bark from Acer saccharum and Betula alleghaniensis trees of different vigor classes." Ind. Crops Prod. Vol. 41, pp 179–187.

62. Chen, W, Peng, J & Bi, XT. (2015) "A state-of-the-art review of biomass torrefaction, densification and applications." Renew. Sustain. Energy Rev. Vol. 44, pp 847–866.

63. Peng, JH. (2012) "A study of softwood torrefaction and densification for the production of high-quality wood pellets." PhD Thesis, The University of British Columbia, Vancouver. pp 260.

64. Yang, H *et al.* (2006) "In-Depth Investigation of Biomass Pyrolysis Based on Three Major Components: Hemicellulose, Cellulose and Lignin." Energy & Fuels. Vol. 20, pp 388–393.

65. Yang, H. (2007) "Characteristics of hemicellulose, cellulose and lignin pyrolysis." Fuel. Vol. 86, pp 1781–1788.

66. Yu, J, Paterson, N, Blamey, J & Millan, M. (2017) "Cellulose , xylan and lignin interactions during pyrolysis of lignocellulosic biomass." Fuel. Vol. 191, pp 140–149.

67. Prins, MJ, Ptasinski, KJ & Janssen, FJJG. (2006) "Torrefaction of wood Part 1. Weight loss kinetics." J. Anal. Appl. Pyrolysis. Vol. 77, pp 28–34.

68. Gašparovič, L, Koreňová, Z & Jelemenský, Ľ. (2010) "Kinetic study of wood chips decomposition by TGA." Chem. Pap. Vol. 64, pp 174–181.

69. Slopiecka, K, Bartocci, P & Fantozzi, F. (2012) "Thermogravimetric analysis and kinetic study of poplar wood pyrolysis." Appl. Energy. Vol. 97, pp 491–497.

70. Fréjaville, T, Carcaillet, C & Curt, T. (2013) "Calibration of charcoal production from trees biomass for soil charcoal analyses in subalpine ecosystems." Quat. Int. Vol. 289, pp 16–23.

71. Sikarwar, S, Zhao, M, Fennell, P, Shah, N & Anthony, E. (2017) "Progress in biofuel production from gasification." Prog. Energy Combust. Sci. Vol. 61, pp 189–248.

72. Anukam, A, Mamphweli, S, Reddy, P & Meyer, E. (2016) "Pre-processing of sugarcane bagasse for gasification in a downdraft biomass gasifier system: A comprehensive review." Renew. Sustain. Energy Rev. Vol. 66, pp 775–801.

73. Branca, C, Giudicianni, P & Di Blasi, C. (2003) "GC/MS Characterization of Liquids Generated from Low-Temperature Pyrolysis of Wood." Ind. Eng. Chem. Res. Vol. 42, pp 3190–3202.

74. Fjellerup, JS, Ahrenfeldt, J, Henriksen, UB, Gøbel, B. (2005) "Formation, Decomposition and Cracking of Biomass Tars in Gasification." Kgs.Lyngby: Technical University of Denmark.

75. Chen, Z, Zhu, Q, Wang, X, Xiao, B & Liu, S. (2015) "Pyrolysis behaviors and kinetic studies on Eucalyptus residues using thermogravimetric analysis." Energy Convers. Manag. Vol. 105, pp 251–259.

76. Ball, R, Mcintosh, AC & Brindley, J. (2007) "Feedback processes in cellulose thermal decomposition: implications for fire-retarding strategies and treatments" Combustion Theory and Modelling. Vol. 8, no 2, pp 281-291.

77. Pattanotai, T, Watanabe, H & Okazaki, K. (2014) "Gasification characteristic of large wood chars with anisotropic structure." Fuel. Vol. 117, pp 331–339.

78. Diebold, JP. (2000) "A Review of the Chemical and Physical Mechanisms of the Storage Stability of Fast Pyrolysis Bio-Oils." Nrel/Sr-570-27613 59.

79. Oasmaa, A, Elliott, DC & Muller, S. (2009) "Quality control in fast pyrolysis bio-oil production and use." Environ. Prog. Sustain. energy. Vol. 28, pp 404– 409.

80. Gwenzi, W, Chaukura, N, Mukome, FND & Machado, S. (2015) "Biochar production and applications in Sub-Saharan Africa : Opportunities, constraints, risks and uncertainties." J. Environ. Manage. Vol. 150, pp 250–261.

81. Kim, J, Mun, T, Kim, J & Kim, J. (2011) "Air gasification of mixed plastic wastes using a two-stage gasifier for the production of producer gas with low tar and a high caloric value." Fuel. Vol. 90, pp 2266-2272.

82. Zulkurnai, NZ, Mohammad Ali, UF, Ibrahim, N & Abdul Manan, NS. (2017) "Carbon Dioxide (CO2) Adsorption by Activated Carbon Functionalized with Deep Eutectic Solvent (DES)." IOP Conf. Ser. Mater. Sci. Eng. Vol. 206.

83. Siedel, A. (2008) "Charcoal in Africa, importance, problems and possible solutions." Deutsche Gesellschaft für Technische Zusammenarbeit (GTZ).

84. NL Agency. (2010) "Making charcoal production in Sub Sahara Africa sustainable." Netherlands Programmes Sustainable Biomass, Maartje.

85. Nisgoski, S. *et al.* (2014) "Anatomical and energy characteristics of charcoal made from five species." Acta Amazonica. Vol. 44, pp 367–372.

86. Ramachandra, TV, Kamakshi, G. (2005) "Bioresource potential of Karnataka (talukwise inventory with management options)." Centre for Ecological Sciences Indian Institute of Science Bangalore. Technical Report Vol. 06.

87. Aref, IM & Megahed, MM. (1996) "Properties of charcoal produced from some endemic and exotic acacia species grown in Riyadh, Saudi Arabia."

88. Sohi, SP, Krull, E, Lopez-Capel, E & Bol, R. (2010) "A review of biochar and its use and function in soil." Adv. Agron. Vol. 105, pp 47–82.

89. Sikarwar, VS *et al.* (2016) "An overview of advances in biomass gasification." Energy Environ. Sci. Vol. 9, pp 2939–2977.

90. Speight, JG. (2015) "Production of syngas, synfuel, bio-oils, and biogas from coal, biomass, and opportunity fuels." Fuel Flexible Energy Generation: Solid, Liquid and Gaseous Fuels. Elsevier Ltd.

91. McKendry, P. (2002) "Energy production from biomass (part 3): gasification technologies." Bioresour. Technol. Vol. 83, no1, pp 55–63.

92. Molino, A. *et al.* (2013) "Electricity production by biomass steam gasification using a high efficiency technology and low environmental impact." Fuel. Vol. 103, pp 179–192.

93. Speight, JG. (2018) "Energy security and the environment." Nat. Gas. pp 361–390.

94. Siedlecki, M, de Jong, W & Verkooijen, AHM. (2011) "Fluidized bed gasification as a mature and reliable technology for the production of bio-syngas and applied in the production of liquid transportation fuels-a review." Energies. Vol 4, pp 389–434.

95. Zhang, Q, Deng, W & Wang, Y. (2013) "Recent advances in understanding the key catalyst factors for Fischer-Tropsch synthesis." J. Energy Chem. Vol. 22, pp 27–38.

96. Basu, P. (2010) Biomass Gasification and Pyrolysis Practical Design. Oxford. Elsevier Inc.

97. Daniell, J, Köpke, M & Simpson, SD. (2012) "Commercial biomass syngas fermentation." Energies. Vol. 5, pp 5417–5417.

98. Habibi, N, Rezaei, M, Majidian, N & Andache, M. (2014) "CH4 reforming with CO2 for syngas production over La2O3 promoted Ni catalysts supported on mesoporous nanostructured γ -Al2O3." J. Energy Chem. Vol. 23, pp 435– 442.

99. Murphy, J, Browne, J, Allen, E & Gallagher, C. (2013) "The resource of biomethane, produced via biological, thermal and electrical routes, as a transport biofuel." Renew. Energy. Vol. 55, pp 474–479.

100. Molino, A *et al.* (2012) "Classification procedure of the explosion risk areas in presence of hydrogen-rich syngas: Biomass gasifier and molten carbonate fuel cell integrated plant." Fuel. Vol. 99, pp 245–253.

101. Roskilly, A, Wang, Y, Mikalsen, R & Yu, H. (2012) "Use of Biofuels in a Range of Engine Configurations." Comprehensive Renewable Energy. pp 343–356. Elsevier.

102. Vilas Boas de Sales, C. *et al.* (2017) "Experimental study on biomass (eucalyptus spp.) gasification in a two- stage downdraft reactor by using mixtures of air, saturated steam and oxygen as gasifying agents." Energy Convers. Manag. Vol. 145, pp 314–323.

103. Di Blasi, C. (2000) "Dynamic behaviour of stratified downdraft gasifiers." Chem. Eng. Sci. Vol. 55, pp 2931–2944.

104. Dogru, M. (2002) "Gasification of hazelnut shells in a downdraft gasifier." Nat. Energy. Vol. 27, pp 415–427.

105. Boldrin, P, Millan-Agorio, M & Brandon, NP. (2015) "Effect of sulfur- and tar- contaminated syngas on solid oxide fuel cell anode materials." Energy and Fuels. Vol. 29, pp 442–446.

106. Huang, J, Schmidt, K & Bian, Z. (2011) "Removal and Conversion of Tar in Syngas from Woody Biomass Gasification for Power Utilization Using Catalytic Hydrocracking." Energies. Vol. 4, pp 1163–1177.

107. Wada, T, Fushimi, C & Tsutsumi, A. (2008) "Effects of Volatile-Char Interaction on the Char Reactivity In the Biomass Gasification." 2008 AIChE Annual Meeting.

108. Ratchahat, S, Kodama, S & Tanthapanichakoon, W. (2015) "CO2 gasification of biomass wastes enhanced by Ni/Al2O3 catalyst in molten eutectic carbonate salt." Int. J. Hydrogen Energy. Vol. 40, no35, pp 11809–11822.

109. Tinaut, FV. (2006) "Method for predicting the performance of an internal combustion engine fuelled by producer gas and other low heating value gases." Fuel Process. Technol. Vol. 87, pp 135–142.

110. Wongsiriamnuay, T, Kannang, N & Tippayawong, N. (2013) "Effect of Operating Conditions on Catalytic Gasification of Bamboo in a Fluidized Bed." Int. J. Chem. Eng. Vol 2013, pp 1–9.

111. Luo, S. *et al.* Hydrogen-rich gas from catalytic steam gasification of biomass in a fixed bed reactor: Influence of particle size on gasification performance. Int. J. Hydrogen Energy 34, 1260–1264 (2009).

112. Franco, C, Pinto, F, Gulyurtlu, I & Cabrita, I. (2003) "The study of reactions influencing the biomass steam gasification process." Fuel. Vol. 82, pp 835–842.

113. Subbaiah, BS, Murugan, DK, Deenadayalan, DB & Dhamodharan, MI. (2014) "Gasification of Biomass Using Fluidized Bed." Int. j. innov. res. sci. eng. technol. Vol. 3, pp 8995–9002.

114. Gil, J, Corella, J, Aznar, MP & Caballero, MA. (1999) "Biomass gasification in atmospheric and bubbling fluidized bed: Effect of the type of gasifying agent on the product distribution." Biomass and Bioenergy. Vol. 17, pp 389–403.

115. Suranani, S & Goli, VR. (2012) "Fuel Particle Size Effect on Performance of Fluidized Bed Combustor Firing Ground Nutshells." Int. J. Chem. Eng. Appl. Vol. 3, pp 147–151.

116. Fjellerup, J, Ahrenfeldt, J, Henriksen, U & Gøbel, B. (2005) "Formation, Decomposition and Cracking of Biomass Tars in Gasification." Renewable Energy. Vol. 30, no2, pp 147–151.

117. Neeft, JPA, Knoef, H. (1999) Behaviour of tar in biomass gasification systems: tar related problems and their solutions. Utrecht. MHP Management & Secretary Services [distr.].

118. Singh, RN, Singh, SP, Balwanshi, JB & Vishwavidhlya, DA. (2014) "Tar removal from Producer Gas: A Review." Res. J. Eng. Sci. Vol. 3, pp 16–22.

119. Sansaniwal, SK, Pal, K, Rosen, MA & Tyagi, SK. (2017) "Recent advances in the development of biomass gasification technology: A comprehensive review." Renew. Sustain. Energy Rev. Vol. 72, pp 363–384.

120. Baker, EG & Mudge, LK. (1984) "Catalysis in biomass gasification." U.S. Department of Energy.

121. Surjosatyo, A. (2012) "Tar Content Evaluation of Produced Gas in Downdraft Biomass Gasifier." Iran. J. Energy Environ. Vol. 3, pp 210–212.

122. Wang, T, Chang, J, Lv, P & Zhu, J. (2005) "Novel catalyst for cracking of biomass tar." Energy and Fuels. Vol. 19, pp 22–27.

123. Mudge, LK, Baker, EG, Mitchell, DH & Brown, MD. (1985) "Catalytic steam gasification of biomass for methanol and methane production." J. Sol. Energy Eng. Trans. ASME. Vol. 107, no1, pp 88–92.

124. Zwart, RWR, Vreugdenhil, BJ. (2009) "Tar formation in pyrolysis and gasification. Energy research Centre of the Netherlands.

125. Sun, S, Zhao, Y, Tian, H, Ling, F & Su, F. (2009) "Experimental study on cyclone air gasification of wood powder." Bioresour. Technol. Vol. 100, no17, pp 4047–4049.

126. Fagbemi, L, Khezami, L & Capart, R. (2001) "Pyrolysis products from different biomasses: application to the thermal cracking of tar." Appl. Energy. Vol. 69, pp 293–306.

127. Scott, D. S. & Plskorz, J. (1984) "The Continuous Flash Pyrolysis of Biomass." Can J Chem Eng. Vol. 62, pp 404–412.

128. Mayerhofer, M. *et al.* (2012) "Influence of pressure, temperature and steam on tar and gas in allothermal fluidized bed gasification." Fuel. Vol. 99, pp 204–209.

129. Corella, J, Orío, A & Toledo, JM. (1999) "Biomass Gasification with Air in a Fluidized Bed: Exhaustive Tar Elimination with Commercial Steam Reforming Catalysts." Energy Fuels. Vol. 13, no3, pp 702–709.

130. Schmid, JC, Pfeifer, C, Kitzler, H, Pröll, T & Hofbauer, H. (2011) "A new dual fluidized bed gasifier design for improved in situ conversion of hydrocarbons" Proc. Int. Conf. Polygeneration Strateg.

131. Henriksen, U. *et al.* (2006) "The design, construction and operation of a 75kW two-stage gasifier." Energy. Vol. 31, pp 1542–1553.

132. Ahrenfeldt, J, Thomsen, TP, Henriksen, U & Clausen, LR. (2013) "Biomass gasification cogeneration - A review of state-of-the-art technology and near future perspectives." Appl. Therm. Eng. Vol. 50, pp 1407–1417.

133. Colantoni, A, Longo, L, Gallucci, F & Monarca, D. (2016) "Pyro-gasification of hazelnut pruning using a downdraft gasifier for concurrent production of syngas and biochar." Contemp. Eng. Sci. Vol. 9, pp 1339–1348.

134. Alipour MR, Yusup, S, Azlina, W, Nehzati, S, Tavasoli, A. (2014) “Investigation on Syngas Production via Biomass Conversion through the Integration of Pyrolysis and Air-Steam Gasification Processes.” Energy Convers. Manag. Vol. 87, 670–675.

135. Chen, G, Andries, J, Spliethoff, H, Fang, M, van de Enden, PJ. “Biomass Gasification Integrated with Pyrolysis in a Circulating Fluidised Bed.” Sol. Energy. Vol. 76 (1–3), 345–349.

136. Department of Environmental Affairs South Africa. (2016) "Government Gazette - Alien and Invasive species lists, 2016" Vol. 375. [Available online]. https://cer.org.za/wp-content/uploads/2010/05/Alien-and-Invasie-Species-List.pdf.

137. Ayeni, AO, Adeeyo, OA, Oresegun, OM & Oladimeji, E. (2015) "Compositional analysis of lignocellulosic materials : Evaluation of an economically viable method suitable for woody and non-woody biomass" Am. J. Eng. Res. Vol. 4, no 4, pp 14–19 (2015).

138. Sluiter, a. *et al.* (2012) "NREL/TP-510-42618 analytical procedure - Determination of structural carbohydrates and lignin in Biomass. Laboratory Analytical Procedure (LAP)" [Available online] http://www.nrel.gov/docs/gen/fy13/42618.pdf.

139. Maekawa, E, Ichizawa, T & Koshijima, T. (1989) "An Evaluation of the Acid-Soluble Lignin Determination in Analyses of Lignin by the Sulfuric Acid Method." J. Wood Chem. Technol. Vol. 9, pp 549–567.

140. Sahito, AR & Siddiqui, Z. (2013) "Estimating calorific values of lignocellulosic biomass from estimating calorific values of lignocellulosic biomass from volatile." Int. J. Biomass Renewables. Vol. 2, pp 1–6.

141. Acar, S & Ayanoglu, A. (2012) "Calculation of higher heating values of biomass fuels." Energy Educ. Sci. Technol. Vol. 28, pp 749–758.

142. Channiwala, SA & Parikh, PP. (2002) "A unified correlation for estimating HHV of solid , liquid and gaseous fuels." Fuel. Vol. 81, pp 1051–1063.

143. ASTM International. (2013) "ASTM E872-82, Standard Test Method for Volatile Matter in the Analysis of Particulate Wood Fuels." [Available online]. https://www.astm.org/Standards/E872.htm.

144. ASTM International. (2015) "ASTM E1755-01, Standard Test Method for Ash in Biomass." [Available online]. https://www.astm.org/DATABASE.CART/HISTORICAL/E1755-01.htm.

145. ASTM International. (2015) "ASTM E1756-08, Standard Test Method for Determination of Total Solids in Biomass." [Available online]. https://www.astm.org/Standards/E1756.htm.

146. Azubuike, CP & Okhamafe, AO. (2012) "Physicochemical , spectroscopic and thermal properties of microcrystalline cellulose derived from corn cobs." Int. j. recycl. org. waste agric. Vol. 1. pp 1–7.

147. Eloy, E, Da Silva, DA, Caron, BO & De Souza, VQ. (2015) "Capacidade energética da madeira e da casca de acácia-negra em diferentes espaçamentos." Pesqui. Florest. Bras. Vol. 35, pp 163.

148. Friedman, HL. (2007) "Kinetics of thermal degradation of char-forming plastics from thermogravimetry. Application to a phenolic plastic." J. Polym. Sci. Part C Polym. Symp. Vol. 6, no 1, pp 183–195.

149. Bilgic, E, Yaman, S & Kucukbayrak, S. (2016) "Limits of variations on the structure and the fuel characteristics of sunflower seed shell through torrefaction." Fuel Process. Technol. Vol. 144, pp 197–202.

150. White, RH. (1987) "Effect of lignin content and extractives on the higher heating value of wood." Wood Fiber Sci. Vol. 19, pp 446–452.

151. Novaes, E, Kirst, M, Chiang, V, Winter-sederoff, H & Sederoff, R. (2010) "Lignin and Biomass: A Negative Correlation for Wood Formation and Lignin Content in Trees 1." Plant Physiol. Vol. 154, pp 555–561.

152. Carder, AC. (1995) Forest giants of the world, past and present. Fitzhenry & Whiteside.

153. Hernandez, RE. (2007) "Moisture sorption properties of hardwoods as affected by their extraneous substances, wood density, and interlocked grain." Wood Fiber Sci. Vol. 39, pp 146–158.

154. Spalt, H. (1957) "The sorption of water by domestic and tropical woods." For. prod J. Vol. 7, pp 331–335.

155. Mitchual, SJ, Frimpong-mensah, K & Darkwa, NA. (2014) "Evaluation of Fuel Properties of Six Tropical Hardwood Timber Species for Briquettes." J. Sustain. Bioenergy Syst. Vol. 4, pp 1–9.

156. Hielg, W & Janssen, R. (2009) "Advancement of pellets-related European standards." WIP Renewable Energies. [Available online]. https://pelletsatlas.info/wp-content/uploads/2015/09/D75_Standards_WIP_HFA_Final091116.pdf. pp 26.

157. Malan, HL & Day, JA. "Linking flow , water quality and potential effects on aquatic biota within the Reserve determination process." Water SA. Vol. 29, no 3, pp 297–304 (2003).

158. Bryers, RW. (1996) "Fireside slagging, fouling, and high-temperature corrosion of heat-transfer surface due to impurities in steam-raising fuels." Prog. Energy Combust. Sci. Vol. 22, pp 29–120.

159. Theis, M, Skrifvars, BJ, Hupa, M & Tran, H. (2006) "Fouling tendency of ash resulting from burning mixtures of biofuels. Part 1: Deposition rates." Fuel. Vol. 85, pp 1125–1130.

160. Demirbas, A. (2004) "Combustion characteristics of different biomass fuels." Prog. Energy Combust. Sci. Vol. 30, pp 219–230.

161. Vamvuka, D & Zografos, D. (2004) "Predicting the behaviour of ash from agricultural wastes during combustion." Fuel. Vol. 83, pp 2051–2057.

162. Melane, M, Ham, C & Meincken, M. (2017) "Characteristics of selected non- woody invasive alien plants in South Africa and an evaluation of their potential for electricity generation." J. Energy South. Africa. Vol. 28, pp 92.

163. Zevenhoven-Onderwater, M, Blomquist, J, Skrifvars, B, Backman, R & Hupa, M. (2000) "The prediction of behaviour of ashes from five different solid fuels." Fuel. Vol. 79, pp 1353–1361.

164. Miles, TR, Baxter, LL, Bryers, RW, Jenkings, BM & Oden, LL. (1995) "Alkali deposits found in Biomass Power Plants: A preliminary investigation of their extent and nature." National Renewable Energy Laboratory (NREL). Vol. 2 (1995).

165. Van Der Stelt, MJC, Gerhauser, H, Kiel, JHA & Ptasinski, KJ. (2011) "Biomass upgrading by torrefaction for the production of biofuels: A review." Biomass and Bioenergy. Vol. 35, pp 3748–3762.

166. Greaver, TL *et al.* (2012) "Ecological effects of nitrogen and sulfur air pollution in the US : what do we know?" Front. Ecol. Environ. Vol. 10, pp 365–372.

167. Hunter, K A *et al.* (2011) "Impacts of anthropogenic SOx, NOx and NH3 on acidification of coastal waters and shipping lanes." Geophys. Res. Lett. Vol. 38, pp 2–7.

168. Mabhaudhi, C. (2014) "Impact of SOx and NOx Deposition on the Leaching behaviour of soils and water quality in the South African Highveld." MSc Dissertation, University of KwaZulu-Natal, Pietermaritzburg.

169. Moldan, B & Cerny, J. (1994) "Small Catchment Research." eds. Moldan, B. & Cerny, J. Biogeochemistry of Small Catchments. pp 1–30. John Wiley & Sons Ltd.

170. Broer, KM & Brown, RC. (2015) "The role of char and tar in determining the gas-phase partitioning of nitrogen during biomass gasification." Appl. Energy. Vol. 158, pp 474–483.

171. Lu, J & Chen, W. (2015) "Investigation on the ignition and burnout temperatures of bamboo and sugarcane bagasse by thermogravimetric analysis." Appl. Energy. Vol. 160, pp 49–57.

172. Awosusi, AA, Ayeni, AO, Adeleke, R & Daramola, MO. (2017) "Biocompositional and thermodecompositional analysis of South African agro-waste corncob and husk towards production of biocommodities." Asia-Pacific J. Chem. Eng. Vol. 12, pp 960–968.

173. Skoulou, V, Zabaniotou, A, Stavropoulos, G & Sakelaropoulos, G. (2008) "Syngas production from olive tree cuttings and olive kernels in a downdraft fixed-bed gasifier." Int. J. Hydrogen Energy. Vol. 33, pp 1185–1194.

174. Cuiping, L, Chuangzhi, W, Yanyongjie & Haitao, H. (2004) "Chemical elemental characteristics of biomass fuels in China." Biomass and Bioenergy. Vol. 27, pp 119–130.

175. Vassilev, SV, Vassileva, CG & Vassilev, VS. (2015) "Advantages and disadvantages of composition and properties of biomass in comparison with coal: An overview." Fuel. Vol. 158, pp 330–350.

176. Barneto, AG, Hernández, RB & Berenguer, JM. (2011) "Thermogravimetric characterization of eucalyptus wood." O Pap. Vol. 72, pp 53–56.

177. Oyedun, AO, Lam, KL & Hui, CW. (2012) "Charcoal production via multistage pyrolysis." Chinese J. Chem. Eng. Vol. 20, pp 455–460.

178. Demirbaş, A. (2002) “Gaseous Products from Biomass by Pyrolysis and Gasification: Effects of Catalyst on Hydrogen Yield.” Energy Convers. Manag. Vol. 43 (7), 897–909.

179. Ahmed, I, Gupta, AK. (2009) “Syngas Yield during Pyrolysis and Steam Gasification of Paper.” Appl. Energy. Vol. 86 (9), 1813–1821.

180. Baxter, L. (2005) "Biomass-coal co-combustion: Opportunity for affordable renewable energy." Fuel. Vol. 84, pp 1295–1302.

181. Vélez, JF, Chejne, F, Valdés, CF, Emery, EJ & Londoño, CA. (2009) "Co-gasification of Colombian coal and biomass in fluidized bed: An experimental study." Fuel. Vol. 88, pp 424–430.

182. Jayanti, S, Maheswaran, K & Saravanan, V. (2007) "Assessment of the effect of high ash content in pulverized coal combustion." Appl. Math. Model. Vol. 31, pp 934–953.

Appendix A: Determination of Activation energies

A1. Bugweed

Where R = 8.314 J/mol^{-1}.K^{-1}

Hemicellulose:

y = -1606.6x + 6.8658 ≡ $-\frac{E_a}{R} * \text{x} + \ln[A \,.\, f(\alpha)]$ ≡ M*x + C

M = $-\frac{E_a}{R}$ = -1606.6

E_a = 8.314 * 1606.6

E_a (hemicellulose) = 13.36 kJ/mol

Cellulose:

y = -438.69x + 3.1904 ≡ $-\frac{E_a}{R} * \text{x} + \ln[A \,.\, f(\alpha)]$ ≡ M*x + C

M = $-\frac{E_a}{R}$ = -438.69

E_a = 8.314 * 438.69

E_a (Cellulose) = 3.65 kJ/mol

Lignin:

y = -442.36x + 3.1933 ≡ $-\frac{E_a}{R} * \text{x} + \ln[A \,.\, f(\alpha)]$ ≡ M*x + C

M = $-\frac{E_a}{R}$ = -442.36

E_a = 8.314 * 442.36

E_a (Lignin) = 3.68 kJ/mol

A2. Eucalyptus

Where R = 8.314 $J/mol^{-1}.K^{-1}$

Hemicellulose:

y = -1258.5x + 5.2365 ≡ $-\frac{E_a}{R} * \mathrm{x} + \ln[A \,.\, f(\alpha)]$ ≡ M*x + C

M = $-\frac{E_a}{R}$ = -1258.5

E_a = 8.314 * 1258.5

E_a (hemicellulose) = 10.50 kJ/mol

Cellulose:

y = -281.27x + 2.545 ≡ $-\frac{E_a}{R} * \mathrm{x} + \ln[A \,.\, f(\alpha)]$ ≡ M*x + C

M = $-\frac{E_a}{R}$ = -281.27

E_a = 8.314 * 281.27

E_a (Cellulose) = 2.34 kJ/mol

Lignin:

y = -401.65x + 2.8106 ≡ $-\frac{E_a}{R} * \mathrm{x} + \ln[A \,.\, f(\alpha)]$ ≡ M*x + C

M = $-\frac{E_a}{R}$ = -401.65

E_a = 8.314 * 401.65

E_a (Lignin) = 3

A3. Jacaranda

Where R = 8.314 $J/mol^{-1}.K^{-1}$

Hemicellulose:

y = -1367.6x + 5.7833 ≡ $-\frac{E_a}{R} * \mathrm{x} + \ln[A \,.\, f(\alpha)]$ ≡ M*x + C

M = $-\frac{E_a}{R}$ = -1367.6

E_a = 8.314 * 1367.6

E_a (hemicellulose) = 11.40 kJ/mol

Cellulose:

y = -249.6x + 2.5794 ≡ $-\frac{E_a}{R} * \mathrm{x} + \ln[A \,.\, f(\alpha)]$ ≡ M*x + C

M = $-\frac{E_a}{R}$ = -249.6

E_a = 8.314 * 249.6

E_a (Cellulose) = 2.08 kJ/mol

Lignin:

y = -258.86x + 2.6059 ≡ $-\frac{E_a}{R} * \mathrm{x} + \ln[A \,.\, f(\alpha)]$ ≡ M*x + C

M = $-\frac{E_a}{R}$ = -258.86

E_a = 8.314 * 258.86

E_a (Lignin) = 2.15 kJ/mol

A4. Poplar

Where R = 8.314 $J/mol^{-1}. K^{-1}$

Hemicellulose:

y = -1342.7x + 5.8067 ≡ $-\frac{E_a}{R} * \mathrm{x} + \ln[A \,.\, f(\alpha)]$ ≡ M*x + C

M = $-\frac{E_a}{R}$ = -1342.7

E_a = 8.314 * 1342.7

E_a (hemicellulose) = 11.20 kJ/mol

Cellulose:

y = -312.27x + 2.823 ≡ $-\frac{E_a}{R} * \mathrm{x} + \ln[A \,.\, f(\alpha)]$ ≡ M*x + C

M = $-\frac{E_a}{R}$ = -312.27

E_a = 8.314 * 312.27

E_a (Cellulose) = 2.60 kJ/mol

Lignin:

y = -483.63x + 3.233 ≡ $-\frac{E_a}{R} * \mathrm{x} + \ln[A \,.\, f(\alpha)]$ ≡ M*x + C

M = $-\frac{E_a}{R}$ = -483.63

E_a = 8.314 * 483.63

E_a (Lignin) = 4.02 kJ/mol

A5. African mesquite

Where R = 8.314 $J/mol^{-1}. K^{-1}$

Hemicellulose:

y = -813.09x + 3.4703 ≡ $-\frac{E_a}{R} * \text{x} + \ln[A \,.\, f(\alpha)]$ ≡ M*x + C

M = $-\frac{E_a}{R}$ = -813.09

E_a = 8.314 * 813.09

E_a (hemicellulose) = 6.76 kJ/mol

Cellulose:

y = -1430.9x + 5.4992 ≡ $-\frac{E_a}{R} * \text{x} + \ln[A \,.\, f(\alpha)]$ ≡ M*x + C

M = $-\frac{E_a}{R}$ = -1430.9

E_a = 8.314 * 1430.9

E_a (Cellulose) = 11.90 kJ/mol

Lignin:

y = -312.85x + 2.4891 ≡ $-\frac{E_a}{R} * \text{x} + \ln[A \,.\, f(\alpha)]$ ≡ M*x + C

M = $-\frac{E_a}{R}$ = -312.85

E_a = 8.314 * 312.85

E_a (Lignin) = 2.60 kJ/mol

A6. African mahogany

Where R = 8.314 $J/mol^{-1}. K^{-1}$

Hemicellulose:

$y = -1424.5x + 5.7566 \equiv -\frac{E_a}{R} * x + \ln[A . f(\alpha)] \equiv M*x + C$

$M = -\frac{E_a}{R} = -1424.5$

$E_a = 8.314 * 1424.5$

E_a (hemicellulose) = 6.76 kJ/mol

Cellulose:

$y = -442.92x + 2.9925 \equiv -\frac{E_a}{R} * x + \ln[A . f(\alpha)] \equiv M*x + C$

$M = -\frac{E_a}{R} = -442.92$

$E_a = 8.314 * 442.92$

E_a (Cellulose) = 3.68 kJ/mol

Lignin:

$y = -397.8x + 2.9208 \equiv -\frac{E_a}{R} * x + \ln[A . f(\alpha)] \equiv M*x + C$

$M = -\frac{E_a}{R} = -397.8$

$E_a = 8.314 * 397.8$

E_a (Lignin) = 3.31 kJ/mol

A7. African oilbean

Where R = 8.314 J/mol^{-1}. K^{-1}

Hemicellulose:

y = -1461.1x + 6.018 ≡ $-\frac{E_a}{R} * \text{x} + \ln[A \,.\, f(\alpha)]$ ≡ M*x + C

M = $-\frac{E_a}{R}$ = -1461.1

E_a = 8.314 * 1461.1

E_a (hemicellulose) = 12.10 kJ/mol

Cellulose:

y = -544.61x + 3.3458 ≡ $-\frac{E_a}{R} * \text{x} + \ln[A \,.\, f(\alpha)]$ ≡ M*x + C

M = $-\frac{E_a}{R}$ = -544.61

E_a = 8.314 * 544.61

E_a (Cellulose) = 4.53 kJ/mol

Lignin:

y = -595.81x + 3.4547 ≡ $-\frac{E_a}{R} * \text{x} + \ln[A \,.\, f(\alpha)]$ ≡ M*x + C

M = $-\frac{E_a}{R}$ = -595.81

E_a = 8.314 * 595.81

E_a (Lignin) = 4.95 kJ/mol

A8. Opepe

Where R = 8. 314 J/mol^{-1}. K^{-1}

Hemicellulose:

y = -1509x + 5.9767 ≡ $-\frac{E_a}{R} * \mathrm{x} + \ln[A \,.\, f(\alpha)]$ ≡ M*x + C

M = $-\frac{E_a}{R}$ = -1509

E_a = 8.314 * 1509

E_a (hemicellulose) = 12.50 kJ/mol

Cellulose:

y = -299.61x + 2.6758 ≡ $-\frac{E_a}{R} * \mathrm{x} + \ln[A \,.\, f(\alpha)]$ ≡ M*x + C

M = $-\frac{E_a}{R}$ = -299.61

E_a = 8.314 * 299.61

E_a (Cellulose) = 2.49 kJ/mol

Lignin:

y = -435.71x + 2.9514 ≡ $-\frac{E_a}{R} * \mathrm{x} + \ln[A \,.\, f(\alpha)]$ ≡ M*x + C

M = $-\frac{E_a}{R}$ = -435.71

E_a = 8.314 * 435.71

E_a (Lignin) = 3.62 kJ/mol

Appendix B: Pyro-gasification experimental data of wood samples

B1: Pyro-gasification data for Jacaranda sample.

Wood Sample	**JACARANDA 100% (20 g)**			
Gas Sampling Temperature	**Gas component**	**900°C**	**950°C**	**1000°C**
Gas Concentration in Product gas (%)	**H_2**	3.99	5.1	62.15
	CO	95.69	91.82	33.75
	Syngas (H_2+CO)	99.68	96.92	95.9
	CH_4	Undetected	2.59	4.1
	CO_2	0.32	0.49	
Volumetric Dry Gas Flow rate *(mL/min)*		285	526	624
Dry gas production rate *(mL/min/gram of feedstock*)	**H_2**	56.8575	134.13	1939.08
	CO	1363.583	2414.866	1053
	Syngas	1420.44	2548.996	2992.08
Gas yield *(mL/gram of feedstock)*	**H_2**	9.975	12.75	155.375
	CO	239.225	229.55	84.375
	Syngas	249.2	242.3	239.75
Volume of Tar/Bio-oil extracted	3.4 mL			
mass of char residue after run	0 g			
Observations	**At 900°C**	**At 950°C**	**At 1000°C**	
	(a) Quick ignition; (b) poor flame propagation; (c) blue/purple flame	(a) Quick ignition; (b) poor flame propagation; (c) blue/purple flame	(a) Quick ignition; (b) poor flame propagation; (c) blue/purple flame	

B2: Pyro-gasification data for Poplar sample.

Wood Sample	**POPLAR 100% (20 g)**			
Gas Sampling Temperature	**Gas component**	**900°C**	**950°C**	**1000°C**
Gas Concentration in Product gas (%)	**H_2**	4.91	6.68	47.07
	CO	94.5	88.2	48.13
	Syngas (H_2+CO)	99.41	94.88	95.2
	CH_4	Undetected	5.12	0.59
	CO_2	0.59	Undetected	4.2
Volumetric Dry Gas Flow rate *(mL/min)*		530	667	1511
Dry gas production rate *(mL/min/gram of feedstock*)	**H_2**	130.115	222.778	3556.1385
	CO	2504.25	2941.47	3636.2215
	Syngas	2634.365	3164.248	7192.36
Gas yield *(mL/gram of feedstock)*	**H_2**	12.275	16.7	117.675
	CO	236.25	220.5	120.325
	Syngas	248.525	237.2	238
Volume of Tar/Bio-oil extracted	4.3 mL			
mass of char residue after run	0.7 g (carbon residue)			
Observations	**At 900°C**	**At 950°C**	**At 1000°C**	
	(a) Quick ignition; (b) low flame propagation; (c) pure blue flame	(a) Low flame propagation; (b) pure blue flame	(a) Low flame propagation; (b) pure blue flame	

B3: Pyro-gasification data for Bugweed sample.

Wood Sample	**BUGWEED 100% (20 g)**			
Gas Sampling Temperature	**Gas component**	**900°C**	**950°C**	**1000°C**
Gas Concentration in Product gas (%)	**H_2**	6.22	13.86	11.36
	CO	91.83	81.54	87.04
	Syngas (H_2+CO)	98.05	95.4	98.4
	CH_4	1.95	4.25	1.3
	CO_2	Undetected	0.34	0.3
Volumetric Dry Gas Flow rate *(mL/min)*		1714	1716	1697
Dry gas production rate *(mL/min/gram of feedstock*)	**H_2**	533.054	1189.188	963.896
	CO	7869.831	6996.132	7385.344
	Syngas	8402.885	8185.32	8349.24
Gas yield *(mL/gram of feedstock)*	**H_2**	15.55	34.65	28.4
	CO	229.575	203.85	217.6
	Syngas	245.125	238.5	246
Volume of Tar/Bio-oil extracted	4.9 mL			
mass of char residue after run	2.04 g (carbon residue)			
Observations	**At 900°C**	**At 950°C**	**At 1000°C**	
	(a) Quick ignition; (b) low flame propagation; (c) pure blue flame	(a) Low flame propagation; (b) pure blue flame	(a) Low flame propagation; (b) pure blue flame	

B4: Pyro-gasification data for Eucalyptus sample.

Wood Sample	**EUCALYPTUS 100% (20 g)**			
Gas Sampling Temperature	**Gas component**	**900°C**	**950°C**	**1000°C**
Gas Concentration in Product gas (%)	**H_2**	3.48	6.7	19.52
	CO	95.76	84.3	76.65
	Syngas (H_2+CO)	99.24	91	96.17
	CH_4	0.12	8.51	0.67
	CO_2	0.64	0.5	3.16
Volumetric Dry Gas Flow rate *(mL/min)*		915	878	1856
Dry gas production rate *(mL/min/gram of feedstock*)	**H_2**	159.21	294.13	1811.456
	CO	4381.02	3700.77	7113.12
	Syngas	4540.23	3994.9	8924.576
Gas yield *(mL/gram of feedstock)*	**H_2**	8.7	16.75	48.8
	CO	239.4	210.75	191.625
	Syngas	248.1	227.5	240.425
Volume of Tar/Bio-oil extracted	4.2 mL			
mass of char residue after run	3.14 g (carbon residue)			
Observations	**At 900°C**	**At 950°C**	**At 1000°C**	
	(a) Poor ignition, low flame propagation; (b) pure yellow flame	(a) Low flame propagation; (b) yellow flame	(a) High flame propagation; (b) yellow flame	

B5: Pyro-gasification data for Jacaranda - Poplar 50/50 blend ratio.

Blend Ratio	**JACARANDA 50% - POPLAR 50% (20 g)**			
Gas Sampling Temperature	**Gas component**	**900°C**	**950°C**	**1000°C**
Gas Concentration in Product gas (%)	**H_2**	52.11	74.06	63.54
	CO	29.73	25.11	34
	Syngas (H_2+CO)	81.84	99.17	97.54
	CH_4	18.16	0.83	2.46
	CO_2	Undetected	Undetected	Undetected
Volumetric Dry Gas Flow rate *(mL/min)*		1726	1736	2000
Dry gas production rate *(mL/min/gram of feedstock*)	**H_2**	4497.093	6428.408	6354
	CO	2565.699	2179.548	3400
	Syngas	7062.792	8607.956	9754
Gas yield *(mL/gram of feedstock)*	**H_2**	130.275	185.15	158.85
	CO	74.325	62.775	85
	Syngas	204.6	247.925	243.85
Volume of Tar/Bio-oil extracted	6.1 mL			
mass of char residue after run	0.15 g (carbon residue)			
Observations	**At 900°C**	**At 950°C**	**At 1000°C**	
	(a) Quick ignition; (b) high and consistent flame propagation; (c) blue/purple flame colour.	(a) High and consistent flame propagation; (b) blue/purple flame colour.	(a) High and consistent flame propagation; (b) blue/purple flame colour.	

B6: Pyro-gasification data for Jacaranda - Poplar 70/30 blend ratio.

Blend Ratio	**JACARANDA 70% - POPLAR 30% (20 g)**			
Gas Sampling Temperature	**Gas component**	**900°C**	**950°C**	**1000°C**
Gas Concentration in Product gas (%)	**H_2**	26.42	3.08	4.95
	CO	71.26	96.41	94.64
	Syngas (H_2+CO)	97.68	99.49	99.59
	CH_4	0.4	Undetected	Undetected
	CO_2	1.91	0.5	0.4
Volumetric Dry Gas Flow rate *(mL/min)*		2000	1650	660
Dry gas production rate *(mL/min/gram of feedstock*)	**H_2**	2642	254.1	163.35
	CO	7126	7953.825	3123.12
	Syngas	9768	8207.925	3286.47
Gas yield *(mL/gram of feedstock)*	**H_2**	66.05	7.7	12.375
	CO	178.15	241.025	236.6
	Syngas	244.2	248.725	248.975
Volume of Tar/Bio-oil extracted	4.8 mL			
mass of char residue after run	0.03 g (carbon residue)			
Observations	**At 900°C**	**At 950°C**	**At 1000°C**	
	(a) Quick ignition; (b) high and consistent flame propagation; (c) blue/purple flame colour; (d) clean gas;	(a) High and consistent flame propagation; (b) blue/purple flame colour.	(a) High and consistent flame propagation; (b) blue/purple flame colour.	

B7: Pyro-gasification data for Jacaranda - Poplar 30/70 blend ratio.

Blend Ratio	**JACARANDA 30% - POPLAR 70% (20 g)**			
Gas Sampling Temperature	**Gas component**	**900°C**	**950°C**	**1000°C**
Gas Concentration in Product gas (%)	**H_2**	6.99	6.49	9.63
	CO	93.01	90.49	0.61
	Syngas (H_2+CO)	100	96.98	10.24
	CH_4	Undetected	3.02	88.12
	CO_2	Undetected		1.64
Volumetric Dry Gas Flow rate *(mL/min)*		1873	1900	1997
Dry gas production rate *(mL/min/gram of feedstock*)	**H_2**	654.6135	616.55	961.5555
	CO	8710.3865	8596.55	60.9085
	Syngas	9365	9213.1	1022.464
Gas yield *(mL/gram of feedstock)*	**H_2**	17.475	16.225	24.075
	CO	232.525	226.225	1.525
	Syngas	250	242.45	25.6
Volume of Tar/Bio-oil extracted	5.2 mL			
mass of char residue after run	0.2 g (carbon residue)			
Observations	**At 900°C**	**At 950°C**	**At 1000°C**	
	(a) Quick ignition; (b) high and consistent flame propagation; (c) blue/purple flame colour; (d) clean gas.	(a) High and consistent flame propagation; (b) blue/purple flame colour.	(a) Reduced but consistent flame propagation; (b) blue/purple flame colour.	

B8: Pyro-gasification data for Eucalyptus - Bugweed 50/50 blend ratio.

Blend Ratio	**EUCALYPTUS 50% - BUGWEED 50% (20 g)**			
Gas Sampling Temperature	**Gas component**	**900°C**	**950°C**	**1000°C**
Gas Concentration in Product gas (%)	**H_2**	4.17	13.65	14.24
	CO	95.13	49.5	80.73
	Syngas (H_2+CO)	99.3	63.15	94.97
	CH_4	Undetected	11.23	5.03
	CO_2	0.7	25.61	
Volumetric Dry Gas Flow rate *(mL/min)*		1615	1913	662
Dry gas production rate *(mL/min/gram of feedstock*)	**H_2**	336.7275	1305.6225	471.344
	CO	7681.7475	4734.675	2672.163
	Syngas	8018.475	6040.2975	3143.507
Gas yield *(mL/gram of feedstock)*	**H_2**	10.425	34.125	35.6
	CO	237.825	123.75	201.825
	Syngas	248.25	157.875	237.425
Volume of Tar/Bio-oil extracted	3 mL			
mass of char residue after run	0.25 g (carbon residue)			
Observations	**At 900°C**	**At 950°C**	**At 1000°C**	
	(a) Quick ignition; (b) high and consistent flame propagation; (c) blue/yellow flame colour.	(a) Quick ignition; (b) high and consistent flame propagation; (c) blue/yellow flame colour.	(a) Good flame propagation but flame reduced due to carbon depletion in reactor; (b) yellow flame.	

B9: Pyro-gasification data for Eucalyptus - Bugweed 70/30 blend ratio.

Blend Ratio	**EUCALYPTUS 70% - BUGWEED 30% (20 g)**			
Gas Sampling Temperature	**Gas component**	**900°C**	**950°C**	**1000°C**
Gas Concentration in Product gas (%)	**H_2**	65.67	52.09	6.99
	CO	33.6	43.62	91.73
	Syngas (H_2+CO)	99.27	95.71	98.72
	CH_4	0.73	0.63	1.28
	CO_2	Undetected	3.66	Undetected
Volumetric Dry Gas Flow rate *(mL/min)*		851	972	793
Dry gas production rate *(mL/min/gram of feedstock*)	**H_2**	2794.2585	2531.574	277.1535
	CO	1429.68	2119.932	3637.0945
	Syngas	4223.9385	4651.506	3914.248
Gas yield *(mL/gram of feedstock)*	**H_2**	164.175	130.225	17.475
	CO	84	109.05	229.325
	Syngas	248.175	239.275	246.8
Volume of Tar/Bio-oil extracted	4.6 mL			
mass of char residue after run	0.21 g (carbon residue)			
Observations	**At 900°C**	**At 950°C**	**At 1000°C**	
	(a) Quick ignition; (b) high and consistent flame propagation but intensity decreased with time; (c) blue/yellow flame colour.	(a) Flame intensity increases again at 950°C to a high burning yellow flame	(a) High and consistent flame intensity; (b) Blue/yellow flame colour	

B10: Pyro-gasification data for Eucalyptus - Bugweed 30/70 blend ratio.

Blend Ratio	**EUCALYPTUS 30% - BUGWEED 70% (20 g)**			
Gas Sampling Temperature	**Gas component**	**900°C**	**950°C**	**1000°C**
Gas Concentration in Product gas (%)	**H_2**	14.45	3.04	80.01
	CO	83.32	96.96	19.99
	Syngas (H_2+CO)	97.77	100	100
	CH_4	0.51	Undetected	Undetected
	CO_2	1.73	Undetected	Undetected
Volumetric Dry Gas Flow rate *(mL/min)*		1084	694	17
Dry gas production rate *(mL/min/gram of feedstock*)	**H_2**	783.19	105.488	68.0085
	CO	4515.944	3364.512	16.9915
	Syngas	5299.134	3470	85
Gas yield *(mL/gram of feedstock)*	**H_2**	36.125	7.6	200.025
	CO	208.3	242.4	49.975
	Syngas	244.425	250	250
Volume of Tar/Bio-oil extracted	4.1 mL			
mass of char residue after run	0.15 g (carbon residue)			
Observations	**At 900°C**	**At 950°C**	**At 1000°C**	
	(a) Quick ignition; (b) high and consistent flame propagation; (c) blue/yellow flame colour.	(a) High and consistent flame intensity; (b) Blue/yellow flame colour	(a) Reduced flame intensity due to carbon depletion in reactor; (b) Blue/yellow flame colour.	

B11: Pyro-gasification data for Eucalyptus - Poplar 50/50 blend ratio.

Blend Ratio	**EUCALYPTUS 50% - POPLAR 50% (20 g)**			
Gas Sampling Temperature	**Gas component**	**900°C**	**950°C**	**1000°C**
Gas Concentration in Product gas (%)	**H_2**	6.13	6.03	90.97
	CO	92	92.71	8.58
	Syngas (H_2+CO)	98.13	98.74	99.55
	CH_4	1.87	1.26	0.45
	CO_2	Undetected	Undetected	Undetected
Volumetric Dry Gas Flow rate *(mL/min)*		1124	367	261
Dry gas production rate *(mL/min/gram of feedstock*)	**H_2**	344.506	110.6505	1187.1585
	CO	5170.4	1701.2285	111.969
	Syngas	5514.906	1811.879	1299.1275
Gas yield *(mL/gram of feedstock)*	**H_2**	15.325	15.075	227.425
	CO	230	231.775	21.45
	Syngas	245.325	246.85	248.875
Volume of Tar/Bio-oil extracted	3.8 mL			
mass of char residue after run	0.66 g (a mixture of ash and carbon particles)			
Observations	**At 900°C**	**At 950°C**	**At 1000°C**	
	(a) Quick ignition; (b) high and consistent flame propagation; (c) blue/yellow flame colour.	(a) Flame self-extinguishes at 950°C	(a) Gas re-ignited manually but produces blue flame with very low flame propagation.	

B12: Pyro-gasification data for Eucalyptus - Poplar 70/30 blend ratio.

Blend Ratio	**EUCALYPTUS 70% - POPLAR 30% (20 g)**			
Gas Sampling Temperature	**Gas component**	**900°C**	**950°C**	**1000°C**
Gas Concentration in Product gas (%)	**H_2**	53.6	60.93	93.17
	CO	41.82	17.44	4.63
	Syngas (H_2+CO)	95.42	78.37	97.8
	CH_4	3.12	21.63	0.64
	CO_2	1.46	Undetected	1.56
Volumetric Dry Gas Flow rate *(mL/min)*		1969	747	851
Dry gas production rate *(mL/min/gram of feedstock*)	**H_2**	5276.92	2275.7355	3964.3835
	CO	4117.179	651.384	197.0065
	Syngas	9394.099	2927.1195	4161.39
Gas yield *(mL/gram of feedstock)*	**H_2**	134	152.325	232.925
	CO	104.55	43.6	11.575
	Syngas	238.55	195.925	244.5
Volume of Tar/Bio-oil extracted	4 mL			
mass of char residue after run	1.52 g (a mixture of ash and carbon residue, but with greater carbon fraction)			
Observations	**At 900°C**	**At 950°C**	**At 1000°C**	
	(a) Quick ignition; (b) high and consistent flame propagation; (c) blue/yellow flame colour.	(a) Reduced flame intensity	(a) Flame intensity increases considerably.	

B13: Pyro-gasification data for Eucalyptus - Poplar 30/70 blend ratio.

Blend Ratio	**EUCALYPTUS 30% - POPLAR 70% (20 g)**			
Gas Sampling Temperature	**Gas component**	**900°C**	**950°C**	**1000°C**
Gas Concentration in Product gas (%)	**H_2**	3.62	3.04	2.53
	CO	96.38	96.45	97.02
	Syngas (H_2+CO)	100	99.49	99.55
	CH_4	Undetected	Undetected	Undetected
	CO_2	Undetected	0.51	0.45
Volumetric Dry Gas Flow rate *(mL/min)*		370	450	498
Dry gas production rate *(mL/min/gram of feedstock*)	**H_2**	66.97	68.4	62.997
	CO	1783.03	2170.125	2415.798
	Syngas	1850	2238.525	2478.795
Gas yield *(mL/gram of feedstock)*	**H_2**	9.05	7.6	6.325
	CO	240.95	241.125	242.55
	Syngas	250	248.725	248.875
Volume of Tar/Bio-oil extracted	4.8 mL			
mass of char residue after run	0.2 g (ash residue)			
Observations	**At 900°C**	**At 950°C**	**At 1000°C**	
	(a) Quick ignition; (b) high and consistent flame propagation; (c) blue/yellow flame colour.	(a) Reduced flame intensity	(a) Flame intensity increases considerably.	

B14: Pyro-gasification data for Eucalyptus - Jacaranda 50/50 blend ratio.

Blend Ratio	**EUCALYPTUS 50% - JACARANDA 50% (20 g)**			
Gas Sampling Temperature	**Gas component**	**900°C**	**950°C**	**1000°C**
Gas Concentration in Product gas (%)	**H_2**	12.15	12.4	2.53
	CO	86.09	82.15	97.02
	Syngas (H_2+CO)	98.24	94.55	99.55
	CH_4	1.3	4.58	Undetected
	CO_2	0.45	0.87	0.45
Volumetric Dry Gas Flow rate *(mL/min)*		940	1117	498
Dry gas production rate *(mL/min/gram of feedstock*)	**H_2**	571.05	692.54	62.997
	CO	4046.23	4588.0775	2415.798
	Syngas	4617.28	5280.6175	2478.795
Gas yield *(mL/gram of feedstock)*	**H_2**	30.375	31	6.325
	CO	215.225	205.375	242.55
	Syngas	245.6	236.375	248.875
Volume of Tar/Bio-oil extracted	5.3 mL			
mass of char residue after run	1.21 g (carbon residue)			
Observations	**At 900°C**	**At 950°C**	**At 1000°C**	
	(a) Quick ignition; (b) high and consistent flame propagation; (c) blue/yellow flame colour.	(a) high and consistent flame propagation; (b) blue/yellow flame colour.	(a) reduced but consistent flame propagation; (b) blue/yellow flame colour.	

B15: Pyro-gasification data for Eucalyptus - Jacaranda 70/30 blend ratio.

Blend Ratio	**EUCALYPTUS 70% - JACARANDA 30% (20 g)**			
Gas Sampling Temperature	**Gas component**	**900°C**	**950°C**	**1000°C**
Gas Concentration in Product gas (%)	**H_2**	81.21	68.34	12.34
	CO	15.32	27.42	84.49
	Syngas (H_2+CO)	96.53	95.76	96.83
	CH_4	3.47	2.86	2.6
	CO_2	Undetected	1.38	0.57
Volumetric Dry Gas Flow rate *(mL/min)*		572	948	1964
Dry gas production rate *(mL/min/gram of feedstock*)	**H_2**	2322.606	3239.316	1211.788
	CO	438.152	1299.708	8296.918
	Syngas	2760.758	4539.024	9508.706
Gas yield *(mL/gram of feedstock)*	**H_2**	203.025	170.85	30.85
	CO	38.3	68.55	211.225
	Syngas	241.325	239.4	242.075
Volume of Tar/Bio-oil extracted	5.0 mL			
mass of char residue after run	0.8 g (carbon residue)			
Observations	**At 900°C**	**At 950°C**	**At 1000°C**	
	(a) Quick ignition; (b) high and consistent flame propagation; (c) blue/yellow flame colour.	(a) High and consistent flame propagation; (b) blue/yellow flame colour.	(a) Increased and consistent flame propagation; (b) blue/yellow flame colour.	

B16: Pyro-gasification data for Eucalyptus - Jacaranda 30/70 blend ratio.

Blend Ratio	**EUCALYPTUS 30% - JACARANDA 70% (20 g)**			
Gas Sampling Temperature	**Gas component**	**900°C**	**950°C**	**1000°C**
Gas Concentration in Product gas (%)	**H_2**	16.39	4.27	79.89
	CO	80.63	94.42	4.79
	Syngas (H_2+CO)	97.02	98.69	84.68
	CH_4	2.82	1.31	15.32
	CO_2	0.16	Undetected	Undetected
Volumetric Dry Gas Flow rate *(mL/min)*		698	1812	1987
Dry gas production rate *(mL/min/gram of feedstock*)	**H_2**	572.011	386.862	7937.0715
	CO	2813.987	8554.452	475.8865
	Syngas	3385.998	8941.314	8412.958
Gas yield *(mL/gram of feedstock)*	**H_2**	40.975	10.675	199.725
	CO	201.575	236.05	11.975
	Syngas	242.55	246.725	211.7
Volume of Tar/Bio-oil extracted	4.5 mL			
mass of char residue after run	1.03 g (carbon residue)			
Observations	**At 900°C**	**At 950°C**	**At 1000°C**	
	(a) Quick ignition; (b) low flame propagation; (c) blue flame colour.	(a) Increased and consistent flame propagation; (b) blue flame colour.	(a) Very high and consistent flame propagation; (b) blue flame colour but colour changes to blue/yellow with time.	

B17: Pyro-gasification data for Bugweed - Poplar 50/50 blend ratio.

Blend Ratio	**BUGWEED 50% - POPLAR 50% (20 g)**			
Gas Sampling Temperature	**Gas component**	**900°C**	**950°C**	**1000°C**
Gas Concentration in Product gas (%)	**H_2**	3.11	5.41	4.13
	CO	92.74	90.45	95.29
	Syngas (H_2+CO)	95.85	95.86	99.42
	CH_4	4.15	4.14	
	CO_2	Undetected	Undetected	0.58
Volumetric Dry Gas Flow rate *(mL/min)*		680	1087	871
Dry gas production rate *(mL/min/gram of feedstock*)	**H_2**	105.74	294.0335	179.8615
	CO	3153.16	4915.9575	4149.8795
	Syngas	3258.9	5209.991	4329.741
Gas yield *(mL/gram of feedstock)*	**H_2**	7.775	13.525	10.325
	CO	231.85	226.125	238.225
	Syngas	239.625	239.65	248.55
Volume of Tar/Bio-oil extracted	3.1 mL			
mass of char residue after run	0 g			
Observations	**At 900°C**	**At 950°C**	**At 1000°C**	
	(a) Quick ignition; (b) very high and consistent flame propagation; (c) blue flame colour.	(a) very high and consistent flame propagation; (b) blue flame colour.	(a) reduced flame intensity	

B18: Pyro-gasification data for Bugweed - Poplar 70/30 blend ratio.

Blend Ratio	**BUGWEED 70% - POPLAR 30% (20 g)**			
Gas Sampling Temperature	**Gas component**	**900°C**	**950°C**	**1000°C**
Gas Concentration in Product gas (%)	**H_2**	4.12	8.26	4.43
	CO	95.83	88.45	95.57
	Syngas (H_2+CO)	99.95	96.71	100
	CH_4	0.05	Undetected	Undetected
	CO_2	Undetected	3.28	Undetected
Volumetric Dry Gas Flow rate *(mL/min)*		1886	1833	122
Dry gas production rate *(mL/min/gram of feedstock*)	**H_2**	388.516	757.029	27.023
	CO	9036.769	8106.4425	582.977
	Syngas	9425.285	8863.4715	610
Gas yield *(mL/gram of feedstock)*	**H_2**	10.3	20.65	11.075
	CO	239.575	221.125	238.925
	Syngas	249.875	241.775	250
Volume of Tar/Bio-oil extracted	2.5 mL			
mass of char residue after run	0.2 g (carbon residue)			
Observations	**At 900°C**	**At 950°C**	**At 1000°C**	
	(a) Quick ignition; (b) very high and consistent flame propagation; (c) blue flame colour.	(a) very high and consistent flame propagation; (b) flame changes to blue/yellow colour.	(a) very low flame propagation; (b) blue/yellow flame colour	

B19: Pyro-gasification data for Bugweed - Poplar 30/70 blend ratio.

Blend Ratio	**BUGWEED 30% - POPLAR 70% (20 g)**			
Gas Sampling Temperature	**Gas component**	**900°C**	**950°C**	**1000°C**
Gas Concentration in Product gas (%)	**H_2**	4.77	6.74	7.03
	CO	94.82	91.46	91.57
	Syngas (H_2+CO)	99.59	98.2	98.6
	CH_4	Undetected	1.24	1.15
	CO_2	0.41	0.56	0.24
Volumetric Dry Gas Flow rate *(mL/min)*		1196	1250	9
Dry gas production rate *(mL/min/gram of feedstock*)	**H_2**	285.246	421.25	3.1635
	CO	5670.236	5716.25	41.2065
	Syngas	5955.482	6137.5	44.37
Gas yield *(mL/gram of feedstock)*	**H_2**	11.925	16.85	17.575
	CO	237.05	228.65	228.925
	Syngas	248.975	245.5	246.5
Volume of Tar/Bio-oil extracted	2.0 mL			
mass of char residue after run	0.4 g (carbon residue)			
Observations	**At 900°C**	**At 950°C**	**At 1000°C**	
	(a) Quick ignition; (b) very high and consistent flame propagation; (c) blue flame colour.	(a) very high and consistent flame propagation; (b) Blue flame colour	(a) very low flame propagation; (b) yellow flame colour	

B20: Pyro-gasification data for Bugweed - Jacaranda 50/50 blend ratio.

Blend Ratio	**BUGWEED 50% - JACARANDA 50% (20 g)**			
Gas Sampling Temperature	**Gas component**	**900°C**	**950°C**	**1000°C**
Gas Concentration in Product gas (%)	**H_2**	4.5	7.43	4.08
	CO	94.97	83.34	88.7
	Syngas (H_2+CO)	99.47	90.77	92.78
	CH_4	Undetected	8.58	7.22
	CO_2	0.53	0.65	Undetected
Volumetric Dry Gas Flow rate *(mL/min)*		1687	1717	13
Dry gas production rate *(mL/min/gram of feedstock*)	**H_2**	379.575	637.8655	2.652
	CO	8010.7195	7154.739	57.655
	Syngas	8390.2945	7792.6045	60.307
Gas yield *(mL/gram of feedstock)*	**H_2**	11.25	18.575	10.2
	CO	237.425	208.35	221.75
	Syngas	248.675	226.925	231.95
Volume of Tar/Bio-oil extracted	8.5 mL			
mass of char residue after run	2.9 g (ash residue)			
Observations	**At 900°C**	**At 950°C**	**At 1000°C**	
	(a) Quick ignition; (b) very high and consistent flame propagation; (c) blue flame colour.	(a) very high and consistent flame propagation; (b) Blue flame colour	(a) very low flame propagation; (b) yellow flame colour	

B21: Pyro-gasification data for Bugweed - Jacaranda 70/30 blend ratio.

Blend Ratio	**BUGWEED 70% - JACARANDA 30% (20 g)**			
Gas Sampling Temperature	**Gas component**	**900°C**	**950°C**	**1000°C**
Gas Concentration in Product gas (%)	**H_2**	3.7	7.09	6.9
	CO	96.1	90.02	91.75
	Syngas (H_2+CO)	99.8	97.11	98.65
	CH_4	0.21	2.89	0.76
	CO_2	Undetected	Undetected	0.59
Volumetric Dry Gas Flow rate *(mL/min)*		1219	32	12
Dry gas production rate *(mL/min/gram of feedstock*)	**H_2**	225.515	11.344	4.14
	CO	5857.295	144.032	55.05
	Syngas	6082.81	155.376	59.19
Gas yield *(mL/gram of feedstock)*	**H_2**	9.25	17.725	17.25
	CO	240.25	225.05	229.375
	Syngas	249.5	242.775	246.625
Volume of Tar/Bio-oil extracted	7.1 mL			
mass of char residue after run	2.2 g (ash residue)			
Observations	**At 900°C**	**At 950°C**	**At 1000°C**	
	(a) Quick ignition; (b) very high and consistent flame propagation; (c) blue flame colour.	(a) very low flame propagation (b) Blue flame colour	(a) Extremely low flame propagation (b) blue flame colour	

B22: Pyro-gasification data for Bugweed - Jacaranda 30/70 blend ratio.

Blend Ratio	**BUGWEED 30% - JACARANDA 70% (20 g)**			
Gas Sampling Temperature	**Gas component**	**900°C**	**950°C**	**1000°C**
Gas Concentration in Product gas (%)	**H_2**	5.06	7.85	8.62
	CO	94.58	87.44	90.58
	Syngas (H_2+CO)	99.64	95.29	99.2
	CH_4	0.35	4.71	0.2
	CO_2	Undetected	Undetected	0.6
Volumetric Dry Gas Flow rate *(mL/min)*		1096	707	193
Dry gas production rate *(mL/min/gram of feedstock*)	**H_2**	277.288	277.4975	83.183
	CO	5182.984	3091.004	874.097
	Syngas	5460.272	3368.5015	957.28
Gas yield *(mL/gram of feedstock)*	**H_2**	12.65	19.625	21.55
	CO	236.45	218.6	226.45
	Syngas	249.1	238.225	248
Volume of Tar/Bio-oil extracted	6.9 mL			
mass of char residue after run	3.1 g (ash residue)			
Observations	**At 900°C**	**At 950°C**	**At 1000°C**	
	(a) Quick ignition; (b) very high and consistent flame propagation; (c) blue flame colour.	(a) reduced flame flame propagation (b) Blue flame colour	(a) Low flame intensity (b) blue flame colour	

B23: Pyro-gasification data for African mahogany sample.

Wood Sample	**AFRICAN MAHOGANY 100% (20 g)**			
Gas Sampling Temperature	**Gas component**	**900°C**	**950°C**	**1000°C**
Gas Concentration in Product gas (%)	**H_2**	2.88	22.62	8.82
	CO	96.38	69.98	90.21
	Syngas (H_2+CO)	99.26	92.6	99.03
	CH_4	Undetected	6.16	0.1
	CO_2	0.74	1.24	0.86
Volumetric Dry Gas Flow rate *(mL/min)*		172	226	417
Dry gas production rate *(mL/min/gram of feedstock*)	**H_2**	24.768	255.606	183.897
	CO	828.868	790.774	1880.8785
	Syngas	853.636	1046.38	2064.7755
Gas yield *(mL/gram of feedstock)*	**H_2**	7.2	56.55	22.05
	CO	240.95	174.95	225.525
	Syngas	248.15	231.5	247.575
Volume of Tar/Bio-oil extracted	3.2 mL			
mass of char residue after run	0.36 g (ash residue)			
Observations	**At 900°C**	**At 950°C**	**At 1000°C**	
	(a) Quick ignition; (b) low flame propagation; (c) pure blue flame	(a) Low flame propagation; (b) pure blue flame	(a) Low flame propagation; (b) pure blue flame	

B24: Pyro-gasification data for African mesquite sample.

Wood Sample	**AFRICAN MESQUITE 100% (20 g)**			
Gas Sampling Temperature	**Gas component**	**900°C**	**950°C**	**1000°C**
Gas Concentration in Product gas (%)	**H_2**	10.31	13.31	8.68
	CO	88.43	78.25	91.32
	Syngas (H_2+CO)	98.74	91.56	100
	CH_4	0.75	0.05	Undetected
	CO_2	0.51	8.39	Undetected
Volumetric Dry Gas Flow rate *(mL/min)*		155	252	395
Dry gas production rate *(mL/min/gram of feedstock*)	**H_2**	79.9025	167.706	171.43
	CO	685.3325	985.95	1803.57
	Syngas	765.235	1153.656	1975
Gas yield *(mL/gram of feedstock)*	**H_2**	25.775	33.275	21.7
	CO	221.075	195.625	228.3
	Syngas	246.85	228.9	250
Volume of Tar/Bio-oil extracted	2.8 mL			
mass of char residue after run	4.22 g (carbon residue)			
Observations	**At 900°C**	**At 950°C**	**At 1000°C**	
	(a) No ignition	(a) Ignites with low flame propagation; (b) blue flame	(a) Low flame propagation; (b) blue/yellow flame	

B25: Pyro-gasification data for African oilbean sample.

Wood Sample	**AFRICAN OILBEAN 100% (20 g)**			
Gas Sampling Temperature	**Gas component**	**900°C**	**950°C**	**1000°C**
Gas Concentration in Product gas (%)	**H_2**	7.79	5.9	12.17
	CO	85.56	89.28	82.24
	Syngas (H_2+CO)	93.35	95.18	94.41
	CH_4	5.98	4.53	0.86
	CO_2	0.67	0.29	4.74
Volumetric Dry Gas Flow rate *(mL/min)*		678	957	1755
Dry gas production rate *(mL/min/gram of feedstock*)	**H_2**	264.081	282.315	1067.9175
	CO	2900.484	4272.048	7216.56
	Syngas	3164.565	4554.363	8284.4775
Gas yield *(mL/gram of feedstock)*	**H_2**	19.475	14.75	30.425
	CO	213.9	223.2	205.6
	Syngas	233.375	237.95	236.025
Volume of Tar/Bio-oil extracted	3.7 mL			
mass of char residue after run	1.6 g (carbon residue)			
Observations	**At 900°C**	**At 950°C**	**At 1000°C**	
	(a) Quick ignition; (b) extremely low flame propagation; (c) Blue flame colour	(a) Still very low flame propagation; (b) blue flame	(a) Considerably increased flame propagation; (b) pure blue flame.	

B26: Pyro-gasification data for Opepe sample.

Wood Sample	**OPEPE 100% (20 g)**			
Gas Sampling Temperature	**Gas component**	**900°C**	**950°C**	**1000°C**
Gas Concentration in Product gas (%)	**H_2**	3.88	24.05	12.82
	CO	95.9	66.56	86.05
	Syngas (H_2+CO)	99.78	90.61	98.87
	CH_4	Undetected	8.25	0.46
	CO_2	0.22	0.87	0.67
Volumetric Dry Gas Flow rate *(mL/min)*		172	235	271
Dry gas production rate *(mL/min/gram of feedstock*)	**H_2**	33.368	282.5875	173.711
	CO	824.74	782.08	1165.9775
	Syngas	858.108	1064.6675	1339.6885
Gas yield *(mL/gram of feedstock)*	**H_2**	9.7	60.125	32.05
	CO	239.75	166.4	215.125
	Syngas	249.45	226.525	247.175
Volume of Tar/Bio-oil extracted	2 mL			
mass of char residue after run	1.89 g (carbon residue)			
Observations	**At 900°C**	**At 950°C**	**At 1000°C**	
	(a) Quick ignition; (b) extremely low flame propagation; (c) Blue flame colour	(a) Increased flame propagation; (b) blue flame	(a) Consistent flame propagation; (b) pure blue flame.	

B27: Pyro-gasification data for African mahogany - African oilbean 50/50 blend ratio.

Blend Ratio	**AFRICAN MAHOGANY 50% - AFRICAN OILBEAN 50% (20 g)**			
Gas Sampling Temperature	**Gas component**	**900°C**	**950°C**	**1000°C**
Gas Concentration in Product gas (%)	**H_2**	1.94	16.24	28.95
	CO	98.06	79.53	68.1
	Syngas (H_2+CO)	100	95.77	97.05
	CH_4	Undetected	4.23	0.81
	CO_2	Undetected	Undetected	2.15
Volumetric Dry Gas Flow rate *(mL/min)*		502	310	1678
Dry gas production rate *(mL/min/gram of feedstock*)	**H_2**	48.694	251.72	2428.905
	CO	2461.306	1232.715	5713.59
	Syngas	2510	1484.435	8142.495
Gas yield *(mL/gram of feedstock)*	**H_2**	4.85	40.6	72.375
	CO	245.15	198.825	170.25
	Syngas	250	239.425	242.625
Volume of Tar/Bio-oil extracted	3.8 mL			
mass of char residue after run	2.25 g (carbon residue)			
Observations	**At 900°C**	**At 950°C**	**At 1000°C**	
	(a) Quick ignition; (b) low but consistent flame propagation; (c) blue flame colour.	(a) slightly increased flame propagation; (b) blue flame colour	(a) Very high flame propagation; (b) Blue/yellow flame colour	

B28: Pyro-gasification data for African mahogany - African oilbean 70/30 blend ratio.

Blend Ratio	**AFRICAN MAHOGANY 70% - AFRICAN OILBEAN 30% (20 g)**			
Gas Sampling Temperature	**Gas component**	**900°C**	**950°C**	**1000°C**
Gas Concentration in Product gas (%)	**H_2**	84.52	12.5	10.57
	CO	8.46	80.3	88.94
	Syngas (H_2+CO)	92.98	92.8	99.51
	CH_4	7.02	7.2	0.49
	CO_2	Undetected	Undetected	Undetected
Volumetric Dry Gas Flow rate *(mL/min)*		1523	1824	1984
Dry gas production rate *(mL/min/gram of feedstock*)	**H_2**	6436.198	1140	1048.544
	CO	644.229	7323.36	8822.848
	Syngas	7080.427	8463.36	9871.392
Gas yield *(mL/gram of feedstock)*	**H_2**	211.3	31.25	26.425
	CO	21.15	200.75	222.35
	Syngas	232.45	232	248.775
Volume of Tar/Bio-oil extracted	3.1 mL			
mass of char residue after run	1.92 g (carbon residue)			
Observations	**At 900°C**	**At 950°C**	**At 1000°C**	
	(a) Quick ignition; (b) Very high flame burning rate; (c) pure blue flame	(a) Very high flame burning rate; (b) pure blue flame	(a) Very high flame propagation; (b) Blue/yellow flame colour	

B29: Pyro-gasification data for African mahogany - African oilbean 30/70 blend ratio.

Blend Ratio	**AFRICAN MAHOGANY 30% - AFRICAN OILBEAN 70% (20 g)**			
Gas Sampling Temperature	**Gas component**	**900°C**	**950°C**	**1000°C**
Gas Concentration in Product gas (%)	**H_2**	44.52	9.5	6.78
	CO	52.38	89.92	89.8
	Syngas (H_2+CO)	96.9	99.42	96.58
	CH_4	0.62	0.16	3.42
	CO_2	2.48	0.43	Undetected
Volumetric Dry Gas Flow rate *(mL/min)*		984	1140	1785
Dry gas production rate *(mL/min/gram of feedstock*)	**H_2**	2190.384	541.5	605.115
	CO	2577.096	5125.44	8014.65
	Syngas	4767.48	5666.94	8619.765
Gas yield *(mL/gram of feedstock)*	**H_2**	111.3	23.75	16.95
	CO	130.95	224.8	224.5
	Syngas	242.25	248.55	241.45
Volume of Tar/Bio-oil extracted	3.6 mL			
mass of char residue after run	1.2 g (carbon residue)			
Observations	**At 900°C**	**At 950°C**	**At 1000°C**	
	(a) Quick ignition; (b) High flame burning rate; (c) Flame stared with blue/yellow colour and turned pure blue with an increased flame propagation after 10 mins at 900°C	(a) Consistently high flame burning rate; (b) pure blue flame	(a) Flame intensity grossly decreased; (b) Yellow flame colour	

B.30: Pyro-gasification data for Opepe - African oilbean 50/50 blend ratio.

Blend Ratio	**OPEPE 50% - AFRICAN OILBEAN 50% (20 g)**			
Gas Sampling Temperature	**Gas component**	**900°C**	**950°C**	**1000°C**
Gas Concentration in Product gas (%)	**H_2**	0.39	7.31	9.46
	CO	91.74	89.71	87.06
	Syngas (H_2+CO)	92.13	97.02	96.52
	CH_4	2.53	2.53	3.48
	CO_2	5.34	0.45	Undetected
Volumetric Dry Gas Flow rate *(mL/min)*		552	584	952
Dry gas production rate *(mL/min/gram of feedstock*)	**H_2**	10.764	213.452	450.296
	CO	2532.024	2619.532	4144.056
	Syngas	2542.788	2832.984	4594.352
Gas yield *(mL/gram of feedstock)*	**H_2**	0.975	18.275	23.65
	CO	229.35	224.275	217.65
	Syngas	230.325	242.55	241.3
Volume of Tar/Bio-oil extracted	3.8 mL			
mass of char residue after run	2.16 g (carbon residue)			
Observations	**At 900°C**	**At 950°C**	**At 1000°C**	
	(a) Quick ignition; (b) High flame burning rate but flame extinguishes after 1 min; (c) Flame is re-ignited easily and burns consistently but with very low flame propagation; (d) Flame colour is blue.	(a) Increased flame burning rate; (b) blue/yellow flame	(a) Flame intensity remains consistent; (b) Blue/yellow flame colour	

B31: Pyro-gasification data for Opepe - African oilbean 70/30 blend ratio.

Blend Ratio	**OPEPE 70% - AFRICAN OILBEAN 30% (20 g)**			
Gas Sampling Temperature	**Gas component**	**900°C**	**950°C**	**1000°C**
Gas Concentration in Product gas (%)	**H_2**	3.2	5.76	10.3
	CO	88.2	84.9	84.6
	Syngas (H_2+CO)	91.4	90.66	94.9
	CH_4	8.6	9.34	4
	CO_2	Undetected	Undetected	1.1
Volumetric Dry Gas Flow rate *(mL/min)*		297	320	436
Dry gas production rate *(mL/min/gram of feedstock*)	**H_2**	47.52	92.16	224.54
	CO	1309.77	1358.4	1844.28
	Syngas	1357.29	1450.56	2068.82
Gas yield *(mL/gram of feedstock)*	**H_2**	8	14.4	25.75
	CO	220.5	212.25	211.5
	Syngas	228.5	226.65	237.25
Volume of Tar/Bio-oil extracted	3 mL			
mass of char residue after run	2.39 g (carbon residue)			
Observations	**At 900°C**	**At 950°C**	**At 1000°C**	
	(a) Quick ignition; (b) High flame burning rate but flame extinguishes after 1 min; (c) Flame is re-ignited easily but with a very low flame propagation; (d) Flame colour is blue.	(a) Increased flame burning rate; (b) blue/yellow flame	(a) Flame intensity remains consistent; (b) Blue/yellow flame colour	

B32: Pyro-gasification data for Opepe - African oilbean 30/70 blend ratio

Blend Ratio	**OPEPE 30% - AFRICAN OILBEAN 70% (20 g)**			
Gas Sampling Temperature	**Gas component**	**900°C**	**950°C**	**1000°C**
Gas Concentration in Product gas (%)	**H_2**	5.79	9.28	72.64
	CO	94.21	86.84	25.11
	Syngas (H_2+CO)	100	96.12	97.75
	CH_4	Undetected	3.77	2.25
	CO_2	Undetected	0.11	Undetected
Volumetric Dry Gas Flow rate *(mL/min)*		80	150	347
Dry gas production rate *(mL/min/gram of feedstock*)	**H_2**	23.16	69.6	1260.304
	CO	376.84	651.3	435.6585
	Syngas	400	720.9	1695.9625
Gas yield *(mL/gram of feedstock)*	**H_2**	14.475	23.2	181.6
	CO	235.525	217.1	62.775
	Syngas	250	240.3	244.375
Volume of Tar/Bio-oil extracted	4.1 mL			
mass of char residue after run	2.25 g (carbon residue)			
Observations	**At 900°C**	**At 950°C**	**At 1000°C**	
	(a) No ignition	(a) No ignition	(a) Ignition but very low flame propagation (b) Blue/yellow flame colour	

B33: Pyro-gasification data for Opepe - African mesquite 50/50 blend ratio.

Blend Ratio	**OPEPE 50% - AFRICAN MESQUITE 50% (20 g)**			
Gas Sampling Temperature	**Gas component**	**900°C**	**950°C**	**1000°C**
Gas Concentration in Product gas (%)	**H_2**	2.11	0.1	1.3
	CO	96.1	97.41	92.64
	Syngas (H_2+CO)	98.21	97.51	93.94
	CH_4	1.79	0.56	6.06
	CO_2	Undetected	1.93	Undetected
Volumetric Dry Gas Flow rate *(mL/min)*		712	558	825
Dry gas production rate *(mL/min/gram of feedstock*)	**H_2**	75.116	2.79	53.625
	CO	3421.16	2717.739	3821.4
	Syngas	3496.276	2720.529	3875.025
Gas yield *(mL/gram of feedstock)*	**H_2**	5.275	0.25	3.25
	CO	240.25	243.525	231.6
	Syngas	245.525	243.775	234.85
Volume of Tar/Bio-oil extracted	2.2 mL			
mass of char residue after run	1.96 g (carbon residue)			
Observations	**At 900°C**	**At 950°C**	**At 1000°C**	
	(a) poor ignition; (b) moderate flame burning rate but flame; (c) Blue/yellow flame	(a) Very low flame burning rate; (b) Yellow flame	(a) Flame intensity remains very low; (b) Blue/yellow flame colour	

B34: Pyro-gasification data for Opepe - African mesquite 70/30 blend ratio.

Blend Ratio	**OPEPE 70% - AFRICAN MESQUITE 30% (20 g)**			
Gas Sampling Temperature	**Gas component**	**900°C**	**950°C**	**1000°C**
Gas Concentration in Product gas (%)	**H_2**	6.00	11.02	9.65
	CO	90.11	87.94	84.77
	Syngas (H_2+CO)	96.11	98.96	94.42
	CH_4	3.52	0.23	5.37
	CO_2	0.38	0.81	0.21
Volumetric Dry Gas Flow rate *(mL/min)*		1406.00	519.00	625.00
Dry gas production rate *(mL/min/gram of feedstock*)	**H_2**	421.80	285.97	301.56
	CO	6334.73	2282.04	2649.06
	Syngas	6756.53	2568.01	2950.63
Gas yield *(mL/gram of feedstock)*	**H_2**	15.00	27.55	24.13
	CO	225.28	219.85	211.93
	Syngas	240.28	247.40	236.05
Volume of Tar/Bio-oil extracted	2.6 mL			
mass of char residue after run	1.24 g (carbon residue)			
Observations	**At 900°C**	**At 950°C**	**At 1000°C**	
	(a) Quick ignition; (b) High flame propagation; (c) Pure blue colour	(a)Flame remains consistent; (b) Pure blue flame	(a) Very low flame flame propagation; (b) yellow flame	

B35: Pyro-gasification data for Opepe - African mesquite 30/70 blend ratio.

Blend Ratio	**OPEPE 30% - AFRICAN MESQUITE 70% (20 g)**			
Gas Sampling Temperature	**Gas component**	**900°C**	**950°C**	**1000°C**
Gas Concentration in Product gas (%)	**H_2**	33.45	32.74	0.32
	CO	33.96	64.47	92.71
	Syngas (H_2+CO)	67.41	97.21	93.03
	CH_4	22.08	0.54	6.16
	CO_2	10.51	2.21	0.81
Volumetric Dry Gas Flow rate *(mL/min)*		625	632	1377
Dry gas production rate *(mL/min/gram of feedstock*)	**H_2**	1045.3125	1034.584	22.032
	CO	1061.25	2037.252	6383.0835
	Syngas	2106.5625	3071.836	6405.1155
Gas yield *(mL/gram of feedstock)*	**H_2**	83.625	81.85	0.8
	CO	84.9	161.175	231.775
	Syngas	168.525	243.025	232.575
Volume of Tar/Bio-oil extracted	2.6 mL			
mass of char residue after run	2.1 g (carbon residue)			
Observations	**At 900°C**	**At 950°C**	**At 1000°C**	
	(a) Quick ignition; (b) High flame propagation; (c) Blue/ Yellow colour	(a)Flame propagation remains consistent; (b) Blue/ Yellow colour	(a) High flame flame propagation; (b) yellow flame	

B36: Pyro-gasification data for African mesquite - African mahogany 50/50 blend ratio.

Blend Ratio	**AFRICAN MESQUITE 50% - AFRICAN MAHOGANY 50% (20 g)**			
Gas Sampling Temperature	**Gas component**	**900°C**	**950°C**	**1000°C**
Gas Concentration in Product gas (%)	**H_2**	70.1	64.9	87
	CO	27.3	32.6	11.1
	Syngas (H_2+CO)	97.4	97.5	98.1
	CH_4	2.15	1.65	1.35
	CO_2	0.5	0.86	0.6
Volumetric Dry Gas Flow rate *(mL/min)*		810	724	738
Dry gas production rate *(mL/min/gram of feedstock*)	**H_2**	2839.05	2349.38	3210.3
	CO	1105.65	1180.12	409.59
	Syngas	3944.7	3529.5	3619.89
Gas yield *(mL/gram of feedstock)*	**H_2**	175.25	162.25	217.5
	CO	68.25	81.5	27.75
	Syngas	243.5	243.75	245.25
Volume of Tar/Bio-oil extracted	2.9 mL			
mass of char residue after run	1.18 g (carbon residue)			
Observations	**At 900°C**	**At 950°C**	**At 1000°C**	
	(a) Quick ignition; (b) Low flame propagation; (c) Blue/ Yellow colour	(a)Flame propagation remains consistent; (b) Blue/ Yellow colour	(a) Consistent flame propagation; (b) yellow flame	

B37: Pyro-gasification data for African mesquite - African mahogany 70/30 blend ratio.

Blend Ratio	**AFRICAN MESQUITE 70% - AFRICAN MAHOGANY 30% (20 g)**			
Gas Sampling Temperature	**Gas component**	**900°C**	**950°C**	**1000°C**
Gas Concentration in Product gas (%)	**H_2**	18.21	57.41	32.63
	CO	78.04	35.73	64.47
	Syngas (H_2+CO)	96.25	93.14	97.1
	CH_4	3.47	0.6	1.62
	CO_2	0.29	6.26	1.27
Volumetric Dry Gas Flow rate *(mL/min)*		414	539	933
Dry gas production rate *(mL/min/gram of feedstock*)	**H_2**	376.947	1547.1995	1522.1895
	CO	1615.428	962.9235	3007.5255
	Syngas	1992.375	2510.123	4529.715
Gas yield *(mL/gram of feedstock)*	**H_2**	45.525	143.525	81.575
	CO	195.1	89.325	161.175
	Syngas	240.625	232.85	242.75
Volume of Tar/Bio-oil extracted	2.3 mL			
mass of char residue after run	1.7 g (carbon residue)			
Observations	**At 900°C**	**At 950°C**	**At 1000°C**	
	(a) Quick ignition; (b) Low and inconsistent flame propagation flame extinguishes after a few minutes; (c) Blue/ Yellow colour	(a)Flame intensity remains low and inconsistent; (b) Blue/ yellow colour	(a) Flame propagation increases; (b) yellow flame	

B38: Pyro-gasification data for African mesquite - African mahogany 30/70 blend ratio.

Blend Ratio	**AFRICAN MESQUITE 30% - AFRICAN MAHOGANY 70% (20 g)**			
Gas Sampling Temperature	**Gas component**	**900°C**	**950°C**	**1000°C**
Gas Concentration in Product gas (%)	**H_2**	4.52	46.81	25.29
	CO	95.15	37.43	72.97
	Syngas (H_2+CO)	99.67	84.24	98.26
	CH_4	0.33	15.76	0.4
	CO_2	Undetected	Undetected	1.34
Volumetric Dry Gas Flow rate *(mL/min)*		738	1031	1495
Dry gas production rate *(mL/min/gram of feedstock*)	**H_2**	166.788	2413.0555	1890.4275
	CO	3511.035	1929.5165	5454.5075
	Syngas	3677.823	4342.572	7344.935
Gas yield *(mL/gram of feedstock)*	**H_2**	11.3	117.025	63.225
	CO	237.875	93.575	182.425
	Syngas	249.175	210.6	245.65
Volume of Tar/Bio-oil extracted	1.9 mL			
mass of char residue after run	2.04 g (carbon residue)			
Observations	**At 900°C**	**At 950°C**	**At 1000°C**	
	(a) Quick ignition; (b) high inconsistent flame propagation flame; (c) pure blue flame	(a)Flame intensity remains high and more stable; (b) pure blue flame	(a) Flame increases to a much higher flame propagation; (b) blue/ yellow flame	

B39: Pyro-gasification data for African mesquite - African oilbean 50/50 blend ratio.

Blend Ratio	**AFRICAN MESQUITE 50% - AFRICAN OILBEAN 50% (20 g)**			
Gas Sampling Temperature	**Gas component**	**900°C**	**950°C**	**1000°C**
Gas Concentration in Product gas (%)	**H_2**	86.95	5.75	99.13
	CO	11.79	87.29	0.87
	Syngas (H_2+CO)	98.74	93.04	100
	CH_4	1.27	6.66	Undetected
	CO_2	Undetected	0.3	Undetected
Volumetric Dry Gas Flow rate *(mL/min)*		645	1007	1696
Dry gas production rate *(mL/min/gram of feedstock*)	**H_2**	2804.1375	289.5125	8406.224
	CO	380.2275	4395.0515	73.776
	Syngas	3184.365	4684.564	8480
Gas yield *(mL/gram of feedstock)*	**H_2**	217.375	14.375	247.825
	CO	29.475	218.225	2.175
	Syngas	246.85	232.6	250
Volume of Tar/Bio-oil extracted	2.7 mL			
mass of char residue after run	1.2 g (carbon residue)			
Observations	**At 900°C**	**At 950°C**	**At 1000°C**	
	(a) Quick ignition; (b) Low inconsistent flame propagation flame; (c) pure blue flame	(a)Flame intensity increases slightly and more stable; (b) blue/yellow flame	(a) Flame increases to a much higher flame propagation; (b) blue/ yellow flame	

B40: Pyro-gasification data for African mesquite - African oilbean 70/30 blend ratio.

Blend Ratio	**AFRICAN MESQUITE 70% - AFRICAN OILBEAN 30% (20 g)**			
Gas Sampling Temperature	**Gas component**	**900°C**	**950°C**	**1000°C**
Gas Concentration in Product gas (%)	**H_2**	13.51	6.74	7.84
	CO	85.32	87.66	86.54
	Syngas (H_2+CO)	98.83	94.4	94.38
	CH_4	0.24	5.6	5.31
	CO_2	0.93	Undetected	0.31
Volumetric Dry Gas Flow rate *(mL/min)*		508	776	1310
Dry gas production rate *(mL/min/gram of feedstock*)	**H_2**	343.154	261.512	513.52
	CO	2167.128	3401.208	5668.37
	Syngas	2510.282	3662.72	6181.89
Gas yield *(mL/gram of feedstock)*	**H_2**	33.775	16.85	19.6
	CO	213.3	219.15	216.35
	Syngas	247.075	236	235.95
Volume of Tar/Bio-oil extracted	3.1 mL			
mass of char residue after run	0.9 g (carbon residue)			
Observations	**At 900°C**	**At 950°C**	**At 1000°C**	
	(a) Quick ignition; (b) Low inconsistent flame propagation; (c) pure blue flame	(a)Flame propagation remains low and inconsistent; (b) blue/yellow flame	(a) flame propagation increases slightly; (b) blue/ yellow flame	

B41: Pyro-gasification data for African mesquite - African oilbean 30/70 blend ratio.

Blend Ratio	**AFRICAN MESQUITE 30% - AFRICAN OILBEAN 70% (20 g)**			
Gas Sampling Temperature	**Gas component**	**900°C**	**950°C**	**1000°C**
Gas Concentration in Product gas (%)	**H_2**	9.22	7.93	10.05
	CO	90	86.95	89.27
	Syngas (H_2+CO)	99.22	94.88	99.32
	CH_4	0.21	4.76	0.2
	CO_2	0.57	0.36	0.48
Volumetric Dry Gas Flow rate *(mL/min)*		861	1173	1753
Dry gas production rate *(mL/min/gram of feedstock*)	**H_2**	396.921	465.0945	880.8825
	CO	3874.5	5099.6175	7824.5155
	Syngas	4271.421	5564.712	8705.398
Gas yield *(mL/gram of feedstock)*	**H_2**	23.05	19.825	25.125
	CO	225	217.375	223.175
	Syngas	248.05	237.2	248.3
Volume of Tar/Bio-oil extracted	2.8 mL			
mass of char residue after run	1 g (carbon residue)			
Observations	**At 900°C**	**At 950°C**	**At 1000°C**	
	(a) Quick ignition; (b) Low inconsistent flame propagation; (c) pure blue flame	(a)Flame propagation remains low and inconsistent; (b) blue/yellow flame	(a) Flame propagation increases slightly; (b) blue/ yellow flame	

B42: Pyro-gasification data for African mahogany - Opepe 50/50 blend ratio.

Blend Ratio	**AFRICAN MAHOGANY 50% - OPEPE 50% (20 g)**			
Gas Sampling Temperature	**Gas component**	**900°C**	**950°C**	**1000°C**
Gas Concentration in Product gas (%)	**H_2**	8.65	7.05	7.83
	CO	90.71	90.05	89.35
	Syngas (H_2+CO)	99.36	97.1	97.18
	CH_4	Undetected	2.89	2.82
	CO_2	0.64	Undetected	Undetected
Volumetric Dry Gas Flow rate *(mL/min)*		984	796	1072
Dry gas production rate *(mL/min/gram of feedstock*)	**H_2**	425.58	280.59	419.688
	CO	4462.932	3583.99	4789.16
	Syngas	4888.512	3864.58	5208.848
Gas yield *(mL/gram of feedstock)*	**H_2**	21.625	17.625	19.575
	CO	226.775	225.125	223.375
	Syngas	248.4	242.75	242.95
Volume of Tar/Bio-oil extracted	1.7 mL			
mass of char residue after run	0.81 g (carbon residue)			
Observations	**At 900°C**	**At 950°C**	**At 1000°C**	
	(a) Quick ignition; (b) Very high flame propagation; (c) pure blue flame	(a)Flame propagation decreases slightly; (b) Pure blue flame	(a) Flame propagation increases once more; (b) Pure blue flame	

B43: Pyro-gasification data for African mahogany - Opepe 70/30 blend ratio.

Blend Ratio	**AFRICAN MAHOGANY 70% - OPEPE 30% (20 g)**			
Gas Sampling Temperature	**Gas component**	**900°C**	**950°C**	**1000°C**
Gas Concentration in Product gas (%)	**H_2**	1.84	7.43	1.34
	CO	0.44	89.15	97.26
	Syngas (H_2+CO)	2.28	96.58	98.6
	CH_4	97.72	3.42	0.91
	CO_2	Undetected	Undetected	0.49
Volumetric Dry Gas Flow rate *(mL/min)*		575	637	171
Dry gas production rate *(mL/min/gram of feedstock*)	**H_2**	52.9	236.6455	11.457
	CO	12.65	2839.4275	831.573
	Syngas	65.55	3076.073	843.03
Gas yield *(mL/gram of feedstock)*	**H_2**	4.6	18.575	3.35
	CO	1.1	222.875	243.15
	Syngas	5.7	241.45	246.5
Volume of Tar/Bio-oil extracted	2.0 mL			
mass of char residue after run	0.41 g (more Ash than carbon residue)			
Observations	**At 900°C**	**At 950°C**	**At 1000°C**	
	(a) Quick ignition; (b) Very high flame propagation; (c) pure blue flame	(a)High flame propagation; (b) Pure blue flame	(a) Very low flame propagation; (b) Pure blue flame	

B44: Pyro-gasification data for African mahogany - Opepe 30/70 blend ratio.

Blend Ratio	**AFRICAN MAHOGANY 30% - OPEPE 70% (20 g)**			
Gas Sampling Temperature	**Gas component**	**900°C**	**950°C**	**1000°C**
Gas Concentration in Product gas (%)	**H_2**	5.33	9.84	28.94
	CO	92.15	89.59	68.47
	Syngas (H_2+CO)	97.48	99.43	97.41
	CH_4	2.52	0.11	1.88
	CO_2	Undetected	0.46	0.71
Volumetric Dry Gas Flow rate *(mL/min)*		690	541	230
Dry gas production rate *(mL/min/gram of feedstock*)	**H_2**	183.885	266.172	332.81
	CO	3179.175	2423.4095	787.405
	Syngas	3363.06	2689.5815	1120.215
Gas yield *(mL/gram of feedstock)*	**H_2**	13.325	24.6	72.35
	CO	230.375	223.975	171.175
	Syngas	243.7	248.575	243.525
Volume of Tar/Bio-oil extracted	2.5 mL			
mass of char residue after run	0.31 g (more Ash than carbon residue)			
Observations	**At 900°C**	**At 950°C**	**At 1000°C**	
	(a) Quick ignition; (b) Very low flame propagation; (c) yellow flame	(a) Low flame propagation; (b) Yellow flame	(a) Very low flame propagation; (b) Yellow flame	

Appendix C: List of publications from this study

- **Okoro, N.M.,** Harding, K.G., Daramola, M.O. (2019) Thermo-decompositional Analysis of Sawdust Blends of Invasive Alien Plants, *J. Phys.: Conf. Ser.* 1378 022020 https://doi.org/10.1088/1742-6596/1378/2/022020
- **Okoro, N.M.,** Harding, K.G., Daramola, M.O. (2019) Pyro-gasification of Invasive Plants to Syngas, In: Valorization of biomass to value-added commodities: current trend, challenges and future outlook (M.O. Daramola and A.O. Ayeni, eds.), Springer Nature Publishers (In press)
- **Okoro, N.M.,** Harding, K.G., Daramola, M.O. (2018) Fuel evaluation of Invasive Alien Plants and Tropical hardwoods as feedstock in pyro-gasification (presented at the BIORESTEC Sitges 2018)
- **Okoro, N.M.,** Harding, K.G., Daramola, M.O. (2020) The Potentials of Wood Pine sawdust as renewable fuel for Pyro-gasification: Nigerian & South African Context (in preparation)